DIE LOAD AND STRESSES IN PRESS FORGING

By

SANMBO ADEWALE BALOGUN

BSc (Eng) , MSc (Met)

A thesis for consideration for the degree of Doctor of Philosophy of the University of Aston in Birmingham.

December 1971.

SUMMARY

Several axi-symmetric EN3B steel components differing in shape and size were forged on a 100 ton joint knuckle press.

A load cell fitted under the lower die inserts recorded the total deformation forces. Job parameters were measured off the billets and the forged parts. Slug temperatures were varied and two lubricants - aqueous colloidal graphite and oil - were used.

An industrial study was also conducted to check the results of the laboratory experiments. Loads were measured (with calibrated extensometers attached to the press frames) when adequately heated mild steel slugs were being forged in finishing dies. Geometric parameters relating to the jobs and the dies were obtained from works drawings.

All the variables considered in the laboratory study could not, however, be investigated without disrupting production. In spite of this obvious limitation, the study confirmed that parting area is the most significant geometric factor influencing the forging load.

Multiple regression analyses of the laboratory and industrial results showed that die loads increase significantly with the weights and parting areas of press forged components, and with the width to thickness ratios of the flashes formed, but diminish with increasing slug temperatures and higher billet diameter to height ratios. The analyses also showed that more complicated parts require greater loads to forge them.

Die stresses, due to applied axial loads, were investigated by the photoelastic method. The three dimensional frozen stress

technique was employed. Model dies were machined from cast araldite cylinders, and the slug material was simulated with plasticene. Test samples were cut from the centres of the dies after the stress freezing.

Examination of the samples, and subsequent calculations, showed that the highest stresses were developed in die outer corners. This observation partly explains why corner cracking occurs frequently in industrial forging dies.

Investigation of die contact during the forging operation revealed the development of very high stresses.

C O N T E N T S

Symbols

σ_o	Resistance to deformation
$\bar{\sigma}_o$, σ_e	Effective stress
σ_y	Normal stress
σ_r	Radial stress
σ_θ	Circumferential stress
q	Mean stress
Q, P	Total load
h, H	Height of forging
μ	Coefficient of friction
f	Unit friction coefficient
ν	Poisson's ratio
T	Temperature
G	Rigidity modulus
τ	Shear stress
t	time
K	Thermal conductivity
C	Specific heat
ρ	Density
ε_y, ε_r, ε_θ	Axial, radial and circumferential strains
α	Coefficient of expansion
R	Relative retardation in inches
λ	Wavelength of light in Armstrom units
F	Unit fringe value in lb/in fringe

Symbols (continued)

C	Stress optical coefficient
n	Fringe order or no of fringes
ϕ	Displacement potential or rotation angle in degrees
ξ	Stress function
P, Q	Secondary principal stresses
σ_1, σ_2	Principal stresses

INTRODUCTION

The loading cycle to which any pair of forging dies will be subjected determines the composition of the die material required and the hardness level to which the dies must be heat-treated to avoid deformation. The magnitude and distribution of the stresses developed indicate the probable mode of failure of the dies and hence the design modifications necessary to prolong their lives.

If forging load is under-estimated, too big a component may be forged on too small a press. The press may be stalled. Valuable production time will be lost and the dies may be damaged in the process of releasing the tools. Where the component is safely made, maintenance of close dimensional tolerances will be difficult, and the greater machining necessary will increase the unit cost of the component.

If forging load is over-estimated, too big a press may be used to forge too small a part. Press capacity will not be utilised to full advantage and the unit cost of the forging will rise. High die stresses will also be developed, and a reduction in die life may result.

An investigation of die loads and stresses in press forging is, therefore, necessary not only for efficient design but also in the interest of safe and economic use of machinery.

In industrial forging practice, design limits are often so tight that only a few job and process parameters can be varied by the forging designer to obtain the best results. An optimum design characteristic can be determined for each forging by "blending" these factors in a particular fashion.

To this end, loads have been studied in relation to die and process design and with regard to press capacity selection.

Die stresses have been investigated by a simulative method. Effect of die contact (during the press forging operation) has been studied, and a theoretical treatment of thermal stresses has been attempted. A literature survey is included to give a balanced outlook.

2. RELEVANT INDUSTRIAL PRACTICE

Forging load and slug size estimation in industry can be cited as being relevant to the present study.

Jobs with close dimensional tolerances are forged on presses. Others , especially relatively heavy ones and those with long extruded sections , are made on hammers.

The determination of the press capacity needed for a job is almost always[1,2,3] based on the component's width or area at parting line , its maximum height and its least thickness. Forging weight is considered in drop forging.

Deformation force is estimated as the product of the job's parting area (calculated from die drawings) and a pressure value which depends on how "thick" or "thin" the estimator considers the part to be. If thick, a value of 25 to 40 ton/in^2 is used, otherwise the "multiplying factor" is between 40 and 55 ton/in^2. The forging is then made on the press nearest in tonnage capacity to the estimated load.

There is no clear-cut demarcation between the definitions of "thick" and "thin" forgings. A visual comparison of any component's width to its diameter is all it takes to decide the category to which it belongs. Estimators, however, seem aware of the dangers of these loose classifications and try to compensate for any "incidental errors" by overestimating the forging load. This has been confirmed in a study conducted by the author on the differences between the tonnage capacities of presses used for various jobs and the actual deformation forces.

The results of the suvey showed that the actual

forging loads are sometimes less than 25% of the rated tonnages of the presses.

In hammer forging, the tup weight is considered the maximum load deliverable by the machine. Hence each hammer is used for components whose load requirements do not exceed the force due to its (hammer's) tup weight.

"Pressure multiplicant factors" similar to those employed in press forging, are also used here. But some large forges prefer nomograms. Two hammer sizes based on the weight and parting area of a component are read off the graphs (see Fig 2.1) and the part is forged on the hammer whose size is nearest to their mean.

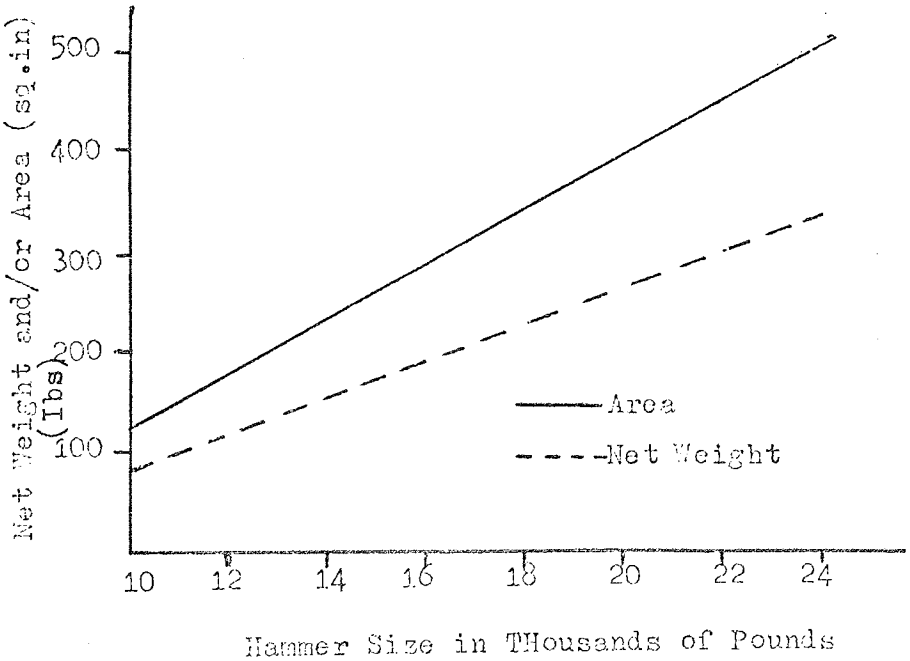

Fig 2.1

The graphs are based on forging load measurements and are to be prefered to the pressure method whose main limitation is the looseness of the classifications.

Forging Stock

Most British forging works are geared to the use of square billets; probably because of their relative cheapness. The cost of round bars often restrict their use to long hubbed and small sectioned forgings. But forgers broadly agree that round stocks are preferable because of the "likelihood of better grain flow".

Forgers avoid large sectioned billets as much as possible. This is partly because of the time and material savings made, and partly because of better grain flow associated with large deformations of croppable small sectioned billets.

The stock size estimation is based entirely on the volume enclosed between the die halves and the degree of difficulty of making the part. Five to forty percent of this volume is generally added on for pierced parts, flash formation and losses due to oxidation.

But yield can be as low as 32% in the non-ferrous industry where finned jobs, like aircraft parts, are common. Forgers accept that such yield rates are undesirable but insist on using oversized billets to ensure complete die filling, because product designers leave little room for manoevre in die design.

It is probable that some stock material saving can be made if adequate consultations are held between product and die designers in the early stages of product development.

3. REVIEW OF FORGING THEORIES

Closed die forging is a non-uniform process. Its tools are complex in shape and worked materials are often inhomogeneous. The process does not, therefore, satisfy the conditions for the application of plasticity theories to a forming process.

But in spite of this obvious limitation, attempts are being made to determine analytically the stress distribution, the forces and the work done in forging processes.

Most of such analyses are confined to simple upsetting and it is assumed in the majority of them that:-

(1) plane cross-sections before compression remain plane after it, and

(2) that the direction of the mean principal stress is perpendicular to the plane of deformation.

In practice, barelling occurs as a result of friction at the job-tool interfaces. The mean principal stress would, therefore, not be perpendicular to the plane of deformation.

Thus, theories based on these assumptions can only be approximate. Some of the models, however, prove to be fair approximations of what obtains in practice.

SIMPLE UPSETTING

One of the earliest attempts to derive expressions for forging load was made by Siebel [4].

In 1932, he obtained a simple equation for the normal stress q on the compressed faces of an upset specimen.

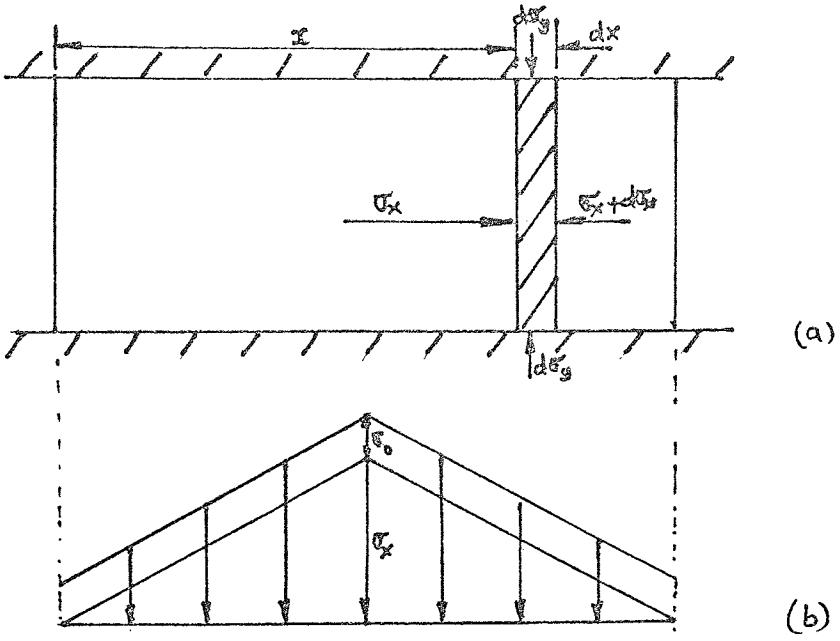

Fig. 3.1

Writing force equilibrium equation for an elemental strip of width dx, Fig (3.1a).

$$\sigma_x = \int_o^x \frac{2\mu\sigma_o dx}{h} = \frac{2\mu\sigma_o x}{h} \qquad \ldots\ldots\ldots (3.1)$$

where μ is the coefficient of friction and σ_o is the resistance to deformation.

Assuming that σ_y and σ_x are principal stresses and that Tresca's shear stress theory is the criterion for yield,

$$\sigma_y = \sigma_x + \sigma_o = \sigma_o \left[1 + \frac{2\mu x}{h}\right] \qquad \ldots\ldots\ldots (3.2)$$

Thus, the mean compression pressure for plane strain deformation is

$$q = \sigma_o\left(1+ \frac{\mu a}{2h}\right) \qquad \ldots\ldots\ldots (3.3)$$

Siebel considered that equation (3.2) is equally true for cylindrical upsetting and hence expressed the mean compression stress on a cylinder radius r and height h as

$$q_c = \frac{2\pi}{\pi r^2}\int^{r} (r-x)\,\sigma_y dx = \sigma_o\left[1 + \frac{2\mu r}{3h}\right] \ldots\ldots (3.4)$$

These equations are, clearly, simple to apply. But they are liable to be inaccurate in view of the assumption that σ_x is a function of σ_o. The lateral compression stress σ_x is a function of the normal compressive stress σ_y; not[44] of the resistance to deformation σ_o. The other assumption that σ_y and σ_x are principal stresses is also liable to introduce an error since metal shearing occurs at the job-tool interfaces.

Geleji[5] and Lippmann[6] derived normal stress equations for plane strain compression in the same way as Siebel. They assumed that $\sigma_y - \sigma_x = \sigma_o$ and that friction resistance f is proportional to the normal stress and obtained a normal stress distribution of the form

$$\sigma_y = \sigma_o e^{\frac{2\mu x}{h}} \qquad \ldots\ldots\ldots (3.5)$$

which gives a mean compression pressure

$$q = \frac{h\sigma_o}{2\mu a}\left[e^{\frac{2\mu a}{h}} - 1\right] \qquad \ldots\ldots\ldots (3.6)$$

Dietrich and Ansel[7] considered that equation (3.5) is

applicable to circular jobs and expressed the force, Q, on the press plates when upsetting a cylinder of radius, r, and height, h, as

$$Q = \int_0^r 2\pi(r - x)dx.q$$

$$= \frac{\pi\sigma_o h}{\mu} \frac{h}{2\mu} \left(e^{\frac{2\mu r}{h}} - 1\right) - r \qquad \ldots\ldots\ldots (3.7)$$

The average pressure is given by

$$q = \frac{Q}{\pi r^2} = \frac{\sigma_o h}{\mu r} \frac{h}{2\mu r} \left(e^{\frac{2\mu r}{h}} - 1\right) - 1 \qquad \ldots\ldots\ldots (3.8)$$

Baraya et al[8] expressed the friction stress f as $\frac{c\sigma_o}{2}$, where c is a constant fraction less than one, and assumed that the normal stress at the edge of the specimen is equal to the resistance to deformation σ_o. The normal stress distribution on the faces of a cylinder of radius r = a, and height, h, is thus given by

$$\sigma_y = \sigma_o \left[1 + c\ (a-r)/h\right] \qquad \ldots\ldots\ldots (3.9)$$

This equation, like Siebel's, suffers from the approximate assumption that the friction stress is a function of the resistance to deformation of the material of the forging.

Later, Schroeder and Webster[9] analysed the effect of friction, area and thickness on pressures required for press forging thin sections.

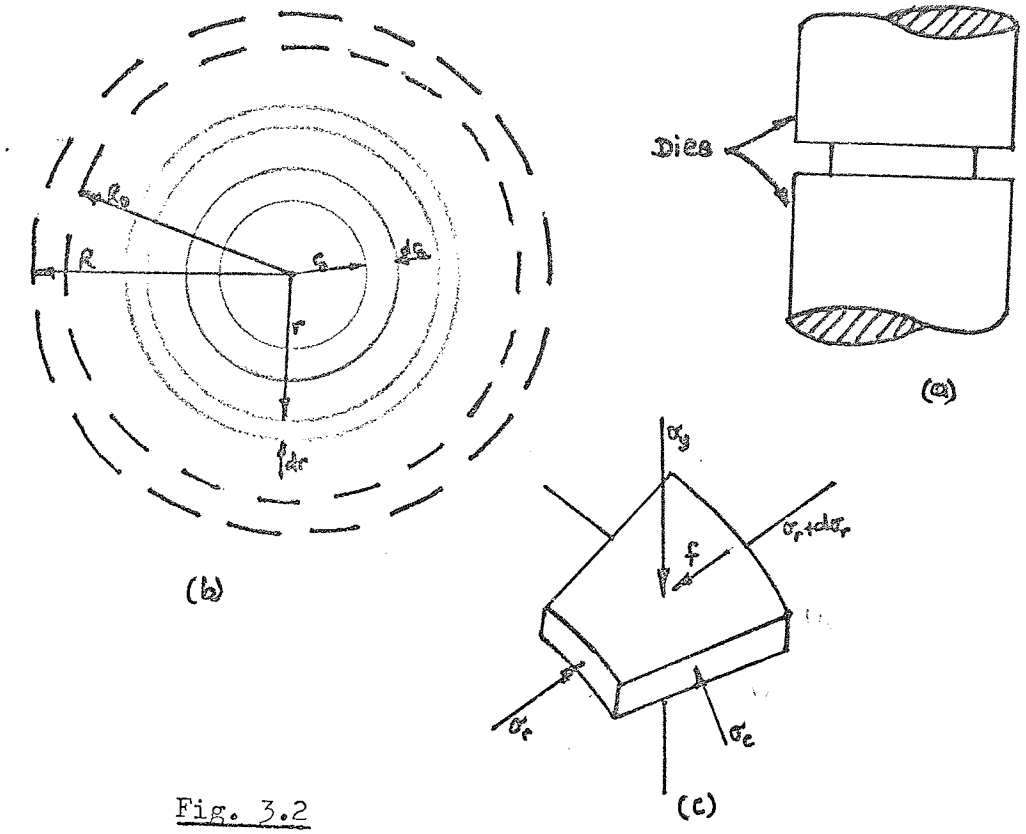

Fig. 3.2

In doing so, they considered the following friction conditions.

(1) Relative sliding motion between the blank and die surface at all points except the blank's geometric centre.

(2) Sticking between surfaces and spreading due to shear strain in the blank surface parallel to the die surface.

and

(3) Sliding in an annular zone near the edge and sticking in the central area.

Writing the force equilibrium equation for an element of the disc shown in Fig (3.2c) gives

$$\frac{d\sigma_r}{dr} + \frac{\sigma_r - \sigma_c}{r} = \frac{-2f}{h} \qquad \ldots\ldots\ldots (3.10)$$

where f is the friction stress.

Using the shear strain energy yield criterion and assuming coulomb's friction conditions, i.e. $f = \mu\sigma_y$ the normal stress distribution for case 1 is given by

$$\sigma_y = \sigma_o \exp\left[2\mu\left(\frac{R}{h} - \frac{r}{h}\right)\right] \qquad \ldots\ldots\ldots (3.11)$$

And the average die pressure, q, is given by

$$q = \frac{2\sigma_o}{C^2}\left[e^C - C - 1\right] \qquad \ldots\ldots\ldots (3.12)$$

where $C = \frac{2\mu r}{h}$

For high values of the unit friction factor f, Schroeder and Webster consider that the restraint to free spreading offered by the dies approximates to a hydrostatic pressure σ_o upon which a shear stress, f, is superimposed Fig (3.3).

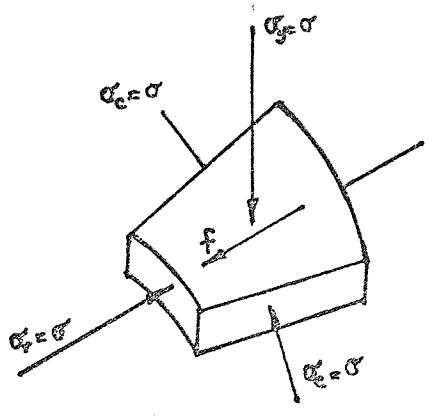

Fig. 3.3

Thus the yield equation becomes

$$\sigma_o = \frac{1}{\sqrt{2}} \left[(2f_o)^2 + f_o^2 + f_o^2 \right]^{\frac{1}{2}}$$

$$\text{and} \quad f_o = 0.577\sigma_o = k\sigma_o \qquad \ldots\ldots\ldots (3.13)$$

Integrating equation (3.10) and substituting $f_o = k\sigma_o$ gives $\frac{\sigma_y}{\sigma_o} = 1 + 2k\left(\frac{R}{h} - \frac{r}{h}\right)$ and the mean compression pressure becomes

$$q = \sigma_o \left(1 + \frac{2kR}{3h}\right) \qquad \ldots\ldots\ldots (3.14)$$

For the intermediate friction condition, i.e. when $\mu < k$ and $R/h > \frac{1}{2\mu} \ln \frac{k}{\mu}$, the stress distribution and the mean stress are expressed respectively as

$$\sigma_y = \sigma_o \left[\frac{k}{\mu} + 2k \left(\frac{r_c}{h} - \frac{r}{h} \right) \right]$$

$$\text{and} \quad \frac{q}{\sigma_o} = \frac{2}{C^2} \left[(D + 1)e^{C - D} - C - 1 \right] + \frac{D^2}{C^2} \left(\frac{k}{\mu} + \frac{2kr_c}{3h} \right)$$

$$\ldots\ldots\ldots (3.15)$$

$$\text{where } D = \frac{2\mu r_c}{h} \quad \text{and} \quad \frac{r_c}{h} = \frac{R}{h} - \frac{1}{2\mu} \ln \frac{k}{\mu}$$

Clearly, the simplifying assumptions made on stress and strain states and on the nature of the material are liable to reduce the accuracy of the models. But they cover a variety of friction conditions and are easy to apply. This probably underlines their broad acceptance, in the literature, for the prediction of loads during disc forging.

Sokolovskii[10] used numerical integration to calculate the normal stress when compressing rectangular strips between parallel platens under conditions of constant friction forces at the contact plane.

Shear stresses at the contact planes are expressed as $\tau = \pm \frac{\sigma_o t}{\sqrt{3}}$ where t is a constant and $o < t < 1$. Sokolovskii then obtained and integrated slip line equations and deduced for frictionless compression, that the normal stress is $\sigma_y = \frac{-2}{\sqrt{3}} \sigma_o$ and the flow stress σ_x is zero. He also observed that if $t \neq o$, stresses depend on the width to height ratio a/h. And when $o \leq a/h \leq 1$, stresses are uniform over the whole strip and are given by

$$\sigma_x = 0, \sigma_y = \frac{-2}{\sqrt{3}} \sigma_o \text{ and } \tau_{xy} = 0.$$

For $1 < a/h < \delta(t)$ where $1 < \delta(t) < 3.66$, conditions at the free end planes and at the vertical axis of symmetry fully determine the solution. Shear and normal stresses, in this case, respectively attain their maximum and minimum absolute values at the edge and centre of the strip and shear stresses do not reach $\pm \frac{\sigma_o t}{\sqrt{3}}$.

When $\delta(t) < a/h < \infty$, the shear stress, τ, equals $\pm \frac{\sigma_o}{\sqrt{3}} t$ in every part of the contact plane except the central area. The normal stress has a constant value in sections $A_1 B_1$ and $A_2 B_2$ of the strip and increases to a maximum at the centre Fig (3.4).

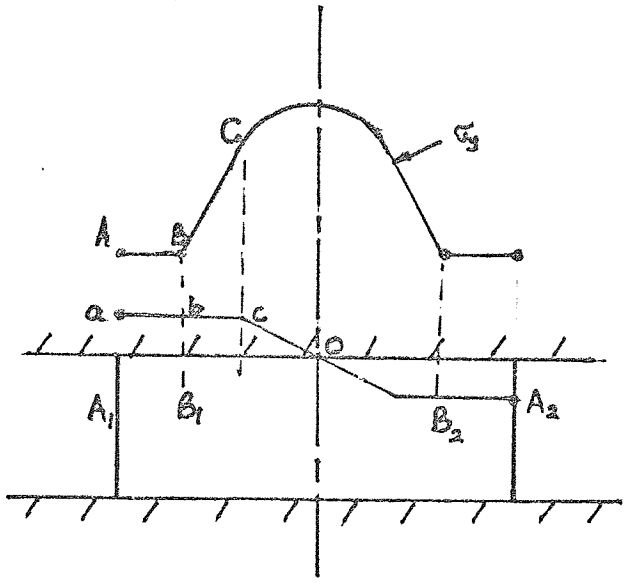

Fig. 3.4

Table 3.1 below shows some of the normal stress equations derived by Sokolovskii.

TABLE 3.1

Coefficient Of Friction, μ	Ratio (a/h)	Specific Pressure (q)
0	Any	$q = \frac{2}{\sqrt{3}} \sigma_o$
0.15	$1 < a/h < 1.7$	$q = \frac{2}{\sqrt{3}} \sigma_o \left[1 + 0.2\ (a/h - 1)\right]$
	$a/h > 1.7$	$q = \frac{2}{\sqrt{3}} \sigma_o \left[0.66 + 0.15\ a/h + 0.41\ \frac{h}{a}\right]$
0.25	$1 < a/h < 1.6$	$q = \frac{2}{\sqrt{3}} \sigma_o \left[1 + 0.39\ (a/h - 1)\right]$
	$a/h > 1.6$	$q = \frac{2}{\sqrt{3}} \sigma_o \left[0.43 + 0.25\ a/h + 0.64\ \frac{h}{a}\right]$
0.30	$1 < a/h < 1.5$	$q = \frac{2}{\sqrt{3}} \sigma_o \left[1 + 0.52\ (a/h - 1)\right]$
	$a/h > 1.5$	$q = \frac{2}{\sqrt{3}} \sigma_o \left[0.51 + 0.25\ a/h + 0.57\ \frac{h}{a}\right]$
0.40	$1 < a/h < 1.4$	$q = \frac{2}{\sqrt{3}} \sigma_o \left[1 + 0.71\ (a/h - 1)\right]$
	$a/h > 1.4$	$q = \frac{2}{\sqrt{3}} \sigma_o \left[0.58 + 0.25\ a/h + 0.5\ \frac{h}{a}\right]$

Fig (3.5) shows the relationship between normal pressure and a/h ratio for different friction coefficients.

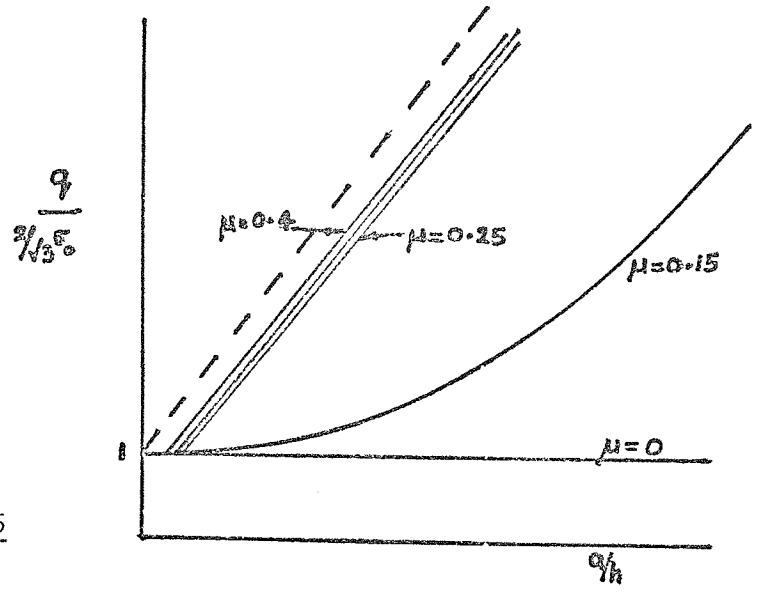

Fig. 3.5

Friction effect on specific pressure is negligible when the coefficient of friction μ is greater than 0.25 . Thereafter, the specific pressure tends to a limiting value given by

$$q = \frac{2}{\sqrt{3}} \sigma_o \left[0.75 + 0.25\ a/h\right] \qquad \ldots\ldots\ldots (3.16)$$

Unksov's upset forging tests [11] have yielded similar results, and have also shown that three friction conditions exist on the surfaces of compressed metal. Billets whose width-to-height ratios a/h exceed a value of six show slip, drag and stick zones Fig (3.6); those with $6 > a/h > 2$, show slip and stick zones Fig (3.7) while those with $1 < a/h < 2$, stick to the platens Fig (3.8).

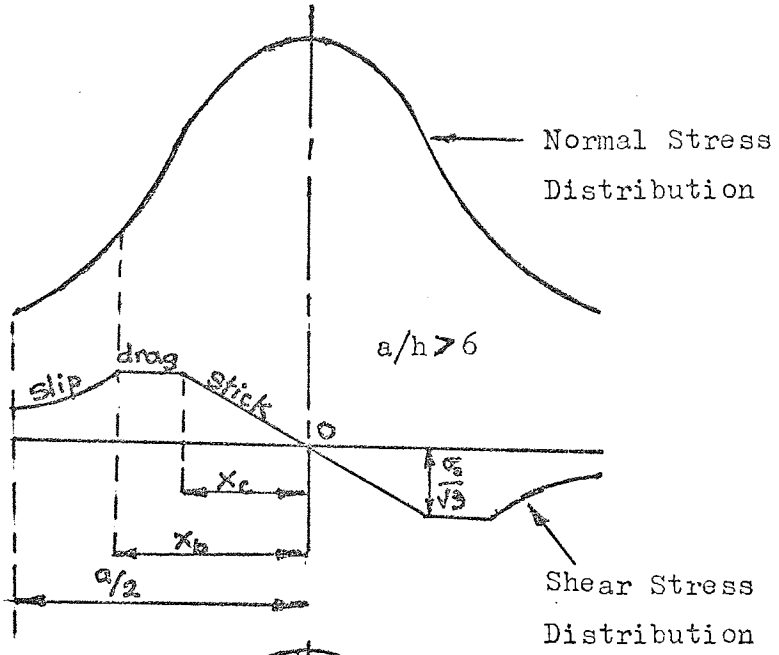

Fig. 3.6

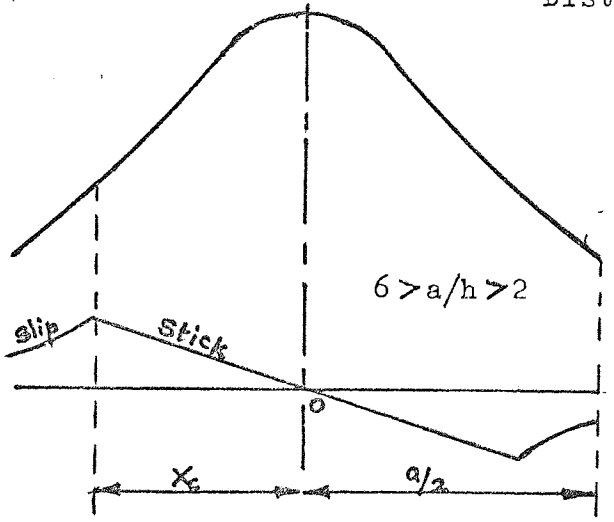

Fig. 3.7

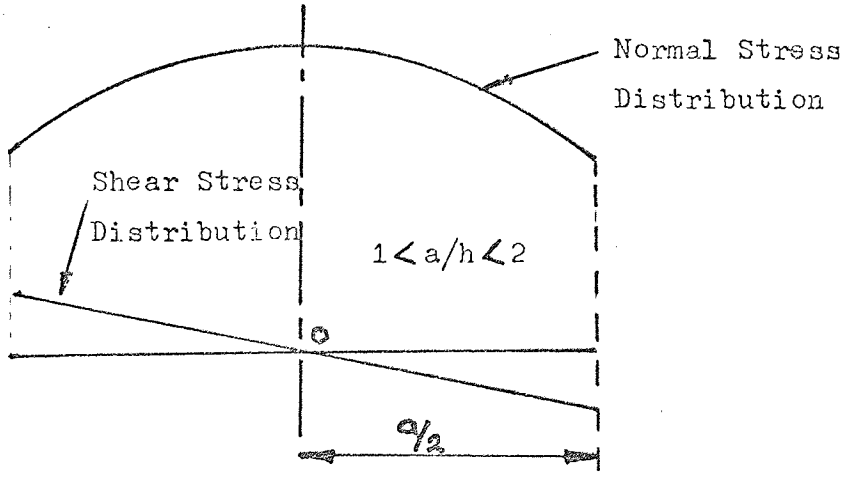

Fig. 3.8

Unksov's tests also showed that the shear stress increases with normal stress in the slip zone and is independent of it in the drag and stick zones. The shear stress, τ, in the slip, drag and stick zones are expressed as $\tau = \pm \mu \sigma_y$, $\tau = \pm \frac{\sigma_o}{\sqrt{3}}$ and $\tau = \pm \frac{\sigma_o}{\sqrt{3}} \cdot \frac{x}{x_c}$ respectively

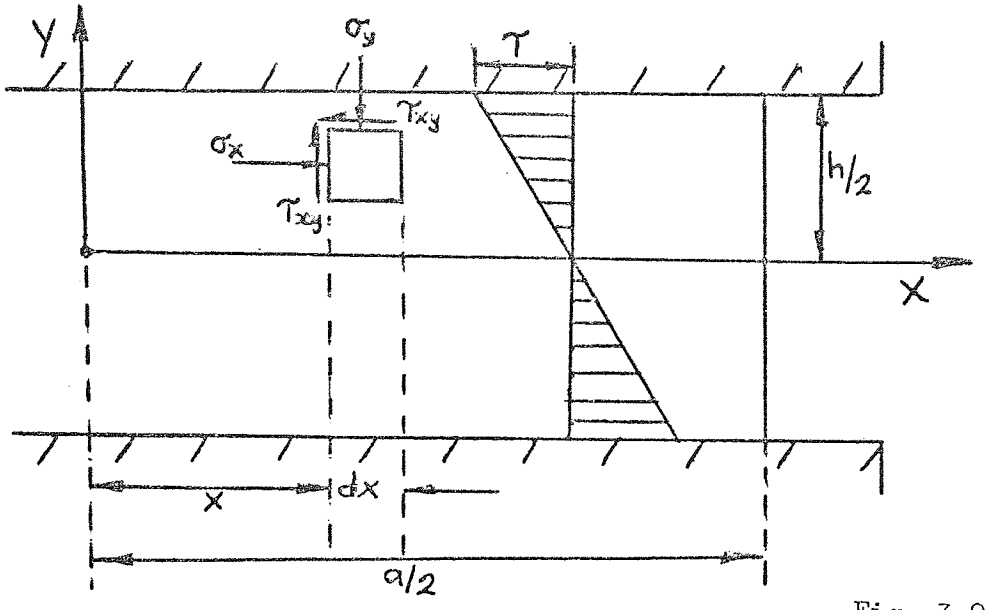

Fig. 3.9

Assuming that the lateral flow stress, σ_x, is independent of y, the equilibrium equation for the element shown in Fig (3.9) is given by

$$\frac{d\sigma_x}{dx} + \frac{2\tau}{h} = 0 \qquad \ldots\ldots\ldots (3.17)$$

Unksov showed that $d\sigma_x = d\sigma_y$ in the areas of the contact surface where τ, is independent of σ_x and σ_y and integrated equation (3.17) with boundary conditions relevant to the three stress distributions.

For $a/h > Mo$ where $Mo = a/h\Big|_{\lim} > 2(1 + \phi)$, the normal compressive stress q is given by

$$q = \frac{2\sigma_o}{\sqrt{3}} \frac{h}{\mu a} \left\{ \left(\tfrac{1}{2}\mu - 1\right) + \left(\frac{a}{2h} - \phi - 1\right) \left[1 + \mu \left(\frac{a}{2h} - \phi - 1\right)\right] + 2\mu \left[\left(\tfrac{1}{2}\mu + \tfrac{1}{3}\right) + \left(\frac{a}{2h} - \phi - 1\right)\right]\right\}$$

$$\text{where } \phi = -\frac{\ln 2\mu}{2\mu} \qquad \ldots\ldots\ldots (3.18)$$

while for $Mo > a/h > 2$,

$$q = \frac{2\sigma_o}{\sqrt{3}} \frac{h}{\mu a} \left[\left(1 + 2\mu + \frac{4}{3}\mu^2\right) \exp \frac{2\mu}{h} (a/2 - h) - 1\right] \qquad \ldots\ldots\ldots (3.19)$$

and

$$q = \frac{2\sigma_o}{\sqrt{3}} \left[1 + \frac{\mu a}{3h}\right] \qquad \ldots\ldots\ldots (3.20)$$

when $1 \leq a/h \leq 2$.

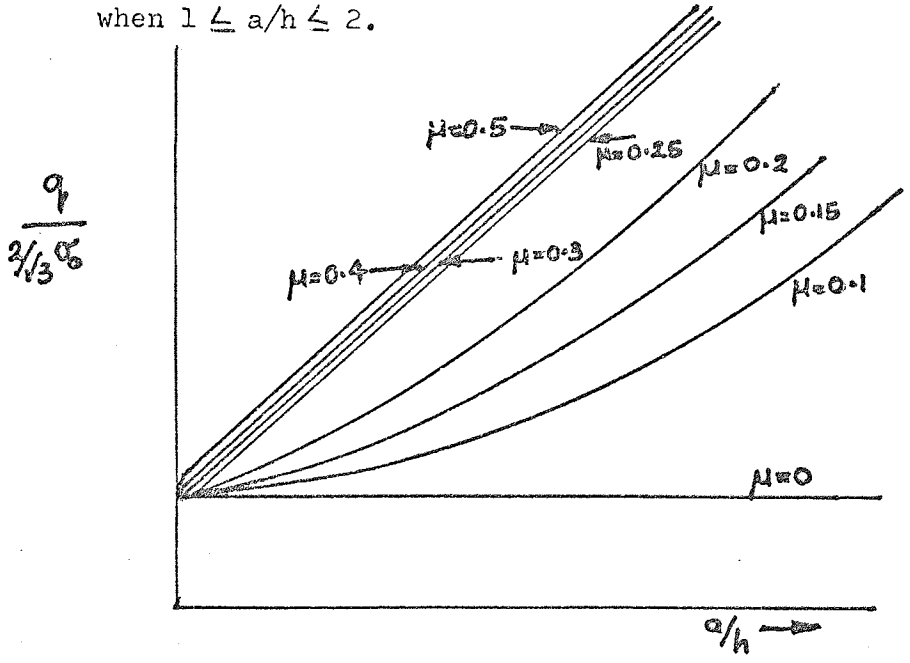

Fig. 3.10

Fig (3.10) shows the relationship between the specific pressures and the ratios a/h and μ. As in Sokolovskii's plots, friction effect on the pressures is negligible for $\mu > 0.25$.

CLOSED DIE FORGING

Pomp, Münker and Lueg are credited in the literature, as the first to analyse die filling and force development in closed die forging.

Unksov's later analyses are based on two assumptions that the metal deforming at the last moment of plane strain forging is a parallelopiped and that the shear stress τ equals $\frac{\sigma_o}{\sqrt{3}}$ at its upper and lower boundaries. The yield stress σ'_o of the metal in the flash is related to that of the body of the forging by

$$\sigma'_o = m\sigma_o \qquad \ldots\ldots\ldots (3.21)$$

where $m > 1$.

And Coulomb's friction is assumed in the flash area.

Thus he deduced that the load P_c for axi-symmetric forging Fig (3.11), is given by

$$P_c = \sigma_o \left[\frac{\pi d^2}{4} Z \left(m \frac{2\mu s}{h_f} + \frac{d}{3\sqrt{3}\, h_k} \right) + \frac{\pi}{4} (D^2 - d^2)\, m \left(1 + \frac{\mu s}{h_f}\right) \right]$$

$\ldots\ldots\ldots (3.22)$

The corresponding load P_p for plane strain compression is given by

$$P_p = \frac{2}{\sqrt{3}} \sigma_o \left[abZ \left(m \frac{2\mu s}{h_f} + \frac{a}{4h_k} \right) + 2bs \left(1 + \frac{\mu s}{h_f}\right) \right]$$

$\ldots\ldots\ldots (3.23)$

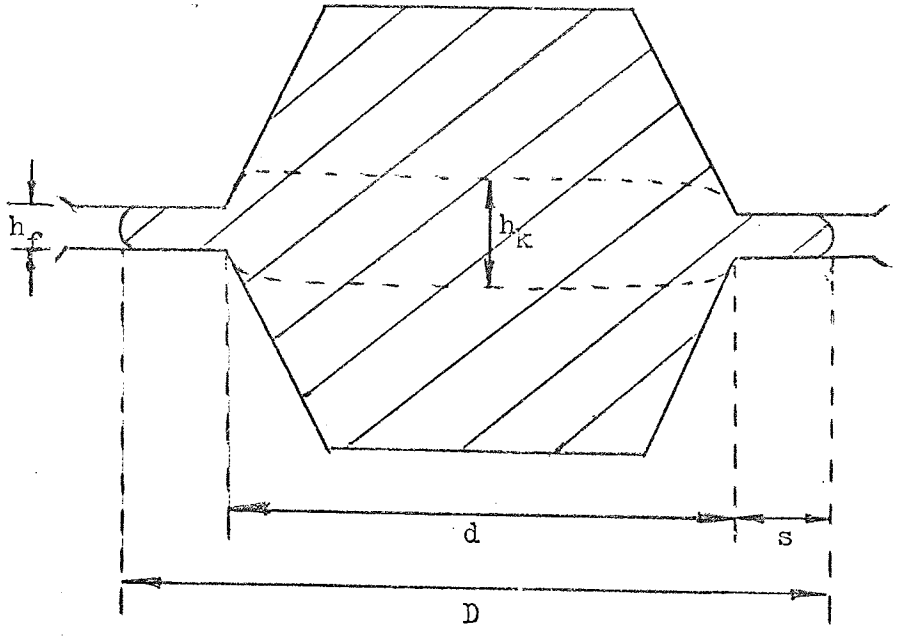

Fig 3.11

ab is the area at the parting line of the forging and h_k is the height of the metal deforming during the final moments of the forging operation. The factor, Z, accounts for die complexity and the unevenness of stress and cooling states of the forging.

Unksov's equations are derived partly from experimental stress distributions and partly from plasticity theories which are very approximate. The introduction of Z is logical but its determination is difficult. Unksov has not suggested how to measure the height h_k.

An approximation that $h_k = h_f$ gives [11] values higher than those obtained in practice. But the substitution of h_k values determined by Gubkin, give reasonable load figures.

Dietrich and Ansel have calculated die forging load by analysing the local forming process in each area of the forging.

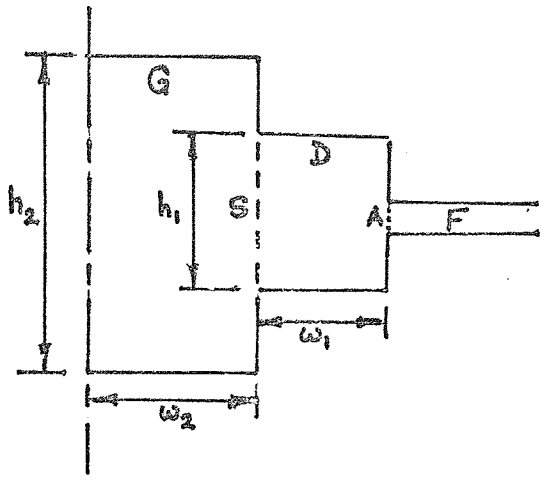

Fig. 3.12

Fig (3.12) shows half the cavity into which a billet is assumed to have been forged. The lateral flow stress σ_x is expressed as

$$\sigma_x = \sigma_o \left[\exp (2\mu x/h) - 1\right] + \sigma_b \exp (2\mu x/h) \qquad \ldots\ldots\ldots (3.24)$$

where σ_b is the back pressure from flash area F on surface A.

The pressure σ_d in section D, distance, x, from surface A is given by

$$\sigma_d = (\sigma_o + \sigma_b) \exp (2\mu x/h) \qquad \ldots\ldots\ldots (3.25)$$

and the total force Q acting on section D is

$$Q = 2\int_0^w \sigma_d dA = \frac{Ah}{2\mu w}(\sigma_o + \sigma_b) \exp(2\mu w/h) - 1 \qquad \ldots\ldots\ldots (3.26)$$

The back pressure σ_b is the sum of pressure σ_b' produced by friction in the adjoining section of lower pressure and the pressure σ_b'' necessary for extrusion from section D to section F.

The back pressure acting on section G due to friction in section D is σ_x at surface S. Thus,

$$\sigma_b' = \sigma_o'' \exp(2\mu w_2/h_2) - 1 + \sigma_{b_2} \exp(2\mu w_2/h_2) \qquad \ldots\ldots\ldots (3.27)$$

where σ_o'' is the deformation resistance in section G.

Dietrich and Ansel then modified Siebel's equation for frictionless extrusion with Sachs' idea that the average deformation resistance is larger in forging than in other processes by a factor of 2 and obtained

$$\sigma_b'' = 2(\sigma_o' + \sigma_o'') \ln \frac{h_1}{h_2} \qquad \ldots\ldots\ldots (3.28)$$

from (3.27) and (3.28)

$$\sigma_b = \sigma_{b_2} \exp(2\mu w_2/h_2) + \sigma_o'' \exp(2\mu w_2/h_2) - (\sigma_o' + \sigma_o'') \ln \frac{h_1}{h_2} \qquad \ldots\ldots\ldots (3.29)$$

The formulae are easy to derive. They account for temperature variations from one part of the forging to the other. But they are difficult to apply and seem only applicable to stepped parts similar to that shown in Fig (3.12). The various yield stresses

necessary for a complete solution are also difficult to determine. Mean values may, however, suffice for rough load estimation.

In addition to his simple upsetting model, Lippman[6] has proposed a forging theory applicable to any forged shape. The method deduces forging pressure from force equilibrium equations and boundary conditions describing the profiles of the forged component.

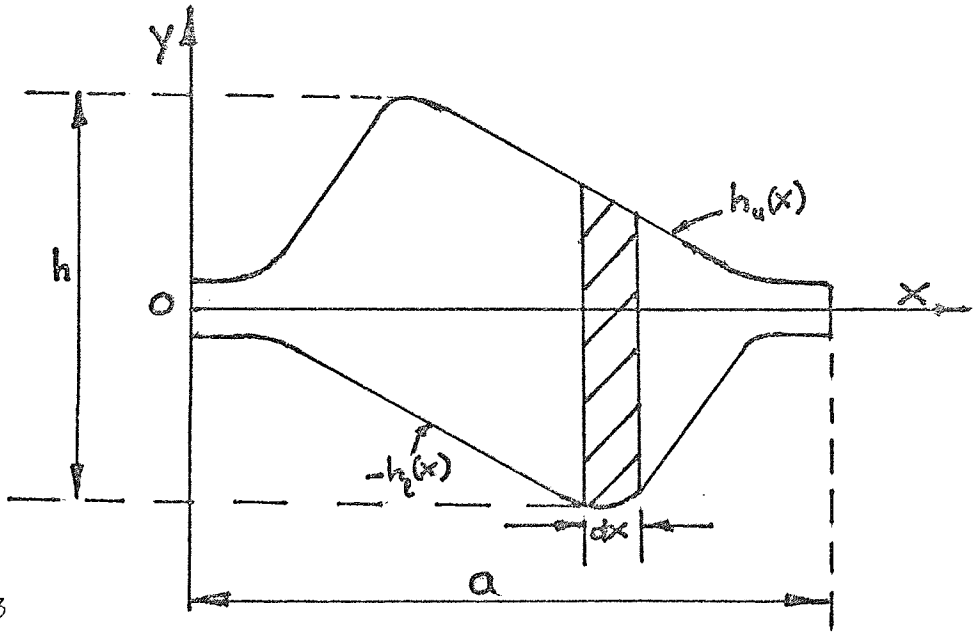

Fig. 3.13

Fig (3.13) shows a hypothetical forging whose boundary equations and their derivatives are assumed known. It is also assumed (a) that the slopes of the boundary curves are small at all points, (b) that the forged material does not stick to the dies, (c) that no material flows at section $x = x_o$ and (d) that plane strain conditions prevail during the compression.

Thus, from equilibrium equations the axial forging pressure distribution σ_y is given as

$$\sigma_y = \exp \int_x^a \frac{h' + f}{h} \left\{ \sigma_o - \int_x^a \frac{(h\sigma_o)'}{h} \left[\exp - \int_x^a \frac{h' + f}{h} \, dx \right] dx \right\} \quad \ldots\ldots\ldots (3.30)$$

where $f = \dfrac{2\mu\,(1 - h_u' h_l') - (1 - \mu^2)\, h'}{(1 + \mu h_u')\,(1 + \mu h_l')}$, h is the maximum height of the forging and $h' = \dfrac{dh}{dx}$, $h_u' = \dfrac{dh_u(x)}{dx}$ and $h_l' = \dfrac{dh_l(x)}{dx}$

The forging load Q is thus given by

$$Q = \int^A \sigma_y \, dA \quad \ldots\ldots\ldots (3.31)$$

where dA is an element of Area A.

This model may well be an accurate one but its complex nature and the assumptions made in deriving it make it difficult to check experimentally. It is also difficult to apply.

The use of profile equations in the derivation assumes a knowledge of what will, more often than not, prove to be complex equations. It is doubtful if the degree of accuracy expected from this model can outweigh the mathematical rigour involved. The main asset of Lippmann's theory seems to be its applicability to any forging at all, providing its profile equations can be determined.

Meanwhile, simpler theories have been proposed.

In their own analyses, Kobayashi et al[12] assumed that the metal deforming in the last moments of closed die forging is a disc of which the flash is part Fig (3.14).

Metal shear below the rigid metal of the forging and sliding between the flash metal and the land are also assumed during the finish forging operation.

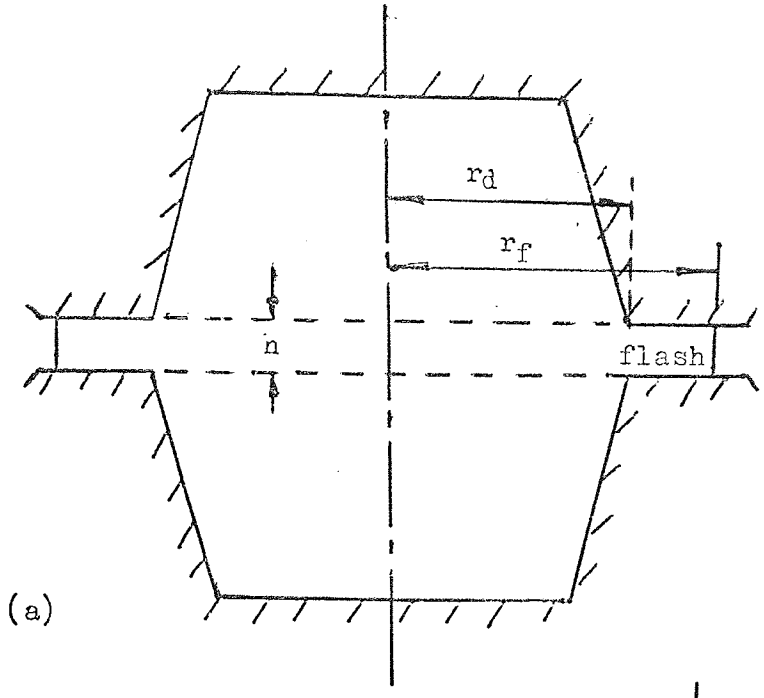

Fig 3.14

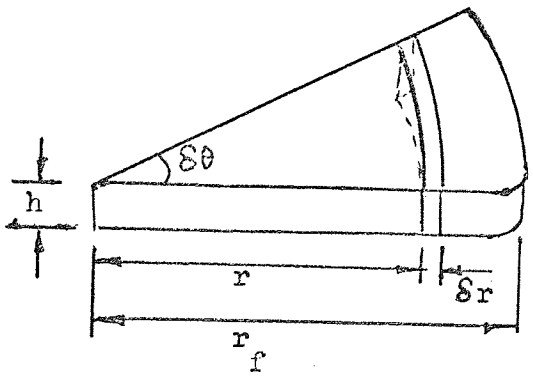

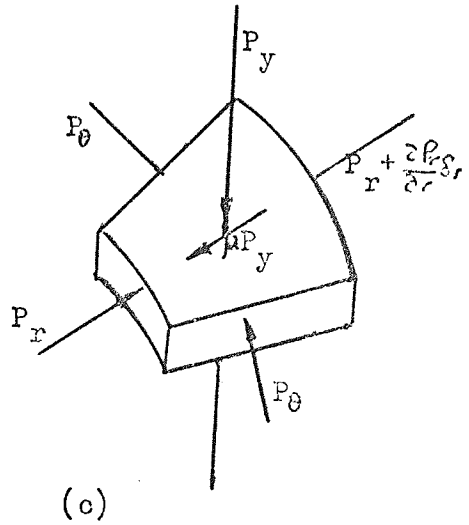

It is then deduced from the equation of radial equilibrium of an element of the disc to which deformation is assumed confined and a yield equation based on Von Mises criterion that,

$$\frac{d\sigma_r}{\sigma_r - \bar{\sigma}_o} = -\frac{2\mu dr}{h} \qquad \ldots\ldots\ldots (3.32)$$

where $\bar{\sigma}_o$ is the effective stress.

By assuming further that shear occurs on the asperities of the disc on which the normal stress σ_y is a hydrostatic pressure, i.e. $\sigma_y = \sigma_r = \sigma_c$ and that the effective stress $\bar{\sigma}_o$ is not a function of specimen radius r, the normal compression pressure q is deduced from equation (3.32) as

$$\frac{q}{\bar{\sigma}_o} = \frac{1}{2}\left[\left(\frac{h}{\mu r_f}\right)^2\left\{\left(\frac{2\mu r_d}{h}+1\right)e^{\frac{2\mu(r_f - r_d)}{h}} - \frac{2\mu r_f}{h} - 1\right\} + \left(\frac{r_d}{r_f}\right)^2\left\{e^{\frac{2\mu(r_f - r_d)}{h}} + \frac{2\sqrt{3}}{9}\frac{r_d}{h}\right\}\right]$$

$\ldots\ldots\ldots (3.33)$

Fig (3.15) shows a typical plot of $\frac{q}{\bar{\sigma}_o}$ against $\frac{h}{h_o}$ for various values of the coefficient of friction μ and one value of $\frac{r_d}{h_o}$.

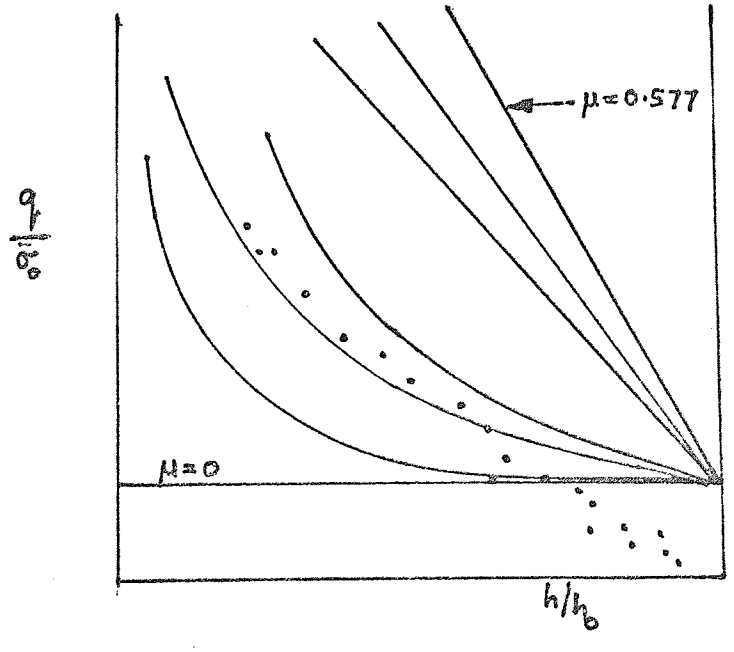

Fig. 3.15

The experimental points are those obtained during press forging tests on 1 15/16" diameter billets of aluminium and lead.

Kobayashi et al blame the assumption that shear occurs only in a thin surface layer of the flash for the discrepancy between experimental results and their theoretical predictions. The assumption that deformation during the later stages of the forging operation is confined to a fictitious disc of which the flash is part is equally likely to introduce an error, since metal flow experiments[11,13,14] have shown that the metal deforming in the final moments of the forging operation is nearly lenticular. Further errors are likely from the assumption that effective stress is independent of specimen radius, r.

From the foregoing, the importance of the coefficient of friction, μ, in forging theories is apparent. For process design, the value of μ has to be known before the operation.

Friction in simple upsetting has been reasonably measured with a push pin device fitted with strain gauges. But there is, as yet, no method for measuring its exact value in closed die forging dies. However, a hope seems offered by a fairly accurate method for its determination[15] during plastic deformation between rigid tools.

Realising the futility of predictions without an accurate knowledge of the coefficient of friction, an attempt to rid forging pressure equations of it has been made by Lippmann and Stoter[16]. They wrote a functional equation for local compression stress in terms of the coefficient of friction μ, the height h of the forging and the

lateral displacement, x, viz

$$\sigma_y = \sigma_o \, f(\mu \, x/h)$$

where by $\sigma_y = \sigma_o \left[1 + A(x/h) + B(x/h)^2 + C(x/h)^4 \right]$

A, B and C were determined experimentally by measuring σ_y for various values of x/h when upsetting Pantal 19 (AlMgSi) samples at room temperature.

Simple Upsetting

Figs (3.16), (3.17), (3.18), (3.19), (3.20) and (3.21) suggest that the normal stress developed when upsetting a specimen varies directly as its width - to - height ratio. Thus all the models conform with the established fact that thinner specimens require more pressure to forge them. The wider the contact area between tool and workpiece, the greater the friction resistance. The higher, therefore, will be the upsetting pressure.

Plain Strain Upsetting

Figs (3.16), (3.17) and (3.18) show the variations of predicted normal stress with the billet width - to - height ratios for three values (0.15, 0.30 and 0.50) of the coefficient of friction μ.

Geleji and Lippmann predict the highest values.

For μ = 0.15, Geleji and Lippmann's pressures are higher than the nearest to them (Siebel's) by as much as 60% for the range of width - to - height ratios considered. For higher coefficients of friction,

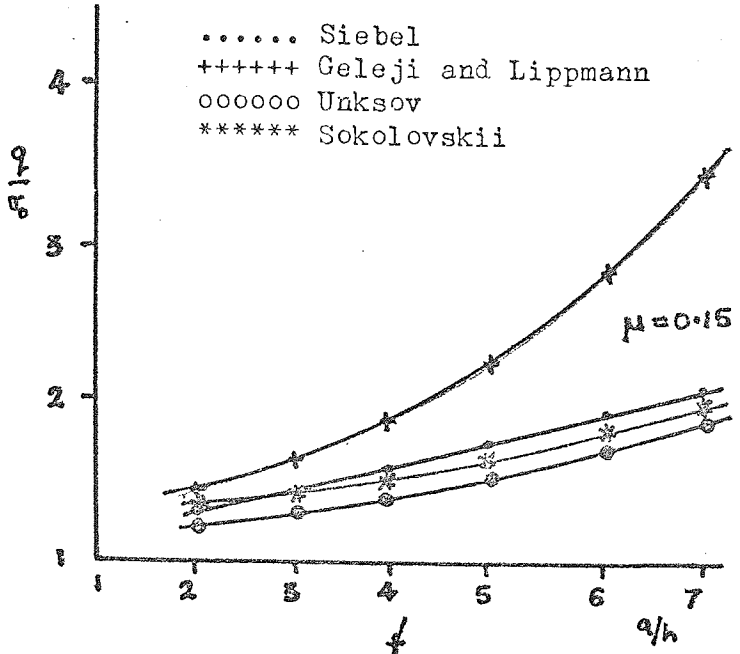

Fig.3.16

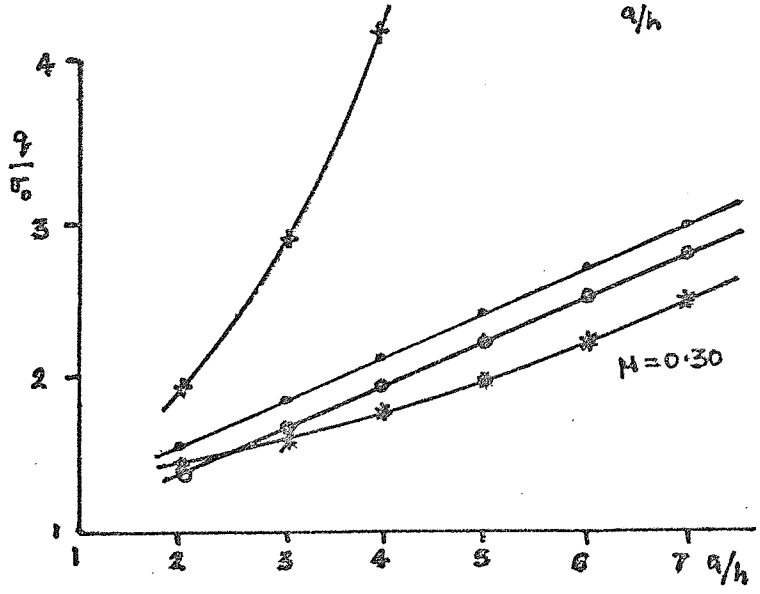

Fig.3.17

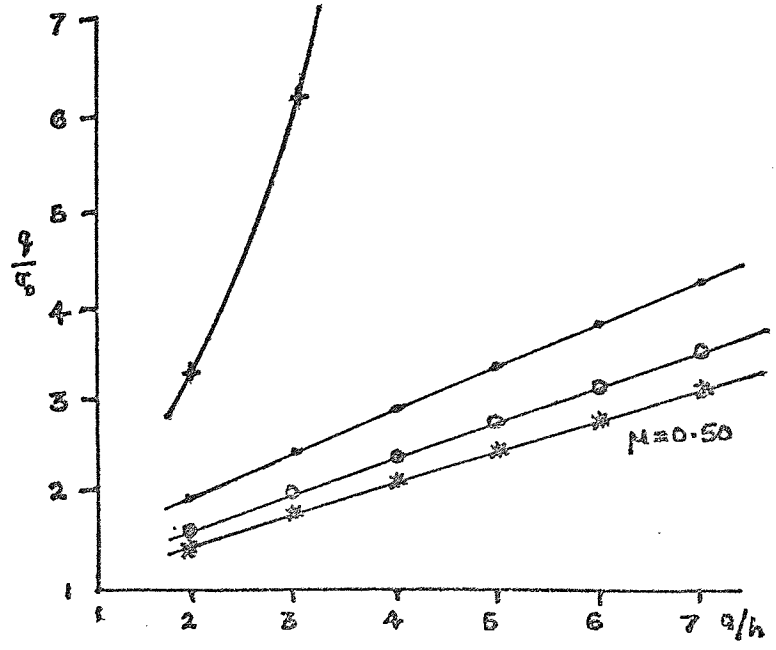

Fig.3.18

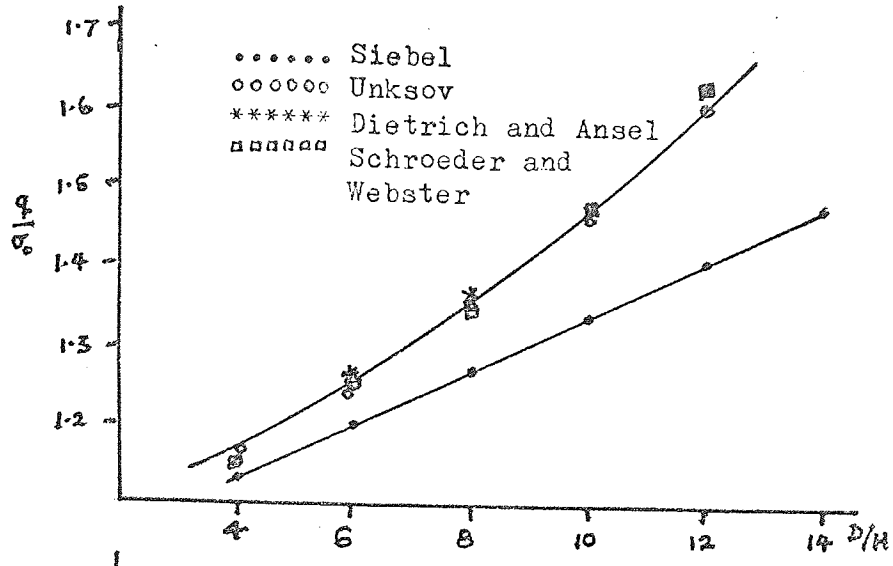

Fig.3.19

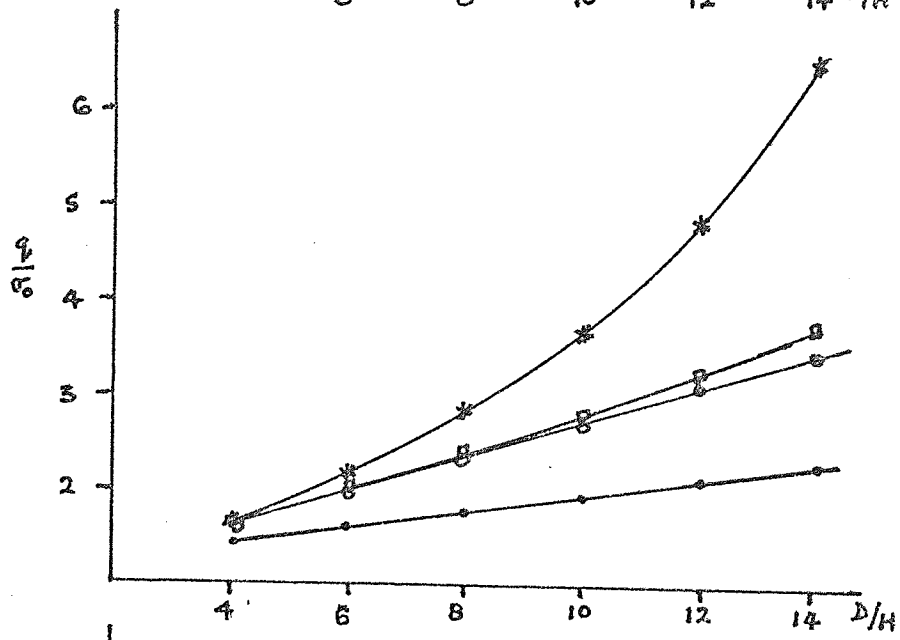

Fig.3.20

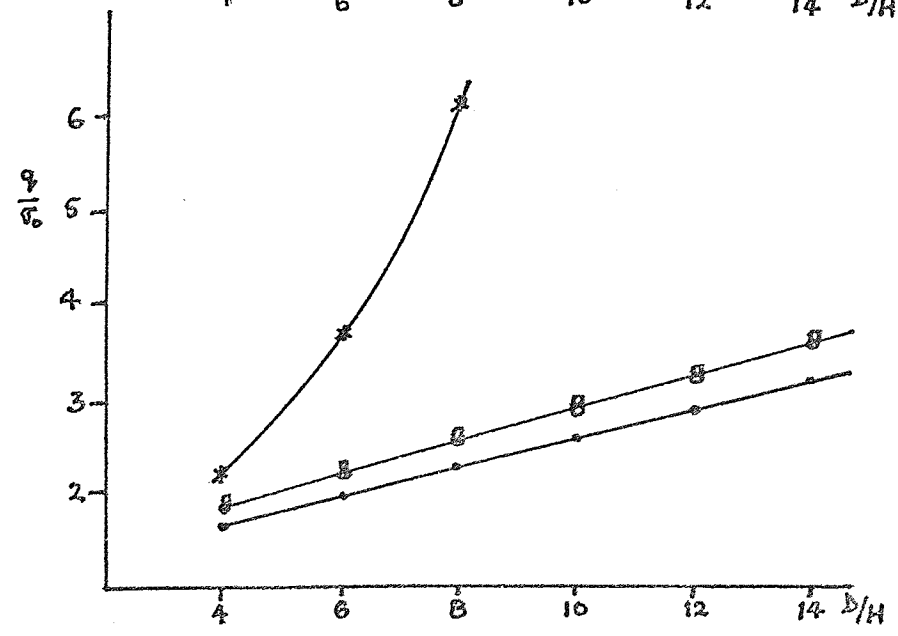

Fig.3.21

their values are very much incompatible with other theories. This is largely due to the assumption that Coulomb's friction occurs on the faces of every compressed specimen. At least two friction conditions - sticking and slipping - occur when upsetting specimens whose width - to - height ratios are greater than 2.

In his analysis, Siebel assumed that friction stress is a function of the resistance to deformation of the forged metal. This can only be true to a small extent. It has been proved that friction is a function of the normal stress. The wider the spread of the compressed metal, the higher the friction resistance. But the amount of spread is jointly determined by the force applied on the piece and the resistance to deformation of the metal. It will be difficult, therefore, to justify that friction stress is mainly a function of the yield stress of the metal - an assumption responsible for Siebel's fairly high pressure values when $\mu = 0.50$. Despite these limitations, investigators favour Siebel's equations for pressure estimations because it is simple to apply and his values are moderately high.

When $\mu = 0.15$ and $\mu = 0.30$, Sokolovskii, Siebel and Unksov predict similar pressures. At $\mu = 0.50$, only Sokolovskii and Unksov's models agree. The agreement between Unksov and Sokolovskii's models is, however, not totally surprising in spite of their different methods of derivation.

They made identical assumptions and both recognised and accounted for two friction zones - slip and stick zones - on the surfaces of specimens considered. Siebel's pressures are probably

slightly higher than Unksov's and Sokolovskii's because of differences in his friction concepts and theirs.

Cylindrical Upsetting

Figs (3.19), (3.20) and (3.21) are the plots of predicted compression pressures against billet diameter - to - height ratios. While Dietrich and Ansel predict the highest pressure values, Siebel's figures are the lowest. Dietrich and Ansel's figures are probably high because of the assumption that only slipping friction prevails on the surfaces of compressed metal.

For all values of the friction coefficient, Unksov and Schroeder and Webster predict identical normal compression pressures. They considered similar friction conditions on the surfaces of the specimens and made identical assumptions on metal plasticity.

Closed Die Forging

Unlike in simple upsetting, there is no common basis for comparing all the closed die forging theories reviewed.

Lippmann's model depends on the profile equations of the boundaries of the forgings. But the profiles of most real forgings are complex and the derivation of their equations is laborious. The use of this model for process design thus depends on the ease of deriving the profile equations. The computer may help in the application of the model to industrial situations.

In contrast, Kobayashi et al's model is simple and easy to apply. But their theory does not seem to agree well with experimental

results. This discrepancy might have arisen from the assumption that deformation in the last moments of the forging operation occurs in a fictitious disc of which the flash is part. Forging experiments have shown[11,13,14,17] that this is only approximately true.

A further source of error is the assumption that the effective stress is not a function of of specimen radius r. This is difficult to justify since effective stress is a function of effective strain which is ,in turn , a function of the specimen radius.

Dietrich and Ansel have exploited the die filling mechanism in deriving their own equation for forging load determination. The model is difficult to use but the consideration of the extrusion aspect of the filling process helps in understanding the mechanism of die filling.

The use , in the theory , of different yield stress values for various sections of the forging is welcome. Temperature differences have been observed[11,18] between the flash areas and the main bodies of forged components. However, the difficulty of application of the model because of its nature and the introduction of various back pressure terms , which are by no means easy to determine , may not lend it to industrial application.

Unksov , in his own derivations , considered three friction conditions in the die impression and introduced a factor Z to account for die complexity and the un-evenness of stress and cooling states. This factor seems logical but its determination is largely intuitive.

Unksov assumed that the deforming metal in the final stages of forging a circular part is a disc thicker than the flash, but did not suggest a method for measuring its height. Reasonable results are, however, obtained by using the height h obtained [21] by assuming that the shape of the deforming metal is lenticular.

Unksov, like Dietrich and Ansel, also assumed different yield stresses for the flash and the body of the forging. His factor $m > 1$ suggests that the flash is colder than the body of the forging. This, thus, restricts the model to press forging since it has been shown [18] that flash temperature is higher in hammer forging and colder in press forging.

4.1. EQUIPMENT AND PROCEDURE

The forging machine was a K100 type Hordern,Mason and Edwards joint knuckle press. Manufacturer's data are listed in Appendix 1. The press and instruments are shown in plate 1. Plate 2 shows a close-up of the tools which included a standard Hazlewood and Dent four-inch bolster, two mild steel shanks and two tool steel (Bestem) die inserts.

The hardness of the tool steel,as supplied, fell within the hardness range of industrial forging dies. They were, therefore, not heat-treated.The impressions were machined on a lathe and polished to a good finish (about 50 microns). Some of the impressions are shown in Fig 4.1.1.

Load Measuring Instruments

The load measuring instruments included a load cell,a power pack and an ultra-violet recorder.

The load cell (see Fig 4.1.3) was made of EN23T steel because of its high tensile strength and was designed to fit under the lower die insert (see Fig4.1.2) and measure compressive loads of up to 120 tonf. To ensure good fitting and uniform straining of its fibres, its flanges were made as wide as the die insert.

The yield strength of the EN23T steel used was 60 tons per square inch. Using a factor of safety of 3, the maximum allowable stress is 60/3 =20 tons/in^2. Since the maximum load to be withstood is 120 tons, the cell's cross-sectional area should be 120/20 =6.0 square inches.

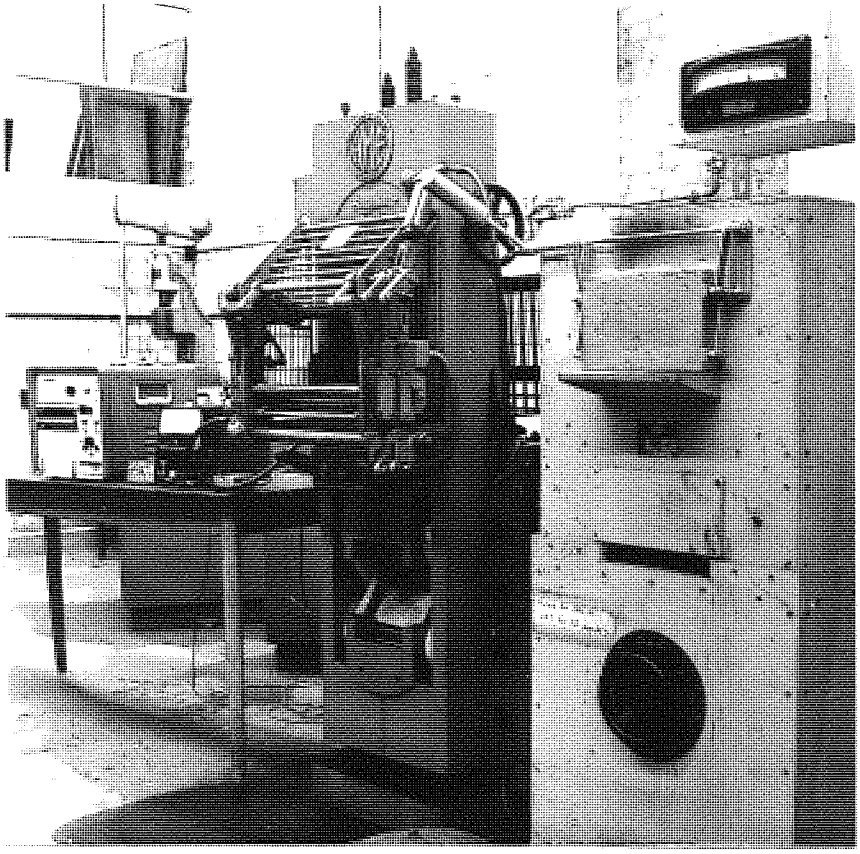

Plate 1 Showing Forging Press, Furnace and Measuring Instruments.

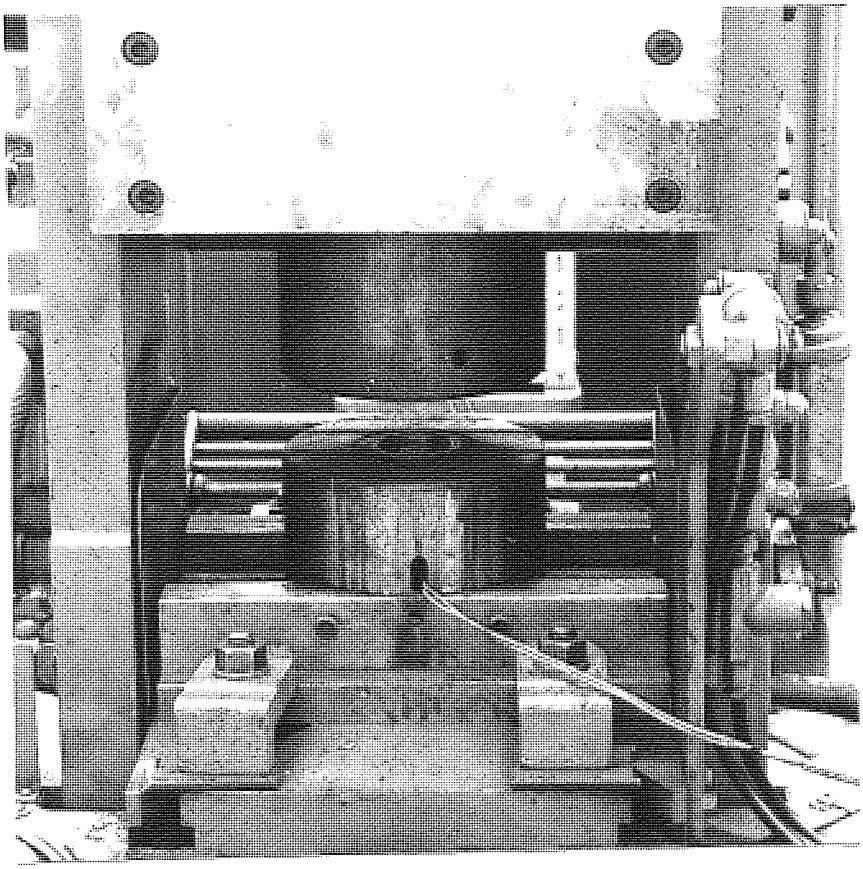

Plate 2 Showing a close-up of Forging tools.

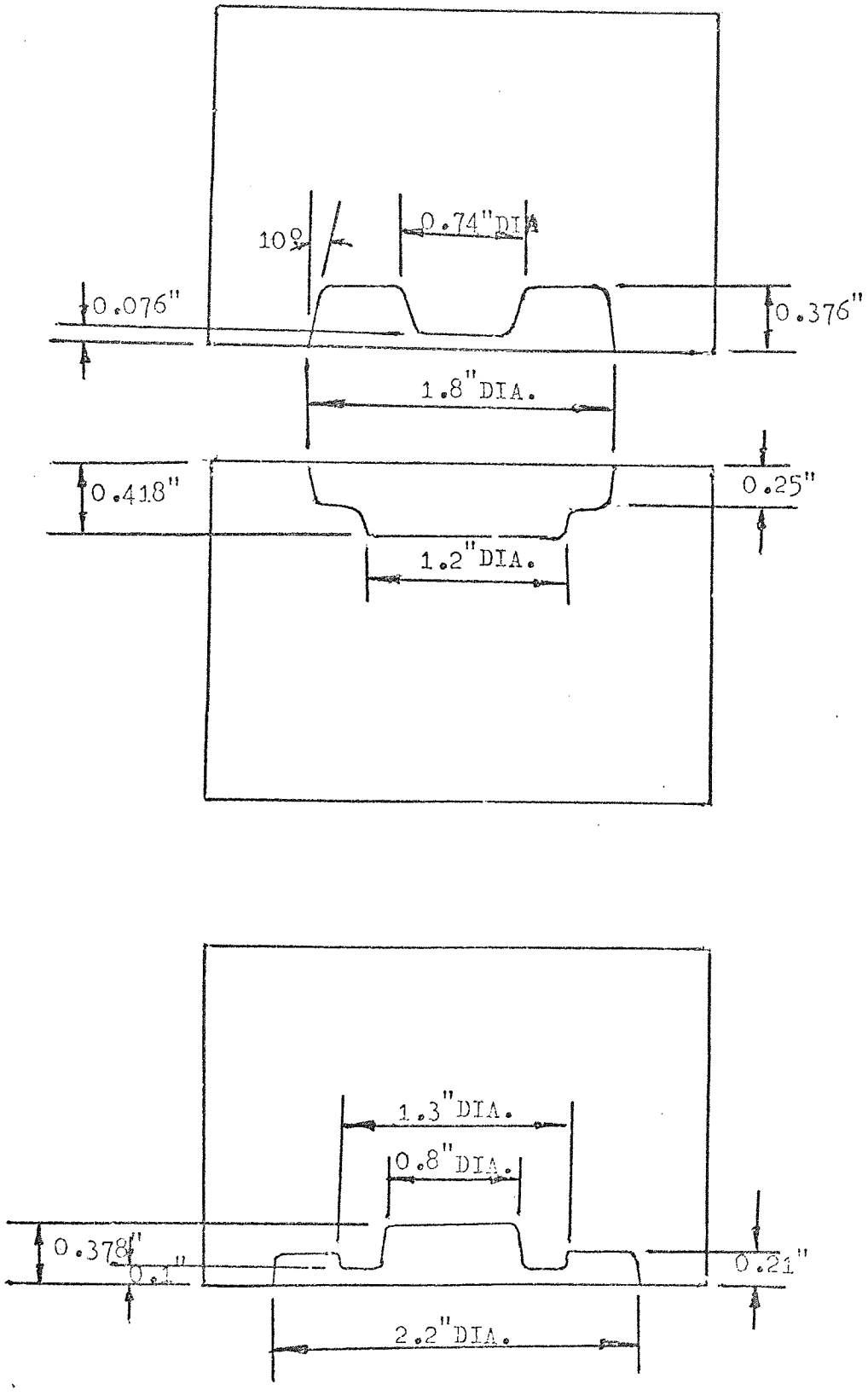

Fig 4.1.1 Showing some of the Forging Die Impressions.

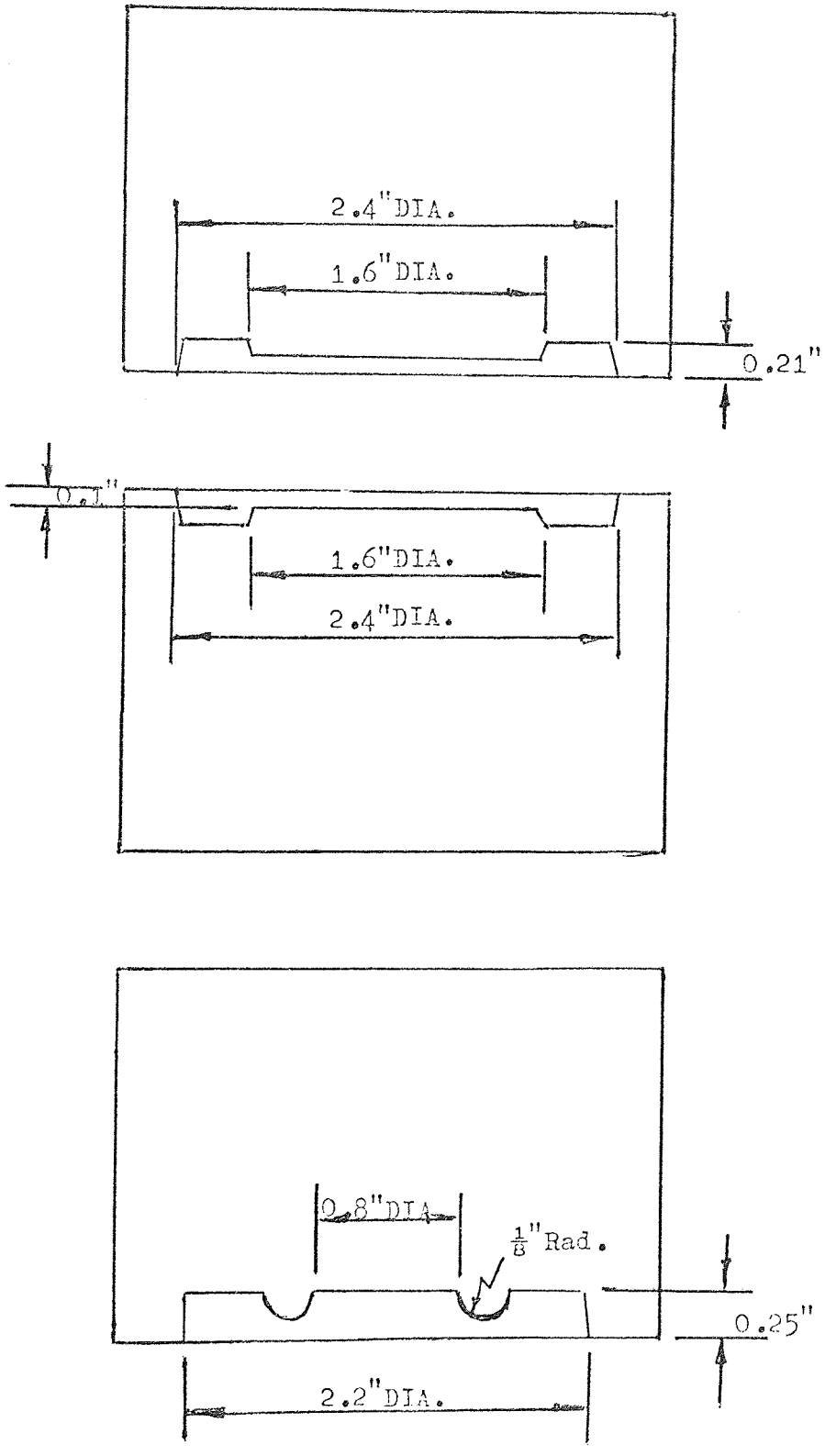

Fig 4.1.1 (contd.)

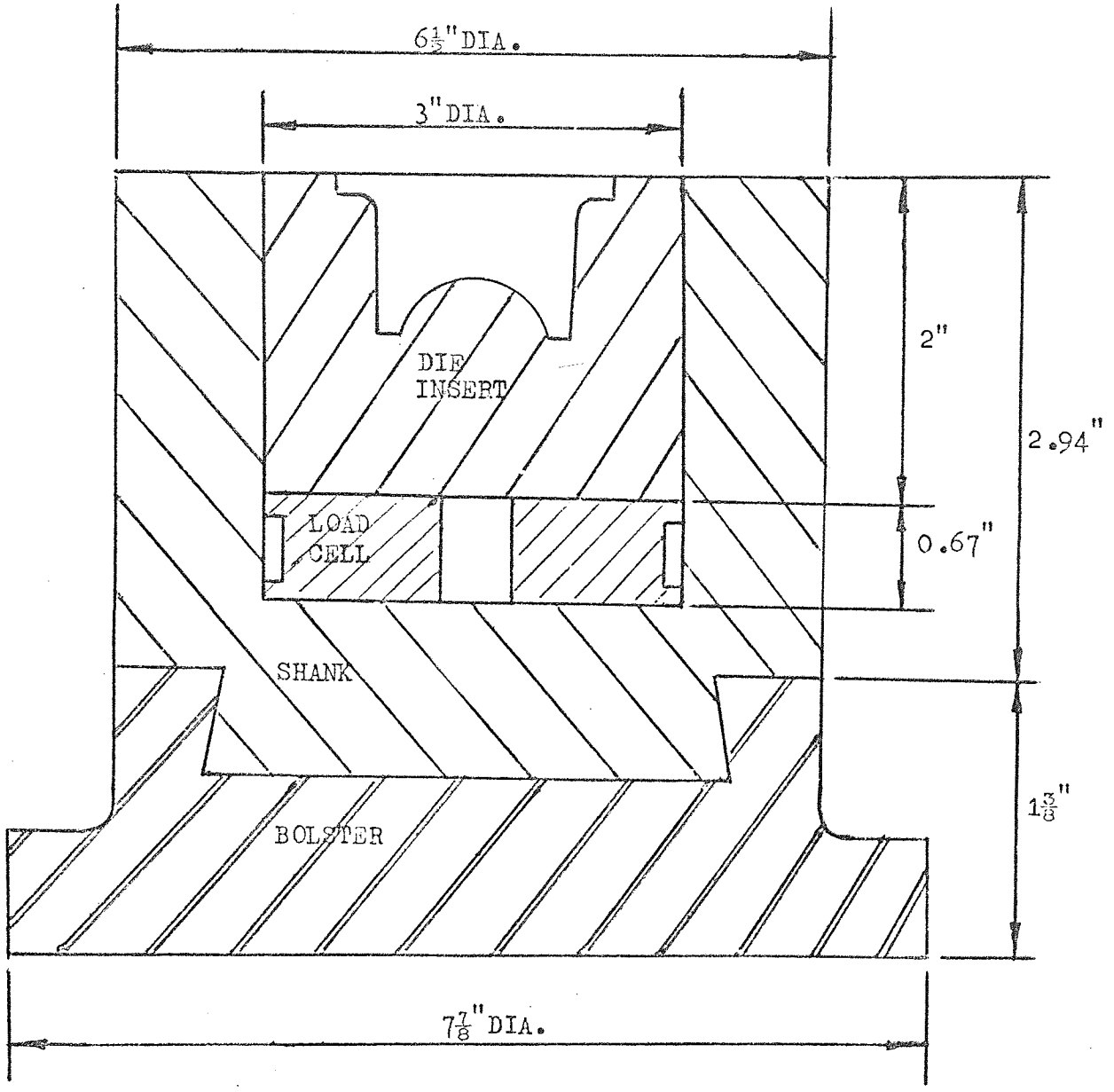

Fig 4.1.2 Showing the positioning of the Load Cell under the lower Die Inserts.

thus $\pi(D^2-d^2)/4 = 6$.

If d= 0.5 inch, D = 2.81 inches.

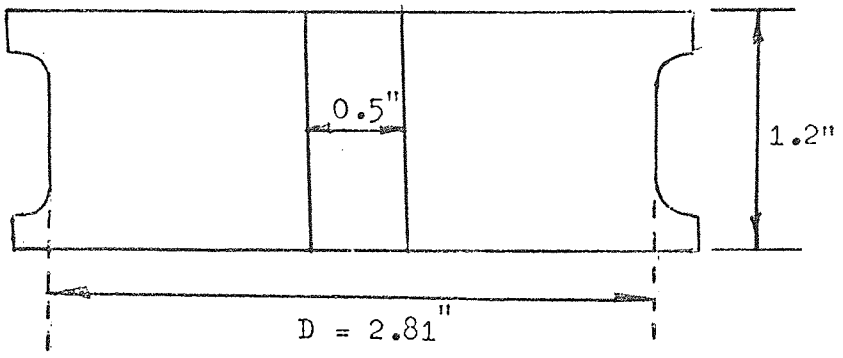

Fig 4.1.3

Expediency was the sole criterion for determining the size of the hole; its main purpose being to ease the withdrawal of die inserts from the bottom shanks.

Eight strain gauges (four active and four dummy) were mounted on the load cell as shown in Fig.4.1.4a and connected in a bridge circuit. One arm of the bridge was connected to the power pack, the other to the ultra-violet recorder Fig.4.1.4b.

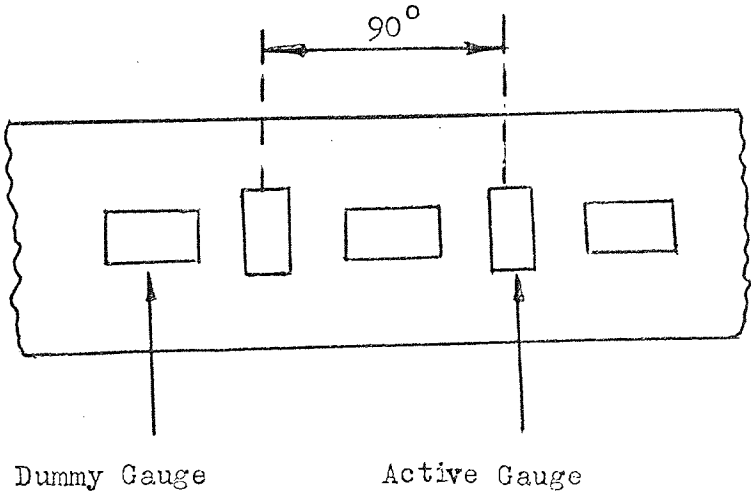

Fig 4.1.4a

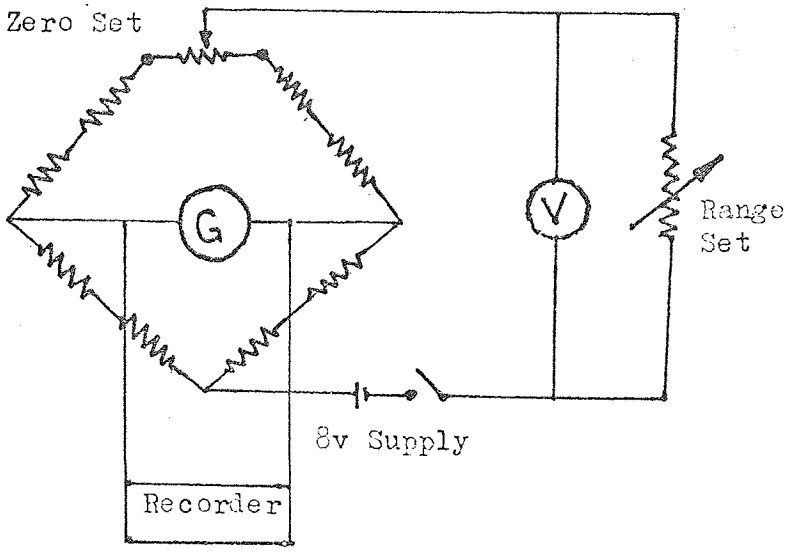

Fig 4.1.4 b

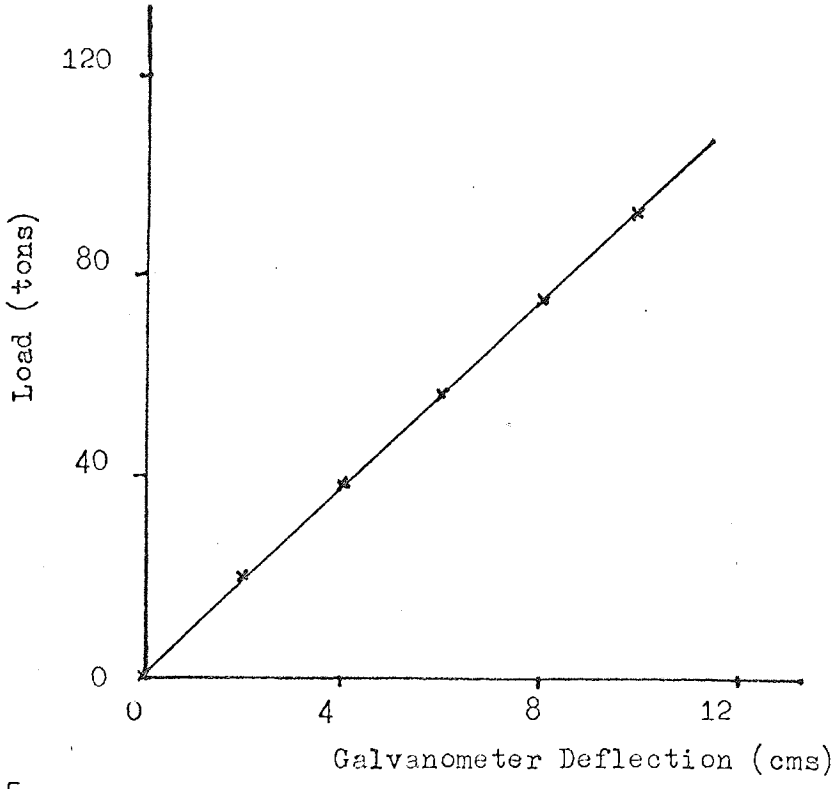

Fig 4.1.5

Calibration of the load cell was on a 300 ton testing machine.Loads of up to 120 tons,in steps of 10 tons,were applied on the load cell and deflections of the recorder galvanometer

were recorded. The transducer stiffness was then deduced from the force-deflection characteristic graph shown in Fig (4.1.5) A compressive load of 9.310 ton caused a centimeter deflection of the recorder galvanometer.

Forging Cycle

Billets were heated in a four-element electric furnace operating at 60% output voltage. Slug temperatures were read off a thermocouple inserted in a dummy billet.

When the preset temperature was reached, the dies were heated to about 120°C and lubricated. Billets were removed from the furnace and descaled on a steel block with a hammer. The tongs used for handling the billets and the steel block on which they were descaled were heated to about 200°C to prevent chilling. The hammer was also heated.

Each billet was then placed centrally (or approximately so) in the dies and forged. Those which could not be positioned well in reasonable time were reheated; so also were those which fell off the steel block during the scale breaking operation.

As a further precaution against errors, forgings which did not fill the dies completely were discarded.

Such situations frequently arose when forging billets into grooved impressions (see Fig 4.1.6).

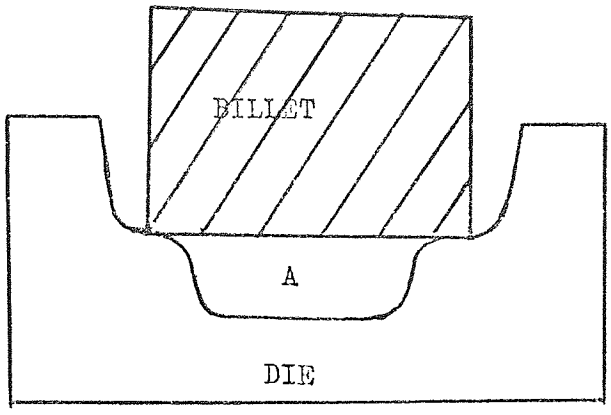

Fig.4.1.6

Air trapped between the job and the tool (position A in Fig 4.1.6) acted as a cushion and prevented metal from completely filling the dies. Furthermore, increased yield strength of the metal flowing into such grooves made die filling more difficult.

Press forging tests[26] on AISI 4340 steel have shown that forging pressure varies with the amount of die fill (Fig4.1.7)

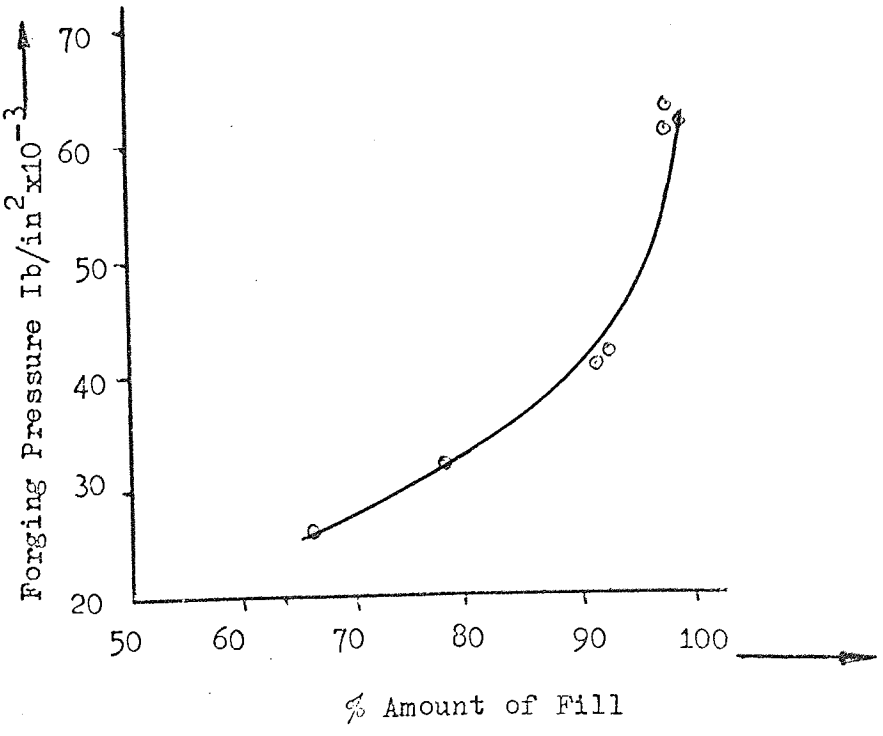

Fig 4.1.7

Parts which did not completely fill the impressions were, therefore, discarded to avoid false readings being recorded for them. The problem of incomplete die filling was subsequently solved by using grooved impressions as top dies. In this way, all corners were filled and perfect forgings were produced.

Two other grades of imperfect forgings were also discarded. These were those whose billets were too small to fill the dies and form adequate flashes, and those whose billets were excessively big that they could not be deformed.

The latter of these two discards occured frequently when forging large billets into the bigger impressions, where deformation loads required exceeded the tonnage capacity of the press and the pressure build up was not enough to cause adequate metal flow.

Experimental Variables

The data obtained from the billets and the forgings can be classified into four groups expressing

(a) the amount of metal and the efficiency of its use

(b) the shape and size of the forging, and

(c) the ease or otherwise of making the forging.

The fourth group is mainly ratios included, in some cases, to check the validity of various claims that they are significant in forging load determination.

(a) Factors Relating To Amount Of Metal

These include the billet and forgingweights, the process

yield and the flash dimensions.

The forging weight is the net weight of the forging after clipping. And the process yield is the ratio of the forging weight to the weight of the billet.

The flash width is the mean width of the flash metal. Flash thicknesses were measured from the unclipped forging.

(b) Factors Relating To Sizes Of Forgings

These are the mean areas at the parting line of the unclipped forgings, the heights of their deepest sections and the depths of those sections nearest in thickness to the flash.

(c) The variable that "measures" the "degree of difficulty" of making a forging is the shape complexity factor.

It is the ratio of the forging weight to the weight of any simple metal shape, cylindrical, cuboidal, cubic, parallelopiped that will completely enclose the outlines of the finished forging.

For example, the shape complexity factor of the round forging shown in Fig (4.1.8) is the weight of the sectioned forging divided by the weight of the enclosing cylinder.

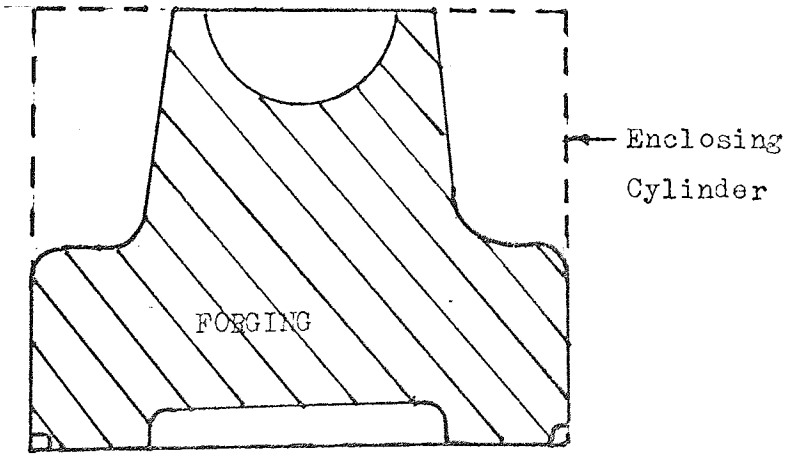

Fig. 4.1.8

Other variables considered include the slug temperature and the lubricant employed. The products of some of the forging ratios were also included to investigate the effects of interactions.

THE EXPERIMENTS

As stated elsewhere , the laboratory experiments were conducted with two main objectives in mind. These were to determine

(a) the influence of forging load in die and process design and

(b) the influence of forging load in press selection.

To achieve these , loads were measured when forging small components differing in weights , height , parting diameters and shape complexity. Various sizes of billets were forged and slug temperatures as well as flash dimensions were varied.

The data thus obtained were analysed statistically, separately for each pair of experimental dies and collectively for all the forgings considered. The individual analyses show the influence of forging load in die and process design while the joint one shows its influence in press capacity selection.

Forging Load in Die and Process Design

It is necessary to study the effects of various job parameters on the loads required in making individual forgings when considering loads in die and process design.

Fig 4.1.9 shows the die sets A and B into which various sizes of billets were forged. The impressions differed in size, shape and height, and their flash lands were parallel.

While Forging "A" was moderate in height, simple in shape and symmetrical about the parting line, "B" was more complex in shape and unsymmetrical about the parting line. The top half of Forging "B" was filled by extrusion.

TABLE 4.1

Billet Diameter (ins)	Billet Height (ins)	Billet Diameter / Billet Height
1.625	0.960	1.694
	0.983	1.655
	1.005	1.617
1.500	1.127	1.331
	1.150	1.271
	1.180	1.025
1.375	1.342	1.025
	1.372	1.003
	1.405	0.980

The Forging Stock

The billets listed in Table 4.1 were sawn and machined from $1\frac{3}{8}$", $1\frac{1}{2}$" and $1\frac{5}{8}$" diameter bars of EN 3B mild steel supplied in the bright drawn condition.

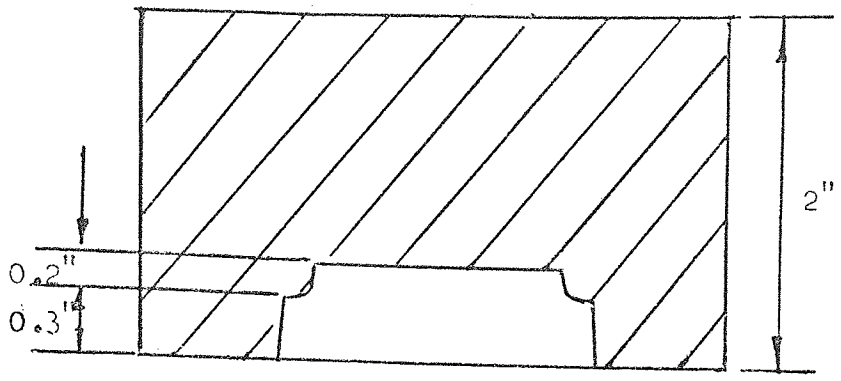

Die Set "A"

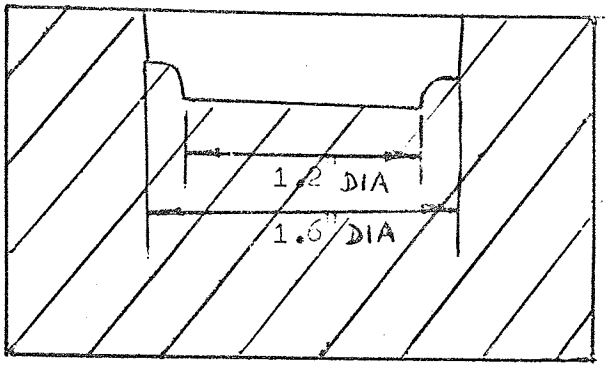

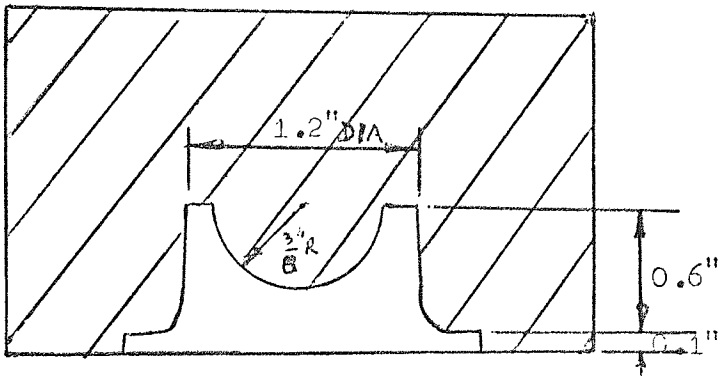

Die Set "B"

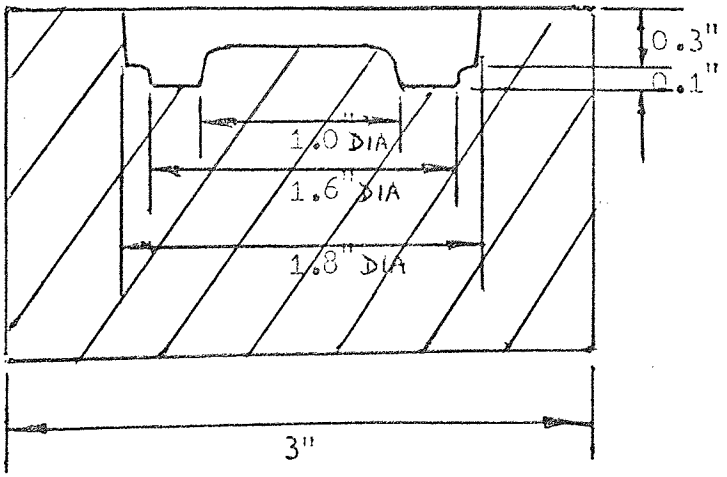

Fig 4.1.9

TABLE 4.2

Billet Temperature (degrees C)	Flash Settings (ins)
1150	0.115
	0.100
1200	0.085
	0.100
1250	0.085
	0.115

Table 4.2 shows the three temperatures at which billets were forged. Fifty degree intervals were chosen to ensure appreciable variations in loads when temperatures were varied. The flash settings included in Table 4.2 were the preset gaps between the faces of the top and bottom dies.

Actual flash thicknesses were greater than the settings, because of the elastic stretch on the press frame. The various combinations of billet temperatures and nominal flash settings on the press were obtained by partial replication [28,29].

Experimental Set Up

The billets, listed in Table 4.1, were weighed before heating them in a furnace to the forging temperatures. They were then forged into the dies at corresponding flash settings and left to cool. Loads were read off the ultra violet recorder, and the parameters listed in

page 45, were measured.

Forging Load in Press Selection

Various forging shapes and sizes can be made on any industrial forging press. It is necessary, in determining the influence of load in press capacity selection, therefore, to collect data from numerous forgings.

To this end, six more impressions (some of which were shown in Fig 4.1.1) were sunk and used for experiments similar to those described above. More data were also obtained by swapping dies whose parting diameters were the same.

To further simulate industrial closed die forging, the above experiments were repeated with flash gutters cut in the dies. The gutters differed in depths and widths and flash lands varied from die to die. The data from this and the previous experiments are tabulated in appendix 2.

Method of Analysis

The statistical method of analysis employed was Multiple Regression. In general, the method expresses a dependent variable Y, say, as a linear function of independent variables x_1, x_2, x_3,.....x_n viz

$$Y = a_1x_1 + a_2x_2 + a_3x_3 \ldots\ldots\ldots\ldots a_nx_n + C$$

C is the constant term and a_1, a_2, a_3,.....a_n are constants known as regression coefficients .

The theory of the technique is extensively treated in Davis[29] and in Barry.[30] It has, therefore, been omitted. For this work, multiple regression programmes developed for ICL 1905 computers have been used. In general, the programmes calculate the regression coefficients, the constant terms and the degree of fit and test for significance of the variables.

Two procedures are available. Their layouts are explained in the computer handbook and in Tognarelli.[31]

Procedure One

In this procedure, the significance level at which the dependent variable should be regressed on a specified number of independent factors is stipulated. Variables significant at the level are output in the regression equation. Others are left out.

Procedure Two

Unlike in Procedure One, significance levels are not specified. Instead, the computer is programmed to determine regression equations with known numbers of independent variables. This is achieved by indicating the minimum and maximum number of factors required in the regression equations.

Presentation Of Results

The results of the analyses are presented in tabular form as well as graphically.

The tables are abridged versions of the computer outputs and

include the names of the significant variables , their correlation coefficients and statistical t-values and the intercept terms. Multiple correlation coefficients and residual errors are also included.

The graphs , for their part , show figuratively how each of the significant variables affects the forging load. Each of the plots has been corrected for the effects of the other factors.

If b_1, b_2, and b_3 ..... are the regression coefficients and a is the intercept term when a dependent variable Y is regressed on independent variables x_1, x_2, x_3.....and t_1, t_2, t_3..... are typical values of x_1, x_2, x_3..... respectively, then

$$Y \text{ (observed)} = Y$$

$$Y \text{ (calculated)} = a + b_1 x_1 + b_2 x_2 + b_3 x_3 + ...$$

and $$Y \text{ (corrected)} = Y - b_1(x_1 - t_1) - b_2(x_2 - t_2) - b_3(x_3 - t_3) ..$$

Thus the values of Y which will be plotted against the variables x_1, x_2, and x_3 are respectively

$$Y(x_1) = Y - b_2(x_2 - t_2) - b_3(x_3 - t_3) .....$$

$$Y(x_2) = Y - b_1(x_1 - t_1) - b_3(x_3 - t_3) .....$$

and $$Y(x_3) = Y - b_1(x_1 - t_1) - b_2(x_2 - t_2) .....$$

The other graphs are those of forging load as calculated from the regression equations against the loads obtained from the experiments. These show the degree of accuracy of predictions from the regression equations and should , for good fit , be distributed about the 45° line.

4.2. EXPERIMENTAL RESULTS

The data obtained from all the laboratory experiments are tabulated in Appendix 2. Results for forgings with parallel flash are in Table 1, and those for forgings with flash gutters in Table 2. The results of the analyses are presented below.

Load In Die and Process Design

Tables 4.3 and 4.4 show the respective regression outputs from the data of die sets A and B. The mathematical models, derived from the tables, expressing forging load as functions of the significant variables are written below each table.

TABLE 4.3

SIGNIFICANT VARIABLES	REGRESSION COEFFICIENTS	T-STAT VALUES	INTERCEPT TERM	MULTIPLE CORRELATION	RESIDUAL ERROR
Flash Width / Flash Thickness	17.573	10.59	77.912	0.860	6.086
Billet Diameter / Billet Height	-7.230	2.26			
Slug Temperature (Degrees C)	-0.050	1.99			

The mathematical interpretation of Table 4.3 is

$$\text{Forging Load (Tons)} = 17.57 \times \frac{\text{Flash Width}}{\text{Flash Thickness}} - 7.23 \times \frac{\text{Billet Diameter}}{\text{Billet Height}}$$

$$- 0.05 \times \text{Slug Temperature } (^{\circ}C) + 77.91$$

TABLE 4.4

SIGNIFICANT VARIABLES	REGRESSION COEFFICIENTS	T-STAT VALUES	INTERCEPT TERM	MULTIPLE CORRELATION	RESIDUAL ERROR
Flash Width / Flash Thickness	28.987	12.91	136.831	0.890	6.209
Billet Diameter / Billet Height	-18.272	5.07			
Slug Temperature (Degrees C)	- 0.099	3.84			

The mathematical interpretation of Table 4.4 is

$$\text{Forging Load (Tons)} = 28.98 \times \frac{\text{Flash Width}}{\text{Flash Thickness}} - 18.27 \times \frac{\text{Billet Diameter}}{\text{Billet Height}}$$

$$- 0.099 \times \text{Slug Temperature } (^{\circ}C) + 136.83$$

The two results are similar and indicate that the load required to forge any given part increases with the width to thickness ratio of the flash formed, and decreases as both the slug temperature and the billet diameter to height ratio increase.

The flash width to thickness ratio is significant at the 1% level, while slug temperature and the ratio of billet diameter to its height are significant at the 10% level. Other forgings investigated showed a similar trend.

In general the multiple correlation coefficient for each of the forgings investigated exceeded 0.85, and their residual errors were less than 7.5ton. Corresponding values for die sets A and B are 0.86

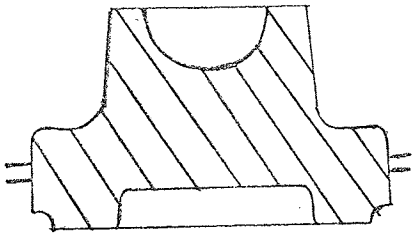

FORGING LOAD (TONS)*10^{-2}
0.360
0.460
0.560
0.660
0.760
0.860
0.960
1.060
1.100
1.500
1.900
2.300
2.700
3.100
FLASH WIDTH/FLASH THICKNESS

Fig. 4.10

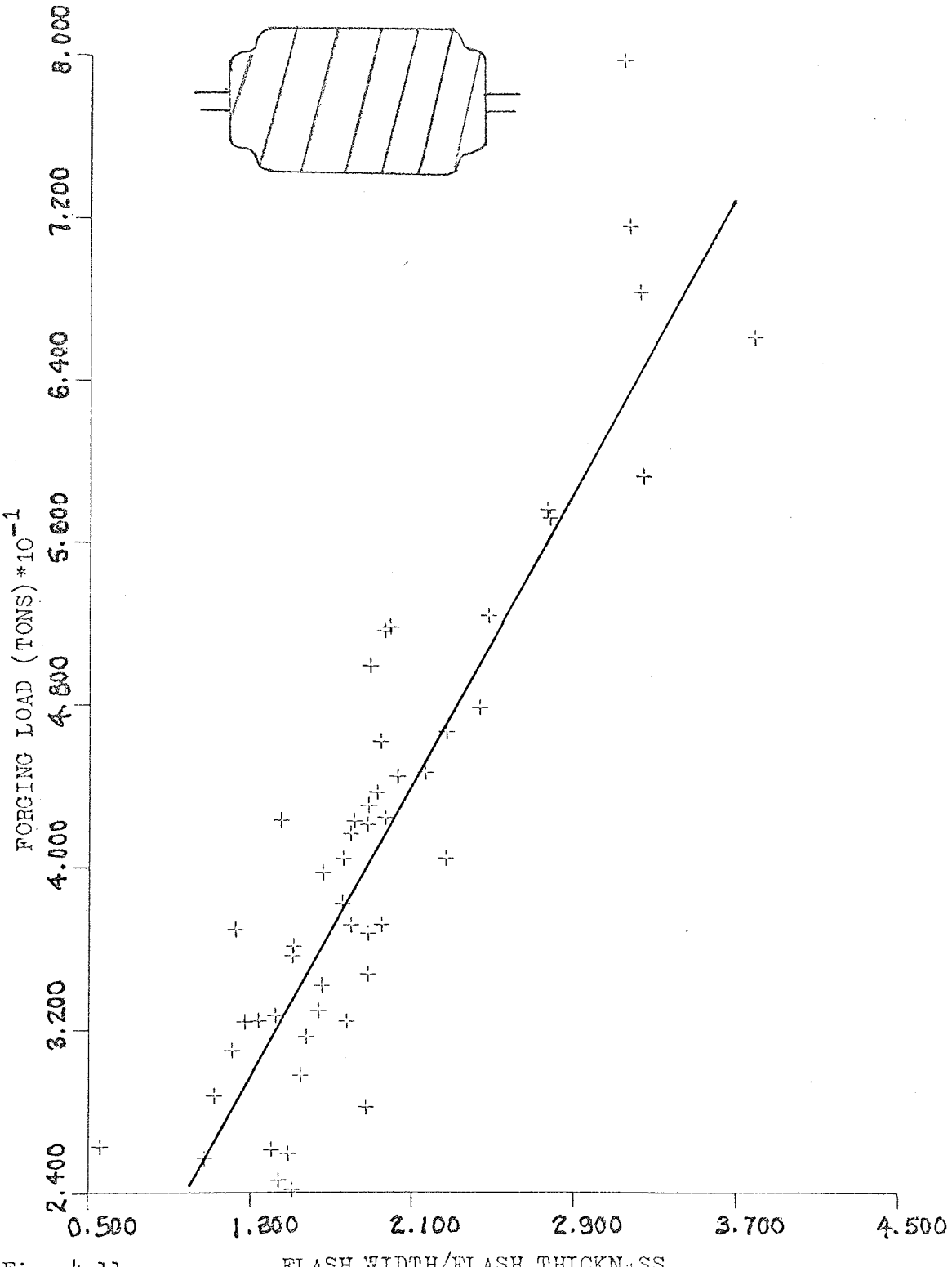
8.000
7.200
6.400
5.600
4.800
4.000
3.200
2.400
FORGING LOAD (TONS)*10⁻¹
0.500
1.300
2.100
2.900
3.700
4.500
FLASH WIDTH/FLASH THICKNESS

Fig. 4.11

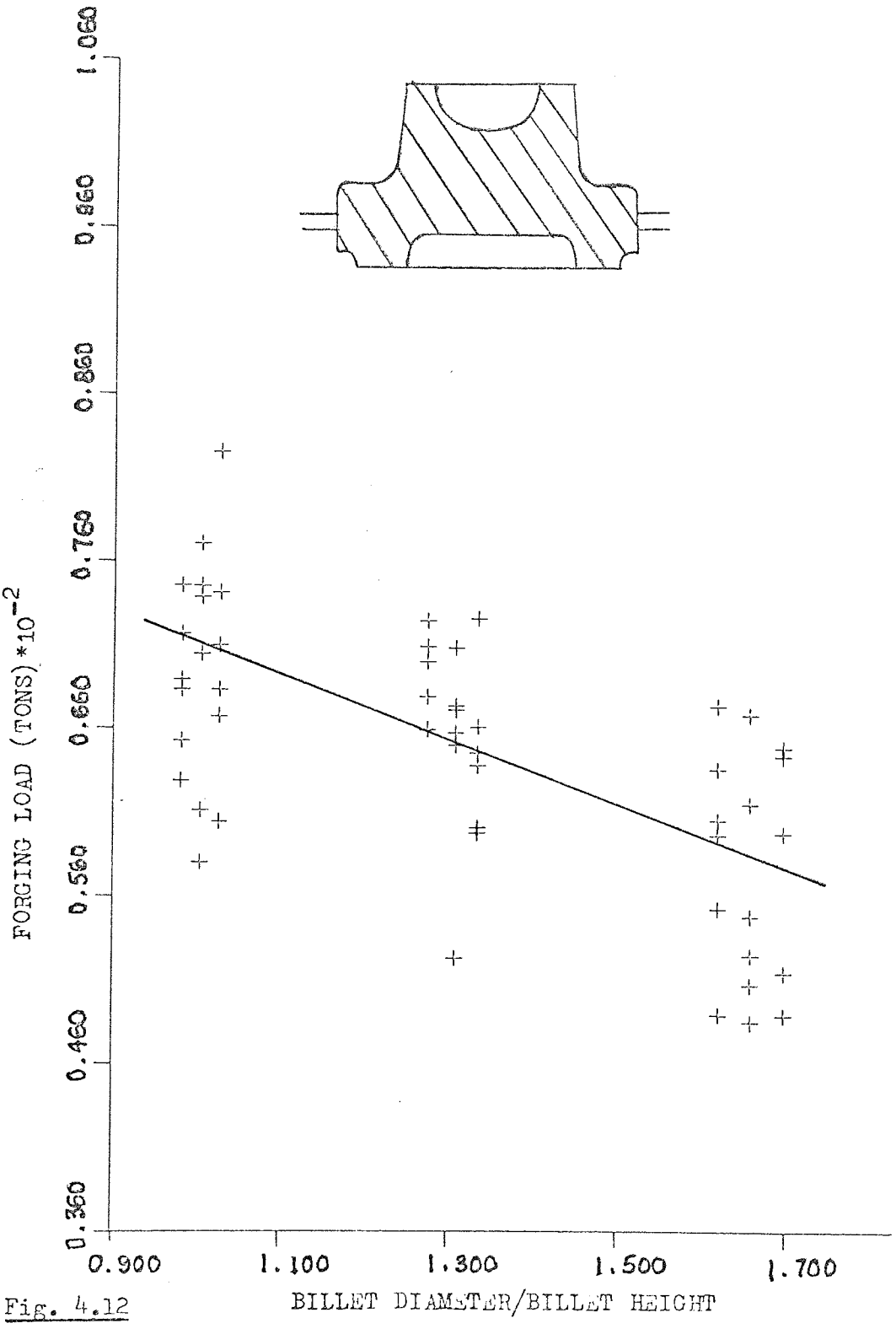
1.060
0.960
0.860
0.760
0.660
0.560
0.460
0.360
FORGING LOAD (TONS)*10^{-2}
0.900
1.100
1.300
1.500
1.700
BILLET DIAMETER/BILLET HEIGHT

Fig. 4.12

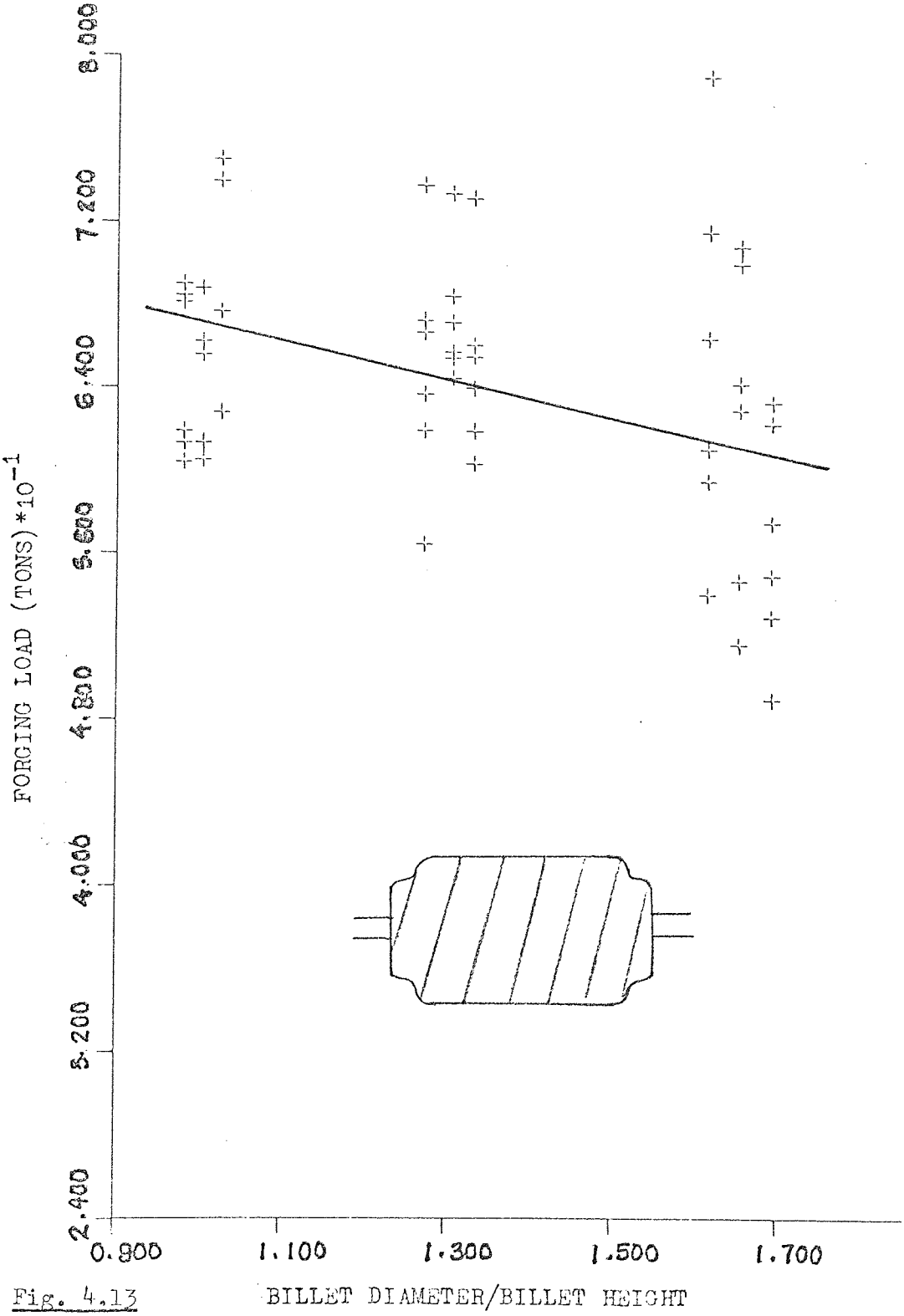
FORGING LOAD (TONS)*10⁻¹
8.000
7.200
6.400
5.600
4.800
4.000
3.200
2.400
0.900
1.100
1.300
1.500
1.700
BILLET DIAMETER/BILLET HEIGHT

Fig. 4.13

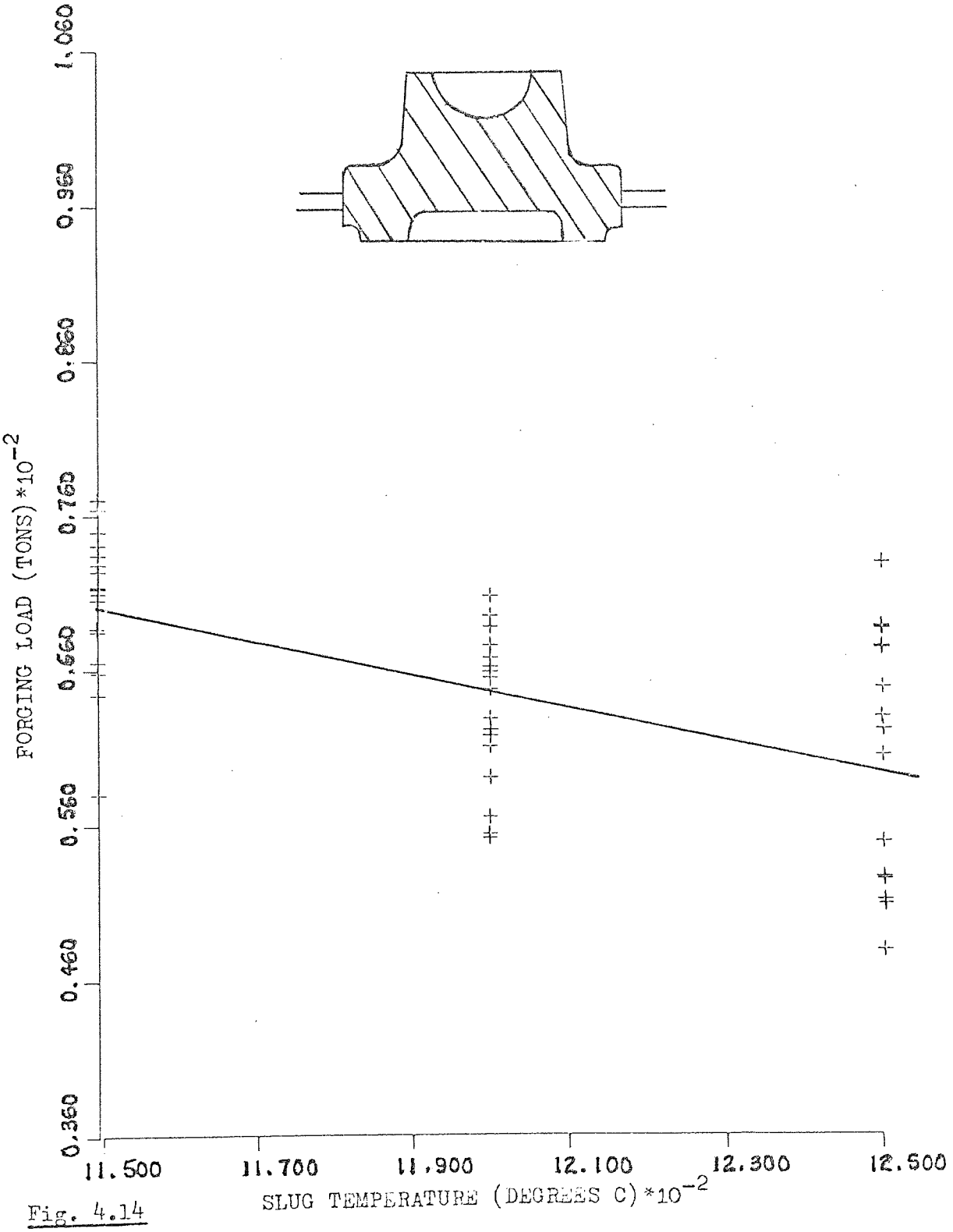
FORGING LOAD (TONS)*10^-2
1.060
0.960
0.860
0.760
0.660
0.560
0.460
0.360
11.500
11.700
11.900
12.100
12.300
12.500
SLUG TEMPERATURE (DEGREES C)*10^-2

Fig. 4.14

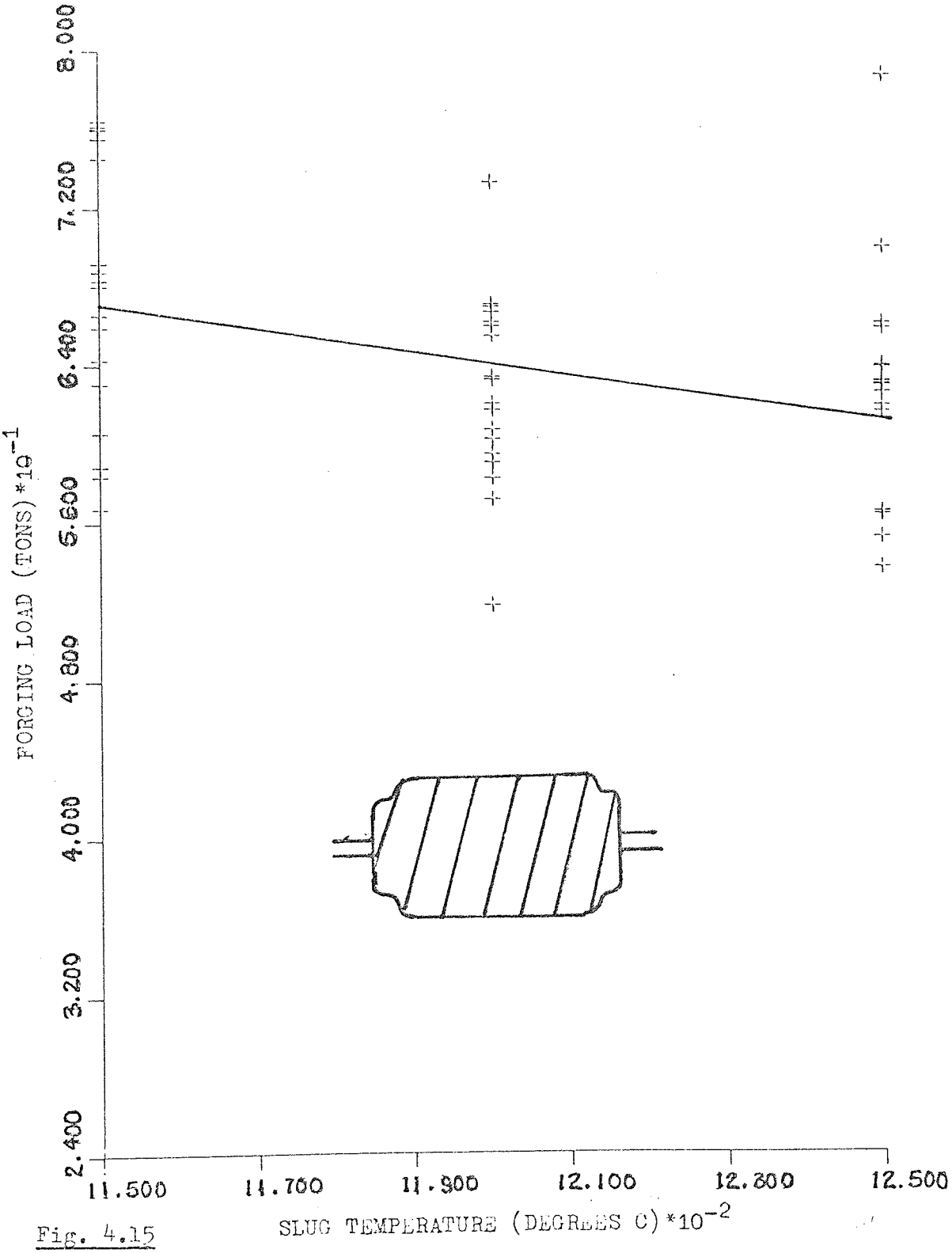
FORGING LOAD (TONS)*10^{-1}
8.000
7.200
6.400
5.600
4.800
4.000
3.200
2.400
11.500
11.700
11.900
12.100
12.300
12.500
SLUG TEMPERATURE (DEGREES C)*10^{-2}

Fig. 4.15

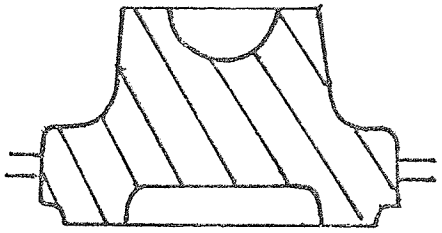

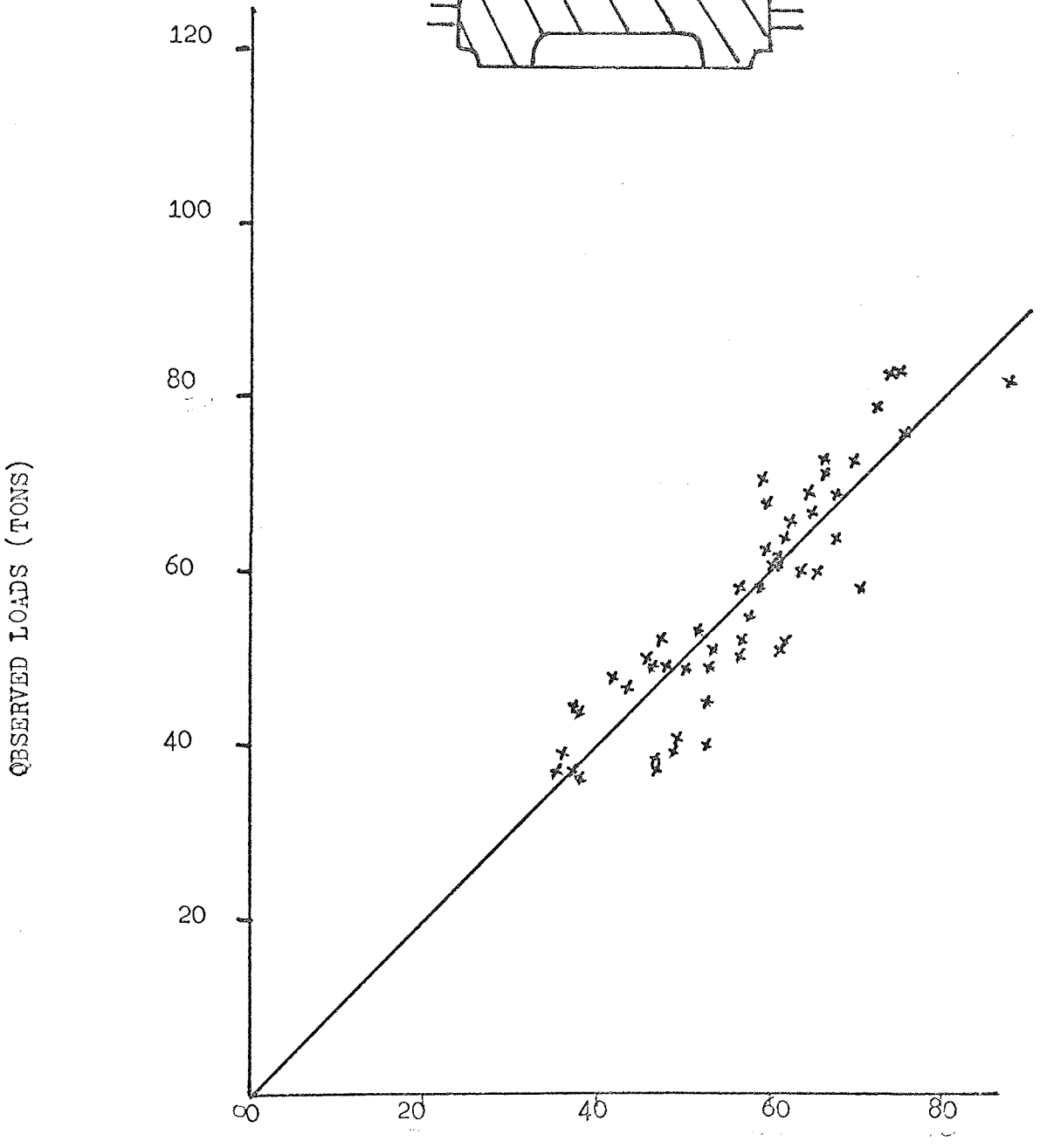
120
100
80
60
40
20
0
20
40
60
80
OBSERVED LOADS (TONS)
CALCULATED LOADS (TONS)

Fig. 4.16

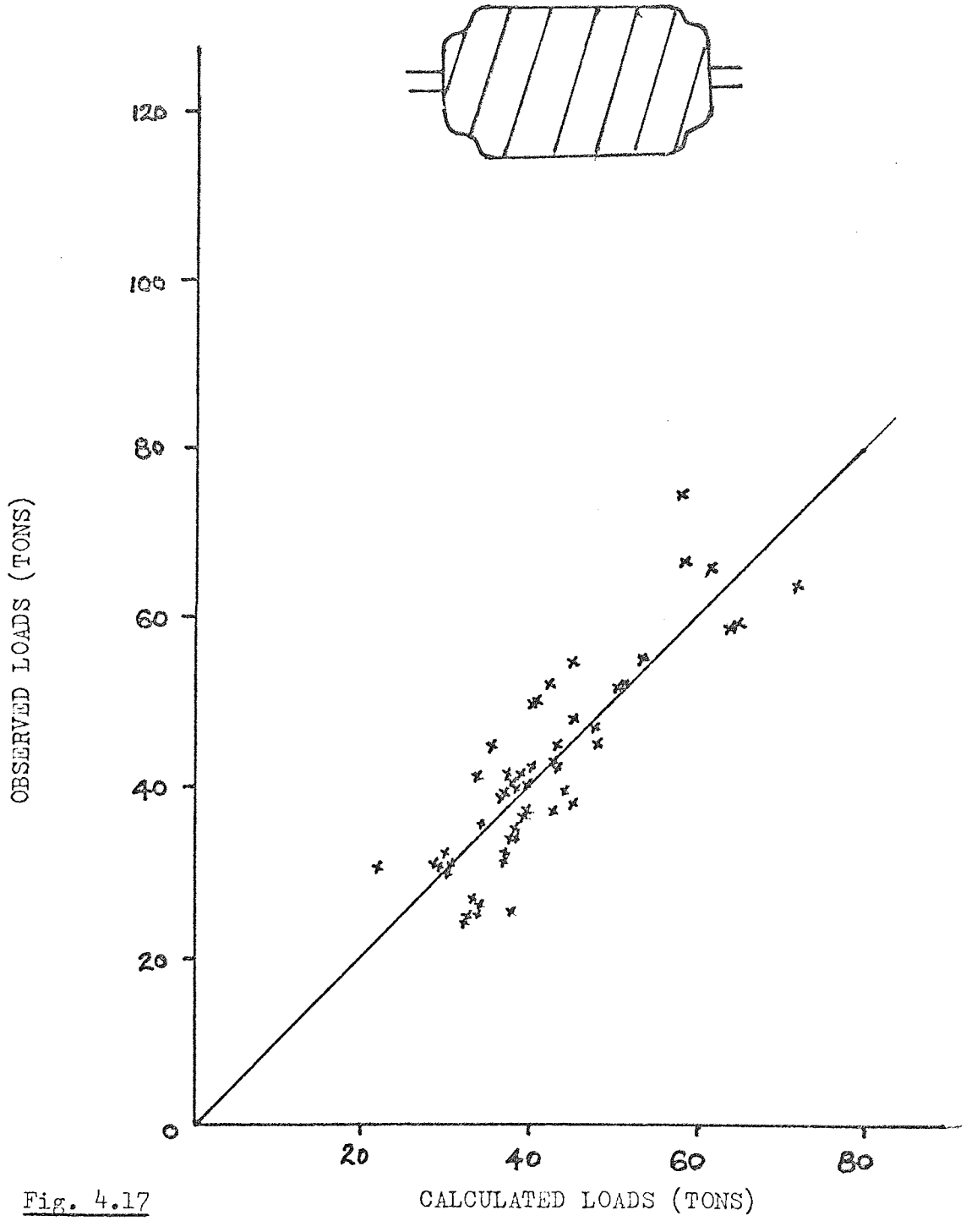
120
100
80
60
40
20
0
20
40
60
80
OBSERVED LOADS (TONS)
CALCULATED LOADS (TONS)

Fig. 4.17

and 6.086 and 0.89 and 6.209 respectively.

The separate effects of each of the significant variables on the load applied on components A and B are shown graphically in Figs (4 . 10 to 4 . 15). Forging loads calculated from the regression equations are plotted against those obtained from experiment in Figs (4 . 16) and (4 . 17).

LOAD IN PRESS CAPACITY SELECTION

The relationship between the various forging parameters considered are shown in the correlation matrix in Appendix 3. A zero coefficient symbolises a complete independence between two variables while a perfect linear relationship produces a coefficient of one. A negative correlation suggests that one factor tends to increase as the other decreases. A possitive one indicates that the two factors tend to increase together. Any coefficient less than 0.4 could have arisen by chance.

The correlation matrix is used to prevent any "chance" correlation from interfering with the regression analyses and to ensure that two or more highly correlated variables do not occur simultaneously in the repression equations.

The areas at parting lines of the forgings were highly correlated with the weights of the billets, the parting diameter to height ratios of the forgings and the process yield. A sensitivity check characterised by the correlation of all the variables investigated with forging load revealed parting area as having the most significant influence on the load. Area was, therefore, included in the analyses at the expense of those highly correlated with it.

The flash width to thickness ratio was in similar circumstances included in the analyses to the exclusion of the flash width and the flash width to clipped forging diameter ratio with which it was highly correlated.

Other variables which are independent of the other parameters were also included in the computations. These were the slug temperature,

the shape complexity factor, the weight of the forging, the billet diameter to height ratio and the flash thickness. The products of some of the variables were also included to investigate the effects of interactions. Definitions of all the parameters are listed in pages 45 and 46.

Forgings with Parallel Flash

Table 4.5 shows the results of regressing forging load (tons) on the job and process variables measured when forging billets into dies with parallel flash.

TABLE 4.5

VARIABLES	REGRESSION CO-EFFICIENTS	T-STAT VALUES	LEVELS OF SIGNI-FICANCE	INTER-CEPT TERM	MULTIPLE CORRE-LATION	RESIDUAL ERROR	DEGREES OF FREEDOM
Parting Area (In^2) (Area)	14.0189	23.94	1.00%	117.857	0.930	7.5906	162
Square Of Flash Width Over Thickness	3.1625	12.82	1.00%				
Slug Temperature (^oC)	- 0.09087	5.95	1.00%				
Billet Diameter / Billet Height	-13.4207	5.41	1.00%				
Shape Complexity	- 8.8357	1.66	10.0%				

The mathematical interpretation of this table is that

$$\text{Forging Load (Tons)} = 14.0189 \times \text{Parting Area} + 3.1625 \times \left(\frac{\text{Flash Width}}{\text{Flash Thickness}}\right)^2$$

$$- 0.09087 \times \text{Slug Temperature} - 13.4207 \times \frac{\text{Billet Diameter}}{\text{Billet Height}}$$

$$- 8.8357 \times \text{Shape Complexity} + 117.857$$

where parting area and slug temperature are in square inches and degrees centigrade respectively.

The physical interpretation of the results is that forging load increases with the area at parting line of the forging and with the width

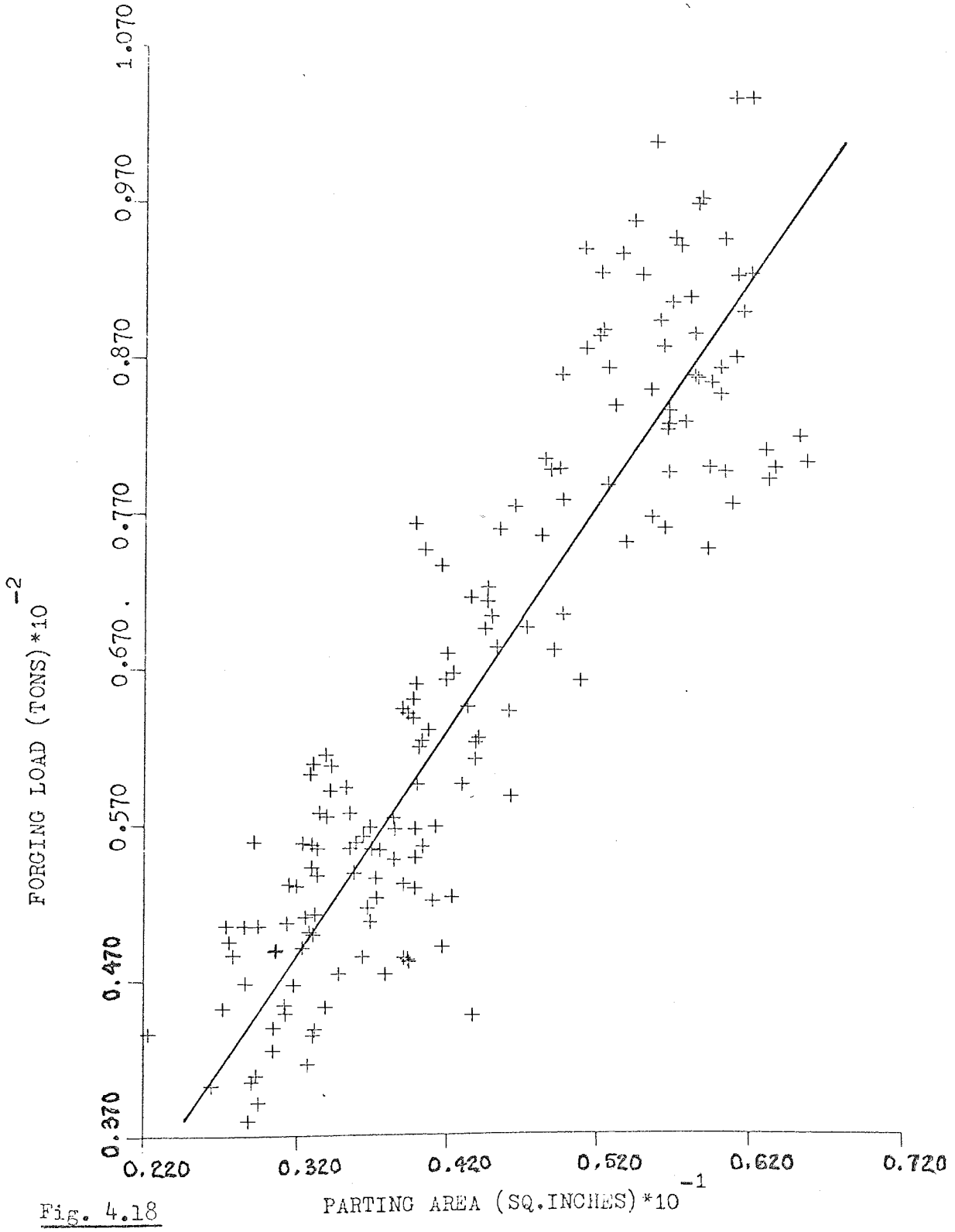
FORGING LOAD (TONS)*10^-2
1.070
0.970
0.870
0.770
0.670
0.570
0.470
0.370
0.220
0.320
0.420
0.520
0.620
0.720
PARTING AREA (SQ.INCHES)*10^-1

Fig. 4.18

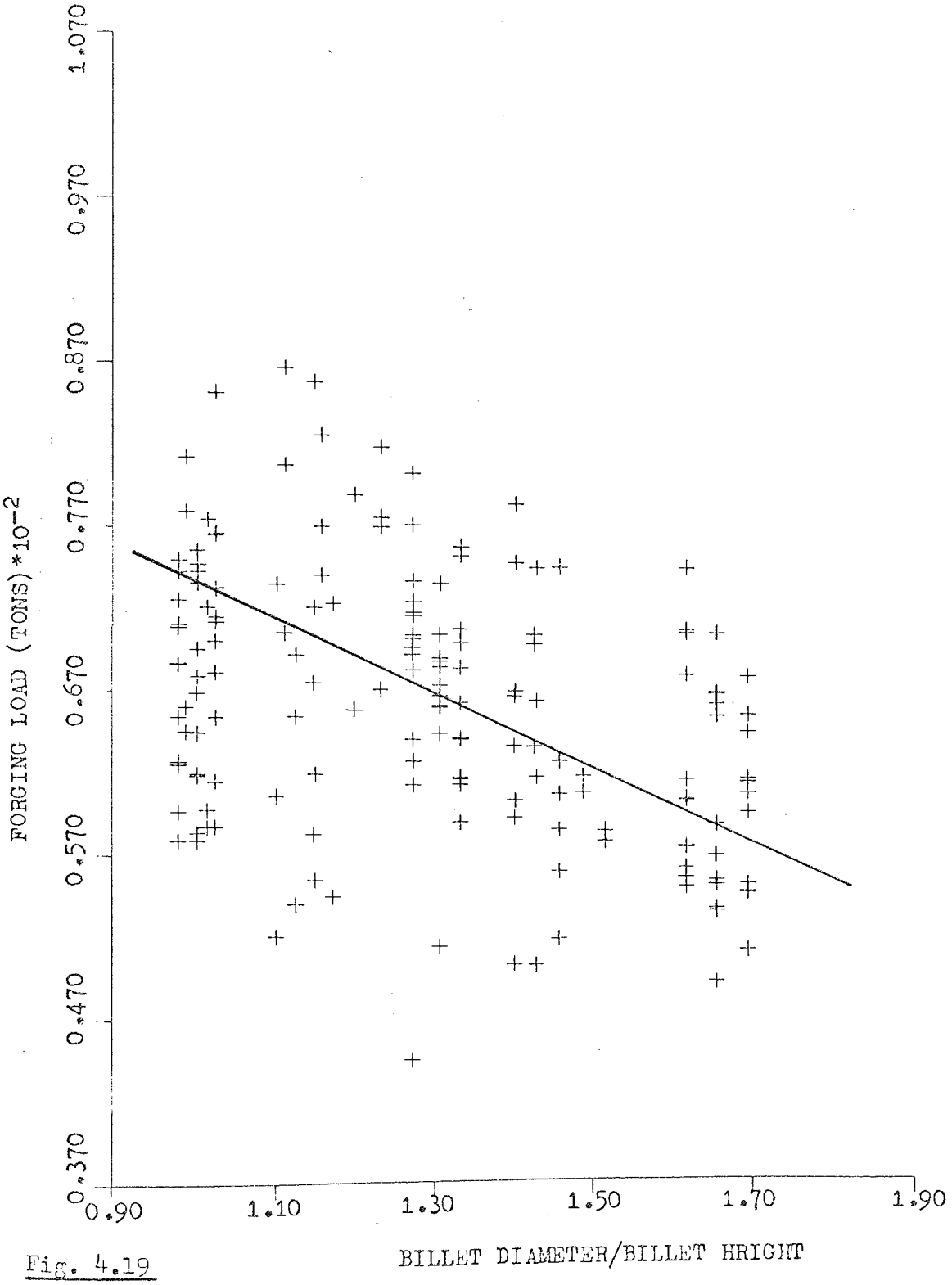
FORGING LOAD (TONS)*10⁻²
1.070
0.970
0.870
0.770
0.670
0.570
0.470
0.370
0.90
1.10
1.30
1.50
1.70
1.90
BILLET DIAMETER/BILLET HRIGHT

Fig. 4.19

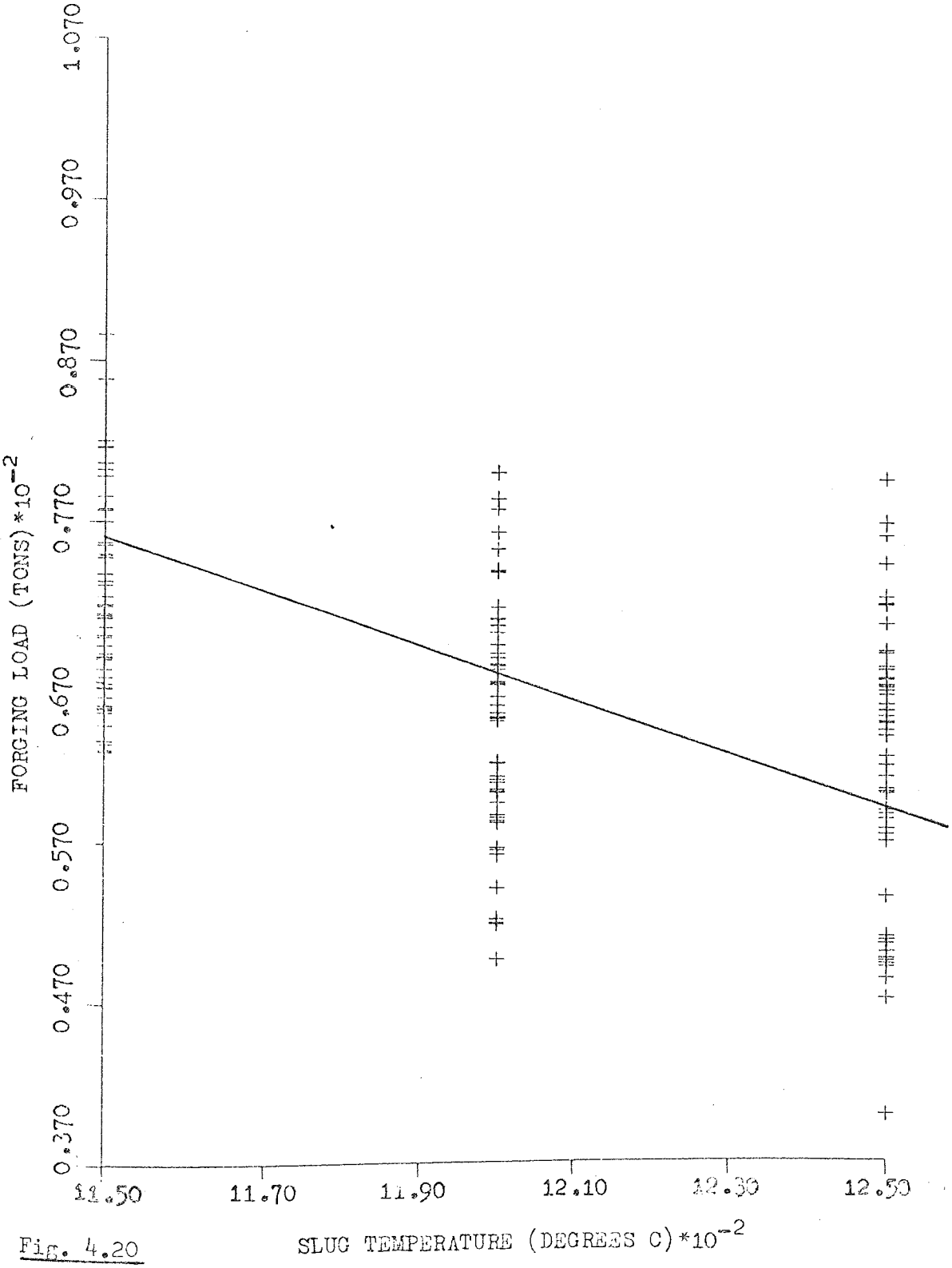
FORGING LOAD (TONS)*10^-2
1.070
0.970
0.870
0.770
0.670
0.570
0.470
0.370
11.50
11.70
11.90
12.10
12.30
12.50
SLUG TEMPERATURE (DEGREES C)*10^-2

Fig. 4.20

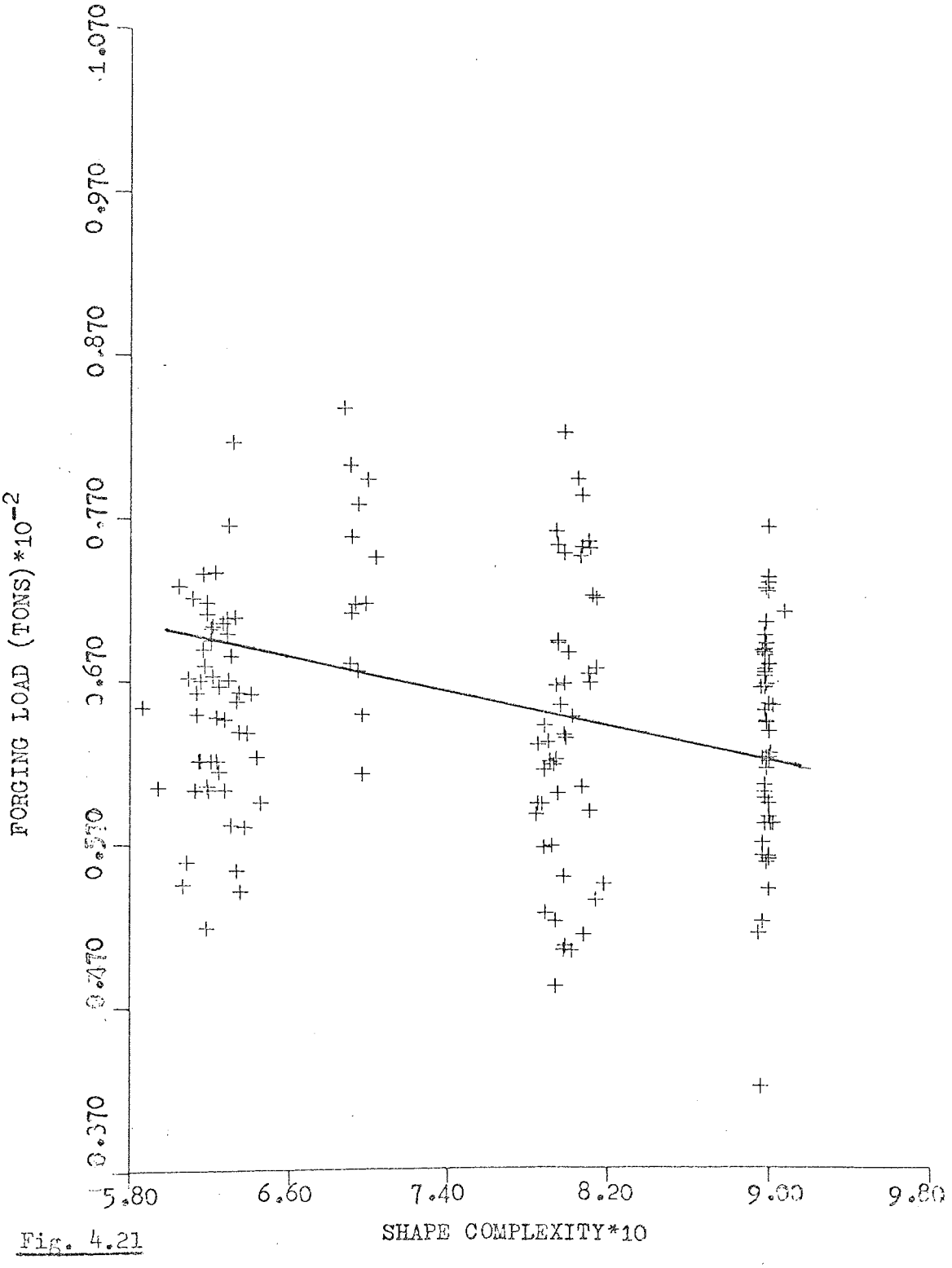
FORGING LOAD (TONS)*10⁻²
1.070
0.970
0.870
0.770
0.670
0.570
0.470
0.370
5.80
6.60
7.40
8.20
9.00
9.80
SHAPE COMPLEXITY*10

Fig. 4.21

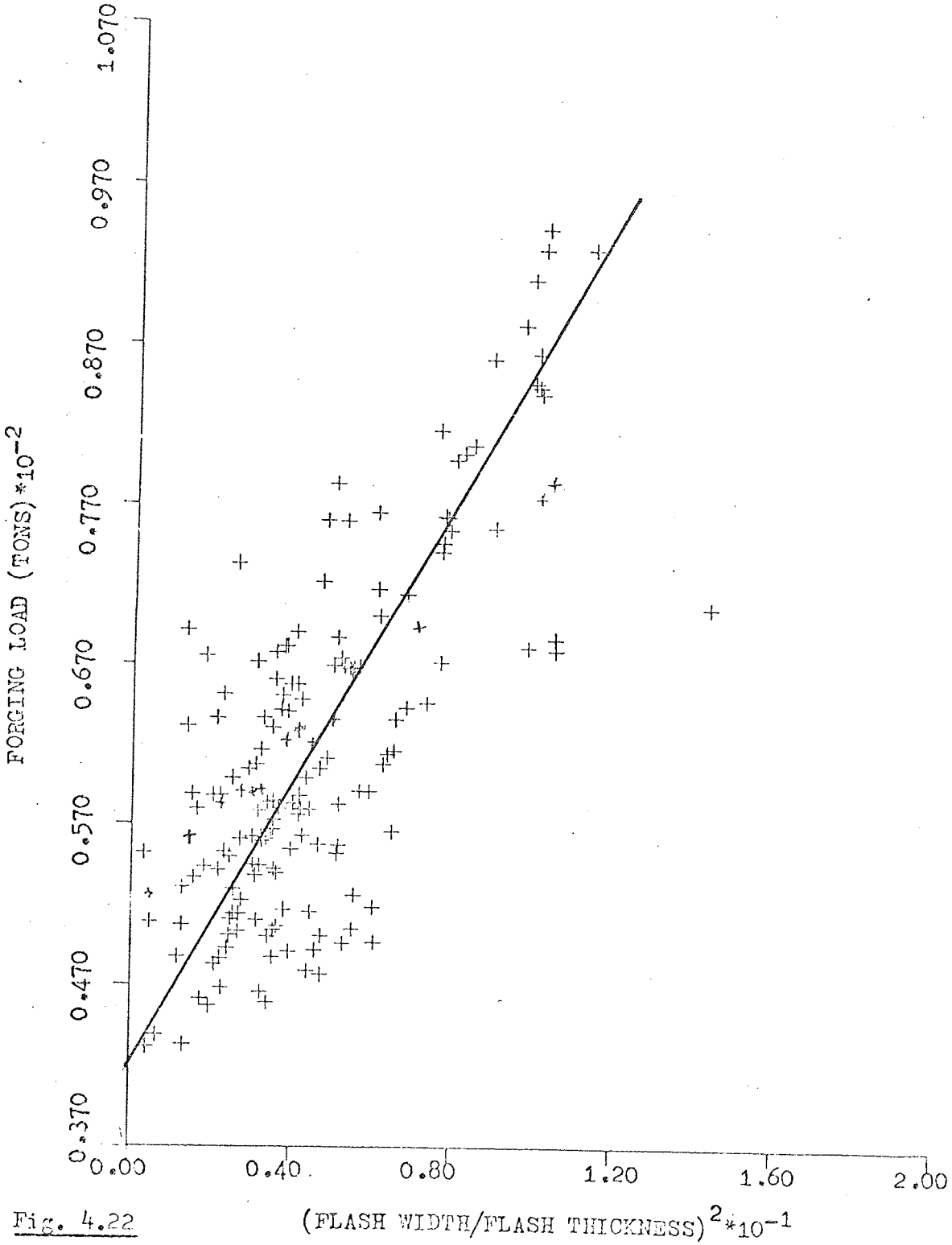
FORGING LOAD (TONS)*10^{-2}
1.070
0.970
0.870
0.770
0.670
0.570
0.470
0.370
0.00
0.40
0.80
1.20
1.60
2.00
(FLASH WIDTH/FLASH THICKNESS)^{2}*10^{-1}

Fig. 4.22

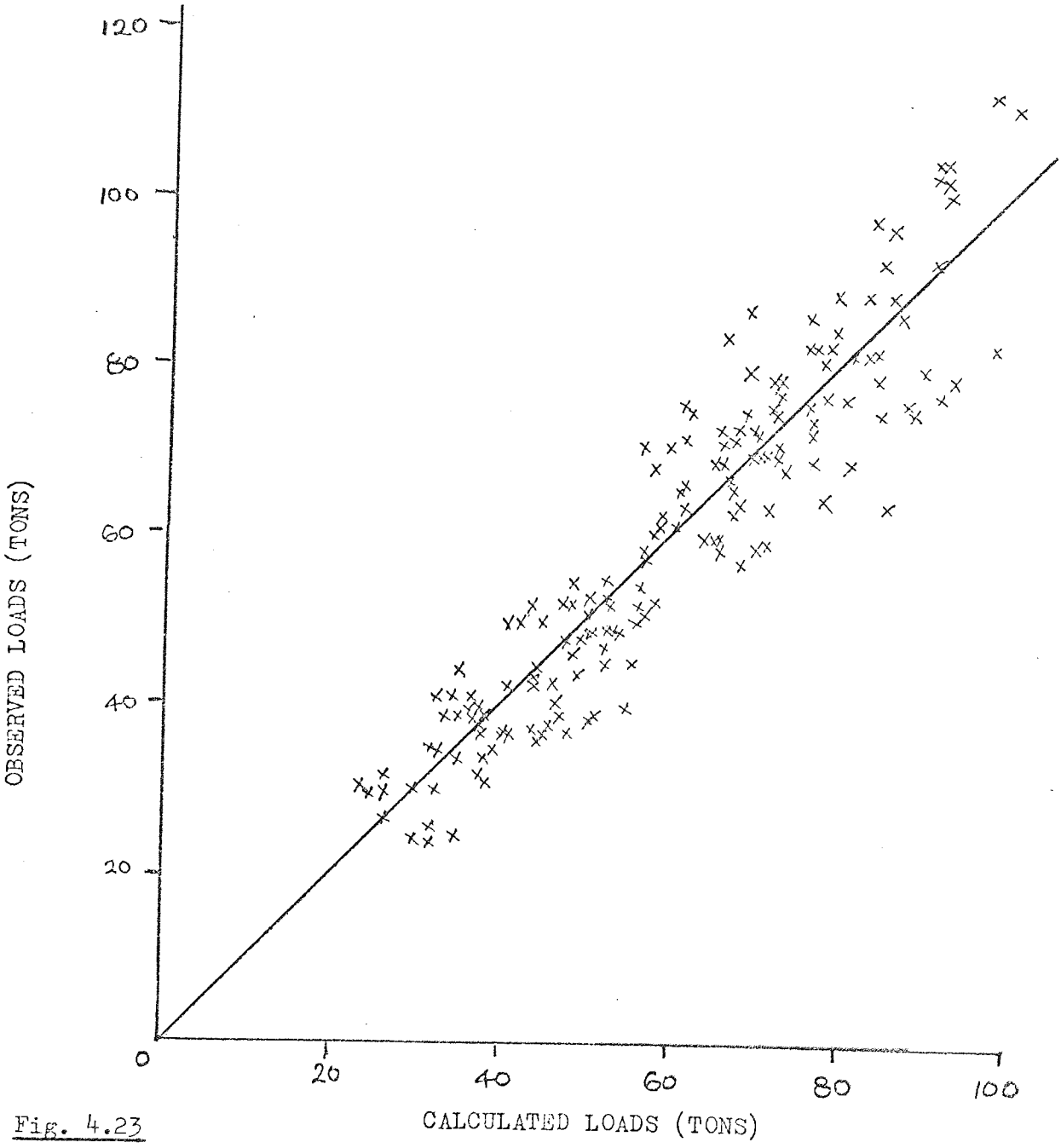
120
100
80
60
40
20
0
20
40
60
80
100
OBSERVED LOADS (TONS)
CALCULATED LOADS (TONS)

Fig. 4.23

to thickness ratio of the flash formed, and diminishes as the slug temperature and billet diameter to height ratio increase. And the more complex the shape of the component, the greater the load required to forge it.

It is pointed out here, for clarity, that the shape complexity factor has been defined such that it tends to one for simple shapes and tends to zero for complicated ones. Hence, the negative sign of its regression coefficient implies that forging load increases as the configuration of the part becomes more complex.

All the variables listed in Table 4.5 are significant at 1.00% level except the shape complexity factor which is significant at the 10% level. A multiple correlation of 0.930 was achieved, and the residual error was $\pm$ 7.5906 tons.

The variations of forging load with each of the significant variables listed above are shown graphically in Figs 4.18 - 4.22. Each plot had been corrected for the effects of the other four variables. Fig 4.23 is the plot of observed loads against those calculated from the regression equation.

Forgings With Flash Gutters

Regression analyses of the data obtained when forging into dies having flash gutters show that forging load increases as

(1) parting area increases

(2) the flash width to thickness ratio increases

(3) the shape of the forging becomes more complicated

(4) slug temperature decreases, and

(5) as the forging weight increases.

All the factors are significant at the 1% level. The multiple correlation was 0.852 and the residual error was ± 6.29 tons.

Table 4.6 shows a summary of the computer output.

TABLE 4.6

VARIABLES	REGRESSION CO-EFFICIENTS	T-STAT VALUES	LEVELS OF SIGNI-FICANCE	INTER-CEPT TERM	MULTIPLE CORRE-LATION	RESIDUAL ERROR	DEGREES OF FREEDOM
Parting Area (In^2)	10.55	17.61	1%	63.045	0.852	6.29	188
Weight Of Forging (lbs)	122.90	9.78	1%				
Slug Temperature (^oC)	- 0.0897	7.21	1%				
Flash Width/ Thickness	15.862	6.06	1%				
Shape Complexity	-27.36	5.18	1%				

Mathematically, the table can be expressed as

$$\text{Forging Load (Tons)} = 10.55 \times \text{Parting Area} + 122.90 \times \text{Forging Weight} - 0.0897 \times \text{Slug Temperature} + 15.862 \times \frac{\text{Flash Width}}{\text{Flash Thickness}} - 27.36 \times \text{Shape Complexity} + 63.045$$

The corrected variation of forging load with each of the significant variables are shown graphically in Figs 4.24 to 4.28, and Fig 4.29 is the plot of forging loads calculated from the regression equation against those measured in the experiments.

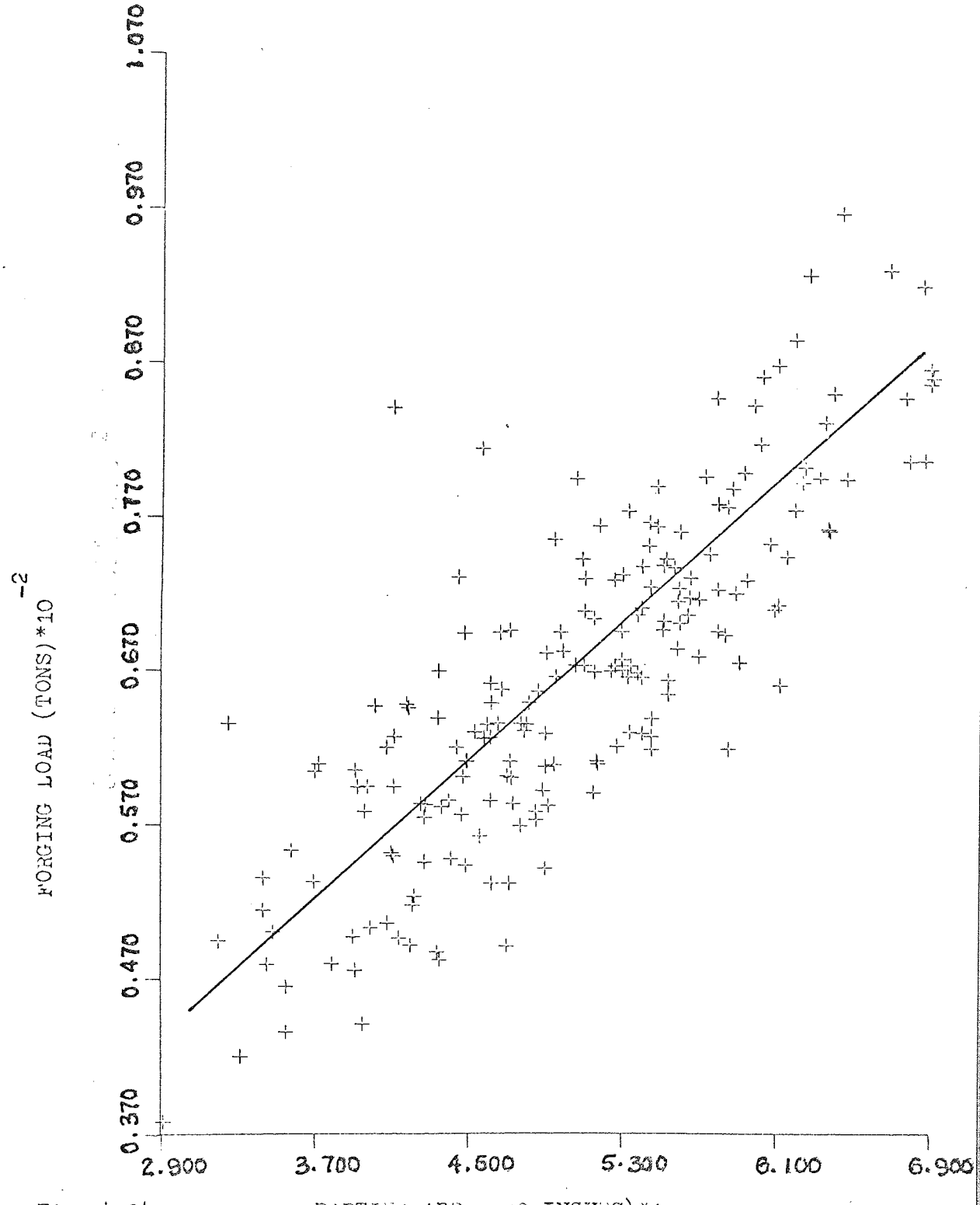
FORGING LOAD (TONS)*10^-2
1.070
0.970
0.870
0.770
0.670
0.570
0.470
0.370
2.900
3.700
4.500
5.300
6.100
6.900
PARTING AREA (SQ.INCHES)*1

Fig. 4.24

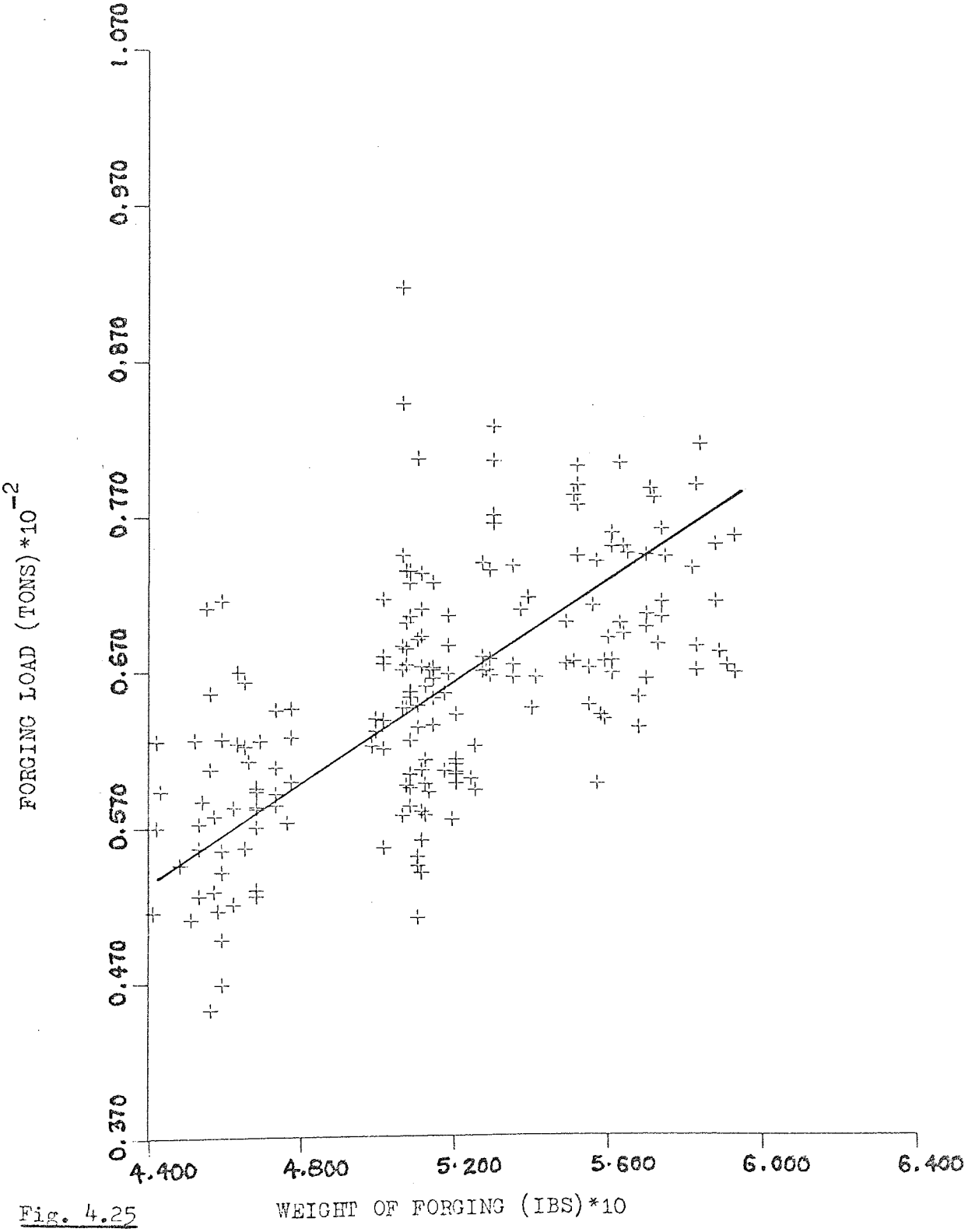
FORGING LOAD (TONS)*10^-2
0.370
0.470
0.570
0.670
0.770
0.870
0.970
1.070
4.400
4.800
5.200
5.600
6.000
6.400
WEIGHT OF FORGING (IBS)*10

Fig. 4.25

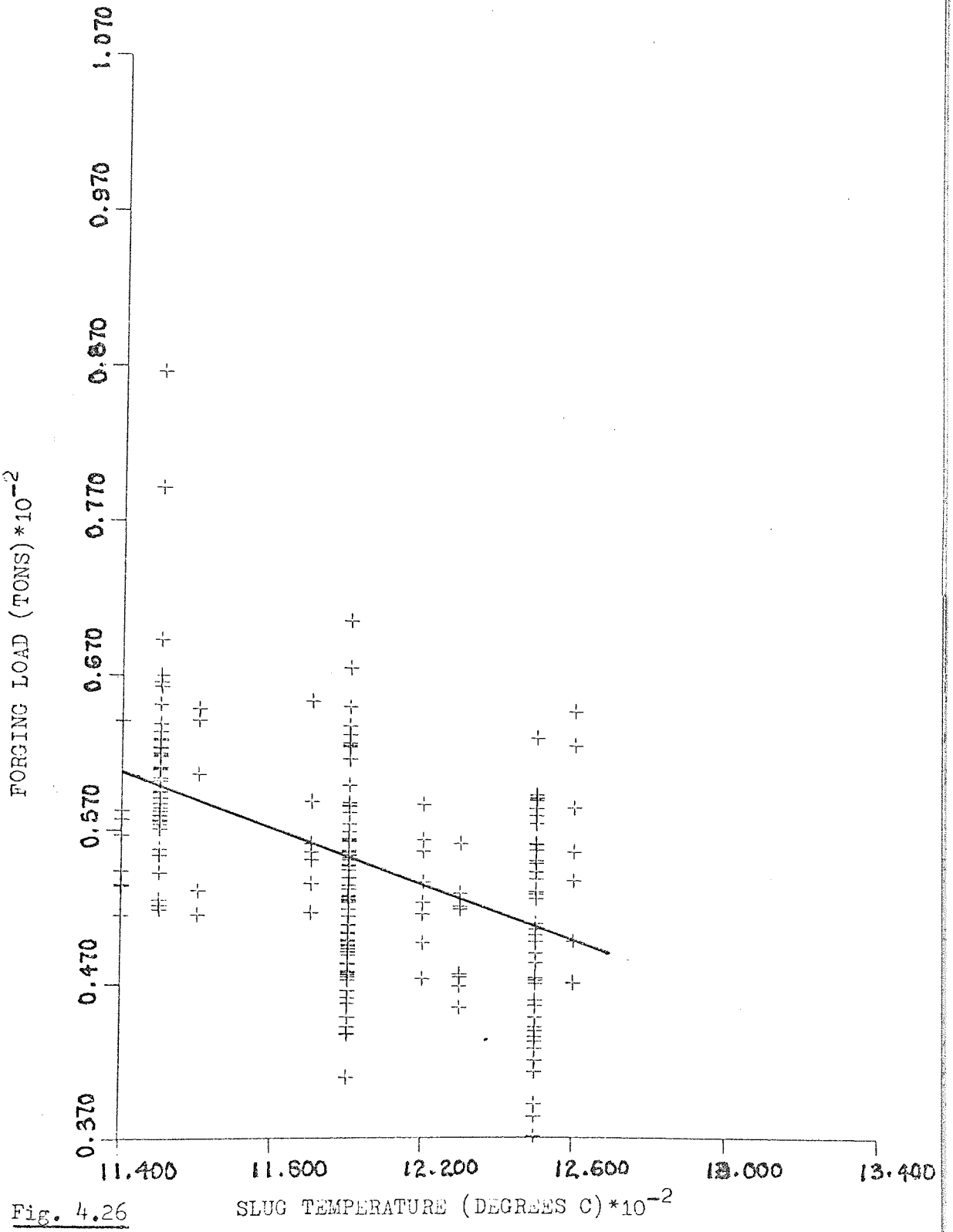
FORGING LOAD (TONS)*10^{-2}
0.370
0.470
0.570
0.670
0.770
0.870
0.970
1.070
11.400
11.600
12.200
12.600
13.000
13.400
SLUG TEMPERATURE (DEGREES C)*10^{-2}

Fig. 4.26

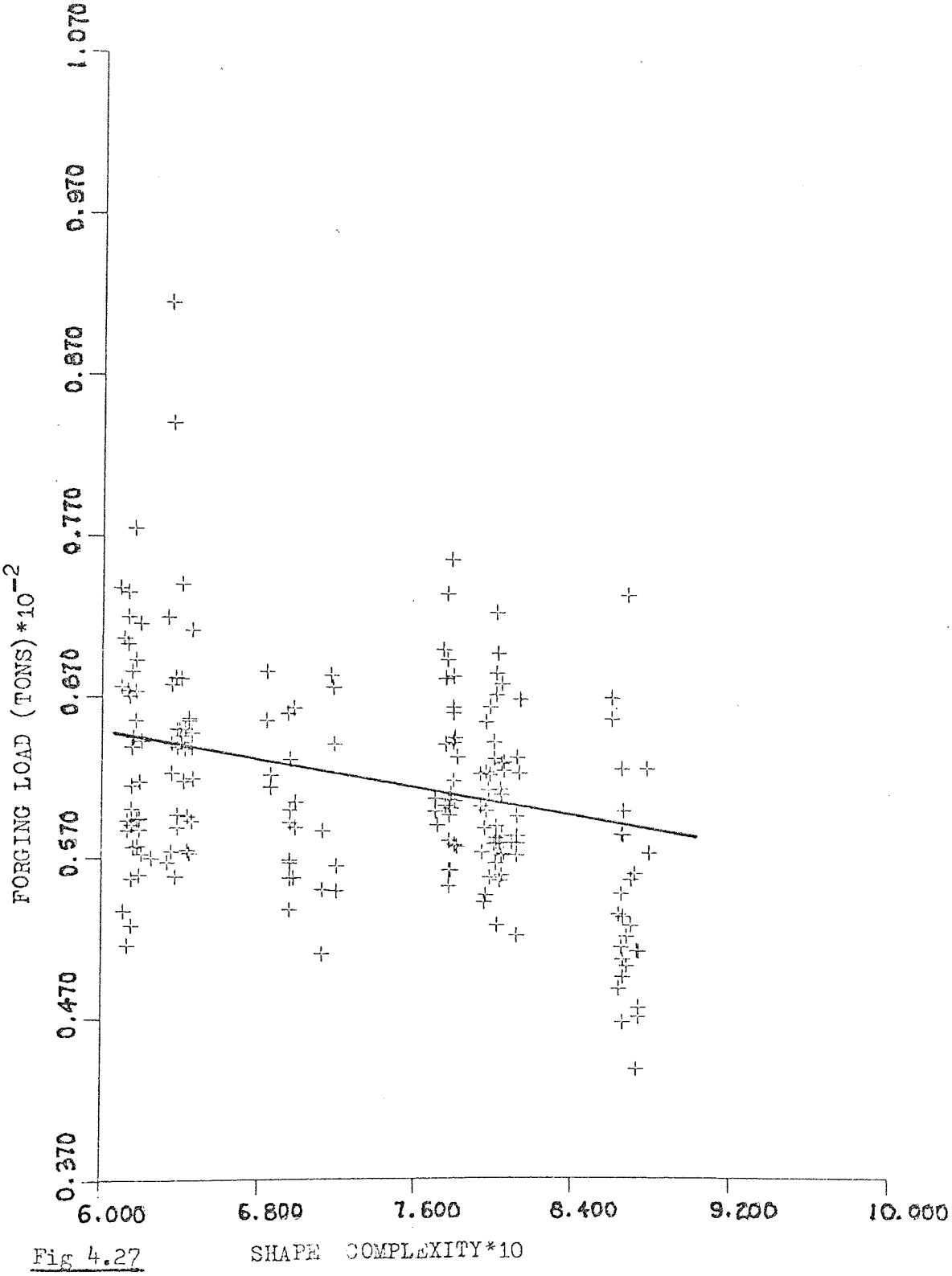
FORGING LOAD (TONS)*10^{-2}
0.370
0.470
0.570
0.670
0.770
0.870
0.970
1.070
6.000
6.800
7.600
8.400
9.200
10.000
SHAPE COMPLEXITY*10

Fig 4.27

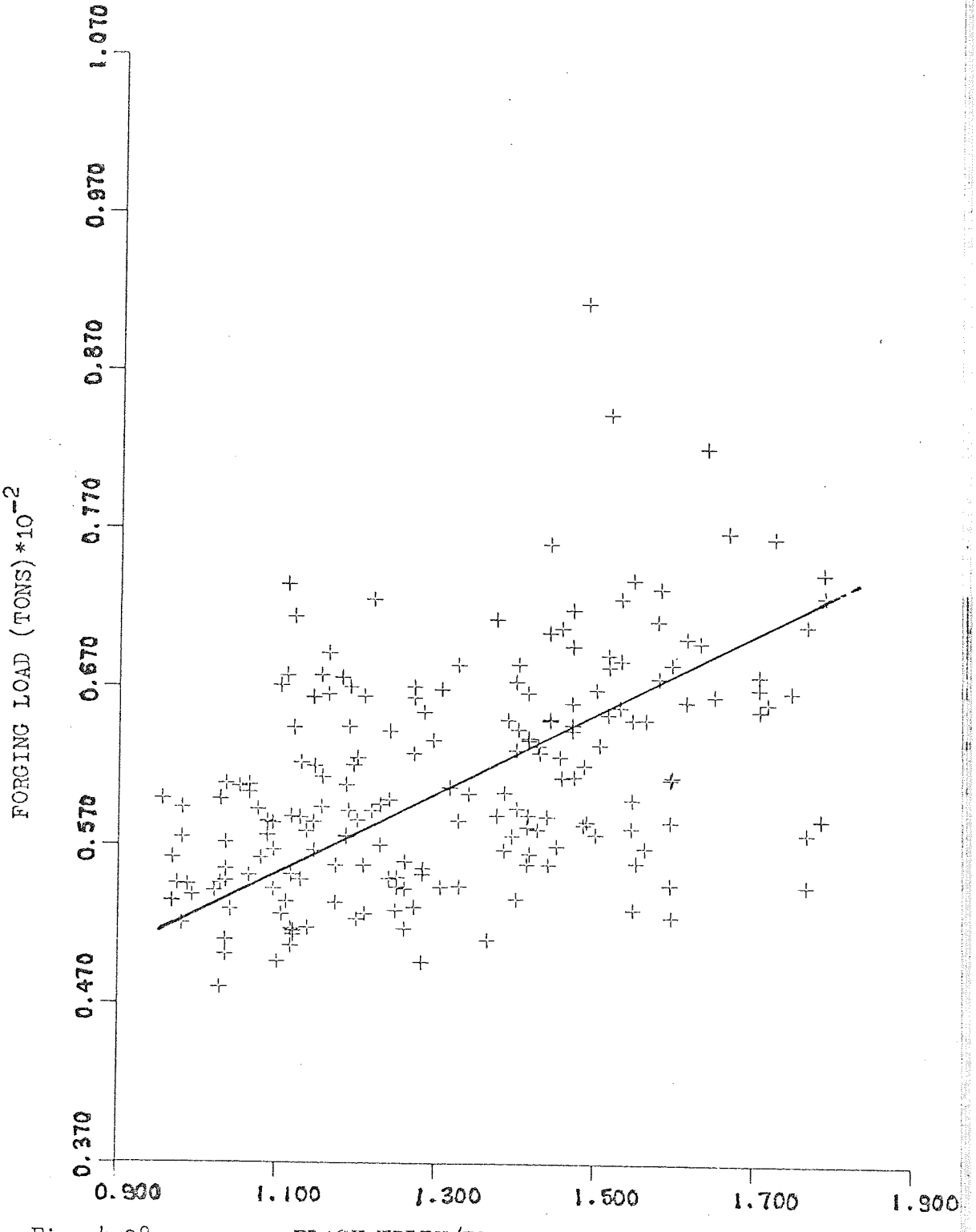
FORGING LOAD (TONS)*10^{-2}
0.370
0.470
0.570
0.670
0.770
0.870
0.970
1.070
0.900
1.100
1.300
1.500
1.700
1.900
FLASH WIDTH/FLASH THICKNESS

Fig. 4.28

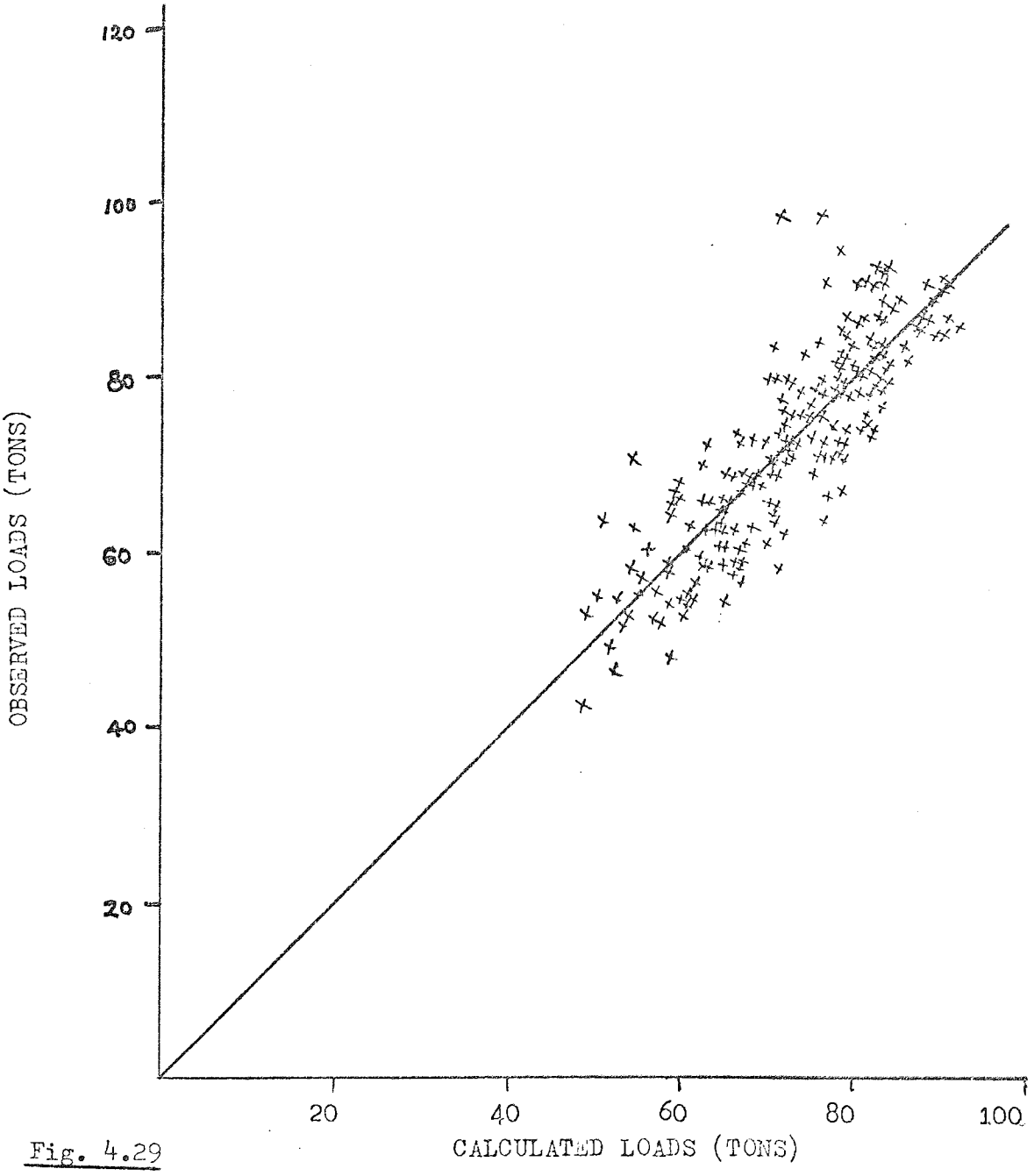
120
100
80
60
40
20
OBSERVED LOADS (TONS)
20
40
60
80
100
CALCULATED LOADS (TONS)

Fig. 4.29

5. FACTORS DETERMINING PRESS FORGING LOAD

DIE AND PROCESS DESIGN

The load necessary to forge any given component varies directly as the width to thickness ratio of the flash formed and inversely as both the billet diameter to height ratio and the slug temperature. As such, careful consideration is necessary in the choice of these parameters.

Effect Of Flash Width To Thickness Ratio

Flash forces increase as flash width to thickness ratio increases[36]. Since forging load increases with flash force, increments in flash width to thickness ratio cause a steady increase in forging load. For low die loads, therefore, the flash width to thickness ratio must be low.

Recent flash gap[35] studies have revealed that forging loads and deformation energy get unnecessarily high when the flash width to thickness ratio exceeds a value of five. Since a sizeable amount of flash forces is required for good die filling, the flash ratio cannot be too low lest die filling will be impeded.

In the present study, all forgings with flash ratios less than $1\frac{1}{2}$ did not fill the dies completely but ratios of between $1\frac{3}{4}$ and $3\frac{3}{4}$ gave very good results.

The choice of flash dimensions in industry seems very much a function of the size of the impression to be filled. Forgers appear to favour higher flash ratios for big impressions and lower ones - say

$1\frac{1}{2}$ to $2\frac{1}{2}$ - for smaller parts. Long hubbed components are generally filled by extrusion and require high flash forces to push metal up their hubs. Their flash ratios should, therefore, be in the higher range. Using the current results and those of Vieregge[35,36] as yard-stick, values of between $2\frac{1}{2}$ and 5 would seem adequate.

Effect of Billet Diameter to Height Ratio

Figs 4.12, 4.13 and 4.19 (later) show that forging load increases as the billet diameter to height ratio decreases. The influence of the variable is marginal; 20% increase in billet diameter to height ratio decreased the force of deformation by only 2.88%. However, the inverse variation of forging load with the billet diameter to height ratio is as expected.

The shorter and wider the billets, the closer they are to the final forging size. Die filling will be easier and temperature losses to the dies will be less.

Apart from this, forging stocks barrel when upset because of friction at the job-tool interfaces and the taller the billet the more important the influence of barrelling on the mode of die filling. For instance, excessive barrelling will cause material to arrive at the die parting line significantly earlier than a billet with a low aspect ratio[25] (also see Appendix 4), and a colder metal will, as a result, be thrown as flash.

Furthermore, contact time between the taller slug and the tools is longer. More heat is transfered to the dies and the yield strength of the material increases. Greater force will, thus, be required to forge the taller billet.

In advising the use of billets with high diameter to height ratios, it is recognised that the size of the cropping machine available often limits the sizes of billets used. But short billets do not necessarily have to be cut from large sectioned bars. The same result will be obtained by upsetting smaller diameter bars to as near as possible to the height of the deepest parts of the die impressions.

Slug upsetting and preforming are not being recommended as new forging techniques. What is being pointed out here is that they offer more, by way of die load reduction, than the breaking of oxide scales and easing of die fill.

It will, however, be ill-advised to forge slugs wider than the impressions into them. When $1\frac{5}{8}$ inch and 2 inch diameter billets were forged into die sets A and B respectively (their respective maximum impression diameters are 1.6" and 1.8"), loads were considerably reduced but die edges "caved" in, filling was incomplete and the forgings produced had laps and tears.

The mode of die filling seems responsible for these observations. In forging the billet shown in Fig 5.0 into the die, for example, the bottom edges of the billet will be sheared and the metal contained within the die tappered. This is similar to the extrusion process where sections leaving the die taper at the exit. The billet metal does not drag along the die wall and may only just have reached the bottom of the die when the crank of the forging press is at the bottom dead centre.

Thus, the die may not fill completely and because of the reduced friction resistance to the flow of the billet metal and the shorter contact time between it and the die (hence the lower rate of

cooling) the forging load will be less.

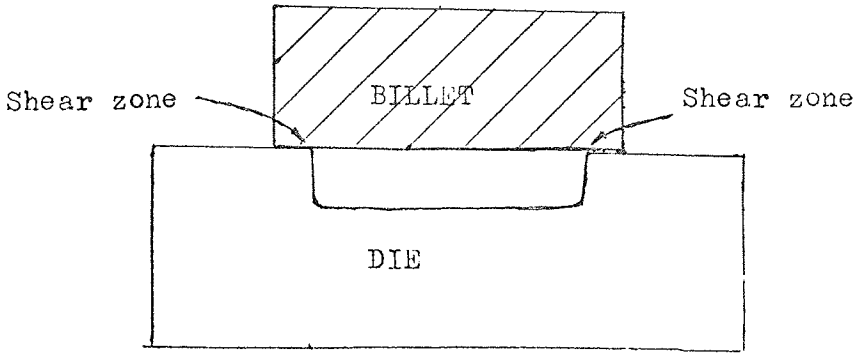

Fig 5.0

A volume of air may also be trapped between the billet and the die (as discussed in page 44). This will act as a cushion and prevent the flow of metal to all corners of the die. This, however, is considered unlikely since some escape channel would have been created when the bottom edges of the billet are sheared in the early stages of the forging operation.

LOADS IN PRESS SELECTION

Die loads in press forging are controlled by the weight and parting area of the forged component, the diameter to height ratio and temperature of the slug, the width to thickness ratio of the flash formed and the shape complexity of the part.

The effects of the flash width to thickness and the billet diameter to height ratios have been discussed in the preceeding text and are, therefore, omitted here.

Effect Of Parting Area

The area at parting line is the most important geometric factor influencing the forging load. It is significant at the 1% level. And the multiple correlation coefficient obtained when forging load is expressed in terms of parting area alone always exceeded 0.8; high enough for reliable load estimation to be made from known values of the parting areas alone.

This is consistent with the industrial forging practice of selecting press capacity for jobs on the basis of their parting areas.

The highly significant effect of parting areas on deformation loads seems easy to explain. Force is theoretically the product of mean stress and area. It is to be expected, therefore, that any increases in area will give rise to an increment in the force.

In any case, the greater spread of metal necessary to cover a wider parting area and the increased frictional resistances to the flow of the metal - both inside the impression and along the flash

land - adequately explain why deformation forces increase with parting areas.

Influence of the Shape Complexity Factor

The regression analysis show that the shape complexity factor, defined in this work as the ratio of the net weight of the forging to the weight of the simplest shape of metal that completely encloses it, is significant at the 1% level for components with stepped flash gutters but less highly significant for parts with parallel flashes. More complex forgings require higher loads to forge them.

The high deformation forces associated with complicated parts is a reflection of the greater effort needed to fill their dies, it being the case that the local yield strength varies more in complex dies than in simple ones. Apart from this, surface areas of complex forgings are often greater. There is thus a wider area of contact between the tools and the workpiece. Frictional resistance to the flow of the slug metal will be greater and the forging load higher.

It is conceded that the shape complexity factor, as defined here, does not adequately reflect the "degree of difficulty" of making all forgings. But all alternative criteria available are only marginally more satisfactory. Of these, Teterin[38] et al's seems the most physically meaningful in that it considers various parameters, e.g. draft angles, corner radii and maximum impression depths, that are likely to define complexity best. Its application, however, to a few of the forgings considered in the present study, showed but little improvement on the level of significance of the complexity factor.

Effects of Temperature

Figs 4.20 and 4.26 show that forging load decreases as slug temperature is raised. The variable is significant at the 1% level and a sensitivity test shows that load decreases 21.5% for a 20% rise in slug temperature. The effect of increasing slug temperature is to decrease its resistance to deformation and hence reduce forces. Fig (5.1) shows the effect of temperature on the yield strengthof EN3B steel, for example.

Thus, for best results, forging stock must be adequately heated to within the recrystallisation temperature of the billet material. It is good practice to soak the billets for a while at the forging temperature. This ensures uniform heating and hence fairly uniform slug resistance to deformation. Too long a soak may, however, cause unnecessary grain growth and cause more oxide scales to be produced.

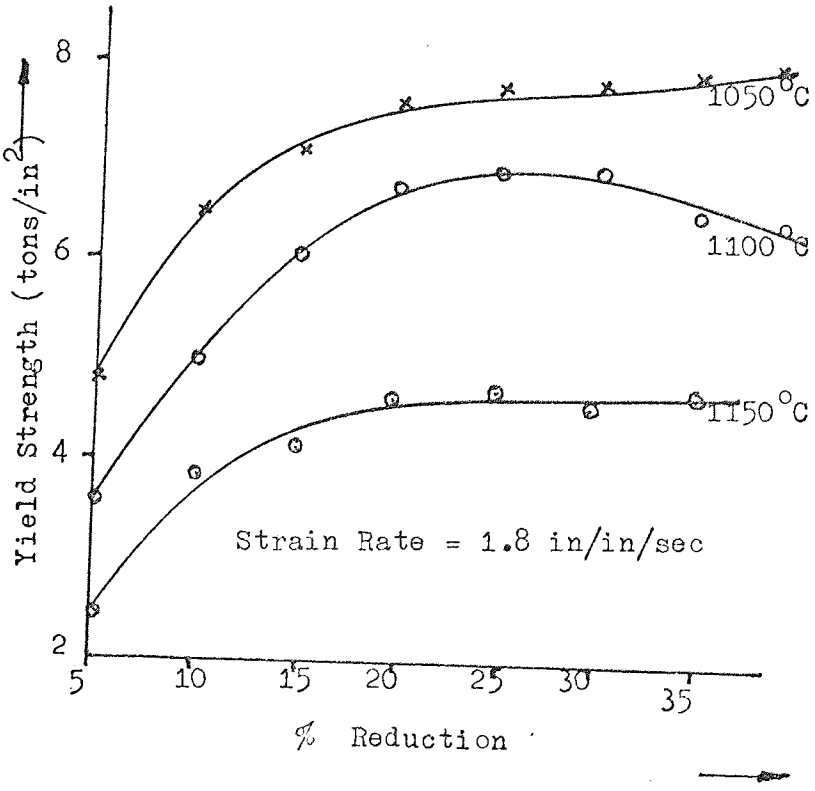

Fig 5.1

Temperature has a considerable effect on die life. Die temperature rises when billets are forged into them, and drops when the dies are lubricated. With time, the temperature rise-drop cycle in the dies causes their surfaces to harden. This minimises die deformation but increases the risk of die failure by cracking.

Temperature also affects the grain structure of forged components. This is true of precipitation hardenable steels, particularly those in the semi austenitic grades. For example[40], forging AM355 alloy steel at too high a temperature (above 1095°C) produces a coarse grain structure which may not transform properly during subsequent heat treatment and may thus leave an undesirable amount of austenite in the finished forging.

Some martensitic steels partly transform to delta ferrite, which reduces forgeability when heated to too high a temperature. Overheating at the centre of heavy sections of some martensitic steel forgings, e.g. 17-4 Ph alloy steel, may cause thermal cracking because of too heavy or too rapid a reduction. Hence their maximum forging temperatures are generally 40°C to 150°C lower than for low alloy steels.

Hot twist tests by Ihrig[41] and Clark and Russ[42] on numerous steels have shown that forgeability increases with temperature until the melting point of the steels is approached (see Fig 5.2), and that forging temperature decreases with increasing carbon content.

	COMPOSITION											
STEEL NAME	C	Mn	Si	Cr	Ni	Mo	Ti	Al	V	Cu	Others	Fe
AM 355	0.13	0.85	0.35	15.5	4.25	2.75	-	-	-	-	0.12N	The rest
17-4 PH	0.04	0.40	0.50	16.5	4.25	0.50	-	-	-	3.6	0.25Cb	The rest

87a

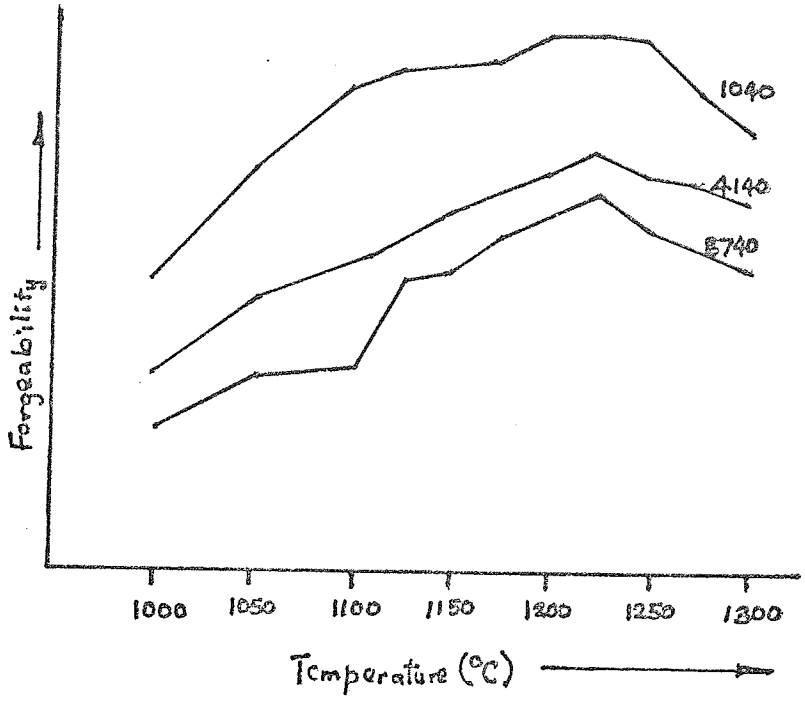

Fig 5.2

Effect Of Flash Shape

Flash and punch loads[25] have been measured when experimenting with different types of flash gutters, to establish the best shape for good die filling. The results plotted in Fig (5.3) show that the closed ended flash shape S_1 has the highest flash and punch forces.

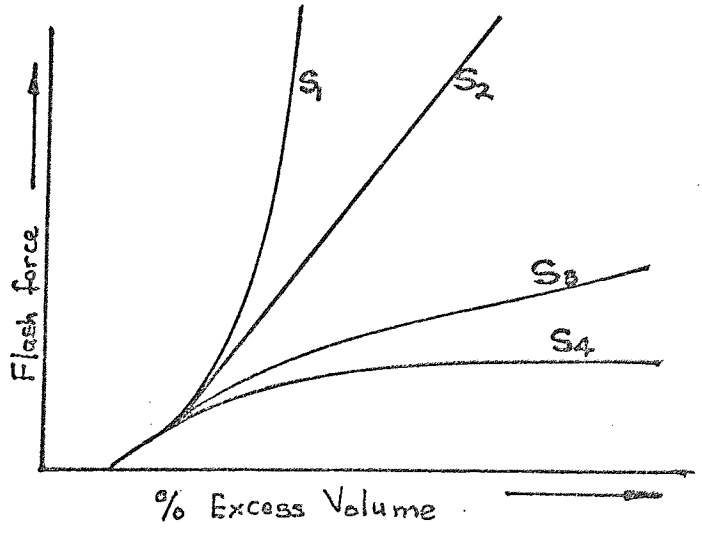

Fig 5.3

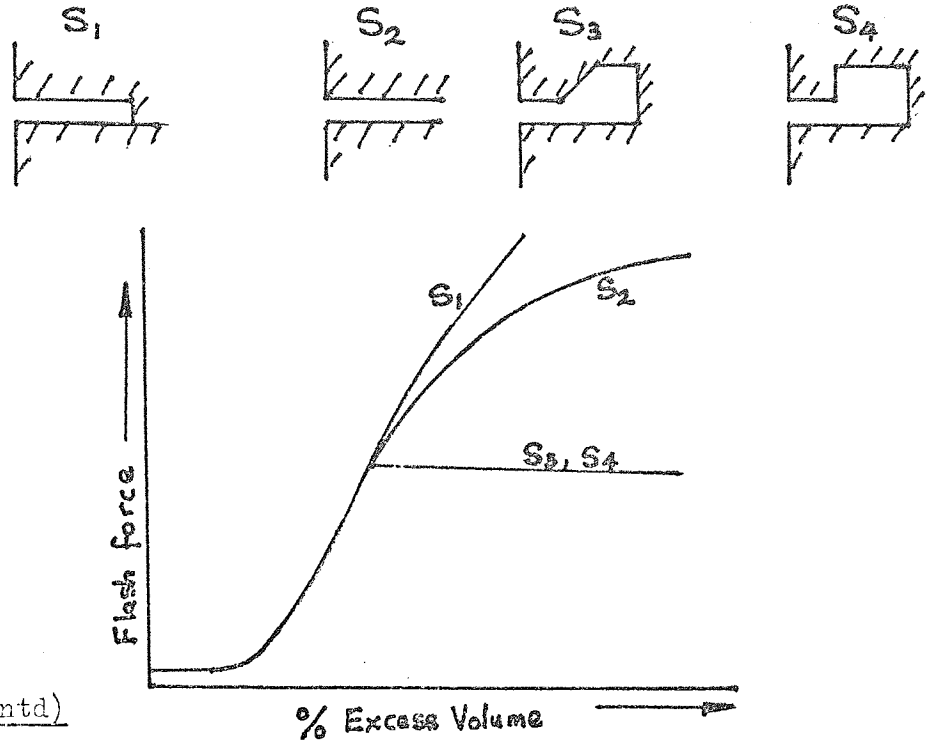

Fig 5.3 (contd)

This is due to the high friction forces resisting the flow of metal into the flash land and the back pressure set up when the metal reaches the end of the gutter. The absence of such a back pressure in flash S_2 explains why its force values are lower than those of S_1.

Flash shapes S_3 and S_4 have the lowest punch forces, but the flash force of S_3 is a little higher than that of S_4. This is probably due to the greater friction resistance to metal flow encountered in flash S_3.

Good die filling is obtained when using shapes S_1 and S_2, because of the high flash forces developed. But the high punch forces and the high rate of die wear associated with high flash forces would not make their use competitive.

A modified version of flash shape S_3 is used in most British forging works. This is not surprising in the light of the results plotted in Fig (5.3); punch loads are low and flash forces are moderately high. While the first advantage can aid overhead costs reduction, the other ensures good die filling.

In the present study, the parallel flash was compared with the open-ended version of die shape S_3 while forging various sizes of billets into two identical dies. The results showed no significant difference in loads when the width of the flash metal was less than that of the land of the die with flash gutter. With greater volumes of billet, loads in the die with parallel flash exceeded those in the other by as much as 16%. This difference is clearly due to the greater flash forces developed in the die with parallel flash because of the increased area of contact between its land and the flash metal, and further strengthens Schey et al's results.

Effect Of Flash Thickness

Figs 5.4 to 5.7 show that forging load increases as the flash thickness decreases. The slopes of the curves are steep and 27% increase in flash thickness causes as much as 40% reduction in load. The rate of increase of forging load with decrease in flash thickness is more rapid when flash thickness is less than 0.115 inches. This is similar to Byan-Grounds[43] earlier observation that press forging loads are considerably high if flash thicknesses of typical carbon and low alloy steel forgings are less than $\frac{1}{8}$ inch, within the temperature range of 1150 and 1200°C.

The inverse variation of forging load with flash thickness is a reflection of the greater deformation necessary to forge thin flashes.

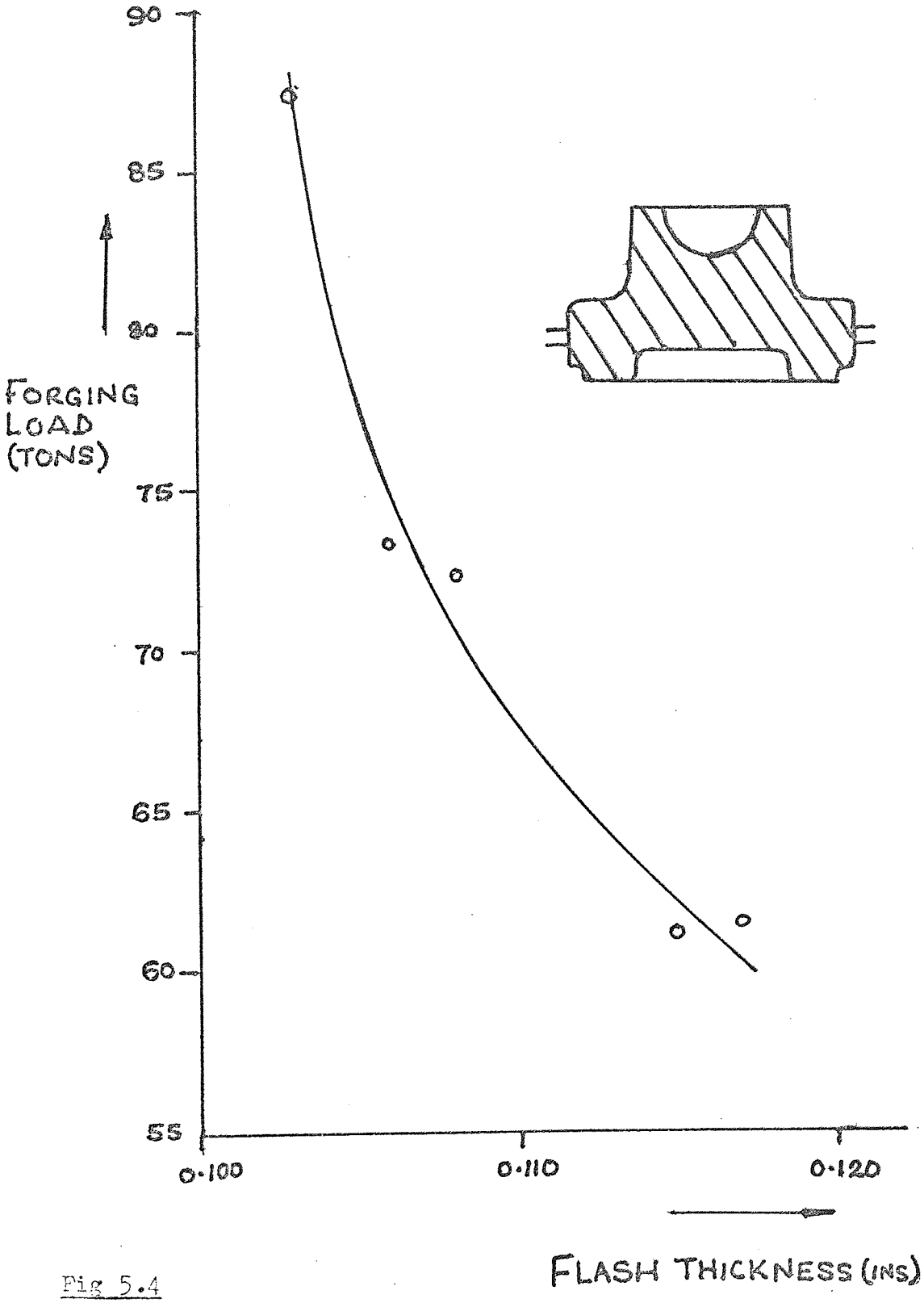
90
85
80
FORGING LOAD (TONS)
75
70
65
60
55
0·100
0·110
0·120
FLASH THICKNESS (INS)

Fig 5.4

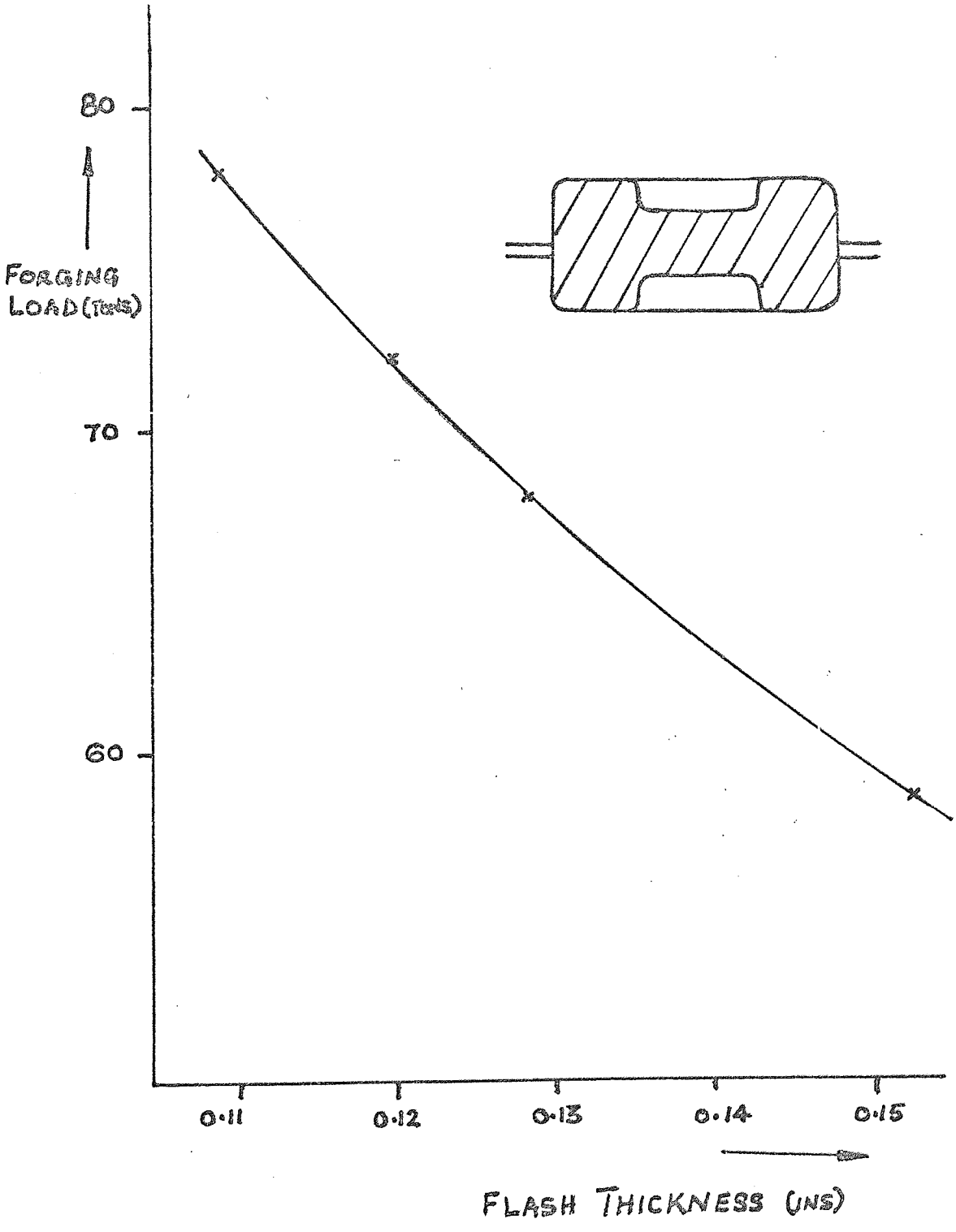
80
70
60
FORGING LOAD (tons)
0·11
0·12
0·13
0·14
0·15
FLASH THICKNESS (ins)

Fig 5.5

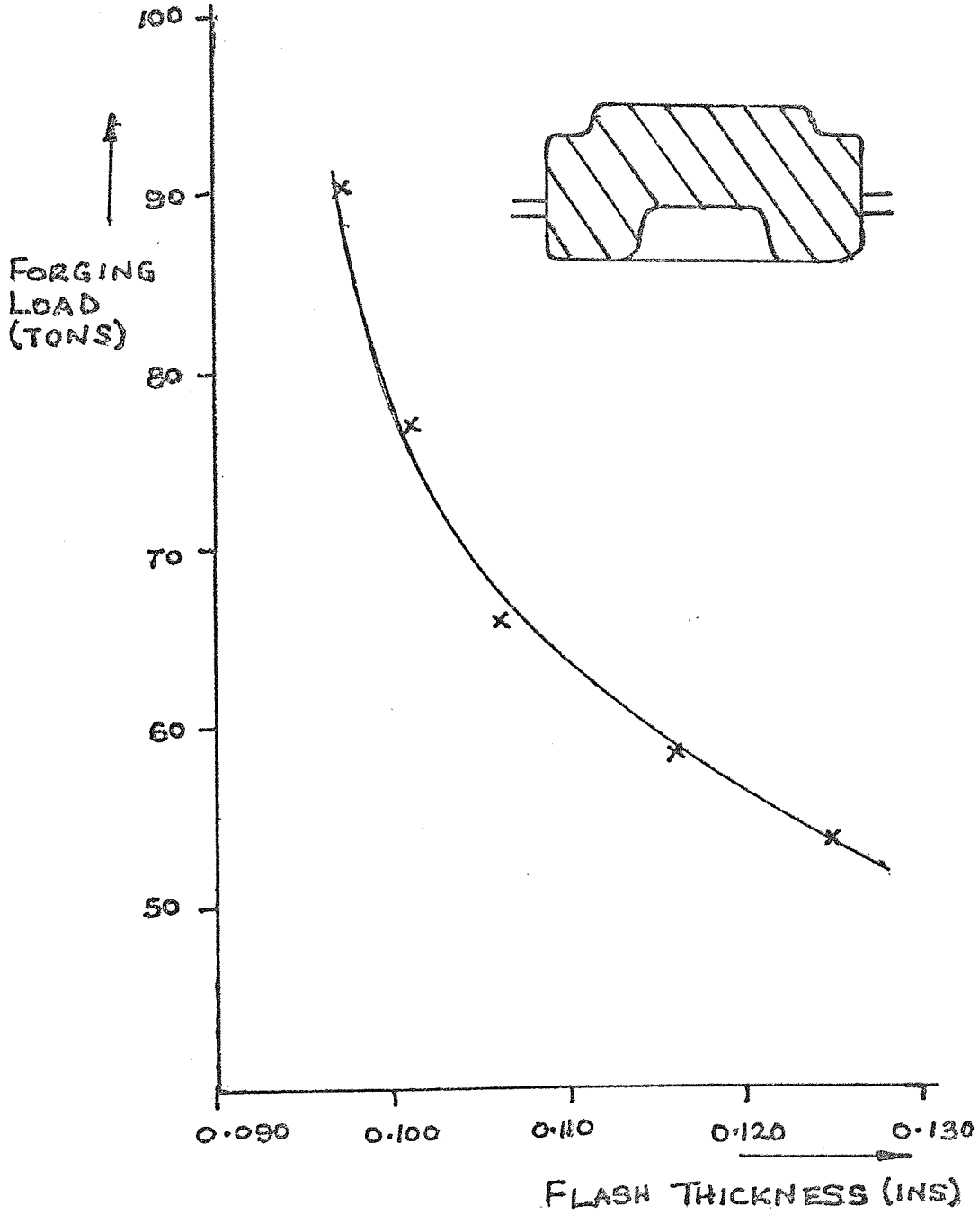
100
90
80
70
60
50
FORGING LOAD (TONS)
0·090
0·100
0·110
0·120
0·130
FLASH THICKNESS (INS)

Fig 5.6

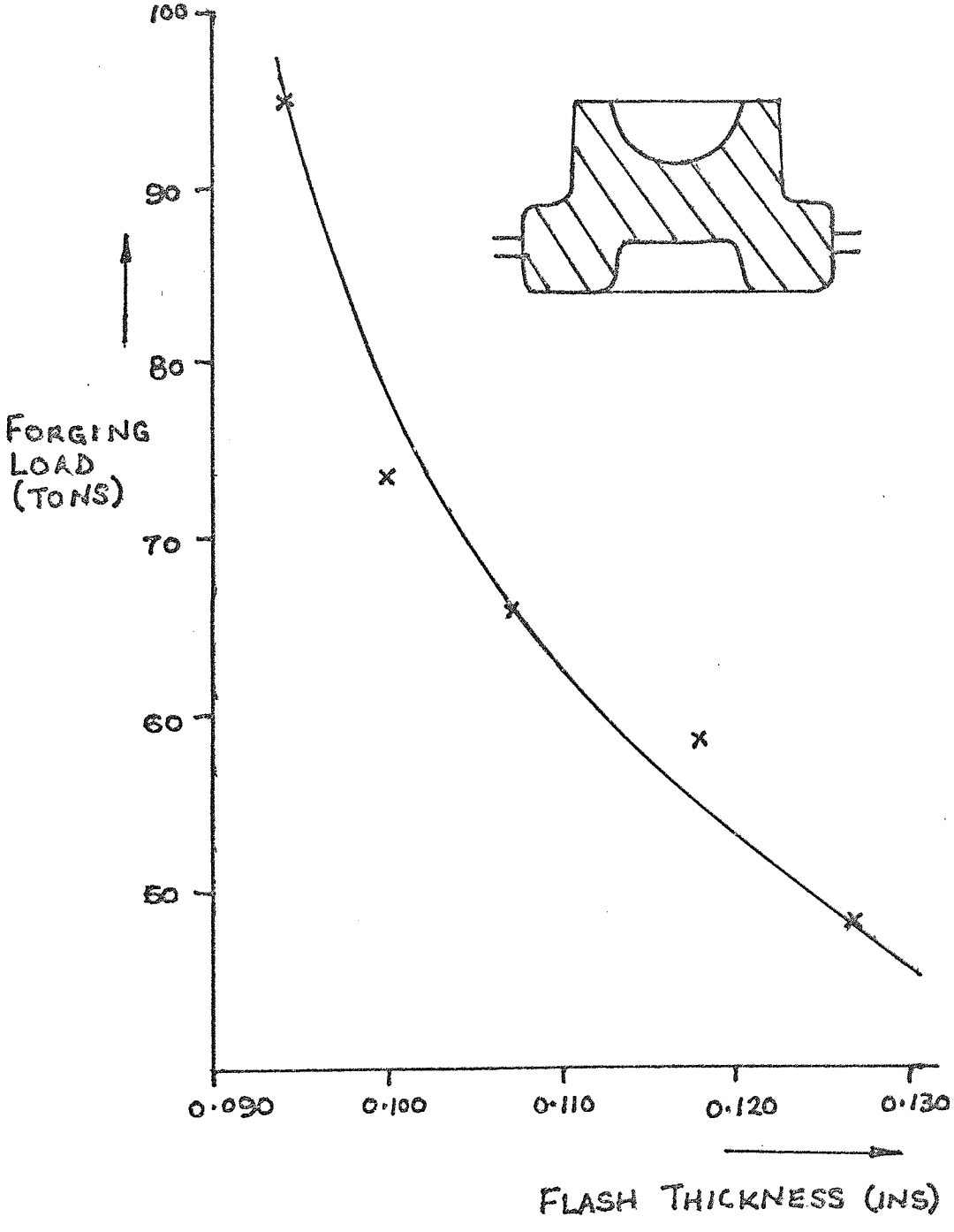
100
90
80
70
60
50
FORGING LOAD (TONS)
0·090
0·100
0·110
0·120
0·130
FLASH THICKNESS (INS)

Fig 5.7

Upset forging tests[40,50] have shown that deformation pressure increases as the reduction in slug height progresses. A greater reduction in flash thickness accordingly results in higher forging load.

Apart from this, thin flashes lose heat to the dies more readily and the attendant increase in their yield strength causes the load to increase.

In industry, flash thickness is always given close attention in die and process design. Forgers realise that the effects of throwing thin flashes are to improve process yields and increase the forces of deformation and vice versa. It is, however, difficult to ascertain what their (forgers') priorities are in terms of choice between thin and thick flashes. While most want to do anything that improves process yield, a good many care more about the forging load.

It seems advisable, in view of the influence of mechanical stressing on die failure and in view of the high costs of die manufacture, to avoid forging too thin a flash without compromising the process yield. This can be done by throwing a moderately thick flash that only just covers the flash land. In this way, smaller capacity presses can be used for such jobs and overhead costs can be reduced, in some cases, by as much as 25%.

Influence of the Amount of Excess Metal

Figs 5.8 to 5.11 show the effect of the amount of excess metal on load for various forgings. All the results were those obtained when forging into dies having flash gutters. It was considered unrealistic to attempt to determine the influence of excess metal in dies with parallel flash since such excess volumes would simply increase the flash

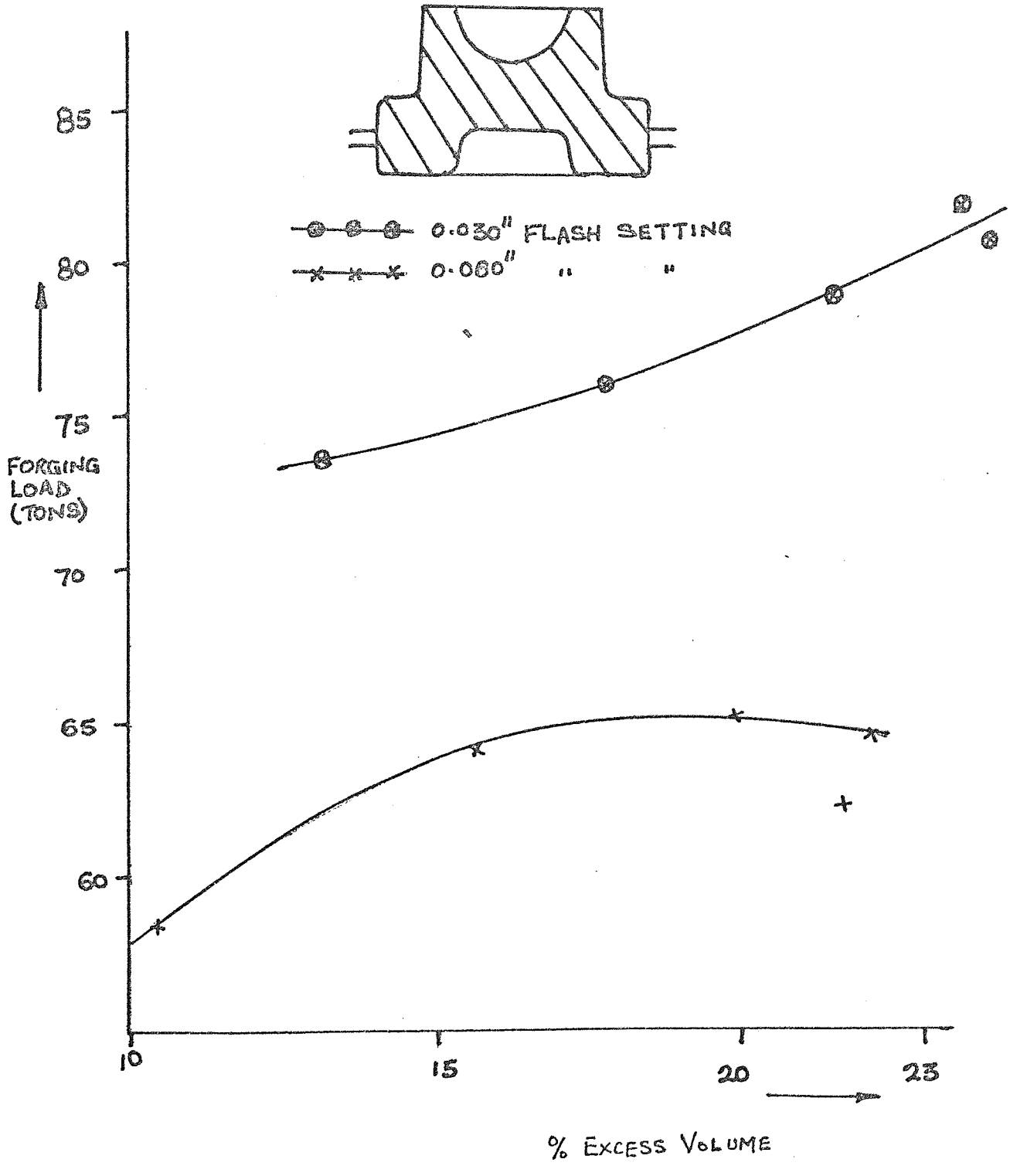
0.030" FLASH SETTING
0.060" " "
85
80
75
70
65
60
FORGING LOAD (TONS)
10
15
20
23
% EXCESS VOLUME

Fig 5.8

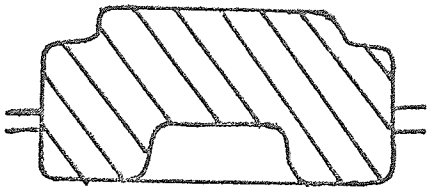

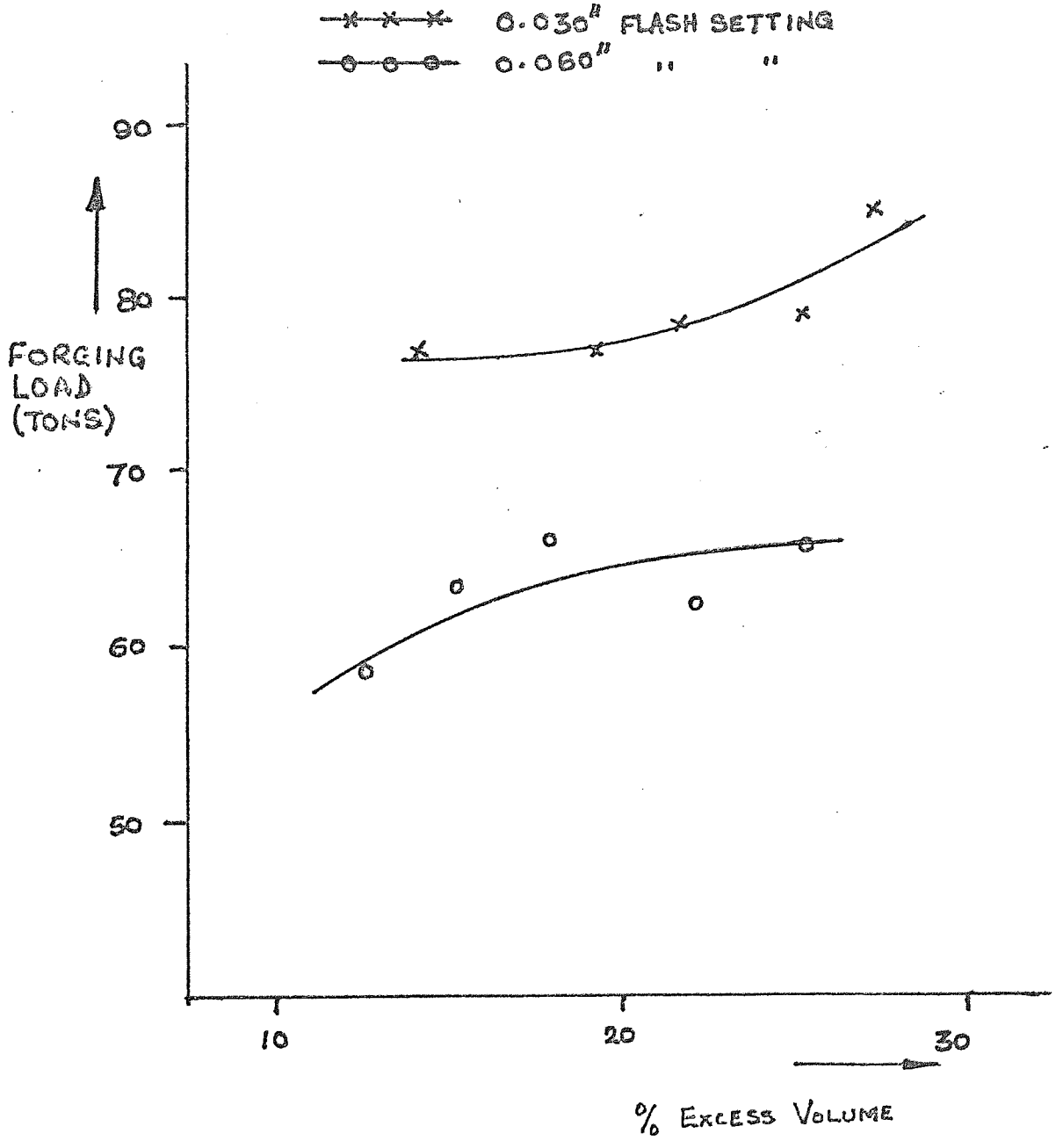
0.030" FLASH SETTING
0.060" " "
90
80
70
60
50
FORGING LOAD (TONS)
10
20
30
% EXCESS VOLUME

Fig 5.9

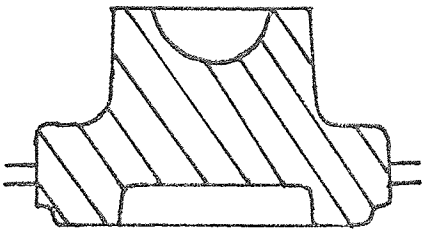

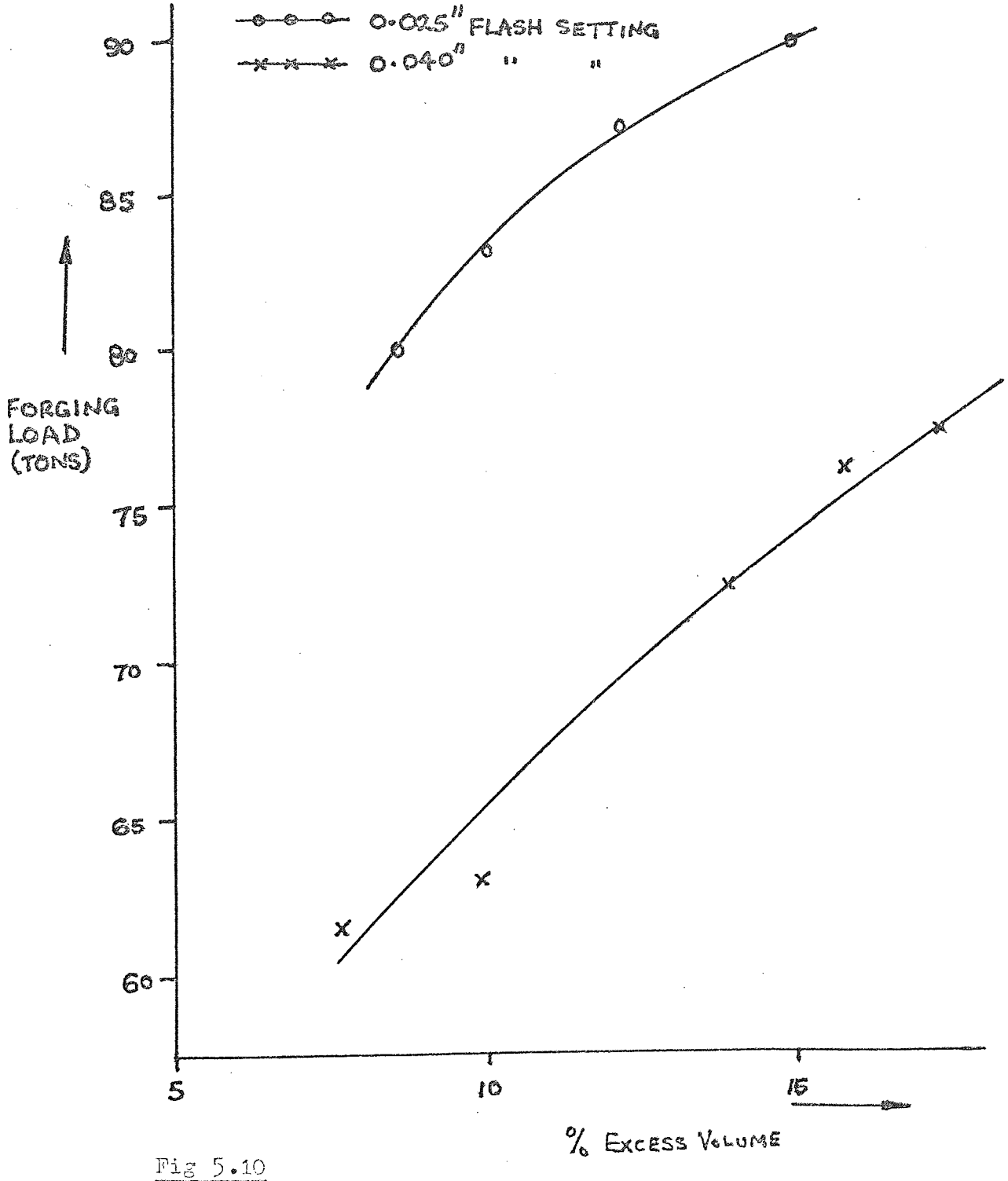
0·025" FLASH SETTING
0·040" " "
90
85
80
75
70
65
60
FORGING LOAD (TONS)
5
10
15
% EXCESS VOLUME

Fig 5.10

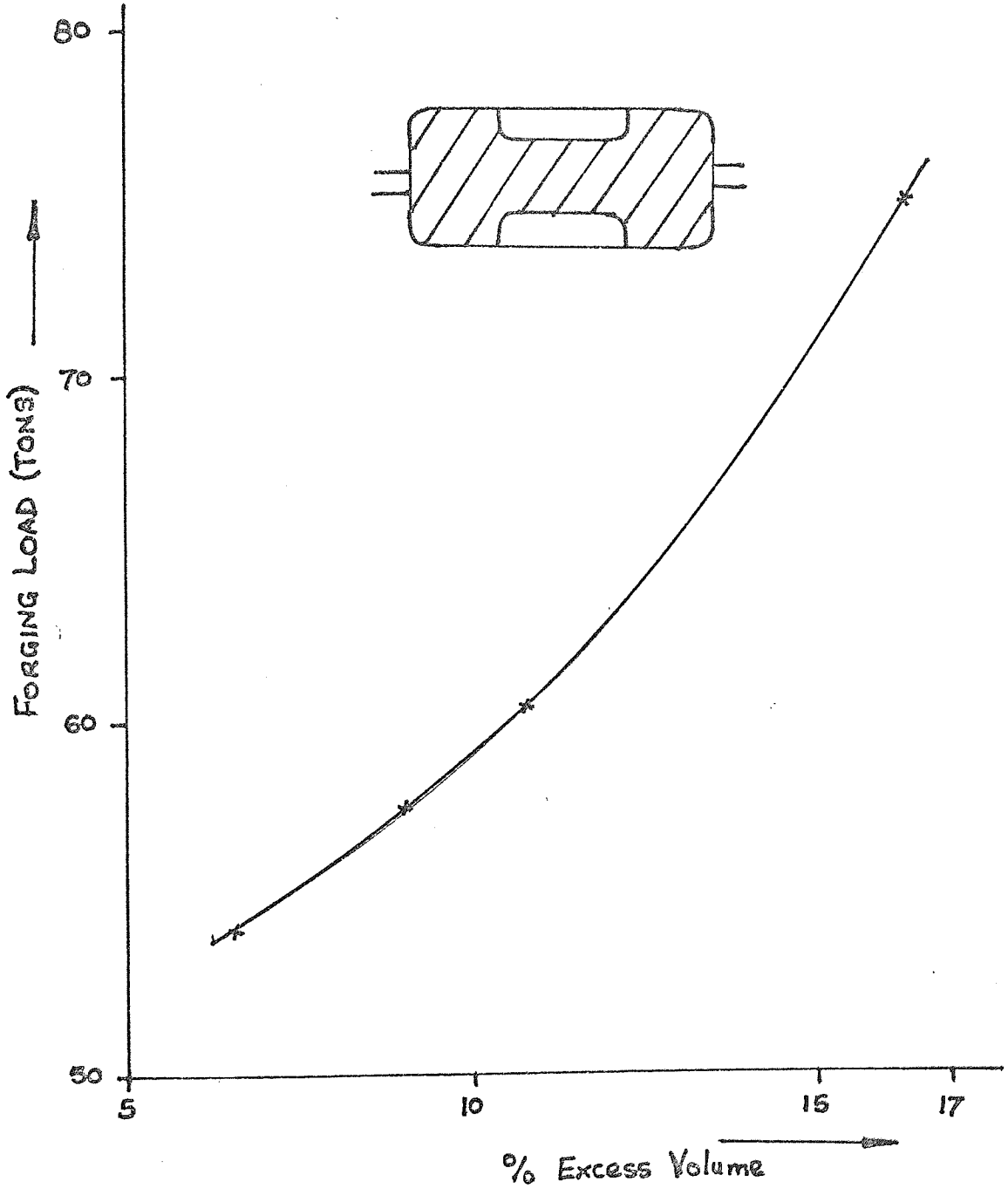

Fig 5.11

area of contact and hence the forging load.

The curves obtained can readily be classified into two distinct categories. These are those which show a progressive increase in forging load as the amount of excess metal increases and those which tend to portray load increases with excess metal to a certain stage and then drops. This later category seems the more reasonable one.

The foregoing view is shared by investigators in Manchester[97] who agree that the effect of increasing the amount of excess metal is to increase the amount of metal thrown as flash without increasing either the frictional resistance to its flow or its resistance to deformation. The theory then is that when a comparatively big billet is being forged, flash is formed before the dies have completely closed. This "initial" flash loses heat to the land and flows into the gutter without being greatly deformed in the final moments of the forging operation. The "real" flash which is then extruded from the metal in the impression, loses little or no heat and in any case generates internal heat as it is further deformed to its final size. Thus, the effective yield strength of the flash metal from a bigger billet will be less. Forging load will accordingly diminish.

This, of course, presupposes that an optimum billet size has caused the load to increase to its maximum value. For the range of forgings considered, the optimum excess volume of metal can broadly be estimated from Figs 5.8 and 5.9 as between 18 and 22 percent.

The other category of curves (those which show a progressive increase in load as the excess metal increases) is more difficult to explain. It is possible that lubrication breakdown occured in the flash land, frictional resistance to flash metal flow increased and

forging load became high. This, however, seems unlikely to explain the observation since lubrication was administered in identical fashion throughout the experiments.

Effect of Radii and Draft Angles

Large corner radii aid die filling and prevent laps and cold shuts but their effect on forging load is insignificant. Aston and Muir[45] have observed that large draft angles promote die failure by mechanical cracking in inner corners. On the other hand, large draft angles make forging ejection easy and slight relief in dies reduces[46] the forging load.

The amount of forging load reduction is, however, only slight. It is, therefore, doubtful if the advantage of this small load reduction and the ease of forging ejection can outweigh the risk of die failure.

Effect of Strain Rate

Fig 5.12 is the result of camplastometer hot compression tests, conducted by the author, on EN3B steel to show the influence of strain rate on its resistance to deformation. The plot shows that the metal's resistance to deformation decreases as the rate of straining is decreased. For 20% reduction in slug height, the resistance to deformation decreased by 33% for 70% drop in strain rate from 6.3in/in/sec to 1.8in/in/sec. Similar results have been reported by Orowan[47], Larke[48], Samanta[49], and Sabroff et al[40].

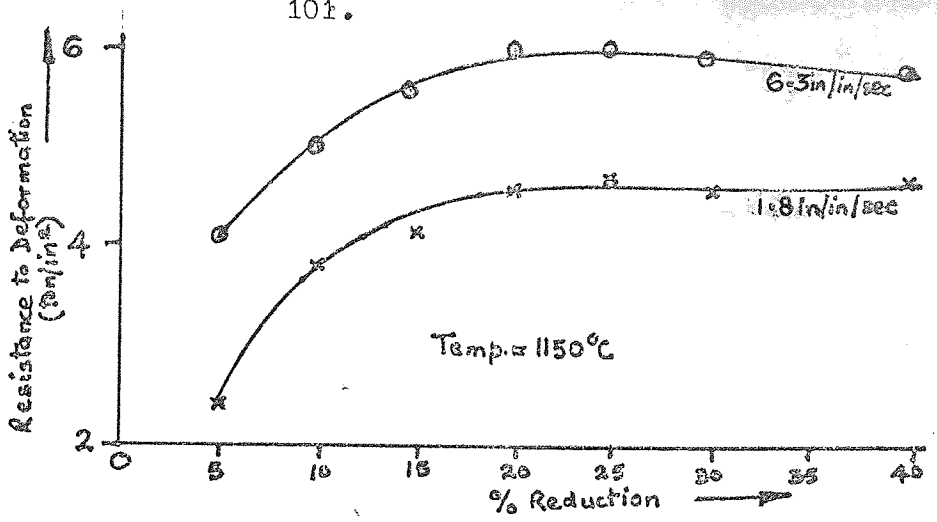

Fig 5.12

The influence of strain rate on deformation forces varies from alloy to alloy. (40) While it is minimal on 4340 steel and 1100 aluminium, effects on the titanium alloy, Ti - 13V - 11Cr - 3Al, is considerable Fig (5.13).

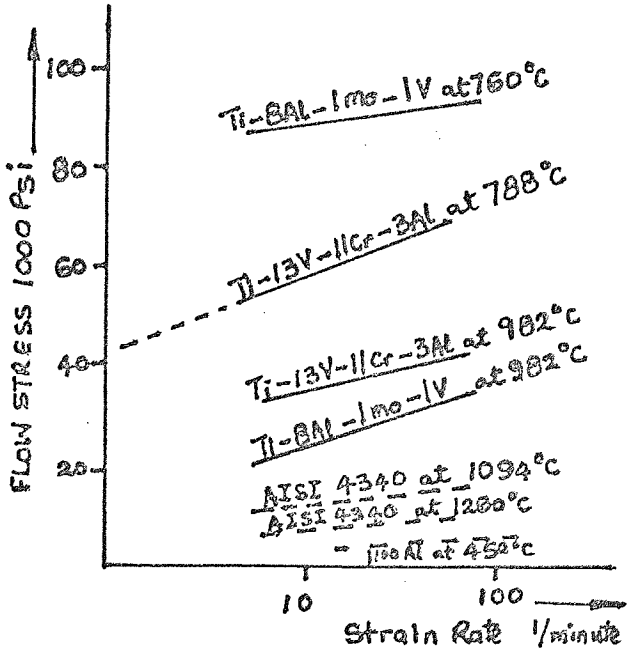

Fig 5.13

Alder and Philip's upset forging tests (50) on low carbon steel have shown that forging pressure increases with strain rate and that the strain effects are more appreciable at higher temperatures Fig (5.14).

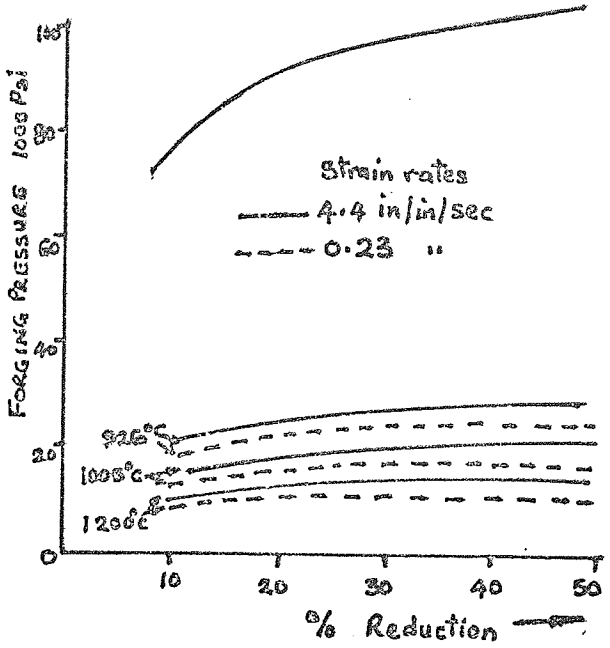

Fig 5.14

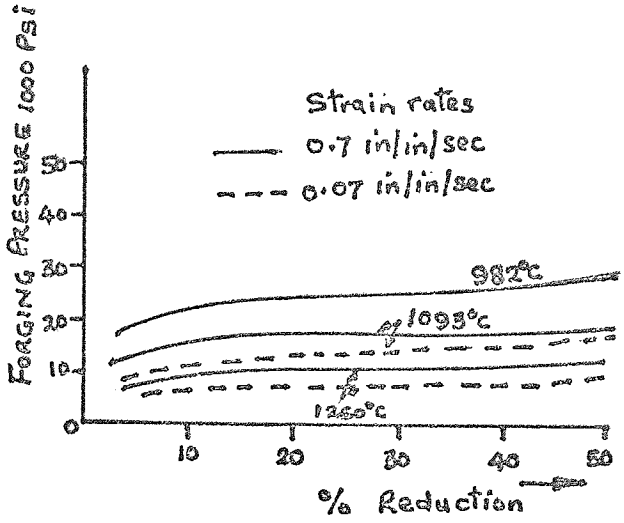

Fig 5.15

Similar results have lately been obtained[40] when AISI 4340 steel were upset forged Fig (5.15).

Deformation energy also increased with strain rate. At 1260°C, upsetting energy more than doubled[40] over a 100 fold increase in strain rate and trebled over a 1000 fold increase.

Effect Of Friction

The three friction zones occuring on surfaces of compression tools, have as yet, not been fully analysed. Nevertheless, friction is known to cause severe barelling when billets are upset.

In hot forging, the billets touch the colder walls of the dies too soon because of barelling. Such contact areas get cooled and the local yield strength of the billet material increases. Thus, the

deformation forces increase and die filling becomes more difficult. Minimisation of friction and hence of barelling should, therefore, be one of the principal qualities of a good forging lubricant.

Compression tests [51] have shown that forging pressure increases with the coefficient of friction. Results obtained during upset forging tests on 2014 aluminium slugs using various lubricants are shown in Table 5.1.

TABLE 5.1

Lubricants	Final Thickness Of Billet (ins)	Final Diameter (ins)	Friction Coefficient	Forging Pressure (lb/in^2)
Silicone Grease	0.103	2.2	0.16	36,000
Flake Graphite In Oil	0.101	2.2	0.15	36,000
25% Flake Graphite + 15% MoS_2 + 5% Mica In Bentone Grease	0.095	2.3	0.13	33,400
Colloidal Graphite In Oil	0.091	2.3	0.12	32,000
Colloidal Graphite In Water	0.086	2.4	0.11	30,000
35% Flake Graphite + 5% Mica In Calcium-Base Grease	0.067	2.7	0.06	23,500

With flaked graphite and mica in calcium-base grease, the forging pressure and the friction coefficient were lowest. Such a lubricant is ideal for wide discs and other flat spreading components where the friction resistance to lateral flow should be minimum. The lubricant's low friction coefficient makes it unsuitable for deep forgings.

Silicone grease and flaked graphite in oil have the worst properties. They combine high friction forces with the least reduction in forging pressure.

The ideal lubricant should reduce deformation forces and minimise die wear by preventing metal contact between the workpiece and the tools. It should also minimise heat transfer from the workpiece to the tools as heat losses from forgings cause the yield strengths of the slug metals to rise.

In all, graphite dispersed in water has shown the best results[51, 52, 53, 56]. Silicone grease and graphite dispersions in oil are less favourable. With the latter, dry lubricant films needed to separate the metal surfaces do not form during the forging operation. With polyalkyleneglycol and diethyleneglycol, high sticking forces which indicate lubrication breakdown were developed.

The main shortcoming of colloidal graphite in water is its poor propellent effect. Oil base graphite lubricants are better in this respect. Sawdust has the best propellent effect but its screening quality is poor as to limit its use in industry.

The current author's experimental study of two lubricants - aqueous colloidal graphite and "forgers' oil" - seem to confirm some of the attributes of colloidal graphite in water reviewed above. The graphite lubricant used in the tests was a sample supplied by Acheson Colloids Ltd[55] and the oil was taken from a stock in use in one of the forging works at which the industrial studies (reported later) were conducted. They were both, therefore, considered of average quality.

About forty billets were forged into a pair of dies using

aqueous colloidal graphite as lubricant. Forging load was recorded for each billet and the hardness of the die impression was measured after the last billet had been forged. The experiment was then repeated with identical dies and billets using forgers's oil as lubricant.

The results showed that forging loads were lower when dies were lubricated with aqueous colloidal graphite than when oil was used by as much as 9%. The die surfaces hardened in relation to their unused states and the rate of hardening was less with the graphite in water lubricant than with oil.

These observations seem to suggest that aqueous colloidal graphite has a better screening quality than oil. In other words, the graphite lubricant is more effective than forgers's oil in minimising contact between the dies and the workpieces.

The primary function of the water in the graphite lubricant is to cool the dies. The water often boiled and dried up leaving graphite particles in the impressions. It is conceivable that such particles formed a more efficient contact barrier between the dies and the deforming metal than the oil lubricant which, no matter how generously sprayed on the dies, always burned off in the last stages of the forging operations.

The result would then be that more billet heat will be lost to the dies when oil is used than will be lost with aqueous colloidal graphite. Thus, the billet resistance to deformation and hence the forging load will be higher in the former case than in the latter.

The hardening temperature of the die material will also be sooner reached with oil.

The load reduction with graphite lubricant as compared with oil may also be partly due to the differing friction conditions existing at the job-tool interfaces. Whereas slight sticking occured with oil, the forgings lubricated with graphite always came out clean without the slightest sign of sticking. It is probable, judging by its burning off, that the oil lubricant brokedown while the graphite particles caused the billets to slip or skid on the dies. The development of higher loads with oil will, thus, not be surprising since flowing metal will encounter a greater frictional resistance.

This would then seem to confirm the suggestion of most of the closed die forging theories reviewed in chapter three that the deformation pressure increases with the coefficient of friction.

On the whole, there is as yet no single lubricant good enough for all conceivable forging conditions. Graphite dispersions in water and oil are good respectively for shallow and deep impressions, and graphite and mica in grease is good for discs. It is, however, claimed (54) that addition of poly-ethylene-glycol may improve the propellent properties of aqueous solutions.

6. INDUSTRIAL EXPERIMENTATION

Forging loads were measured on industrial presses with the aid of instrumented extensometers attached to their frames.

Principle

When dies close during a forging operation, a reaction force is applied on the moving parts of the machine. The force tends to push the dies apart at an instant when the crank is at the bottom dead centre, and thus causes a stretch in the press frame.

The stretch (60) is directly proportional to the resistance to deformation of the material forged and the load applied on the component. Thus the forging load can be determined from the axial strain on the frame of the press.

Experimental Set Up

Fig (6.1) shows the main features of the extensometer used to measure the strains in the press frames. The steel cylinder, housing a two inch strip of hardened and tempered high speed steel, was bolted to the press frame as indicated in the diagram.

Four strain gauges (two on either face) were mounted on the steel strip and connected in a bridge circuit. A power pack was connected across one arm of the bridge and a multi-channel ultra violet recorder was connected across the other.

A 66 inch long tube hung freely from a fixed support and carried a trigger rod, having knife edges designed to suit the steel strip, at its other end. To take a reading, the trigger knife edge was

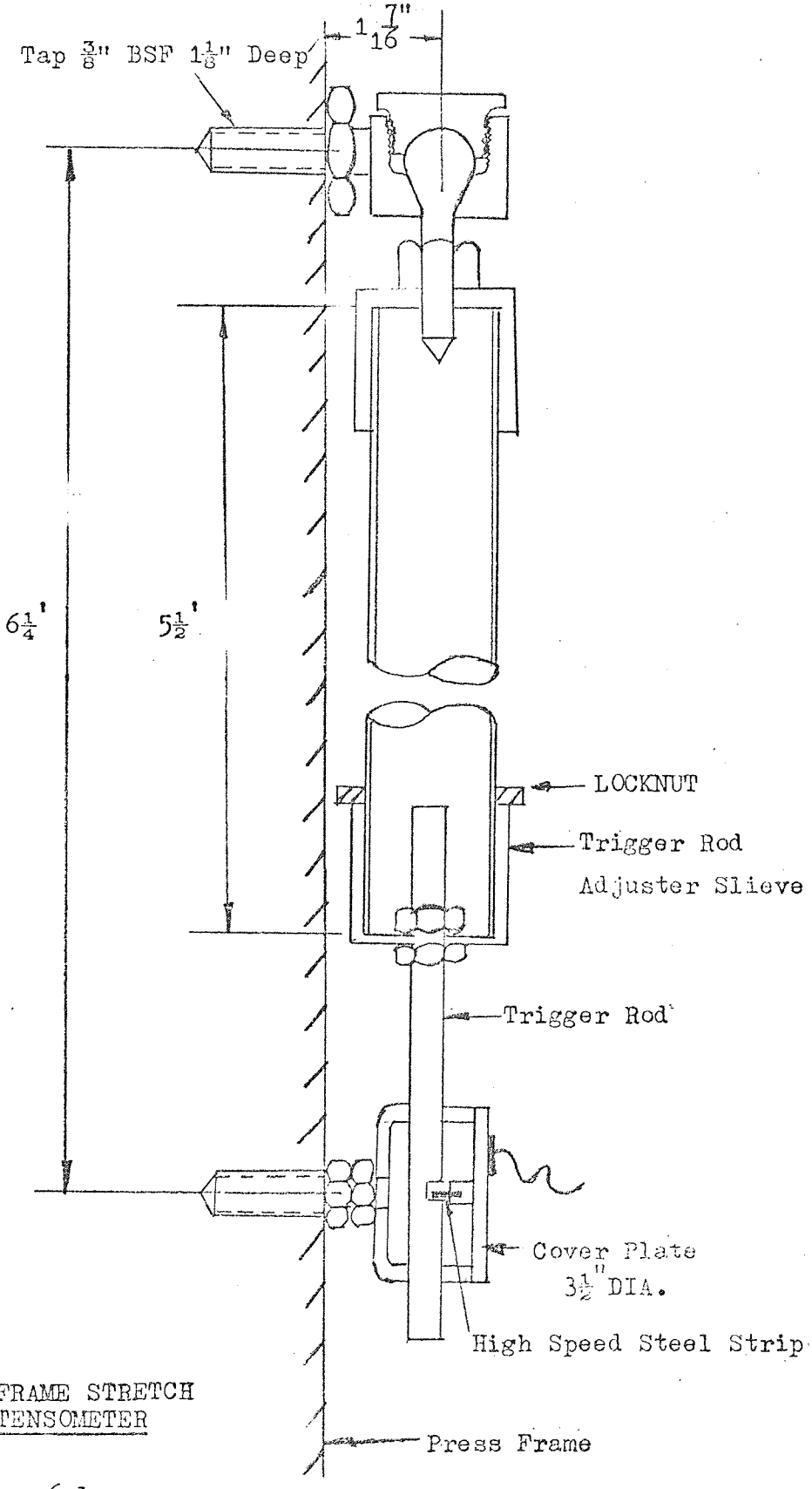

PRESS FRAME STRETCH EXTENSOMETER

Fig. 6.1

made to touch the lower face of the steel strip. When forging commenced, the fixed supports moved apart and the knife edge bent the strip. The bending caused an inbalance in the bridge circuit and a signal proportional to the stretch of the frame was recorded. The product of the height of this trace and the press frame stiffness is the forging load.

Calibration Of the Extensometer

An EN 24 steel load cell, precalibrated on a 300 ton testing machine was used to calibrate the extensometer. The cell was compressed elastically between experimental dies fitted to the press while the extensometer was attached to the frame. The frame extension and the strain on the load cell were recorded on the multi-channel recorder.

Six steel discs, 0.05 inch thick and having the same diameter as the load cell, were then placed (one by one) on it to vary the strain in press frame. The frame strain corresponding to a unit load cell strain was then deduced from a plot of load cell strain versus frame strain. The extensometer stiffness was finally obtained by dividing the load cell stiffness by the frame strain per unit cell strain.

Obtaining The Data

Loads were measured during actual production runs when mild steel billets considered to have been adequately heated were being forged into finishing dies. Other forging data relating to job size and die shape were obtained from relevant die and component drawings.

Colloidal graphite in water was the lubricant and the forgings were classified into two categories - Axi-symmetric or circular, eg. gear blanks and Irregular, eg. connecting rods and spiders. The data for each category were separately analysed.

Forging Variables

The job and process variables considered in the study of circular forgings were similar to those investigated in the laboratory. But the definition of parting area excluded the flash width because it was not practicable to measure the parting diameters of unclipped forgings without disrupting production.

Other geometric parameters considered in the study of irregular forgings were the equivalent parting diameter and the equivalent width. The former was defined as the diameter of a circular part having a parting area equal to that of the irregular forging, and the latter was the breadth of a rectangular part whose length and parting area are equal to those of the irregular component.

The billet diameter to height ratio and the flash width to height ratio were investigated and found highly significant in the laboratory. They have been ignored here. The reasons for abandoning them are given below.

Billet Diameter To Height Ratio

All the billets were upset and preformed before forging them in the finishing dies. It was not practicable to measure the diameter to height ratios just before the finishing operation. They

were, therefore, ignored.

Flash Width To Thickness Ratio

All the dies investigated had flash gutters. The flash width to thickness ratio was, therefore, to be defined as the land width over the flash thickness. It, however, had to be abandoned because it did not vary from forging to forging. This seems a deliberate policy of the works in which the study was conducted.

RESULTS

Circular Forgings

Table 6.1 shows the results when forging load was regressed on the other variables. The table shows that forging load increases with wider parting area and lower forging temperature. It also suggests that complex parts require less load.

TABLE 6.1

Significant Variables	Regression Coefficients	T-Stat Values	Intercept Term	Multiple Correlation
Area At Parting Line (Sq. Inch)	32.7784	5.48	361.9748	0.704
Shape Complexity Factor	565.6566	1.05		
Slug Temperature (^{o}C)	- 0.5293	0.10		

Mathematically,

Forging load (tons) = 32.78 x Parting Area (sq. in)
+ 565.66 x Complexity Factor
- 0.53 x Slug Temp (^{o}C) + 361.97

The variations of forging load with each of the significant factors are shown graphically in Figs 6.2, 6.3 and 6.4. Each plot had been corrected for the effects of the other two variables. Fig 6.5 is the plot of observed loads against those calculated from the regression equation.

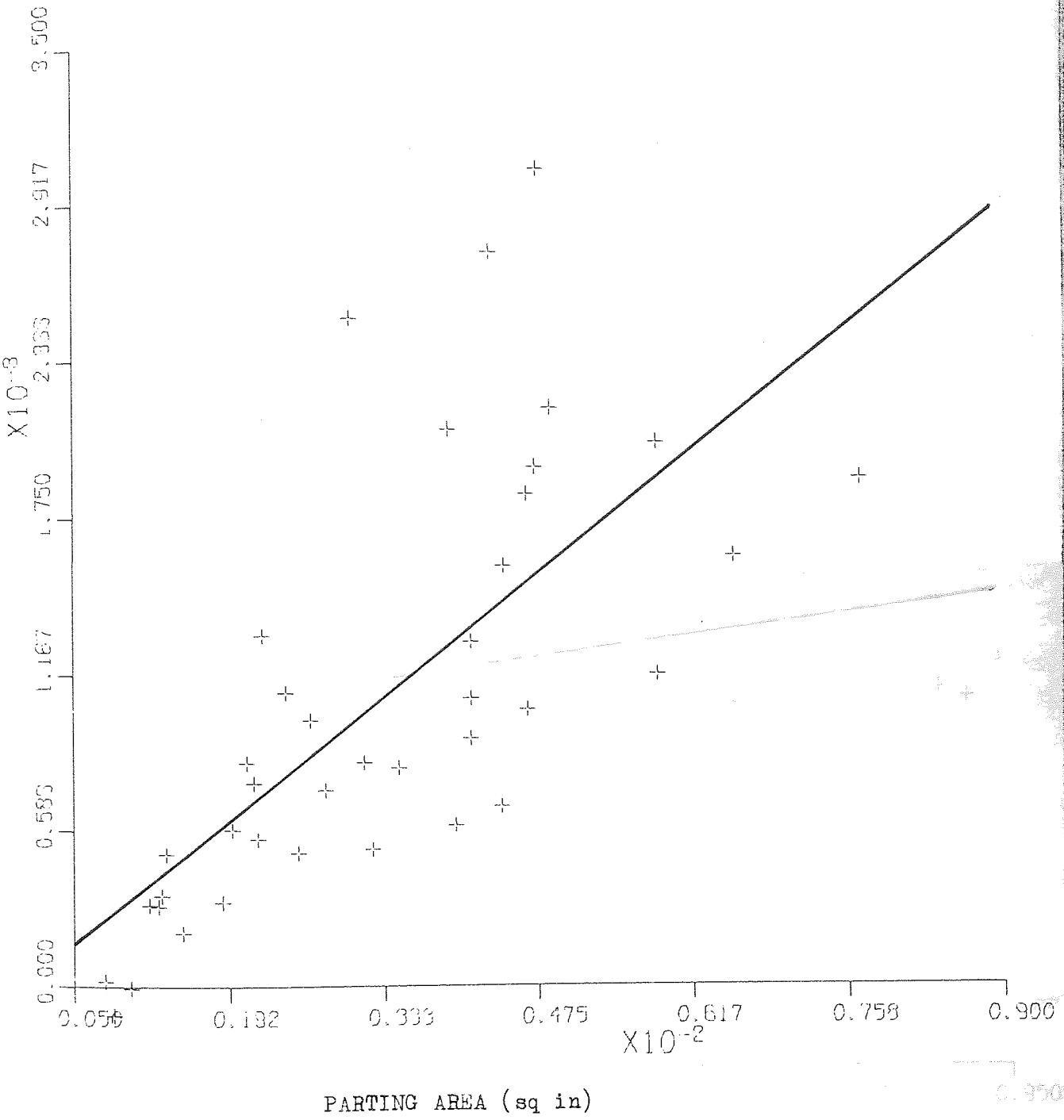
3.500
2.917
2.333
1.750
1.167
0.583
0.000
X10⁻³
0.056
0.192
0.333
0.475
0.617
0.758
0.900
X10⁻²
PARTING AREA (sq in)

Fig 6.6

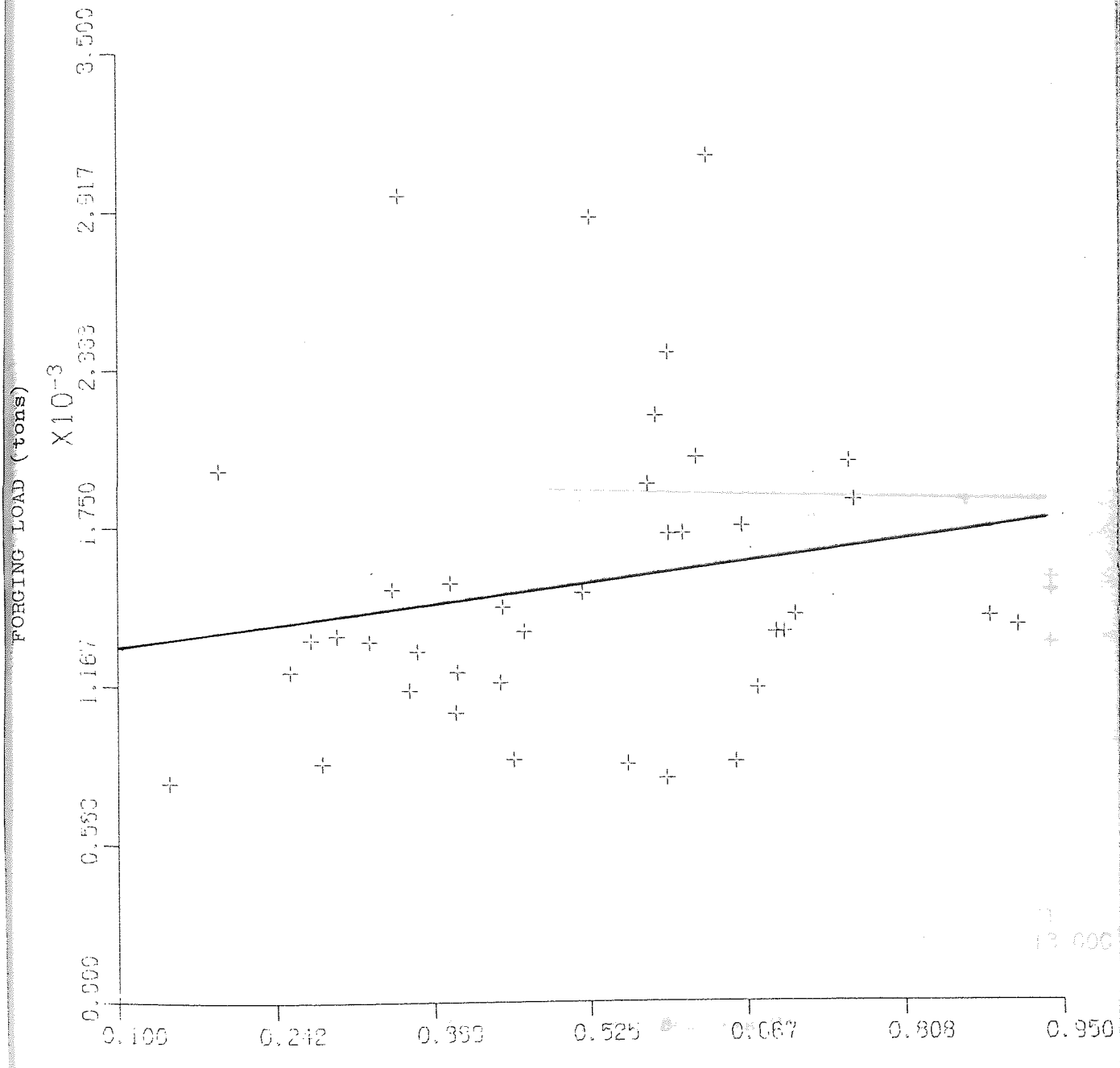
FORGING LOAD (tons)
X10⁻³
3.500
2.917
2.333
1.750
1.167
0.583
0.000
0.100
0.242
0.383
0.525
0.667
0.808
0.950
SHAPE COMPLEXITY FACTOR

Fig 6.7

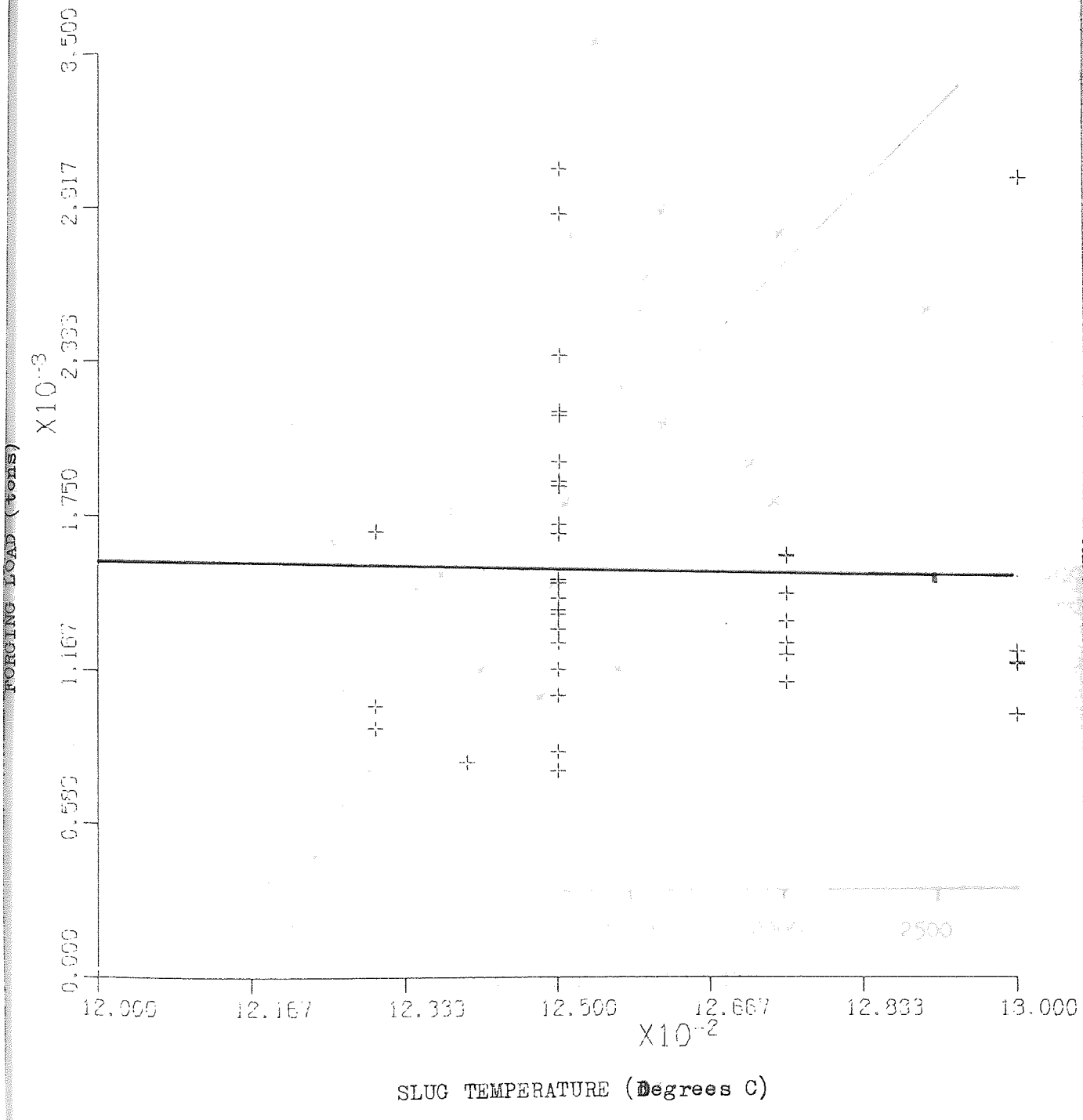
FORGING LOAD (tons)
X10⁻³
0.000
0.583
1.167
1.750
2.333
2.917
3.500
12.000
12.167
12.333
12.500
12.667
12.833
13.000
X10⁻²
SLUG TEMPERATURE (Degrees C)

Fig 6.8

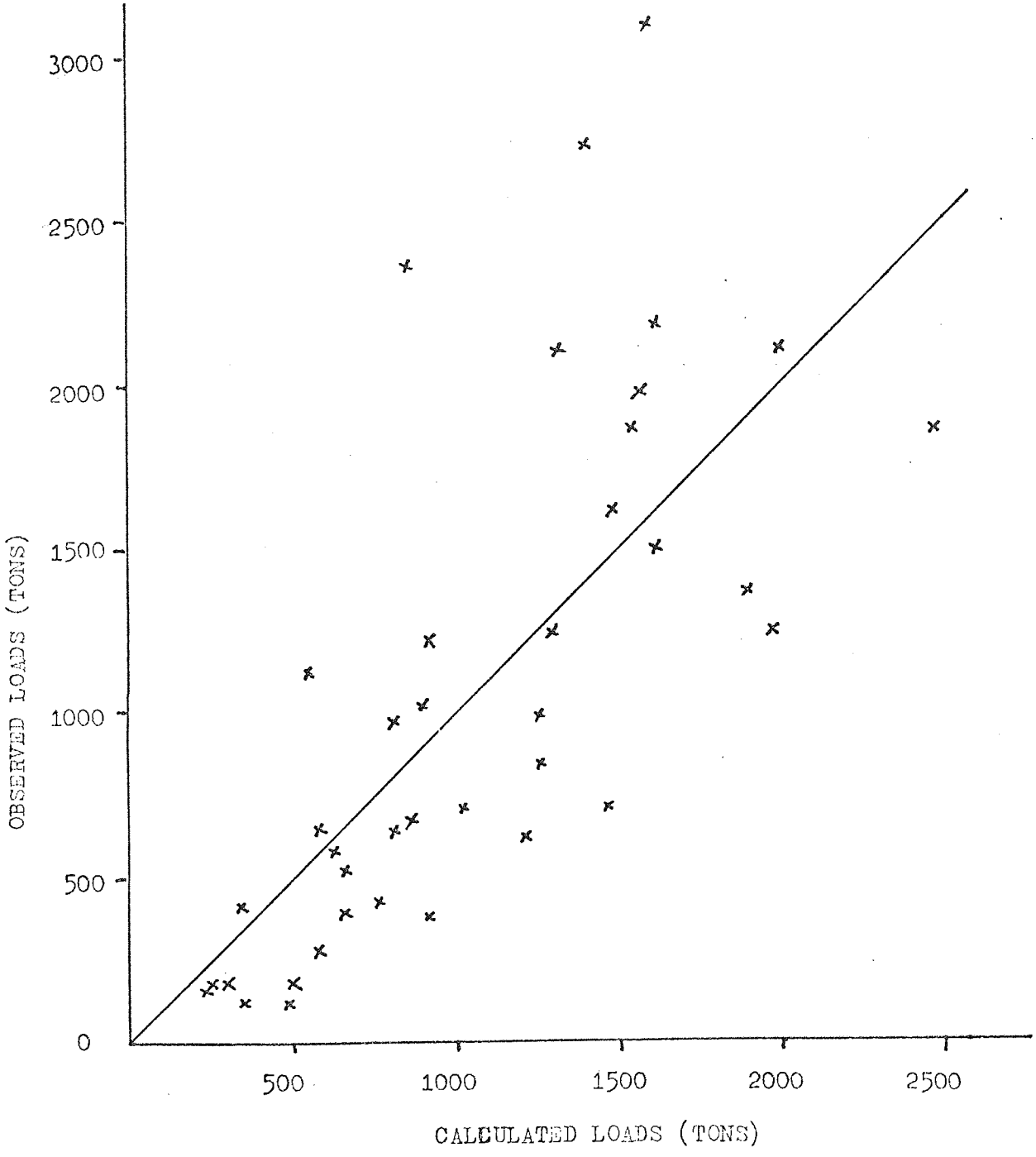
3000
2500
2000
1500
1000
500
0
OBSERVED LOADS (TONS)
500
1000
1500
2000
2500
CALCULATED LOADS (TONS)

Fig 6.5

Irregular Forgings

The results of regressing load on the job and process parameters of the irregular components investigated are summarised in Table 6.2 below.

Forging load increases with parting area and diminishes with increasing slug temperature. More complicated forgings require higher loads to forge them.

TABLE 6.2

Significant Variables	Regression Coefficients	T-Stat Values	Intercept Term	Multiple Correlation
Parting Area (Sq. Inches)	35.7322	5.49	785.6934	0.734
Shape Complexity Factor	-57.8492	0.13		
Slug Temperature (^{o}C)	- 0.2991	0.07		

The mathematical interpretation of the table is that

Forging load (tons) = 35.73 x Parting Area (sq. in)
- 57.85 x Complexity Factor
- 0.30 x Slug Temp (^{o}C) + 785.69

The influence of the parameters on the forging load are shown in Figs 6.6 to 6.8, and observed loads are plotted against the calculated ones in Fig 6.9 .

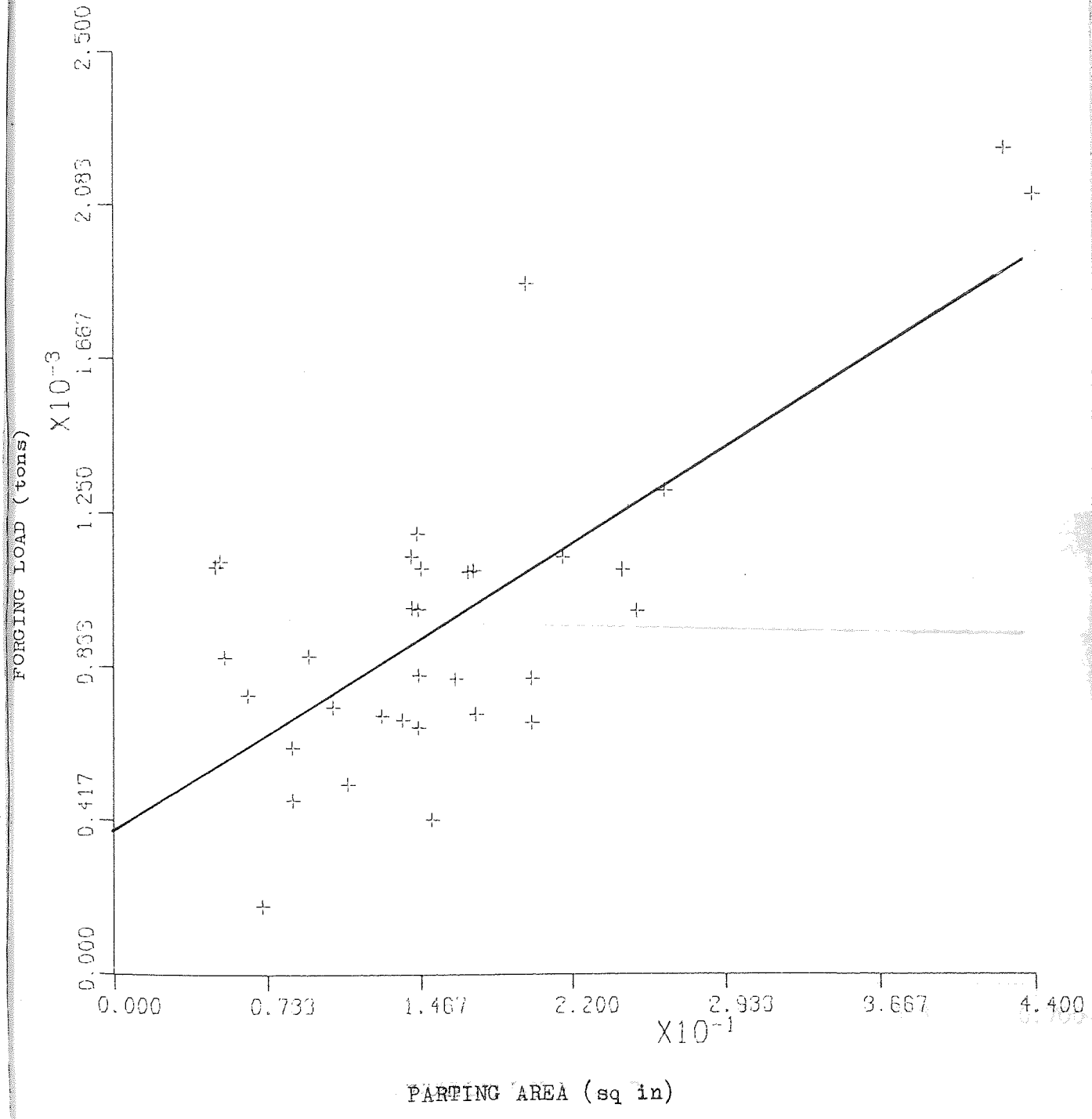
FORGING LOAD (tons)
X10⁻³
2.500
2.083
1.667
1.250
0.833
0.417
0.000
0.000
0.733
1.467
2.200
2.933
3.667
4.400
X10⁻¹
PARTING AREA (sq in)

Fig 6.2

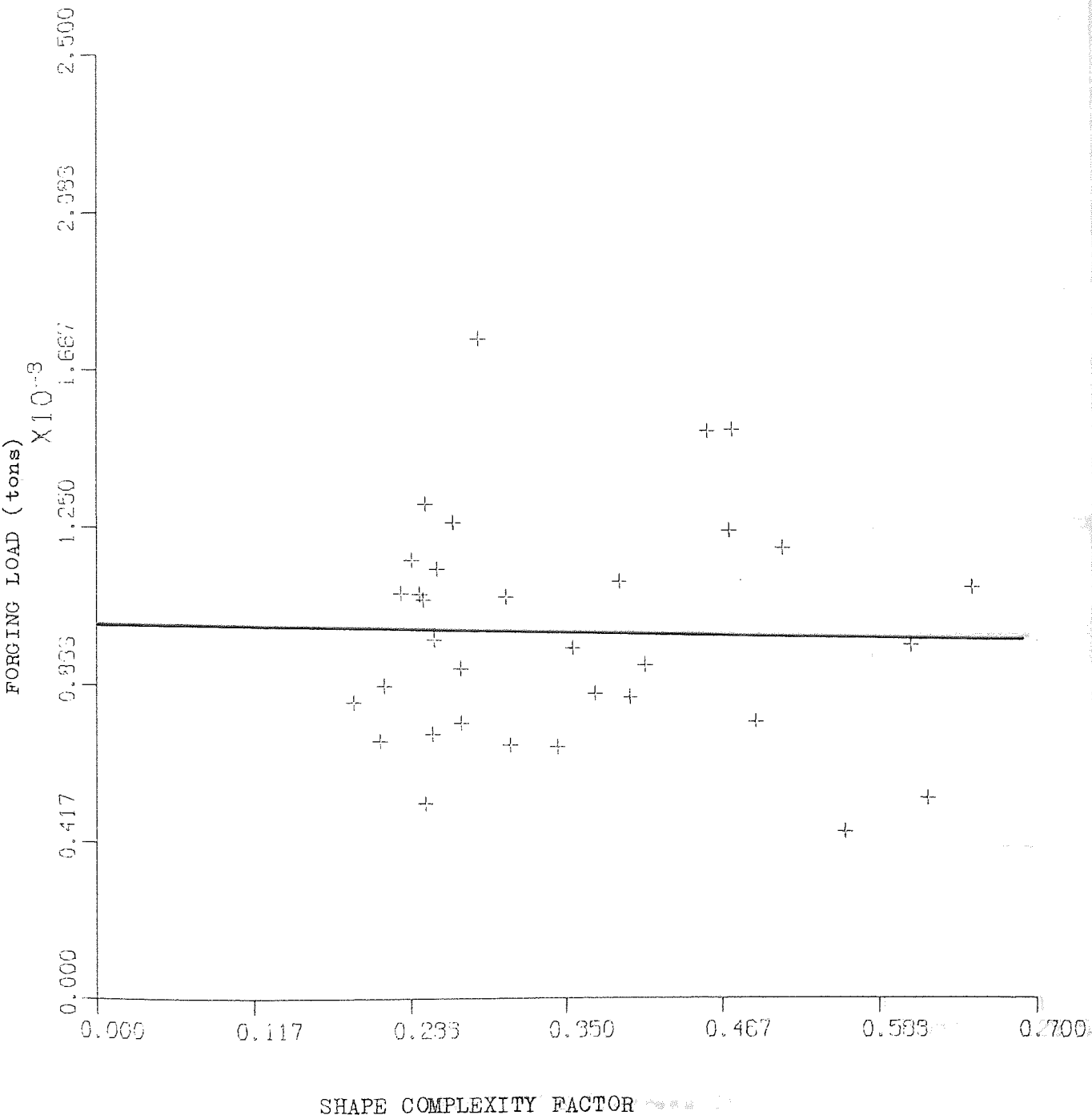
FORGING LOAD (tons)
X10⁻³
2.500
2.333
1.667
1.250
0.833
0.417
0.000
0.000
0.117
0.233
0.350
0.467
0.583
0.700
SHAPE COMPLEXITY FACTOR

Fig 6.3

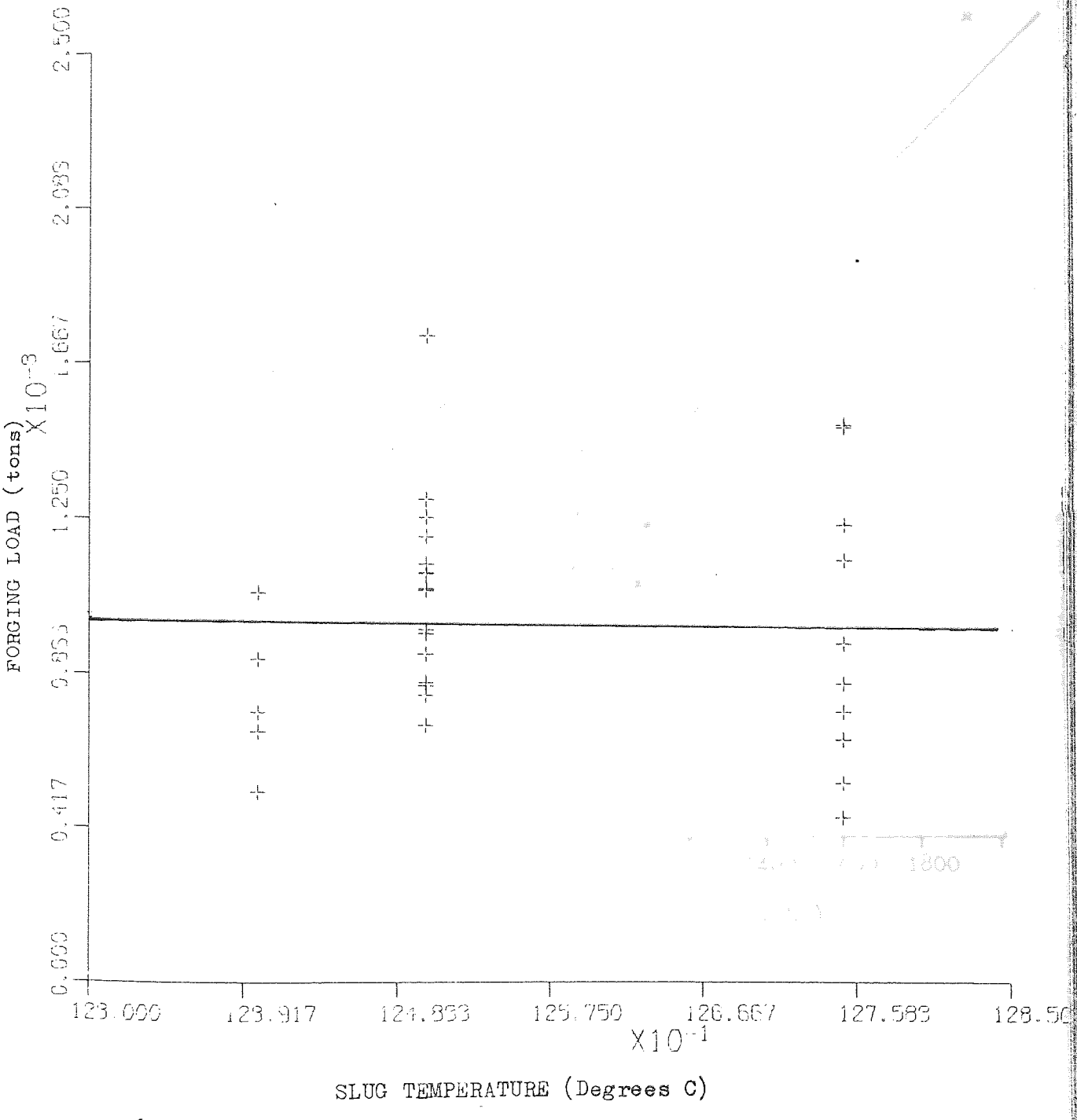
FORGING LOAD (tons)
X10⁻³
2.500
2.083
1.667
1.250
0.833
0.417
0.000
123.000
123.917
124.833
125.750
126.667
127.583
128.50
X10⁻¹
SLUG TEMPERATURE (Degrees C)

Fig 6.4

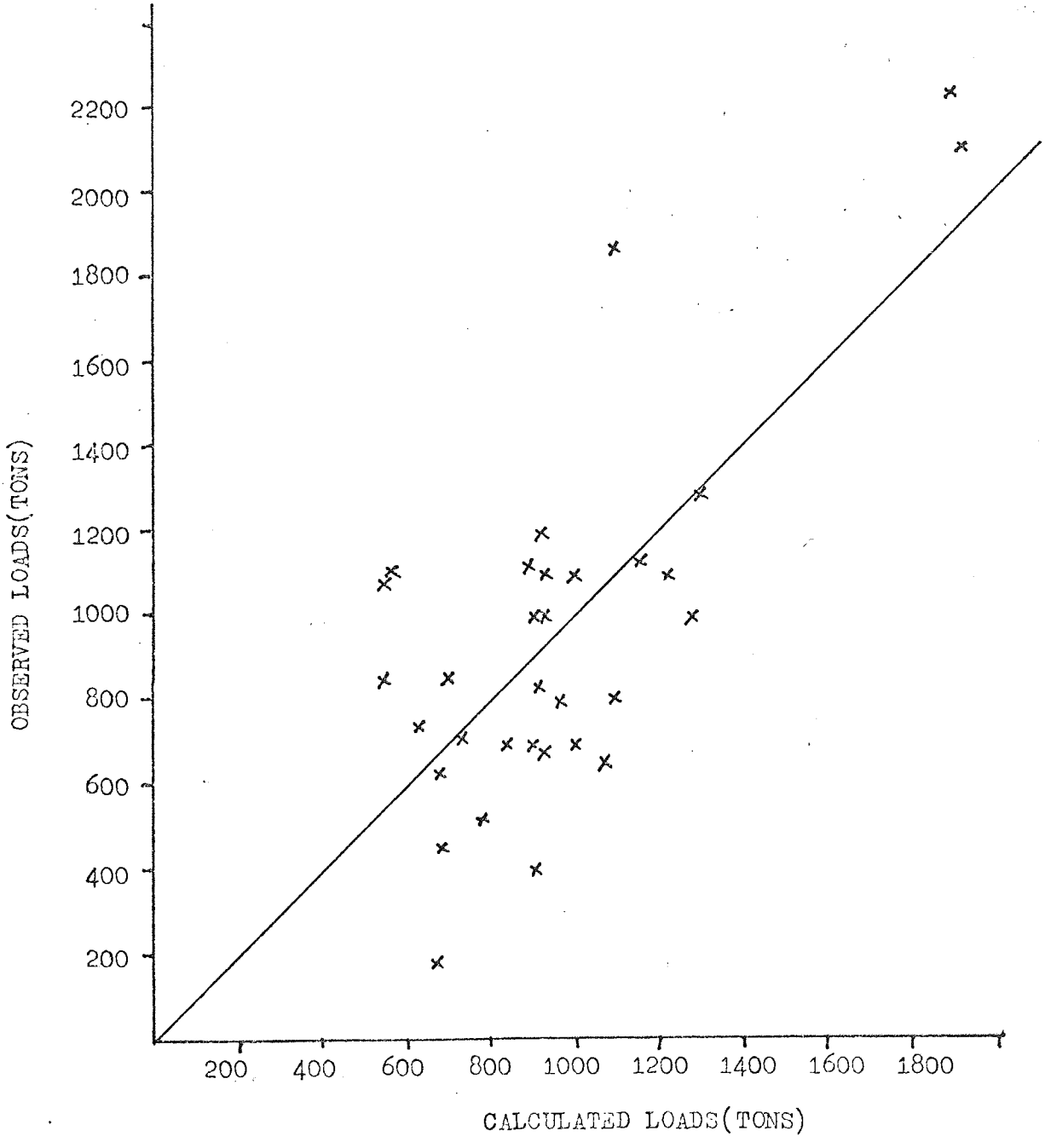
OBSERVED LOADS(TONS)
2200
2000
1800
1600
1400
1200
1000
800
600
400
200
200
400
600
800
1000
1200
1400
1600
1800
CALCULATED LOADS(TONS)

Fig 6.9

DISCUSSION

Both multiple regression results show that forging load increases with parting area and decreases with increasing slug temperature. This is as expected and in agreement with the laboratory study.

But while the results from the irregular forgings data show an increase in load as forging shape becomes more complex, the results of the circular ones suggest the reverse.

It is thought that more complicated parts should require higher loads, partly because of the greater variation in metal resistance to deformation and partly because of the greater difficulty in die filling. This has been confirmed by the laboratory study.

It is somewhat difficult, therefore, to see why loads applied to circular forgings varied as they did with the shape complexity. One probable reason is the contrasting thicknesses of the circular and irregular forgings. While the circular parts were hardly less than $2\frac{1}{2}$ inches in thickness and included a few with long extruded hubs, the irregular components were much thinner with most not thicker than one inch.

If this be the reason, the result seems to confirm the doubts expressed elsewhere about the inadequacy of the definition of the shape complexity, in reflecting the degree of difficulty involved in forging tall components.

Even then, the level at which the parameter is significant is comparable with its level of significance in the laboratory study.

The parting area is significant at the 1%, the slug temperature at 99%.

The insignificance of the variation of forging load with temperature is not surprising. A few of all the forgings investigated were made at 1300°C. The rest were produced at two temperatures (1200°C and 1250°C) and no single component was made at any two of these temperatures. Clearly, an element of bias has been introduced. The significance of slug temperature cannot, therefore, be adequately indicated.

In general, the industrial study confirmed the corresponding results obtained in the laboratory. It showed that the parting area is the most significant parameter influencing the forging load, and thus vindicates the industrial practice of press capacity selection from parting areas of components to be forged.

Correlation between Theory and Practice

The simple upsetting theories reviewed suggest that forging pressure increases with billet diameter to height ratio and the experiments have shown that the reverse is the case in closed die press forging. This seeming disparity between theory and practice is to be expected. In simple upsetting, there are no constraints whatsoever to the spread of slug material as obtains in closed die forging operations. The effect of increasing the billet diameter to height ratio is to increase the contact area between the tools and the workpiece. Forging load will, thus, increase with billet diameter to height ratio because of the increased frictional resistance to the flow of the slug material.

In closed die forging, the taller the billet, the colder the metal thrown as flash and the greater the heat losses to the dies. Consequently, forging load decreases as billet diameter to height ratio

increases.

Most of the closed die forging theories reviewed seek to predict deformation forces from the parting areas of forged components. They also suggest that forging load increases with the flash width to thickness ratio. Both ideas have been vindicated by the results of the experimental studies which showed that press forging loads significantly increase as both the components' parting areas and the aspect ratios of the flashes formed increase. The shape complexity factor which Unksov[11] accounted for in his theory and the slug temperature which both Unksov and Dietrich and Ansel[6] compensated for have been shown to be significant in press load determination.

The pressures predicted by two of the closed die forging theories, namely those of Unksov and Kobayashi et al[12], have been checked against experimental results. The models were used to calculate the pressure required to forge a billet having a diameter to height ratio of 1.025 and a weight of 0.563 pounds into a pair of dies A (shown in Fig 4.1.9) at a temperature of 1150°C and produce a flash 0.067" wide and 0.121 inch thick. In practice, a pressure of 13.8 tons/in^2 was required.

In the calculations, a friction coefficient of 0.20 was assumed for the graphite in water lubricant. Shaw et al[51] have obtained a value of 0.11 for the lubricant during upset forging tests on aluminium samples and Peterson and Johnson's press forging experiments[98] have indicated that graphite containing lubricants usually result in friction coefficients ranging from 0.1 to 0.4. A summary, by Unksov, of the results of several friction investigators has also shown that the friction coefficient of graphite in various types of solvents varies between 0.1

and 0.2 during extrusion and piercing in closed dies. The assumed friction value can, therefore, be considered adequate.

To use Unksov's model (Equation 3.22, Page 19) , values must be assumed for the factor "Z" accounting for die complexity and the un-evenness of stress and cooling states of the forging and the factor "m" which reflects the differences between the resistances to deformation of the metal in the die impression and that in the flash land. Unksov has suggested that Z varies between 1.5 and 2.0 for hot metal working operations. The lower value of 1.5 was used in the calculations because of the simplicity of the die shape under consideration. For the factor m, a value of 1.1 was assumed. This corresponds to a 5% difference in the flash and forging temperatures of components made of EN3B steel. This seems a realistic value since, as far as the author can ascertain, no investigation has revealed a greater temperature differetial between the body of a component and its flash.

The only unknown quantity now left in the equation is the height h_k of the metal deforming in the last stages of the forging operation. Unksov has not suggested how to determine its value but has indicated that pressure values higher than those occuring in practice will be obtained if h_k is assumed to be equal to the height h_f of the flash. The author's calculations showed this to be the case. When h_k was assumed equal to h_f, a pressure value of 17.8 tons/in^2 which represents a 29% over-estimation was obtained. The theory (Unksov's) agreed with practice when h_k was assumed equal to $1.3h_f$.

It is evident from the foregoing that Unksov's model is bedevilled by too many factors whose determination can hardly be precise.

It is possible to obtain accurate figures for factor m by experiment but the determination of Z is less certain and the height h_k of the metal deforming in the last stages of the forging operation can probably only be determined approximately by studying interpenetration of dead metal zones in the forging stock.

Unksov's theory takes account of most of the load influencing parameters in closed die forging. If factor Z, whose determination at the moment is largely intuitive, can be readily assessed it seems likely that the model can be satisfactorily employed for press shop load estimations.

The application of Kobayashi et al's model to the forging data listed earlier yielded a pressure of 8.57 tons/in^2. This represents a 37% underestimation of the forging load. It must be said, however, that whereas Kobayashi et al defined the effective stress $\bar{\sigma}_o$ (see equation 3.33, Page 26) as the instantaneous resistance to deformation of the billet material at the moment of peak loading, an average yield stress value has been used in the calculations. Even then, the difference between these two stress values must be only slight and cannot, therefore , explain the wide disparity between this theory and practice. Possible reasons for this discrepancy have been put forward in chapter three. A pressure value of 14.35 tons/in^2, which agrees broadly with the experimental results, was obtained when a friction coefficient of 0.4 was assumed.

7 DIE STRESSES

Stresses in forging dies are mainly mechanical and thermal, due respectively to the applied axial loads and to the contact between the dies and the hot deforming metal.

Apart from other physical and metallurgical factors they determine the mode of failure of most forging dies. Thermal shock speeds die wear and mechanical fatigue - the cumulative effect of continual mechanical stressing - causes cracks to develop in die corners.

In general, each forging cycle involves the crushing of a hot slug in a colder pair of dies. The temperature of the latter is raised mainly by conduction and then suddenly dropped by spraying lubricants into them. Thermal stresses are thus developed in the forging dies.

The rise - drop cycle of the die temperature also has a characteristic of hardening the die surface. This reduces the chance of die deformation but increases the risk of die failure by cracking.

The thermal stress developed in a die when a billet is forged into it can be determined approximately by calculating the temperature distribution in the die and using thermoelastic theory to deduce the stress.

7.1 Temperature Distribution

By considering heat balance in an element of a forging die and assuming that heat transfer is by conduction alone, it can be shown that the temperature T at a point (x, y, z) in the die, time t after being in contact with a hot billet is given by

$$\frac{\partial^2 T}{\partial x^2} + \frac{\partial^2 T}{\partial y^2} + \frac{\partial^2 T}{\partial z^2} + \frac{H}{K} = \frac{c\rho}{K} \frac{\partial T}{\partial t} \qquad \ldots\ldots\ldots \quad 7.1.1$$

where K is the thermal conductivity of the die material (assumed constant), H is the rate of internal heat generation, c is the specific heat and ρ is the density.

If H is ignored, then

$$\frac{\partial^2 T}{\partial x^2} + \frac{\partial^2 T}{\partial y^2} + \frac{\partial^2 T}{\partial z^2} = \frac{1}{a} \frac{\partial T}{\partial t} \qquad \ldots\ldots\ldots \quad 7.1.2$$

$$\text{i.e.} \nabla^2 T = \frac{1}{a} \frac{\partial T}{\partial t} \qquad \ldots\ldots\ldots \quad 7.1.3$$

where $a = \frac{K}{c\rho}$ is the thermal diffusivity of the die material.

In cylindrical co-ordinates, the laplacian operator ∇^2 is given by

$$\nabla^2 = \frac{\partial^2}{\partial r^2} + \frac{1}{r} \frac{\partial}{\partial r} + \frac{\partial^2}{\partial z^2} \qquad \ldots\ldots\ldots \quad 7.1.4$$

Assumptions And Boundary Conditions

Apart from assuming that heat transfer from the billet to the die is by conduction alone, other assumptions to be made include

(a) that the preheat temperature of the die is constant throughout the die surface.

(b) that the billet temperature is constant throughout its section.

(c) that at all times the temperature of the free surfaces of the die remains constant.

(d) that the billet is placed centrally in the die, and

(e) that the centre of the die impression attains the billet temperature as soon as contact is made with it.

The following boundary conditions can thus be formulated

(1) $T = To$ (die preheat temperature) at $t = o$ at all points on the die surface.

(2) $T = To$ for all values of t in areas where there is no contact with the billet material.

(3) $T = T_1$ at $t = o$, $r = o$, $z = o$.

Solution of $\nabla^2 T = \frac{1}{a}\frac{\partial T}{\partial t}$ By Finite Difference Method

A complete solution of the differential equation for temperature distribution can be obtained by superimposing a grid of small squares on the die profile as in Fig (7.1) and integrating from point to point.

In cylindrical co-ordinates, the equation is

$$\frac{\partial^2 T}{\partial r^2} + \frac{1}{r}\frac{\partial T}{\partial r} + \frac{\partial^2 T}{\partial z^2} = \frac{1}{a}\frac{\partial T}{\partial t} \qquad \ldots\ldots\ldots \quad 7.1.5$$

For a typical node, expansion of each term of the equation by Taylor's series gives

$$\frac{\partial^2 T}{\partial r^2} = \frac{1}{\Delta r^2}\left[T(r+\Delta r, z, t) - 2T(r, z, t) + T(r-\Delta r, z, t)\right] \qquad \ldots\ldots\ldots \quad 7.1.6$$

$$\frac{\partial^2 T}{\partial z^2} = \frac{1}{\Delta z^2}\left[T(r, z+\Delta z, t) - 2T(r, z, t) + T(r, z-\Delta z, t)\right] \qquad \ldots\ldots\ldots \quad 7.1.7$$

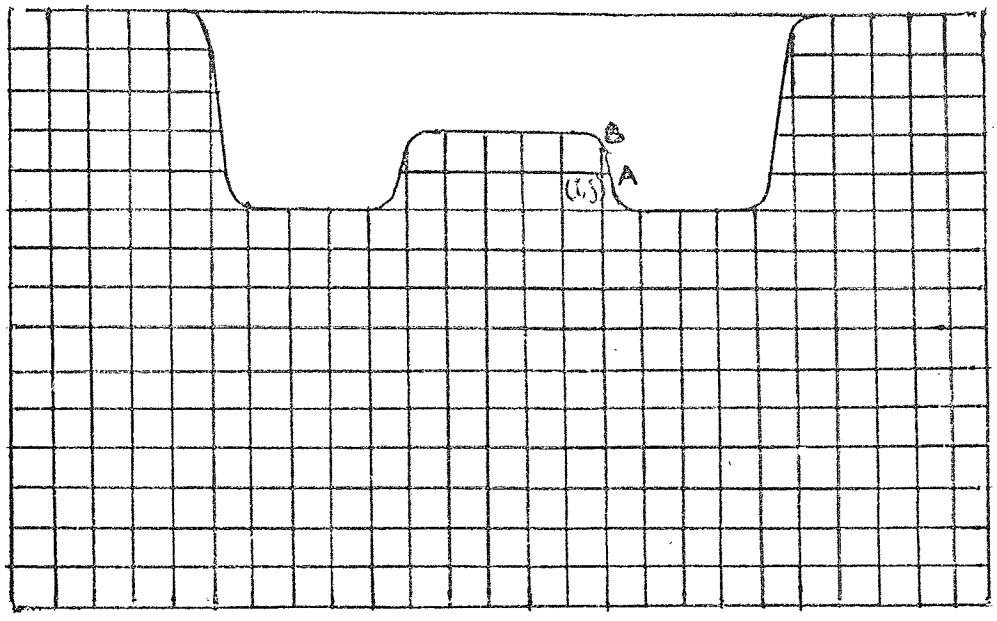

Typical Mesh Spacing for Finite Difference Approximations

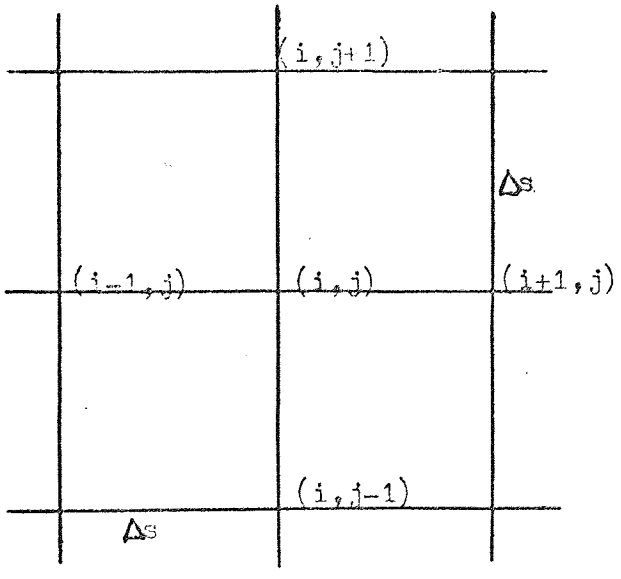

Fig 7.1

$$\frac{1}{r}\frac{\partial T}{\partial r} = \frac{1}{r}\left[\frac{T(r+\Delta r,z,t) - T(r-\Delta r,z,t)}{2\Delta r}\right] \quad \ldots\ldots\ldots \quad 7.1.8$$

$$\text{and } \frac{\partial T}{\partial t} = \frac{1}{\Delta t}\left[T(r,z,t+\Delta t) - T(r,z,t)\right] \quad \ldots\ldots\ldots \quad 7.1.9$$

Thus for a node (i,j) shown in Fig (7.1), where $\Delta r = \Delta z = \Delta s$ equation (5) reduces to

$$\frac{1}{\Delta s^2}\left[T_{i+1,j} - 4T_{i,j} + T_{i-1,j} + T_{i,j+1} + T_{i,j-1}\right]$$

$$+ \frac{T_{i+1,j} - T_{i-1,j}}{2r\Delta s} - \frac{T_{ijt_1} - T_{ijt_o}}{a\Delta t} = 0$$

from which $T_{i,j,t_1} = T_{i,j,t_o} + \frac{a\Delta t}{\Delta s}\left[\frac{T_{i+1,j} - T_{i-1,j}}{2r} + \right.$

$$\left.\frac{1}{\Delta s}\left\{T_{i+1,j} - 4T_{i,j} + T_{i-1,j} + T_{i,j+1} + T_{i,j-1}\right\}\right] \quad \ldots\ldots\ldots \quad 7.1.10$$

This solution applies to evenly spaced nodes only; not to those on curved boundaries which in general are unevenly spaced.

Fig (7.2) shows two nodal points A and B on a curved section of the die surface. Assuming they are located respectively at distances n_1 and n_2, less than unity, from the node (i,j).

Then

$$T_A = T_{i,j} + \Delta s\, n_1 \frac{\partial T_{i,j}}{\partial r} + \frac{1}{2}\Delta s^2 n_1^2 \frac{\partial^2 T_{ij}}{\partial r^2} \quad \ldots\ldots\ldots \quad 7.1.11$$

for point (i - 1,j)

$$T_{i-1,j} = T_{i,j} - \Delta s \frac{\partial T_{i,j}}{\partial r} + \frac{1}{2}\Delta s^2 \frac{\partial^2 T_{i,j}}{\partial r^2} \quad \ldots\ldots\ldots \quad 7.1.12$$

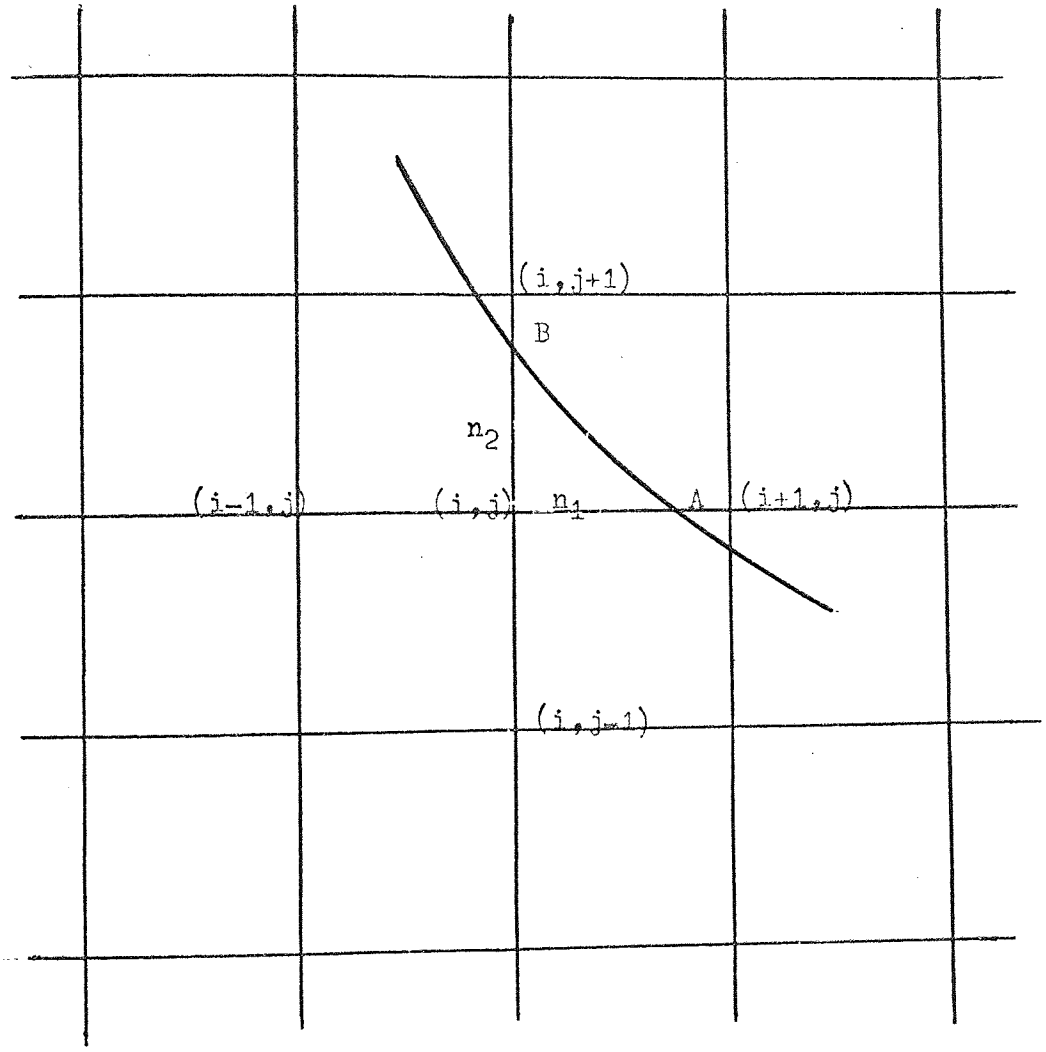

Fig 7.2

from (11) and (12)

$$\frac{\partial^2 Ti,j}{\partial r^2} = \frac{2}{\Delta s^2}\left[\frac{TA}{n_1(1+n_1)} + \frac{Ti-1,j}{(1+n_1)} - \frac{Ti,j}{n_1}\right]$$

..... 7.1.13

$$\text{and } \frac{1}{r}\frac{\partial Ti,j}{\partial r} = \frac{1}{rn_1(1+n_1)}\left[T_A - n_1^2\, Ti-1,j - (1-n_1^2)\, Ti,j\right]$$

..... 7.1.14

By similarity

$$\frac{\partial^2 Ti,j}{\partial z^2} = \frac{2}{\Delta s^2}\left[\frac{T_B}{n_2(1+n_2)} + \frac{Ti,j-1}{(1+n_2)} - \frac{Ti,j}{n_2}\right]$$

..... 7.1.15

Substituting (13), (14) and (15) with

$$\frac{1}{a}\frac{\partial T}{\partial t} = \frac{1}{a\Delta t}\left[Ti,j,t_1 - Ti,j,t_o\right] \text{ into equation 7.1.5}$$

$$\frac{2}{\Delta s^2}\left[\frac{TA}{n_1(1+n_1)} + \frac{Ti-1,j}{(1+n_1)} - \frac{Ti,j}{n_1}\right] + \frac{1}{rn_1(1+n_1)\Delta s}$$

$$\left[T_A - n_1^2\, Ti-1,j - (1-n_1^2)\, Ti,j\right] + \frac{2}{\Delta s^2}\left[\frac{T_B}{n_2(1+n_2)} + \frac{Ti,j-1}{(1+n_2)}\right.$$

$$\left. - \frac{Ti,j}{n_2}\right] - \frac{1}{a\Delta t}\left[Ti,j,t_1 - Ti,j,t_o\right] = 0$$

from which

$$Ti,j,t_1 = Ti,j,t_o + \frac{a\Delta t}{\Delta s^2}\left[\left\{\frac{2r+\Delta s}{rn_1(1+n_1)}\right\}TA + \frac{2T_B}{n_2(1+n_2)} + \frac{2}{(1+n_2)}\right.$$

$$Ti,j-1 + \left\{\frac{2r - n_1\Delta s}{r(1+n_1)}\right\}Ti-1,j - \left\{\frac{2r(n_1+n_2) + n_2(1-n_1)\Delta s}{r\, n_1\, n_2}\right\}$$

..... 7.1.16

Stress Determination From Temperature Distribution

The thermoelastic strains ε_y, ε_x and ε_z are composed of the strain related to stress by Hooke's law and that due to free thermal expansion and are given by

$$\varepsilon_x = \frac{1}{E}\left[\sigma_x - \nu(\sigma_y + \sigma_z)\right] + \alpha T \quad \ldots\ldots\ldots \quad 7.1.17$$

$$\varepsilon_y = \frac{1}{E}\left[\sigma_y - \nu(\sigma_x + \sigma_z)\right] + \alpha T \quad \ldots\ldots\ldots \quad 7.1.18$$

and $$\varepsilon_z = \frac{1}{E}\left[\sigma_z - \nu(\sigma_x + \sigma_y)\right] + \alpha T \quad \ldots\ldots\ldots \quad 7.1.19$$

where α is the coefficient of thermal expansion, T is the temperature predicted in the temperature distribution equation and ν is poisson's ratio.

Solving equations (17), (18) and (19) give

$$\sigma_x = \lambda e + 2G\varepsilon_x - \frac{\alpha E T}{1 - 2\nu} \quad \ldots\ldots\ldots \quad 7.1.20$$

$$\sigma_y = \lambda e + 2G\varepsilon_y - \frac{\alpha E T}{1 - 2\nu} \quad \ldots\ldots\ldots \quad 7.1.21$$

$$\sigma_z = \lambda e + 2G\varepsilon_z - \frac{\alpha E T}{1 - 2\nu} \quad \ldots\ldots\ldots \quad 7.1.22$$

where $\lambda = \frac{\nu E}{(1+\nu)(1-2\nu)}$ and $e = \varepsilon_x + \varepsilon_y + \varepsilon_z$

In polar coordinates, σ_r, σ_θ and σ_z are given by

$$\sigma_r = 2G\left(\varepsilon_r + \frac{\nu}{1-2\nu}e - \frac{1+\nu}{1-2\nu}\alpha T\right) \quad \ldots\ldots\ldots \quad 7.1.23$$

$$\sigma_\theta = 2G\left(\varepsilon_\theta + \frac{\nu}{1-2\nu}e - \frac{1+\nu}{1-2\nu}\alpha T\right) \quad \ldots\ldots\ldots \quad 7.1.24$$

$$\sigma_z = 2G\left(\varepsilon_z + \frac{\nu}{1-2\nu}e - \frac{1+\nu}{1-2\nu}\alpha T\right) \quad \ldots\ldots\ldots \quad 7.1.25$$

and $\varepsilon_r = \frac{du}{dr}$, $\varepsilon_\theta = \frac{u}{r}$, $\varepsilon_z = \frac{dw}{dz}$, $\gamma_{rz} = \gamma_{zr} = \frac{du}{dz} + \frac{dw}{dr}$

and $e = \varepsilon_r + \varepsilon_\theta + \varepsilon_z$ $\quad \ldots\ldots\ldots \quad 7.1.26$

The stresses are independent of θ, and $\tau_{r\theta}$ and $\tau_{\theta z}$ varnish because of symmetry.

Disregarding body forces, it can be shown by considering radial and axial equilibrium of an element of the die, that σ_r, τ_{rz} σ_θ and σ_z are related by

$$\frac{\partial \sigma_r}{\partial r} + \frac{\partial \tau_{rz}}{\partial z} + \frac{\sigma_r - \sigma_\theta}{r} = 0 \quad \ldots\ldots \quad 7.1.27$$

and $$\frac{\partial \tau_{rz}}{\partial r} + \frac{\partial \sigma_z}{\partial z} + \frac{\tau_{rz}}{r} = 0 \quad \ldots\ldots \quad 7.1.28$$

Substituting for σ_r, σ_θ and σ_r in equations (27) and (28) and then substituting in the strain equations (26) gives

$$\nabla u^2 - \frac{u}{r^2} + \frac{1}{1-2\nu}\frac{\partial e}{\partial r} - \frac{2(1+\nu)}{(1-2\nu)}\alpha\frac{\partial T}{\partial r} = 0 \quad \ldots\ldots \quad 7.1.29$$

and $$\nabla^2 w + \frac{1}{1-2\nu}\frac{\partial e}{\partial z} - \frac{2(1+\nu)}{(1-2\nu)}\alpha\frac{\partial T}{\partial z} = 0 \quad \ldots\ldots \quad 7.1.30$$

where $$\nabla^2 = \frac{\partial^2}{\partial r^2} + \frac{1}{r}\frac{\partial}{\partial r} + \frac{\partial^2}{\partial z^2}$$

If a displacement potential of ϕ is defined such that $u = \frac{\partial \phi}{\partial r}$, $w = \frac{\partial \phi}{\partial z}$ and $e = \nabla^2\phi$, equations (29) and (30) transform to

$$\frac{\partial}{\partial r}\left[(1-\nu)\nabla^2\phi - (1+\nu)\alpha T\right] = 0 \quad \ldots\ldots \quad 7.1.31$$

and $$\frac{\partial}{\partial z}\left[(1-\nu)\nabla^2\phi - (1+\nu)\alpha T\right] = 0 \quad \ldots\ldots \quad 7.1.32$$

A particular solution of these equations can be obtained from

$$\nabla^2\phi = \frac{1+\nu}{1-\nu}\alpha T \quad \ldots\ldots \quad 7.1.33$$

The stresses are, thus, given in terms of ϕ by

$$\sigma_r = 2G \left(\frac{\partial^2 \phi}{\partial r^2} - \nabla^2 \phi\right) \quad \ldots\ldots \quad 7.1.34$$

$$\sigma_\theta = 2G \left(\frac{1}{r}\frac{\partial \phi}{\partial r} - \nabla^2 \phi\right) \quad \ldots\ldots \quad 7.1.35$$

$$\sigma_z = 2G \left(\frac{\partial^2 \phi}{\partial z^2} - \nabla^2 \phi\right) \quad \ldots\ldots \quad 7.1.36$$

$$\tau_{rz} = 2G \frac{\partial^2 \phi}{\partial r \partial z} \quad \ldots\ldots \quad 7.1.37$$

The stresses, as calculated from the particular solution, will in general, not satisfy the boundary conditions. A complementary solution, obtained from equations (31) and (32) when T = 0 needs, therefore, be superposed on the particular solution.

If a stress function ξ is introduced such that $\nabla^4 \xi = 0$, then the stresses to be superposed on the solution may be obtained from

$$\sigma'_r = \frac{\partial}{\partial z}\left(\nu \nabla^2 \xi - \frac{\partial^2 \xi}{\partial r^2}\right) \quad \ldots\ldots \quad 7.1.38$$

$$\sigma'_\theta = \frac{\partial}{\partial z}\left(\nu \nabla^2 \xi - \frac{1}{r}\frac{\partial \xi}{\partial r}\right) \quad \ldots\ldots \quad 7.1.39$$

$$\sigma'_z = \frac{\partial}{\partial z}\left[(2 - \nu)\nabla^2 \xi - \frac{\partial^2 \xi}{\partial z^2}\right] \quad \ldots\ldots \quad 7.1.40$$

$$\tau'_{rz} = \frac{\partial}{\partial r}\left[(1 - \nu)\nabla^2 \xi - \frac{\partial^2 \xi}{\partial z^2}\right] \quad \ldots\ldots \quad 7.1.41$$

The entire thermal stress state can thus be calculated with the relevant boundary conditions.

For an example, consider the case of thermal stress determination across the surface of a flat die. The variation of the displacement potential O along the Z axis can be ignored. Hence equation 7.1.33 i.e $\nabla^2\phi = \frac{1+\nu}{1-\nu}\alpha T$ reduces to $\frac{\partial^2\phi}{\partial r^2} + \frac{1}{r}\frac{\partial\phi}{\partial r} = \frac{1+\nu}{1-\nu}\alpha T$ .....(1)

If the assumptions are made (page 124) (1) that the die temperature rises tothe mean of the die preheat temperature and that of the billet as soon as contact is made between the slug and the die and (2) that the progression with time of temperature is negligible , then the right hand side of equation (1) is a constant

$$\text{i.e } \frac{1+\nu}{1+\nu}\alpha T = a = \text{constant}$$

Therefore equation (1) becomes $\frac{\partial^2\phi}{\partial r^2} + \frac{1}{r}\frac{\partial\phi}{\partial r} = \text{constant}$.

which since ϕ is now only a function of r can be written as

..... (2)

To solve this equation let $r=e^t$ then $\frac{dr}{dt} = e^t$ and $\frac{dt}{dr} = \frac{1}{r}$

$$\text{Now } \frac{d\phi}{dr} = \frac{d\phi}{dt}\cdot\frac{dt}{dr} = \frac{1}{r}\frac{d\phi}{dt}$$

$$\text{i.e } r\frac{d\phi}{dr} = \frac{d\phi}{dt} \quad \ldots\ldots\ldots \quad (3)$$

Differentiating (3) with respect to r, we have

$$\frac{d\phi}{dr} + r\frac{d^2\phi}{dr^2} = \frac{\partial^2\phi}{\partial t\,\partial r} = \frac{1}{\partial t}\left(\frac{\partial\phi}{\partial r}\right)$$

$$= \frac{d}{dt}\left(\frac{d\phi}{dt}\cdot\frac{dt}{dr}\right)$$

$$= \frac{d}{dt}\left(\frac{1}{r}\frac{d\phi}{dt}\right)$$

$$= \frac{1}{r}\frac{d^2\phi}{dt^2}$$

$$r\frac{d\phi}{dr} + r^2\frac{d^2\phi}{dr^2} = \frac{d^2\phi}{dt^2} \quad \text{.....(4)}$$

substituting (4) in (2) gives

$$\frac{d^2\phi}{dt^2} = a\, e^{2t}$$

which after integrating tields

$$\phi + ae^{2t} + K_1 t + K_2 \quad \text{.....(5)}$$

where K_1 and K_2 are constants determined by the initial conditions.

Substituting for t in (5) gives

$$\phi = \frac{ar^2}{4} + K_1 \log r + K_2$$

At the die centre where r=0, ϕ=0 and $\frac{d\phi}{dr}$ =0

$$K_1 = K_2 = 0$$

Hence $\phi = \frac{ar^2}{4}$

The stress components can then be calculated from equations 34, 35, 36 and 37 as

$$\sigma_r = 2G\left(\frac{\partial^2\phi}{\partial r^2} - \nabla^2\phi\right) = 2G(\, a/2 - a) = -Ga$$

$$\sigma_\theta = 2G\left(\frac{1}{r}\frac{\partial\phi}{\partial r} - \nabla^2\phi\right) = 2G(\, a/2 - a) = -Ga$$

and $$\sigma_z = 2G\left(\frac{\partial^2\phi}{\partial z\, \partial r} - \nabla^2\phi\right) = 2G(\, 0 - a) = -2Ga$$

$$\tau_{rz} = 2G\,\frac{\partial^2\phi}{\partial r\, \partial z} = 0$$

Since $T_{rz} = 0$, σ_θ, σ_r and σ_z can be regarded as principal stresses.

Therefore, the effective stress $\bar{\sigma}_o$ can be expressed as

$$\bar{\sigma}_o = \frac{1}{\sqrt{2}} \left[(\sigma_r - \sigma_\phi)^2 + (\sigma_\phi - \sigma_z)^2 + (\sigma_z - \sigma_r)^2 \right]^{\frac{1}{2}}$$

$$= \frac{1}{\sqrt{2}} \left[(0)^2 + (-Ga)^2 + (-Ga)^2 \right]^{\frac{1}{2}}$$

$$= \pm Ga$$

The above stresses are the values obtained from the particular solution of equations 31 and 32. They, however, also represent the actual operating stresses since the stress values to be superposed on them (equations 38, 39, and 40) are partial derivatives with respect to z of terms which are only functions of r.

Thus the effective stress is independent of the size of the flat die and parallel in distribution to its face. For a die preheated to 200°C, if the slug temperature is 1200°C, then

$$T = \frac{1200 + 200}{2} = 700$$

If the die is made of tool steel whose poisson's ratio is 0.285 and its coefficient of linear expansion is 7.1×10^{-6} in/in/°F, then

$$a = \frac{1+\nu}{1+\nu} \alpha T = \frac{1+0.285}{1-0.285} \times 7.1 \times 10^{-6} \times 1292$$

$$= 0.0165$$

where 700°C = 1292°F

The rigidity modulus of tool steel being 1.12×10^6 lb/in^2 the effective thermal stress $\bar{\sigma}_o$ is given by

$$\bar{\sigma}_o = \frac{1.12 \times 10^6 \times 0.0165}{2240} \text{ tons/in}^2$$

$$= 8.25 \text{ tons/in}^2$$

The flat die case considered above is clearly a simple one. In closed die forging and indeed in simple upsetting, there is a progression of temperature across the die surface with time since the slug does not, in general, cover the die surface instantaneously. Temperature will not therefore be entirely constant across the die surface.

Reliable results may, however.be obtained for thermal stresses in closed die forging dies by calculating the stresses from the mean temperature attained by each point of interest along the die surface. The problem will be much easier if such temperatures are determined by experiment but the numerical integration technique can also be of tremendous value insofar as temperatures in at least two points each in r and z directions are predetermined. The displacement potential will vary in both the r and z directions and the solution of the equation $\nabla^2\phi = \frac{1+\nu}{1-\nu}\alpha T$ will be in the form of Bessel functions.

Although time precluded the consideration of a more realistic forging problem the simple example has shown the signs of the various stress components and allowed a broad comparison between thermal and mechanical stresses .

For the sort of die configuration considered in the example, the effective mechanical stress value is of the order of 25 to 30 tons/in^2. This represents between three and four times the thermal stress. The thermal stresses are, thus, not nearly as insignificant as would otherwise be imagined.

7.2 Mechanical Stresses

Mechanical stresses in simple upsetting dies have been extensively investigated. Available experimental and analytical data show that the normal stress is maximum at the centre of the die and minimum at its extremes, although there are slight differences of opinion as to the actual shape of the stress distribution curves. Such differences have been discussed in Chapter Three.

In closed die forging, die impressions are so complex that reliable analytical treatment is not feasible. Unfortunately, earlier die stress experimentations have been restricted to the determination of normal stresses - their distributions being obtained by the use of carbon pick ups and pin sized strain gauges inserted along the faces of forging dies.

To fully appreciate the effects of mechanical stressing on forging dies, the relevant stress components need be studied. In attempting to accomplish this objective, the photoelastic stress analysis technique, which is essentially a simulative one, has been employed. It is assumed in the subsequent text that the reader is conversant with normal working of plane and circular polariscopes.

Photoelasticity

The photoelastic method for stress determination is based on the quasi-crystalline behaviour of stressed transparent materials. When a beam of plane polarised light falls on a strained bi-refringent model, it is split at the point of entry into two components in the

directions of the principal stresses. And the components are later transmitted at different speeds Fig (7.2.1).

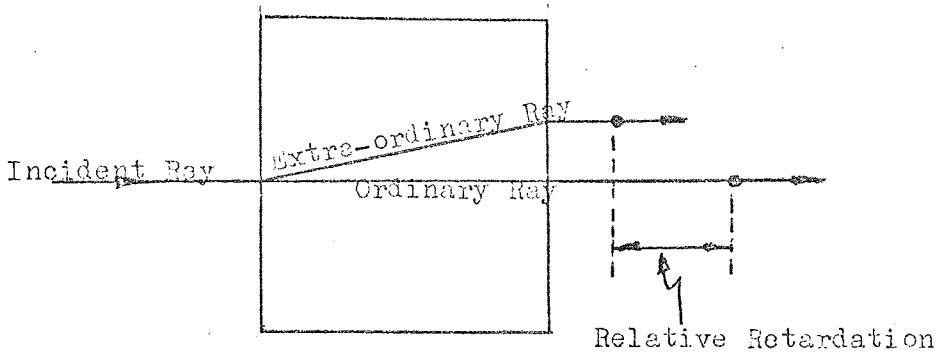

Fig 7.2.1

The resulting relative path retardation R is proportional to the thickness t of the plate and the difference of the principal stresses.

thus $R = Ct\ (\sigma_A - \sigma_B)$ 7.2.1

C is the stress optical coefficient of the material of the model and σ_A and σ_B are the principal stresses.

Since $R = n\lambda$ and $C = \frac{\lambda}{F}$ where λ is the wavelength of the light used, n is the fringe order and F is the fringe value of the material of the model, equation 7.2.1 can be re-written as

$$n = \frac{t}{F}\ (\sigma_A - \sigma_B) \qquad \text{..... 7.2.2}$$

Thus the number of fringes observed when a stressed model is observed in the polariscope is directly proportional to the difference of the principal stresses and the thickness of the model. This is the fundamental basis of the photoelastic method.

For the present study, the three dimensional version of this theory is required since plane strain analysis of closed die forging will

not reveal the true stress state existing. The experimental method employed for the investigation is the frozen stress technique.

The Frozen Stress Technique

The frozen stress method is based on the di-phasic property of some transparent materials.

If a block of such a material is stressed at an elevated temperature, and cooled to room temperature while still under load, it exhibits birefringence even after the load has been removed. And the fringe patterns developed are not disturbed when the block is cut, ground or polished.

The explanation of this phenomenon lies in the molecular structure of such materials, which can be considered as consisting of two phases. The first is rigid at room temperature and becomes fluid at elevated temperatures. The second maintains its rigidity at elevated temperatures, though at a much lower level than that of the first phase at room temperature.

Thus, it is possible to explore the state of stress in forging dies internally, by cutting slices off model dies made of such materials and examining the fringe patterns developed.

Manufacture Of Model Dies

The experimental dies were machined from cast cylinders of hardened araldite CT200.

The Casting Operation

Six pounds of resin was melted in a small electric oven at 150°C. Two pounds of powdered HT 901 hardener was then stirred into the melt and the heating continued. The mixture was intermittently withdrawn from the oven and stirred to ensure the release of gases.

After about $1\frac{3}{4}$ hours, the hardener melted completely. The melt was then slowly poured into two warm copper moulds lubricated with silicone grease.

Oven temperature was dropped to 105°C and the casts were put in for gelation to occur. Subsequently, oven temperature was raised to 120°C and the castings were left to cure for 24 hours.

Die Machining And Finishing

The dies were first rough machined on a lathe to within 1/16" of the finished impression. They were then heat-treated to relieve residual stresses and eliminate self-weight effects.

The heat treatment comprised heating the dies to 150°C in a glycerine bath, cooling them at the rate of half a degree centigrade per hour to 90°C. when all phase changes in araldite are supposed to have ceased, and finally cooling them in air to ambient temperature.

The dies were then finish-machined, polished to a good finish and taken through the stress relieving cycle again to ensure no residual stresses interfered with the subsequent stress analysis. Figs (7.2.3), (7.2.4) and (7.2.5) show the three main die shapes manufactured.

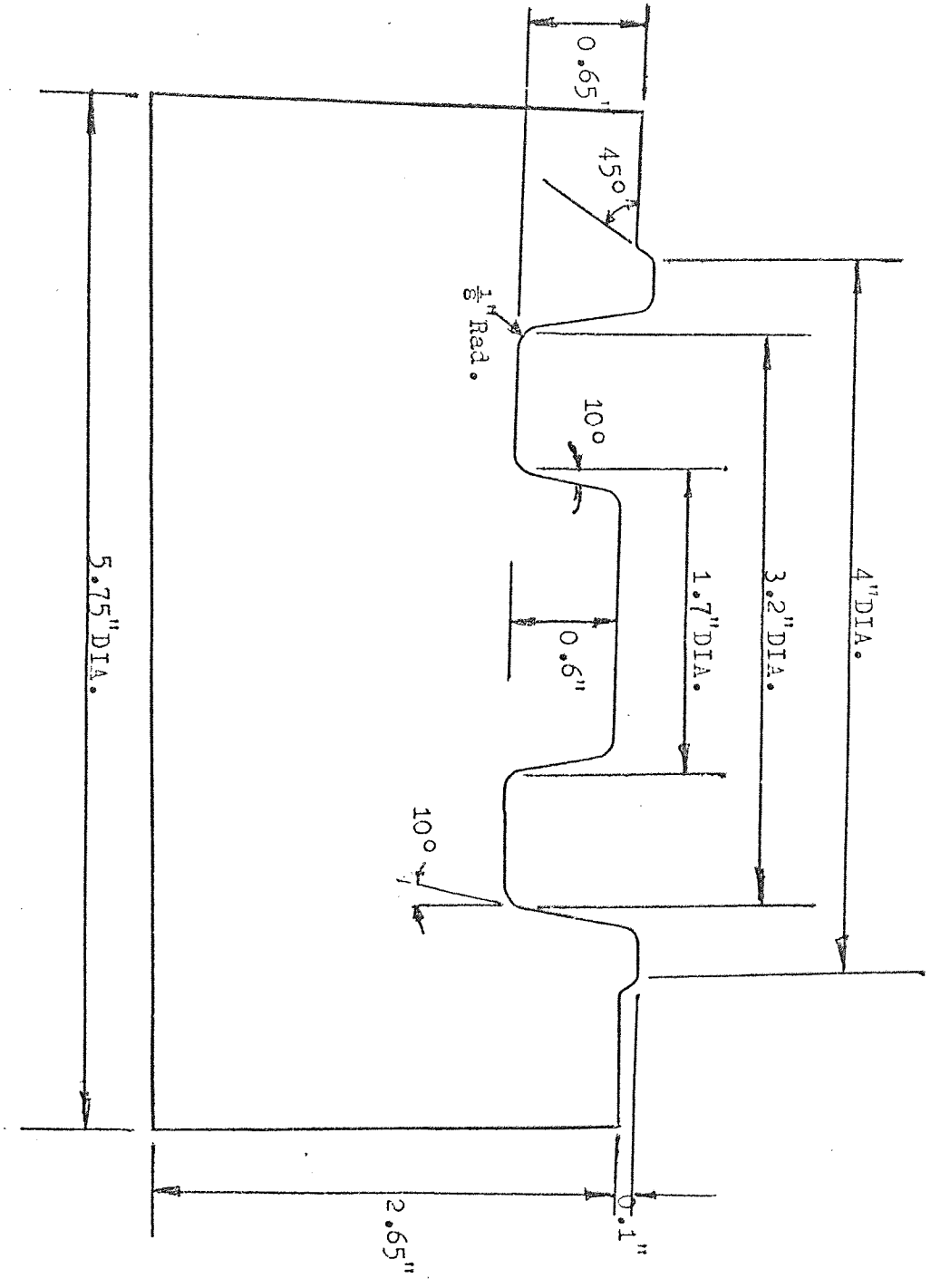

Die D_1

Fig 7.2.3

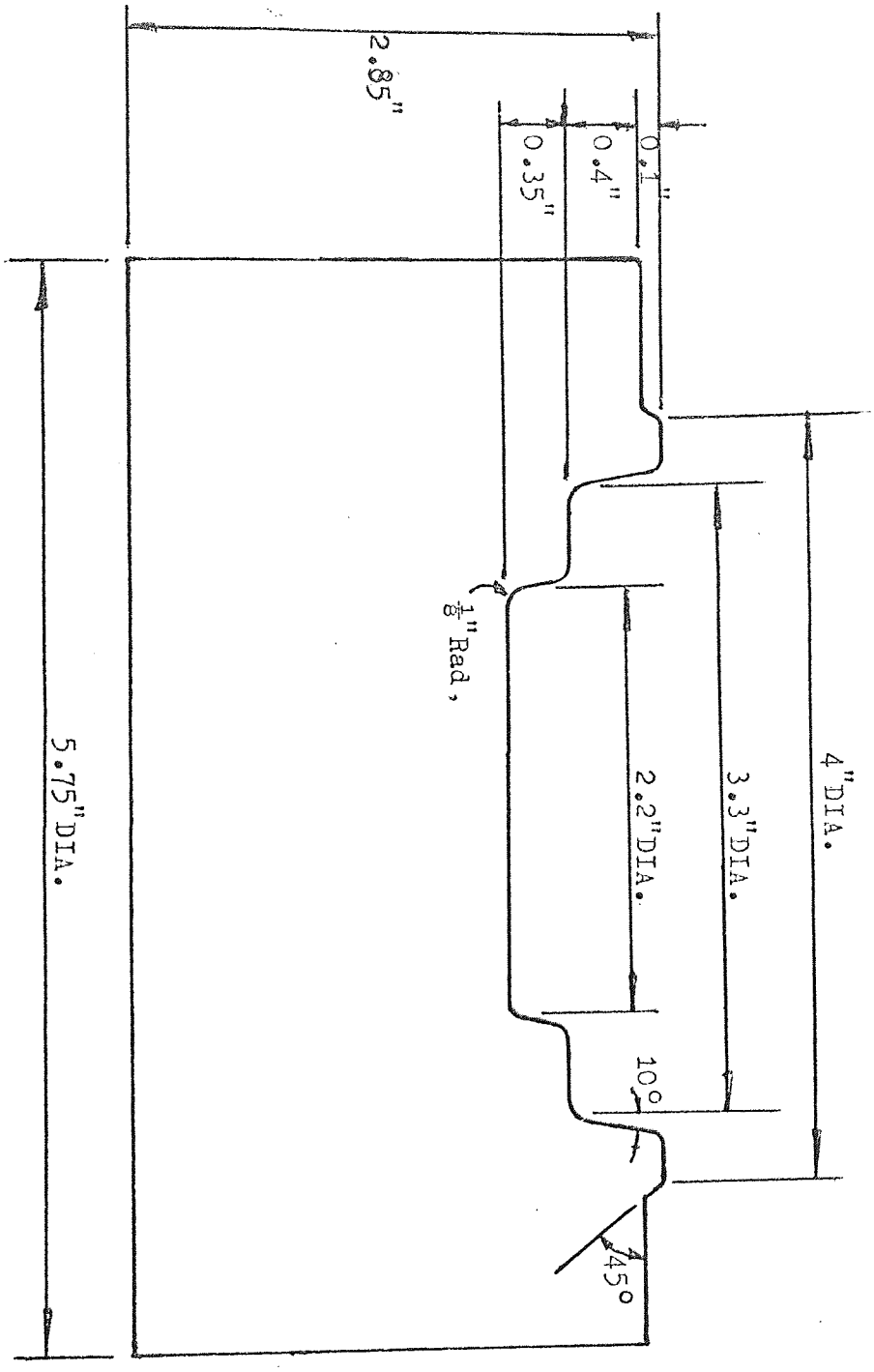

Die D2

Fig 7.2.4

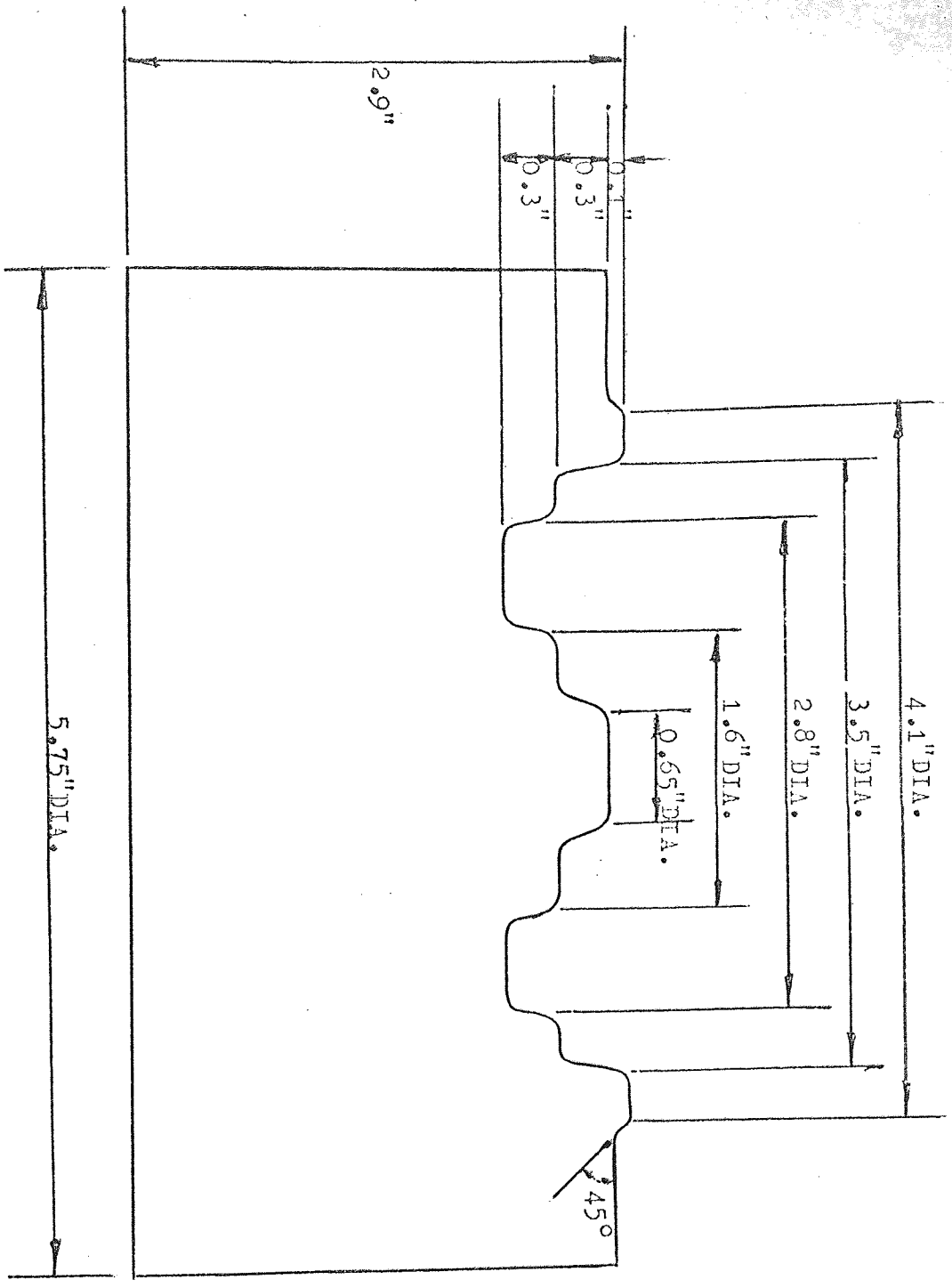

Die D3

Fig 7.2.5

The Billet Material

Several soft materials including aluminium, lead, plastics and wax were considered. Lead and wax were rejected because their stress-strain characteristics substantially differ from those of steel, the prototype metal.

The plastics considered were mainly phenolic resins, e.g. polystyrene. They too were deemed unsuitable because of their considerable physical recovery after deformation. Aluminium was rejected because it needs relatively high load - the type that is physically impossible to apply in the circumstances of the experiments - to deform it plastically when cold.

In the end, plasticene was chosen. It flows easily under moderate loads and its stress-strain characteristics are similar to those of steel.(83,84,95,96)

The Stress Freezing

The amount of plasticene required to fill a pair of dies and form a flash was cut off a two inch diameter bar stock and upset and preshaped to the form of the die impression. The dies were lubricated with a 50/50 mixture of glycerine and teepol before "forging" the pre-formed slugs into them with the aid of a universal testing machine.

The closed dies were then placed in an oven, loaded as shown in Fig (7.2.6), quickly heated to 125°C, allowed to soak for five hours and slowly cooled at the rate of half a degree centigrade per hour to below 30°C. A thin tin strip was used to prevent the outflow of the

flash part of the plasticene forging at high temperature. Care was taken to ensure that the dies were centrally loaded.

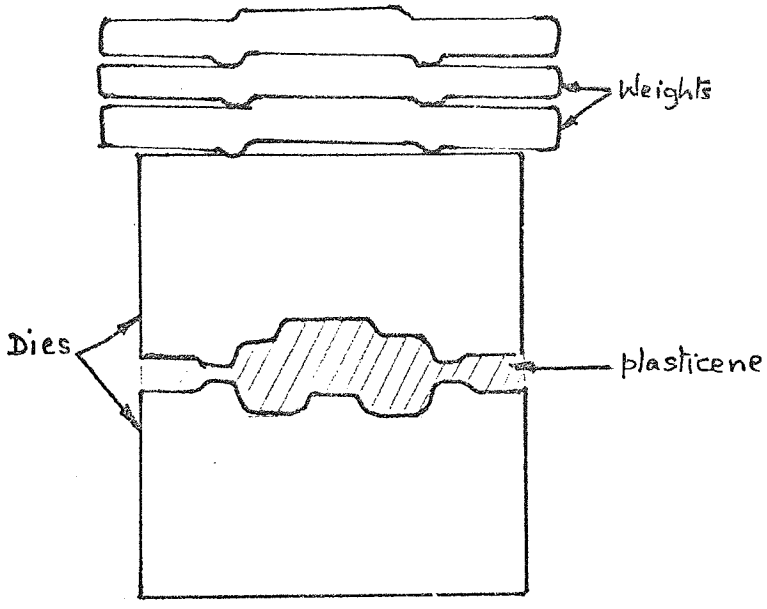

Fig 7.2.6

Preparation Of Test Slices

0.200 inch thick slices were carefully cut off the centres of the dies on a milling machine. Cutting speeds were slow and a generous flow of cooling suds was maintained to avoid any local overheating which might impair the fringes.

The slices were then held firmly on the table of a surface grinder with the aid of double-faced tape and ground. They were later polished to a glass finish ready for examination.

Rough polishing was accomplished by sticking the slices to smooth wooden blocks, as shown in Fig (7.2.7), and rubbing them length-wise and widthwise on various grades of silicon carbide paper under a

tap of cold water. Glass finish transparency was achieved by rubbing the slices on two fine grades of diamond paste.

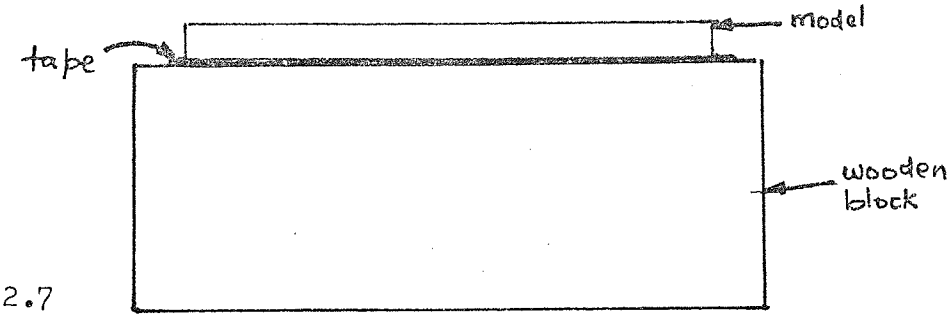

Fig. 7.2.7

The Photoelastic Examination

All the models were examined with the polariser axis inclined at 90° to that of the analyser. Such a set up gives a dark field of view and an integral number of fringes.

The isoclinics - the locii of points where the inclinations of the principal stresses to an arbitrary reference line are equal - were determined at the points of interest. So also were the fringe distributions along the faces of the impressions, at normal and oblique incidence. Fractional fringe orders were obtained by Tardy compensation.

Plate (7.1) shows the apparatus used to incline the models at 30° to the light beam. Its tilting stage allows model inclination from zero to 45°. The glass tank surrounding the model holder was filled with glycerine to eliminate light scattering and the polarising

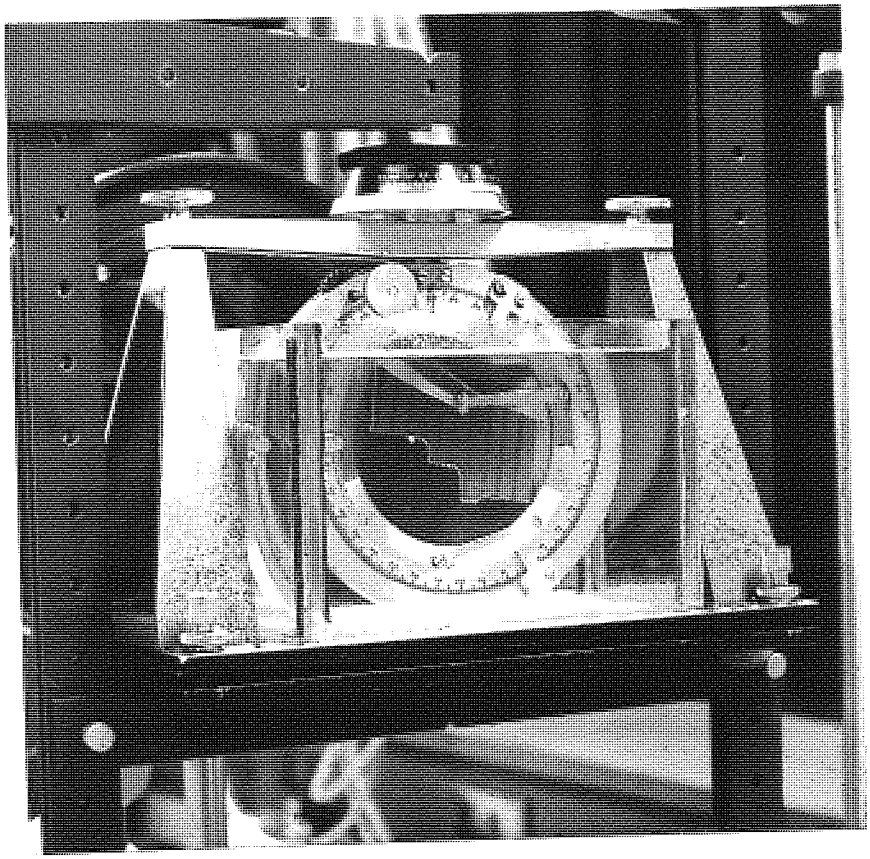

Plate 7.1 Showing part of a model slice mounted ready for Photoelastic examination.

effects on the faces of the models.

Figs (7.2.8), (7.2.9) and (7.2.10) show the fringe distributions at normal and oblique incidence, along the faces of the model dies.

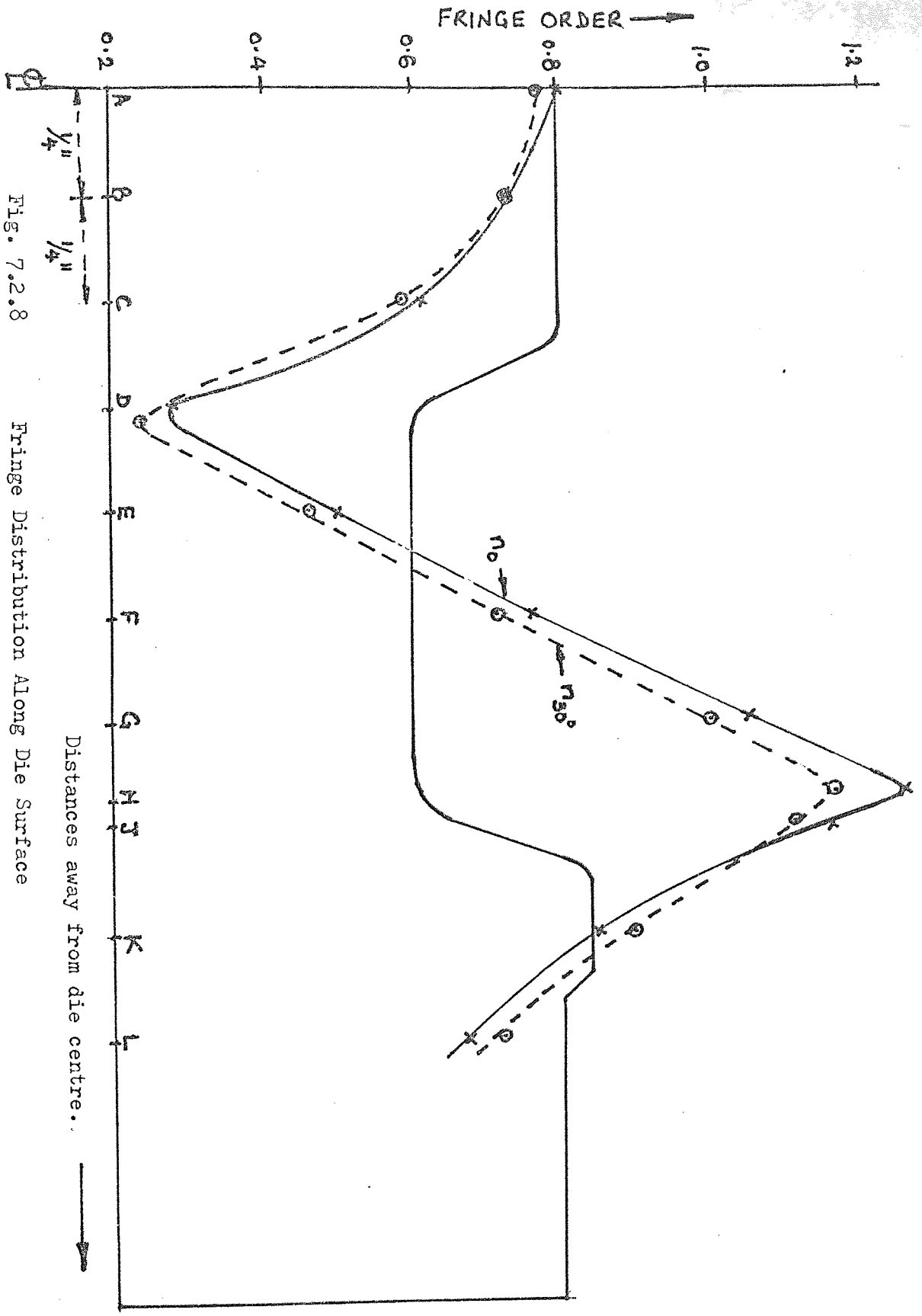

Fig. 7.2.8 Fringe Distribution Along Die Surface

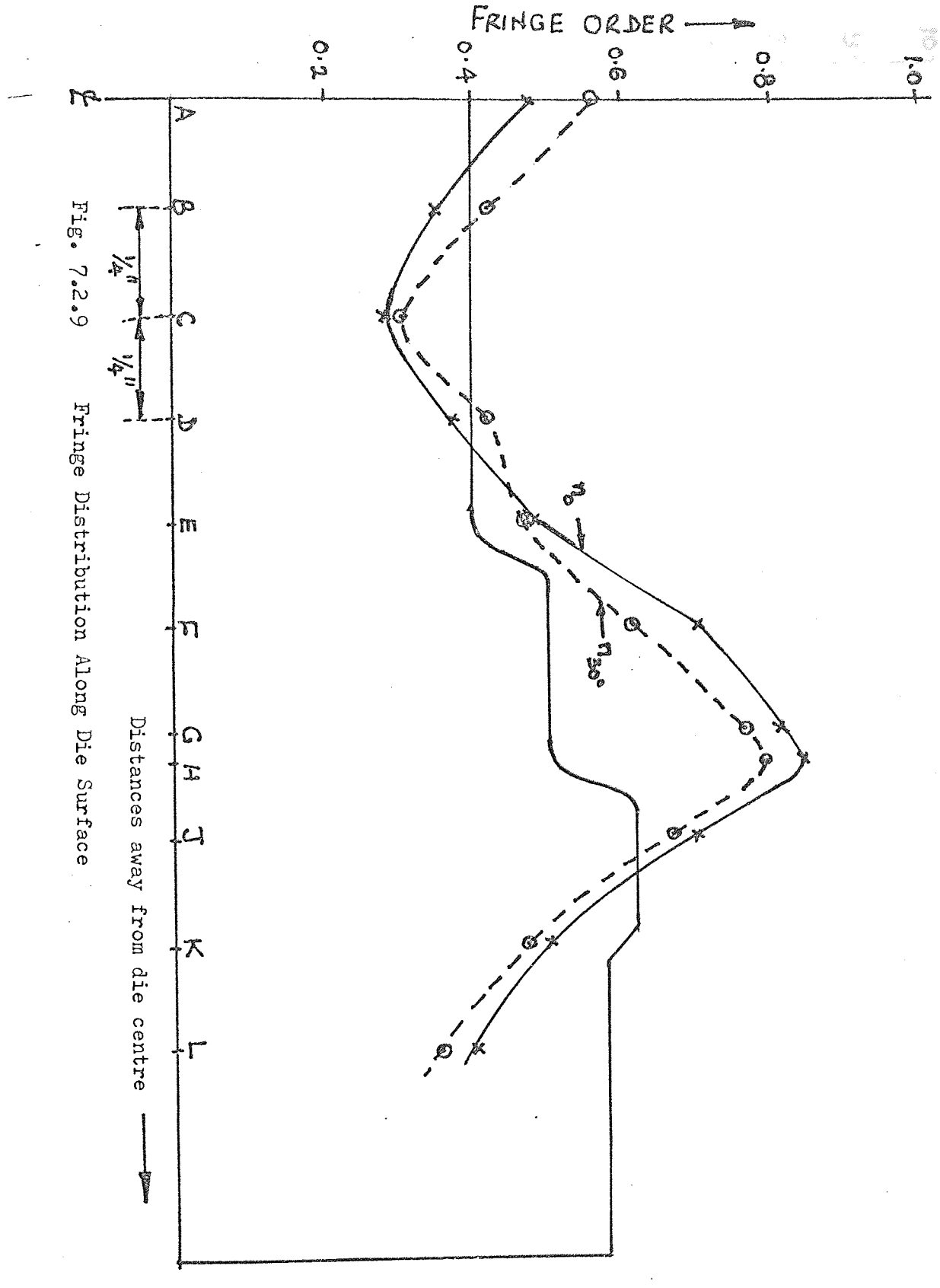

Fig. 7.2.9 Fringe Distribution Along Die Surface

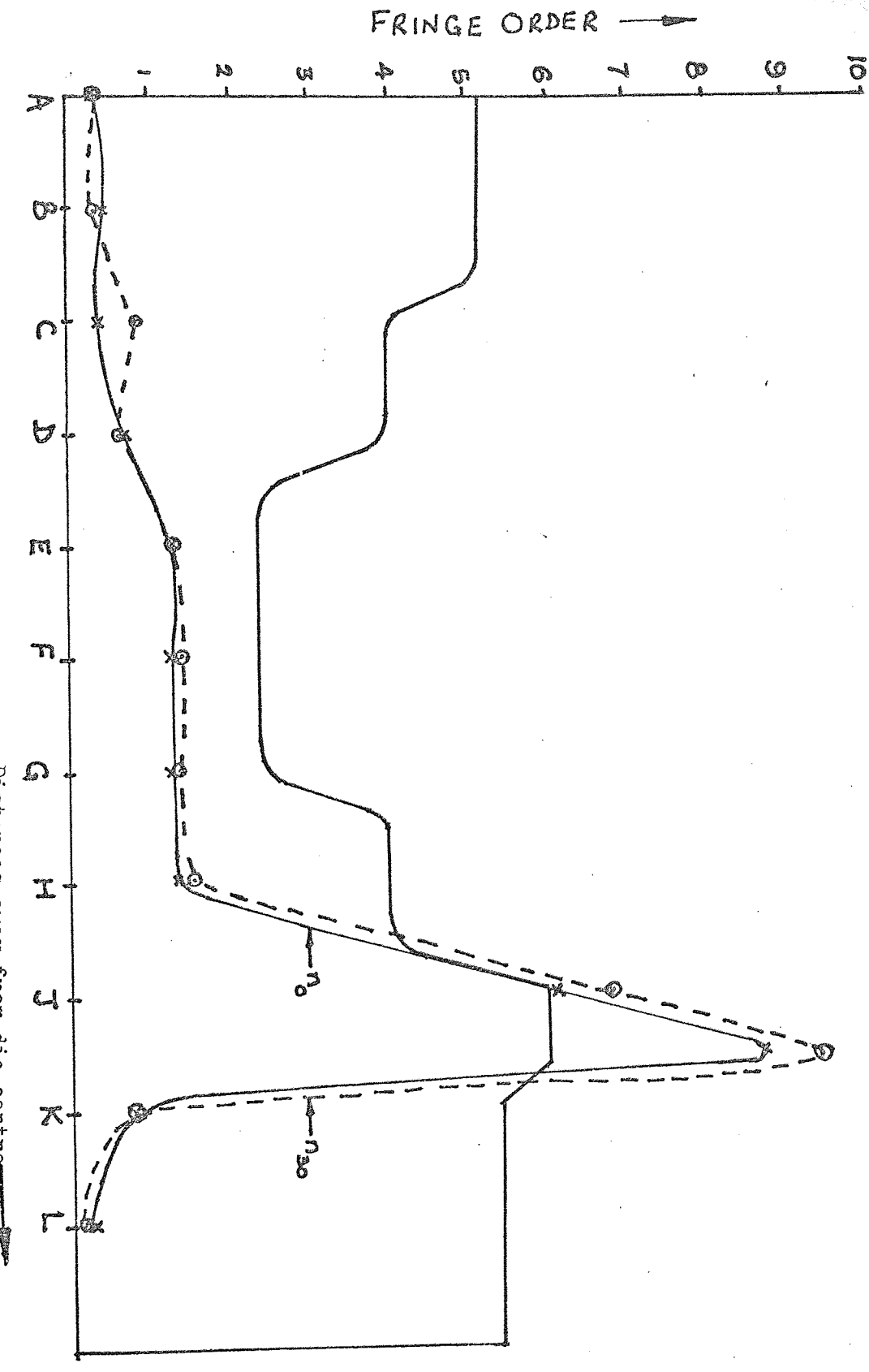

Fig. 7.2.10 Fringe Distribution Along Die Surface

Calculations

Let the normal, radial and circumferential stresses acting on the die be σ_z, σ_r and σ_θ respectively. The shear stress on the surface of the die impression will be τ_{rz} and $\tau_{z\theta}$ will be zero.

If the principal stresses acting on the plane of the model slice are σ_1 and σ_2, and the direction of σ_1 makes an angle ϕ with the direction of σ_r (see Fig 7.2.11), it can be shown that

$$\sigma_r = \sigma_1 \cos^2 \phi + \sigma_2 \sin^2 \phi = (\sigma_1 - \sigma_2) \cos^2 \phi + \sigma_2 \quad \ldots\ldots\ldots (7.2.3)$$

$$\sigma_z = \sigma_1 \sin^2 \phi + \sigma_2 \cos^2 \phi = (\sigma_1 - \sigma_2) \sin^2 \phi + \sigma_2 \quad \ldots\ldots\ldots (7.2.4)$$

$$\text{and } \tau_{rz} = \frac{\sigma_1 - \sigma_2}{2} \sin 2\phi \quad \ldots\ldots\ldots (7.2.5)$$

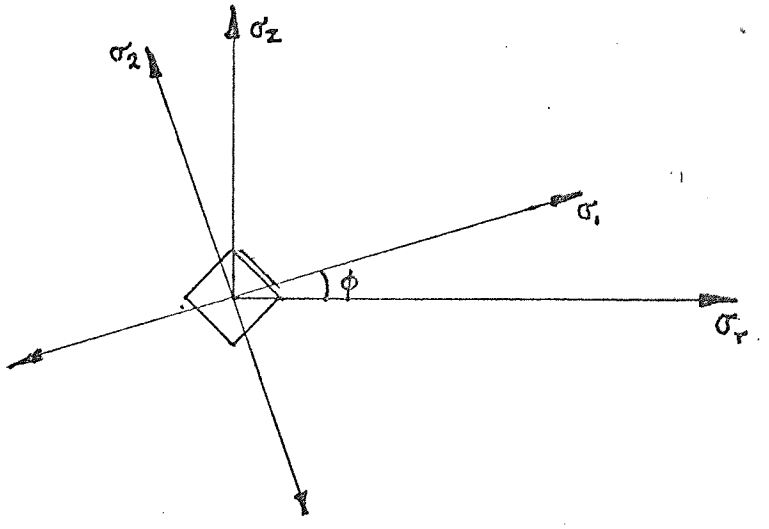

Fig. 7.2.11

If n_o is the fringe order of a point, A, when the model slice is examined in a normal incident light beam, then

$$n_o = (\sigma_1 - \sigma_2) \frac{t}{F} \quad \ldots\ldots\ldots (7.2.6)$$

t is the thickness of the slice and F is the material unit fringe value.

When the model is rotated in the horizontal plane (see Fig 7.2.12), such that the angle between the wave normal and the normal to the surface of the slice is θ, the fringe order n_θ of the point is given by

$$n_\theta = \frac{(P - Q)t}{F \cos \theta} \qquad \ldots\ldots\ldots (7.2.7)$$

$\frac{t}{\cos \theta}$ is the new length of the path traversed by the light, and P and Q are secondary principal stresses given by

$$P - Q = \sqrt{\left[\sigma_r \cos^2\theta + \sigma_\theta \sin^2\theta - \sigma_z\right]^2 + 4\tau_{rz}^2 \cos^2\theta} \qquad \ldots\ldots\ldots (7.2.8)$$

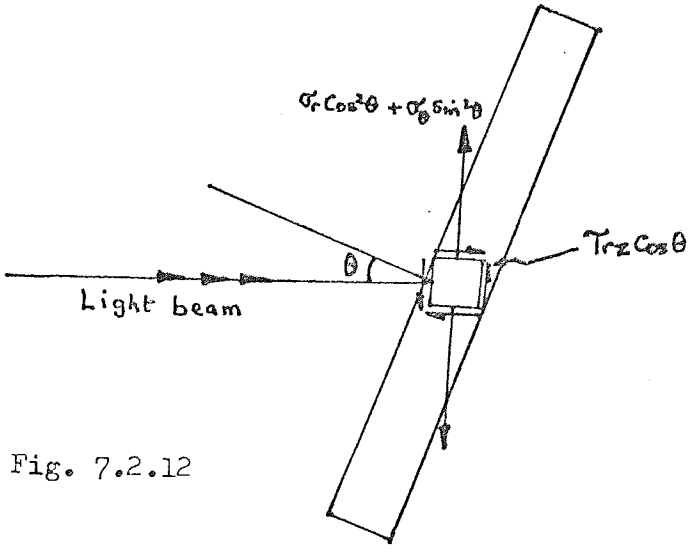

Fig. 7.2.12

Substituting first for (P - Q), and then σ_r, σ_θ, σ_z and τ_{rz} in equation (7.2.7) gives

$$\sigma_\theta - \sigma_2 = \frac{F}{t \sin^2\theta}\left\{\cos\theta\sqrt{n_\theta^2 - n_o^2 \sin^2\phi} - n_o\left[\cos^2\theta - \sin^2\phi\,(1 + \cos^2\theta)\right]\right\} \quad \ldots\ldots\ldots (7.2.10)$$

Thus, the principal stress differences $(\sigma_1 - \sigma_2)$, $(\sigma_\theta - \sigma_2)$ and $(\sigma_1 - \sigma_\theta)$ can, in general, be obtained from equations (7.2.6) and (7.2.10). In the special cases where $\theta = 0$ and $\theta = 90$, $\sigma_\theta - \sigma_2$ are given by

$$(\sigma_\theta - \sigma_2)_{\theta = 0} = \frac{F}{t \sin^2\theta}\left[n_\theta \cos\theta - n_o \cos^2\theta\right] \quad \ldots\ldots\ldots (7.2.11)$$

$$\text{and } (\sigma_\theta - \sigma_2)_{\theta = 90^o} = \frac{F}{t \sin^2\theta}\left[n_\theta \cos\theta + n_o\right] \quad \ldots\ldots\ldots (7.2.12)$$

The effective stress, σ_e, can now be determined at each point of interest from

$$\sigma_e = \frac{1}{\sqrt{2}}\left[(\sigma_1 - \sigma_2)^2 + (\sigma_\theta - \sigma_2)^2 + (\sigma_1 - \sigma_\theta)^2\right]^{\frac{1}{2}} \quad \ldots\ldots\ldots (7.2.13)$$

For example, at point, K, in Fig (7.2.8) $n_o = 0.86$, $n_{30} = 0.90$ and $\phi = 15^o$. The material fringe value F = 1.39 lb/in fringe and the thickness, t, of the model is 0.133 ins.

$$\therefore\ \sigma_1 - \sigma_2 = \frac{n_o F}{t} = \frac{0.86 \times 1.39}{0.133} = 9 \text{ lb/in}^2$$

$$\text{and } \sigma_\theta - \sigma_2 = \frac{1.39}{0.133}\sin^2 30\left[\cos 30\sqrt{0.90^2 - 0.86^2 \sin^2 30} - 0.86\left\{\cos^2 30 - \sin^2 15\,(1 + \cos^2 30)\right\}\right]$$

which simplifies to

$$\sigma_o - \sigma_2 = 5.85 \text{ lb/in}^2$$

$$\therefore \quad \sigma_1 - \sigma_o = (\sigma_1 - \sigma_2) - (\sigma_o - \sigma_2) = 9 - 5.85 = 3.15 \text{ lb/in}^2$$

$$\therefore \quad \sigma_e = \frac{1}{\sqrt{2}} \left[9^2 + 5.85^2 + 3.15^2\right]^{\frac{1}{2}}$$

$$= \underline{7.9} \text{ lb/in}^2$$

And at point, C, where $\phi = 0$, $^{n}_{o} = 0.61$ and $^{n}_{30} = 0.59$

$$\sigma_1 - \sigma_2 = \frac{0.61 \times 1.39}{0.133} = 6.38 \text{ lb/in}^2$$

$$\sigma_o - \sigma_2 = \frac{1.39}{0.133} \sin^2 30 \left[0.59 \cos 30 - 0.61 \cos^2 30\right]$$

$$= \underline{2.217} \text{ lb/in}^2$$

and $\sigma_1 - \sigma_o = 6.38 - 2.217 = 4.163 \text{ lb/in}^2$

$$\therefore \quad \sigma_e = \frac{1}{\sqrt{2}} \left[6.38^2 + 2.217^2 + 4.163^2\right]^{\frac{1}{2}}$$

$$= \underline{5.61} \text{ lb/in}^2$$

The principal stress differences and the effective stresses along the faces of dies D_1, D_2 and D_3 are shown respectively in Tables (7.1), (7.2) and (7.3). The effective stresses are also superimposed on the die impressions in Figs (7.2.13), (7.2.14) and (7.2.15).

TABLE (7.1)

Point On Die Surface	$\sigma_1 - \sigma_2$ lb/in^2	$\sigma_1 - \sigma_\theta$ lb/in^2	$\sigma_\theta - \sigma_2$ lb/in^2	Effective Stress σ_e (lb/in^2)
A	8.36	5.22	3.14	7.33
B	7.63	4.81	2.82	6.68
C	6.37	4.14	2.13	5.61
D	2.926	3.01	-0.084	3.01
E	5.23	4.97	0.251	5.1
F	8.15	6.9	1.26	7.6
G	11.20	8.87	2.32	10.24.
H	13.06	9.86	3.20	11.77
J	12.22	8.36	3.86	10.81
K	8.99	3.14	5.85	7.90
L	7.0	1.96	5.04	6.26

TABLE (7.2)

Point On Die Surface	$\sigma_1 - \sigma_2$ lb/in^2	$\sigma_1 - \sigma_\theta$ lb/in^2	$\sigma_\theta - \sigma_2$ lb/in^2	Effective Stress σ_e (lb/in^2)
A	4.040	-0.168	4.208	4.130
B	2.940	-0.472	3.410	3.210
C	2.356	0.674	1.682	2.100
D	3.120	0.200	2.920	3.026
E	4.050	2.465	1.585	3.540
F	5.640	4.480	1.160	5.160
G	6.900	5.460	1.440	6.310
H	7.075	5.223	1.852	6.380
J	5.975	4.375	1.600	5.360
K	4.295	3.470	0.825	3.940
L	3.452	3.300	0.152	3.373

TABLE (7.3)

Point On Die Surface	$\sigma_1 - \sigma_2$ lb/in^2	$\sigma_1 - \sigma_\theta$ lb/in^2	$\sigma_\theta - \sigma_2$ lb/in^2	Effective Stress σ_e (lb/in^2)
A	3.050	0.542	2.508	2.82
B	3.480	0.159	3.321	3.39
C	3.305	13.900	-10.595	12.57
D	5.94	1.288	4.652	5.42
E	10.94	4.510	6.430	9.51
F	10.850	7.400	3.450	9.61
G	10.760	6.170	4.590	9.35
H	11.030	2.034	8.996	10.15
J	51.70	-24.4	76.1	67.3
K	5.68	5.275	0.405	5.49
L	2.035	-1.995	4.030	4.93

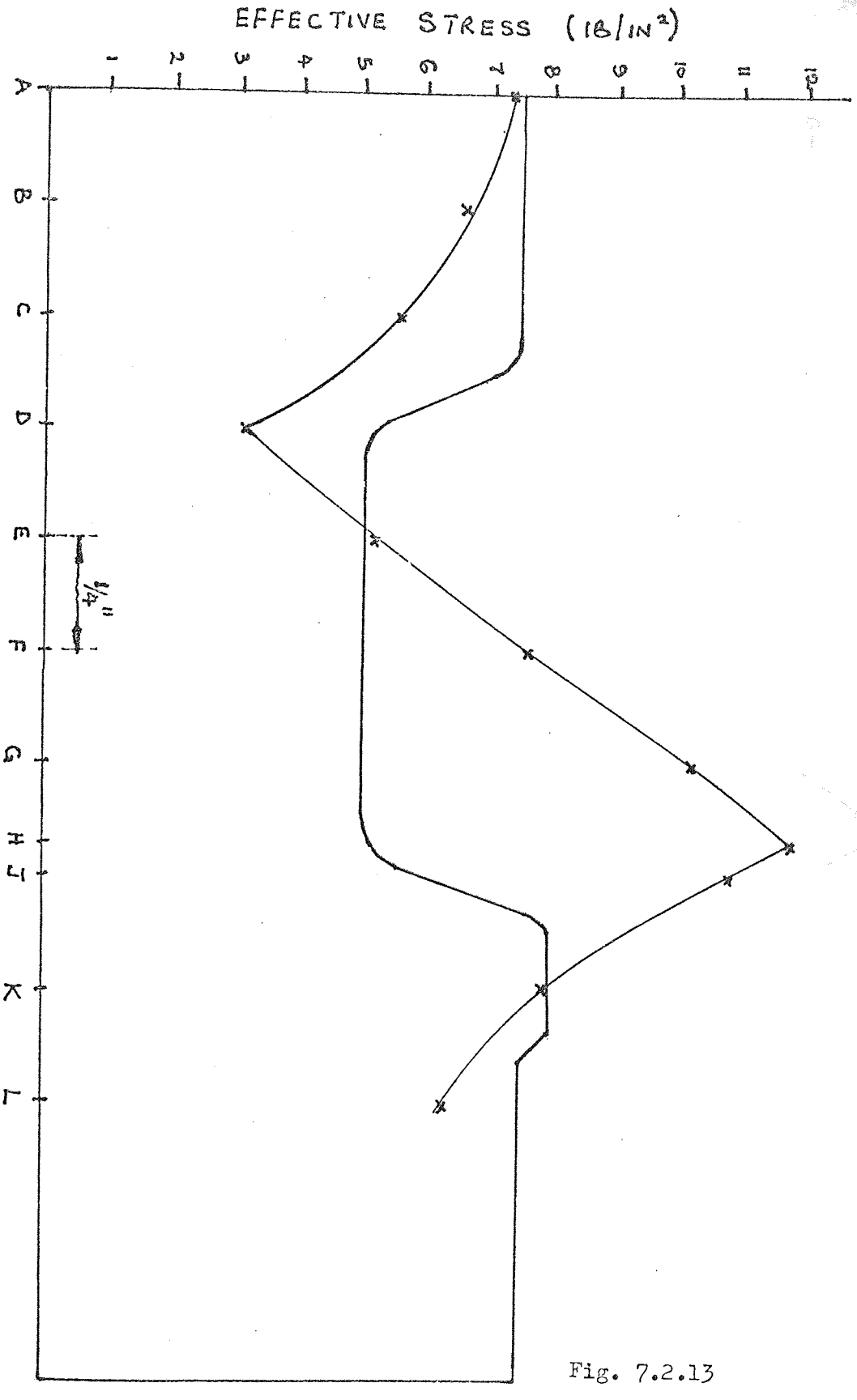

Effective Stress Distribution across Die Surface.

Fig. 7.2.13

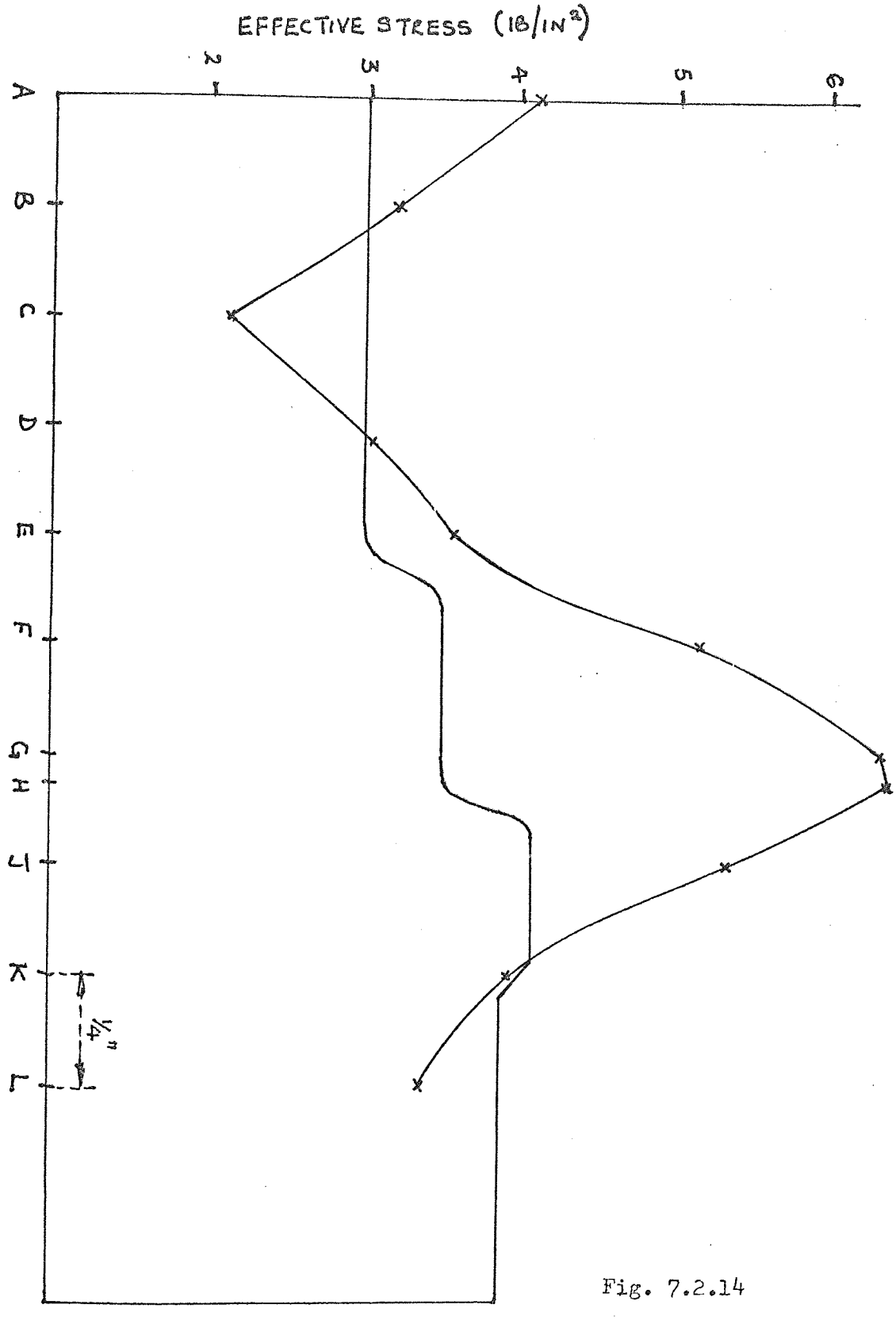

Effective Stress Distribution across Die Surface.

Fig. 7.2.14

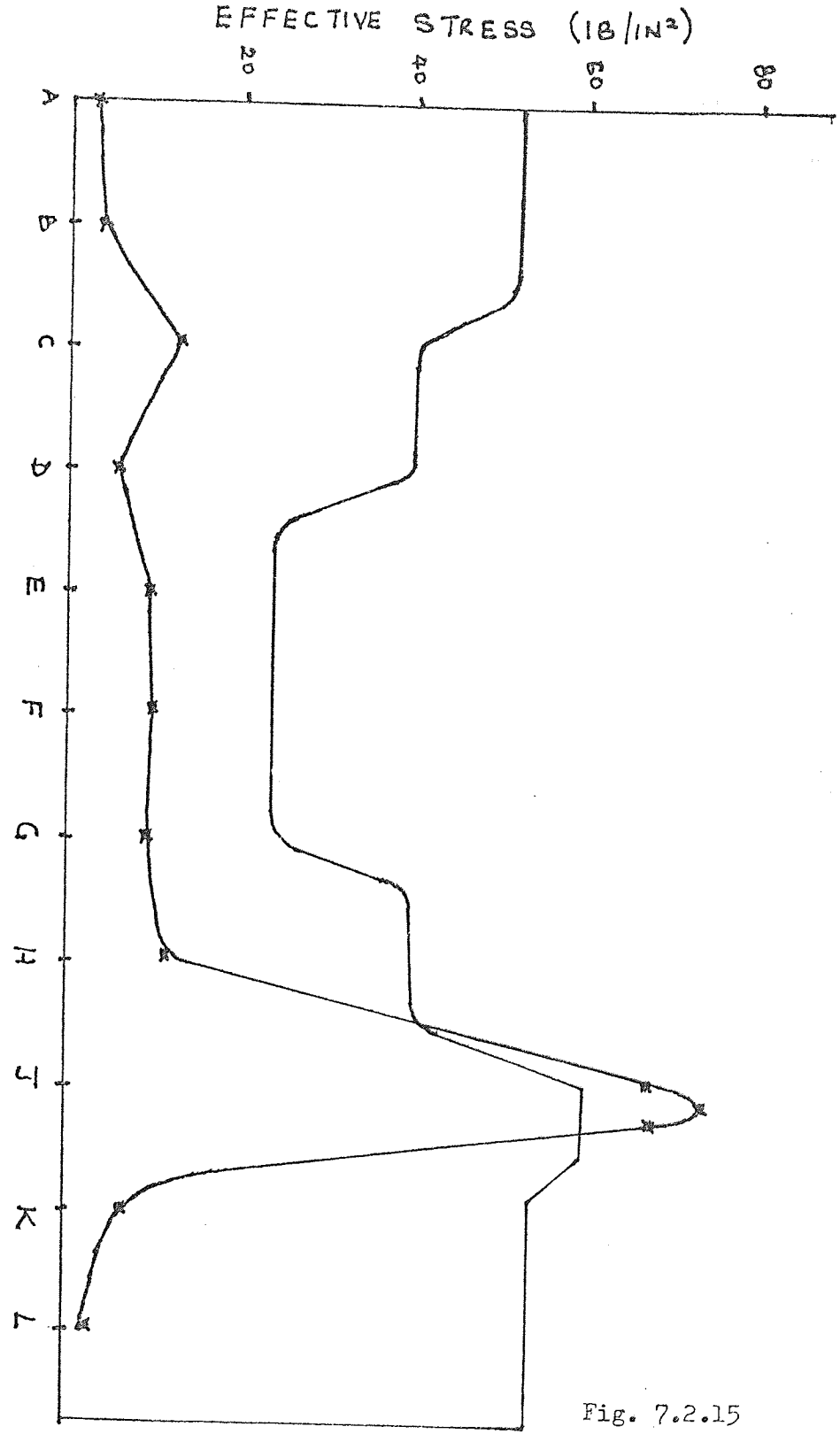

Effective Stress Distribution across Die Surface.

Fig. 7.2.15

Transposition of Model Stresses to the Prototype

Let the mean stress due to the load Pm applied on the araldite die of radius Rm be σ_m. The dimensionless stress is then given by

$$\frac{Pm}{\pi Rm^2 \sigma_m}$$

If the load applied to the steel die of radius Rs is Ps, the dimensionless stress is

$$\frac{Ps}{\pi Rs^2 \sigma_s}$$

Assuming geometric similarity between the dies,

$$\frac{Pm}{\pi Rm^2 \sigma_m} = \frac{Ps}{\pi Rs^2 \sigma_s}$$

$$\therefore \quad \sigma_s = \sigma_m \frac{Ps}{Pm} \left(\frac{Rm}{Rs}\right)^2 \qquad \ldots\ldots\ldots (7.2.13)$$

In a general case where the model and prototype differ not only in scale and applied loads but also in shape, equation (7.2.13) becomes

$$\sigma_s = \sigma_m \frac{Ps}{Pm} \left(\frac{lm}{ls}\right)^2 \qquad \ldots\ldots\ldots (7.2.14)$$

where ls and lm are typical length dimensions of the steel and araldite dies respectively.

The accuracy of the predicted stress distribution depends on the poisson's ratios of the prototype and of the model, which in this study are 0.293 at 200°C and 0.5 at 125°C respectively.

Fessler and Lewin[93] have observed little effect of poisson's ratio on strain concentration factor of a Tee Type branched pipe and Rose and Fessler[90] have shown that a change of poisson's ratio from $\frac{1}{2}$ to $\frac{1}{4}$ caused a 3% change in the maximum stress developed in a pressurised hemispherical head. The latter also observed a more appreciable ratio effect in areas of lower stresses.

Similar results were obtained by Clutterbuck[91], who concluded that "any effect due to a change in poisson's ratio is of an order not greater than that of the errors of observation, that is, about 7%".

In the light of these observations, it is reasonable to suggest a 3 to 10% modification (increment) to the predicted prototype stresses. Such modifications, however, are not expected to affect the basic shape of the stress distributions immensely, nor will they alter the areas in which forging dies are most likely to fail in service.

DISCUSSION

Figs (7.2.8) and (7.2.9) show the fringe distribution in dies D_1 and D_2 respectively. In both cases, the fringes drop from a value at the die centre to a minimum at a point about $\frac{3}{4}$" from the centre, and then rises to a maximum at the die outer corner. Thereafter, the fringes diminish steadily towards the sides of the die.

The effective stress is the stress component largely responsible for fatigue failure in forging dies. Its distribution is shown for dies D_1 and D_2 in Fig (7.2.13) and (7.2.14) respectively. The stresses are maximum at the die outer corners. This is as expected.

Apart from friction, outer relief sides offer the first significant barrier to the flow of slug materials in closed die forging operations. They constrain the metal in the die impression and are, therefore, subject to a stress system which, in the main, have shearing and bending effects [illegible]. The sides tend to be bent about, and sheared off the die corners. Thus high stresses are developed in the corners.

Cracking in die corners occurs frequently in industrial forging practice. The cracks often run round the die corners at an angle to the adjoining areas of the die. The effective stress is a most likely factor responsible; the catalysing agent being the martensitic structure of the die surface. This latter factor renders the die surface brittle and therefore more susceptible to the damaging influence of the effective stress.

Greater rigidity is necessary to minimise the effects of

the stress. This can be achieved by making the "clearance width" of the die (shown in Fig 7.2.16) as large as possible, and by reinforcing the die with a back-up shank.

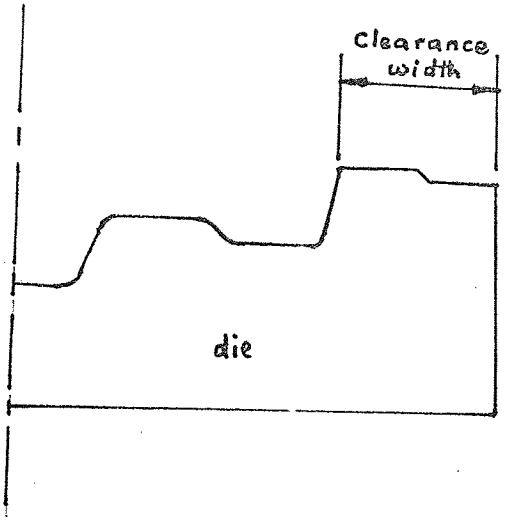

Fig. 7.2.16

It also seems advisable to allow generous radii at outer corners. Such a step will reduce the level of stress concentration and hence lessen the influence of the effective stress. The effect of the stress component tending to bend the relief sides about the corners may also be reduced by giving dies greater draft angles.

These steps will admittedly cause the unit costs of forged components to increase, but it seems more likely than not that the advantages of any prolonged die life would offset such cost increases.

Shearing On Die Surfaces

The isoclinic angle and hence the shear stress was zero at all points on the die surface except those on the relief sides. This is not an adequate reflection of the shear stress state in a forging die.

It is, however, a fair result in the context of this experiment, since there was no relative movement between the die and the plasticene at the points in question.

Whereas the slug metal spreads momentarily in real closed die forging operations, the plasticene had to be forged into the dies before the stress freezing cycle, partly to ensure uniform slug deformation and partly to ascertain that the dies were completely filled. Shearing continually occured in the slug material. But the expected movement of the plasticene mass, on the die impression surface, after softening at high temperature (125°C) must have been too slight as to be unable to set up a significant stress pattern.

Effect of Die Contact on Stress Distribution

When experimenting with die D_3, a very thin flash material of the order of 0.05 inch separated the die halves. At the highest stress freezing temperature the plasticene softened and most of the flash material oozed out, thus allowing the dies to touch.

Figs 7.2.10 and 7.2.15 show respectively the fringe distribution obtained and the distribution of the corresponding effective stresses.

Unlike in the other two dies, the stresses are minimum at the die centre and increase to a maximum in the flash land. Stresses developed in the die outer corners are incompatibly higher (up to about six times in the area of maximum stress level) than those developed in dies D_1 and D_2.

It is thus easy to deduce that dies which repeatedly touch during closed die forging operations are liable to fail much sooner than would otherwise have been.

The obvious explanation of this result is the die contact. Whereas the load applied to dies D_1 and D_2 were supported by the plasticene mass, the land area has carried the bulk of the load in die D_3, and a very small percentage had acted on the workpiece.

It is thought that, barring any gross carelessness, this sort of stress situation is more likely to arise in the coining process where no flashes are formed than in closed die press or hammer forging operations.

Applicability of model results to prototype

Some care needs be taken in using the simulative results for die stress determination in closed die forging of steel. Since stress freezing temperatures far below its melting point were used in the photoelastic study the araldite dies can be considered rigid enough throughout the experiments. They must, therefore, be regarded as adequate for die simulation.

The photoelastic stress analysis technique has also been demonstably shown to be applicable to closed die forging die stress evaluation. But because the frozen stress technique is essentially a low deformation-rate process, there is considerable disparity between the rates of deformation of actual steel billets and those practicable on the model slug. It is, thus, possible that creep might have interfered with the simulation.

This would have caused a lowering of the stress levels

within the die impressions and any predictions made from the results would then be an under-estimation. However, creep influence on the shapes of the stress distributions will be expected to be only slight as to be unable to alter the positions of areas most prone to failure.

Except during the study of die contact, the stress freezing temperatures were not high enough to cause the plasticene to soften considerably and ooze out at the die parting lines. If they have been, the model slug would have flowed like an hydraulic fluid and the effective stress would have been constant within the die impression. This did not seem to happen. Both halves were always completely full of plasticene when separated after the stress freezing operations, the final flash thicknesses did not deviate from the expected values by more than 5% and the distributions dropped from a height in the die to a minimum level before rising to a peak at the die outer corners.

CONCLUSIONS

The laboratory and industrial experiments showed that the shape and size of forged components, the width-to-thickness ratios of the flashes formed and the size and temperature of the forging stocks jointly determine closed die press forging loads.

In general, loads were lower in dies with flash gutters than in those without them. Bigger, wider and more complicated forgings required more loads to forge them. And deformation forces decreased with higher forging temperatures and with increasing billet diameter-to-height ratios.

Reduction in load with higher slug temperature is a direct result of the reduction in metal resistance to deformation and local cooling associated with longer contact time between tall billets and the dies explains why loads increased with decreasing billet diameter-to-height ratios.

Forging loads also increased with strain rate, flash thickness and the percentage amount of excess metal. Forces rose steeply when metal less than 0.115 inches were thrown as flash.

When billets wider than the impressions were forged into them, deformation forces were low but the forgings produced were imperfect. They had laps and tears and die edges "caved in" as more forgings were produced.

Forgings whose flash width-to-thickness ratios were less than $1\frac{1}{2}$ did not fill the impressions completely. Ratios of between $1\frac{3}{4}$ and $3\frac{1}{2}$ gave good results. Die fill was also inadequate when deep impressions were used as bottom dies. Perfect forgings were

produced by using such impressions as top dies.

Light oils are unsuitable as forging lubricants. When used, sticking (characteristic of lubrication breakdown) occured at the job-tool interfaces and extremely high loads were developed. The forgers' oil was adequate and colloidal graphite in water seems an even better lubricant. The die surfaces hardened after forging a sizeable number of billets and the rate of hardening was less with aqueous collidal graphite than with oil. This suggests that the former has a better screening quality .

On the average, forging loads were higher with forgers' oil than with aqueous collidal graphite. This broadly agrees with the observations of an earlier research group(51). Investigators in a large forging works have, however, obtained results which suggest the contrary. This seeming disparity probably confirms their claim that the effect of die lubricant on deformation forces is a function of the type of slug heating employed.

DIE STRESSES

The effective stress distribution dropped from a value at the die centre to a minimum at a point between half an inch and one inch from the centre and thereafter rose to a peak at the outer corner. This is to be expected since, apart from friction, the die outer corners offer the first significant barrier to the flow of the slug metal.

The stress acting on the outer walls of the die can be

approximated to a uniformly distributed loading whose effect is partly to shear and partly to bend the wall about the die corner. Effective stress will thus be higher in the outer corners than in areas where it is essentially due to the three polar stresses. It is therefore thought that forging dies will be more susceptible to mechanical cracking in such zones.

Such view is supported in industry where dies which crack have been observed to do so along their outer corners at varying angles to the containing walls.

This raises obvious design problems. An arrangement whereby areas most susceptible to the effects of the stresses are made softer than the adjoining areas is unlikely to work since sudden variations in metal texture cannot enhance strength. The use of backing-up dies is advisable. Such dies will, apart from holding the inserts in position, curtail the deflection of their outer walls.

For similar results outer relief angles and corner radii may be made more generous. Greater relief would reduce the effect of the bending stress component and more generous corner radii should effectively reduce the degree of stress concentration.

But the most effective method of dealing with the problem seems to be the division of the die insert into small units (Fig 8.1) This has the advantage of eliminating the die corners altogether. Such arrangements are common in coining and are already being employed in certain drop forging works.

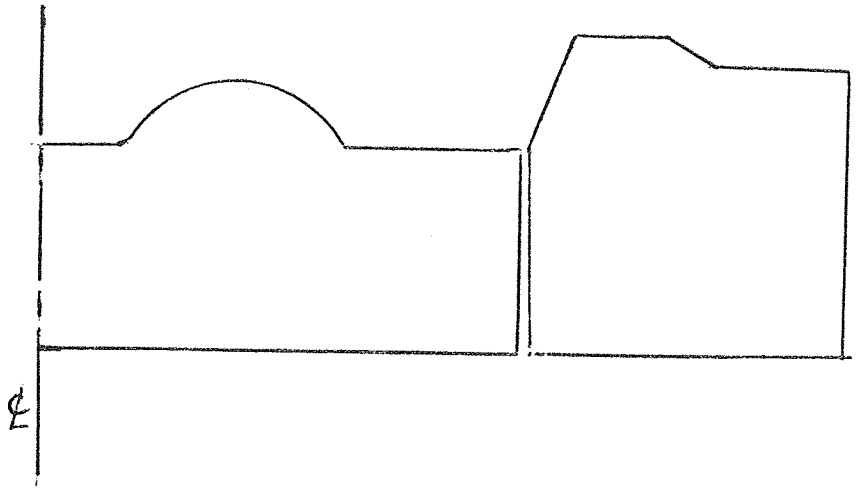

Fig 8.1

Die contact

Die contact significantly affected the stress distribution. Maximum stress was developed in the flash area and the least occured at the die centre. Stresses were also significantly higher . Increases of up to 600% were observed.

The discrepancy in the magnitude and distribution of the stresses is a direct result of the differences in the mode of die loading. Whereas the slug material bore the deformation load when there was no contact, most of the load was now applied on the dies; particularly the flash area.

While die contact occurs infrequently in closed die forging operations, it is just as well to anticipate an earlier tool failure if and when it does continually.

Shear Stresses

In general, shearing occurs within the bodies of forged components and friction shear occurs at the job-tool interfaces. The former was apparent in the simulative study but friction shear situations on the die faces were not properly reflected. Isoclinic angles were zero in all areas of the impressions except along the external restraining walls. The indication is that the expected slug flow at high temperature was not enough to set up an appreciable shear stress pattern.

Such movements are difficult to simulate by the photoelastic frozen stress technique without compromising some of the basic requirements of a perfect forging. Although the present study has not dertermined its distribution, the author considers that interface friction is a significant factor in forging load determination.

SUGGESTIONS FOR FURTHER WORK

The joint knuckle press used for the load study had a maximum tonnage capacity of 100 tons. This limited the diameters of components forged to no more than four inches. And long hubbed parts which, in general, require high loads for good die filling, could not be investigated. It is recommended, therefore, that any further load tests be carried out on a bigger press.

The shape complexity factor as defined in the thesis is inadequate in reflecting the degree of difficulty of making all forgings. This is probably why it was not nearly as significant as expected. The author considers that this factor may be more significant than the present report has portrayed. A more detailed study of the variable, therefore, seems called for.

The stress measurements have shown the effect of mechanical stressing on die failure, and the frozen stress technique has been found inadequate for investigations into shear stress effects on die impressions. The necessary relative motion between the tools and the job is difficult to simulate without compromising some of the features relevant in real press forging operations.

It seems worthwhile, for better understanding of the phenomenon of die wear, to investigate these stresses. A likely method is the determination of normal stresses at the points of interest, probably with the aid of pin-sized load cells, and converting them with friction coefficients predetermined by the ring method (15). The

results will admittedly be approximate. But they will adequately indicate or predict the mode of any likely wear.

More vigorous wear tests with different forging lubricants also seem worthwhile. As far as the author can ascertain, only one (53) of the tests on lubricants reported in the literature is related to die wear. Experiments designed to determine the "wear retardation or acceleration" qualities of several forging lubricants seem likely to bridge this information gap.

APPENDIX I

Press Specifications

Maximum Pressure	100 tons
Daylight Bolster To Top Tool Face	$11\frac{3}{4}$ inches
Maximum Stroke	$1\frac{3}{4}$ inches
Top Tool Adjustment	$\frac{1}{2}$ inch
Speed	70 strokes per minute
Main motor - Horsepower	3
Main motor - Speed	1440 revs per minute

APPENDIX 2

KEY

COLUMNS	VARIABLE NAMES
1	Billet Diameter-to-Height Ratio
2	Weight of Billets (IBS)
3	Area at Parting Lines (SQ. INCHES)
4	Parting Diameter/ Maximum Forging Height
5	Weight of clipped Forging (IBS)
6	Shape Complexity Factor
7	Process Yield
8	Flash Width-to-Thickness Ratio
9	Slug Temperature (DEGREES C)
10	Forging Loads (TONS)

TABLE 1

1,003	0,576	2,750	1,057	0,5260	0,899	0,913	1,274	1250	32,06
0,980	0,588	2,940	1,061	0,5270	0,898	0,897	1,508	1250	35,50
1,331	0,563	2,850	1,057	0,5250	0,897	0,933	1,426	1250	30,00
1,305	0,576	3,290	1,064	0,5280	0,898	0,916	1,966	1250	40,00
1,271	0,588	3,230	1,064	0,5280	0,898	0,898	1,926	1250	41,50
1,694	0,563	3,060	1,055	0,5240	0,899	0,931	1,776	1250	27,10
1,655	0,576	3,340	1,061	0,5270	0,899	0,916	2,024	1250	39,50
1,617	0,588	3,280	1,062	0,5270	0,899	0,897	1,941	1250	41,50
1,025	0,563	2,730	1,063	0,5275	0,899	0,954	1,225	1150	41,50
1,003	0,576	3,175	1,065	0,5285	0,898	0,918	1,755	1150	43,00
0,980	0,588	3,300	1,067	0,5300	0,900	0,902	1,880	1150	48,00
1,331	0,563	2,910	1,066	0,5300	0,900	0,941	1,450	1150	44,70
1,305	0,576	3,250	1,066	0,5300	0,900	0,920	1,877	1150	44,70
1,271	0,588	3,410	1,073	0,5330	0,898	0,906	1,985	1150	54,70
1,694	0,563	3,140	1,064	0,5280	0,898	0,939	1,756	1150	40,20
1,655	0,576	3,300	1,070	0,5320	0,900	0,924	1,884	1150	50,00
1,617	0,588	3,380	1,070	0,5320	0,900	0,904	1,958	1150	52,00
1,003	0,576	3,905	1,046	0,5180	0,897	0,900	3,239	1250	59,10
0,980	0,588	3,940	1,046	0,5175	0,895	0,880	3,241	1250	59,20
1,331	0,563	3,540	1,043	0,5175	0,896	0,918	2,760	1250	55,00
1,305	0,576	3,990	1,050	0,5200	0,897	0,903	3,221	1250	66,00
1,271	0,588	4,370	1,050	0,5200	0,896	0,883	3,790	1250	64,00
1,694	0,563	3,515	1,040	0,5160	0,898	0,916	2,772	1250	52,00
1,655	0,576	3,980	1,050	0,5200	0,898	0,903	3,170	1250	66,70
1,617	0,588	4,040	1,054	0,5240	0,900	0,890	3,139	1250	75,20
1,025	0,563	3,325	1,040	0,5160	0,898	0,916	2,472	1250	52,00
1,025	0,563	2,710	1,070	0,5325	0,902	0,946	1,123	1200	30,80
1,003	0,576	3,040	1,070	0,5325	0,902	0,925	1,550	1200	32,00
0,980	0,588	3,050	1,074	0,5330	0,899	0,908	1,515	1200	38,50
1,331	0,563	2,775	1,070	0,5310	0,900	0,943	1,211	1200	30,80
1,305	0,576	3,190	1,074	0,5330	0,899	0,925	1,659	1200	39,80
1,271	0,588	3,325	1,077	0,5360	0,900	0,911	1,811	1200	42,60
1,694	0,563	3,270	1,065	0,5330	0,900	0,941	1,875	1200	25,40
1,655	0,576	3,290	1,073	0,5330	0,900	0,926	1,792	1200	39,20
1,617	0,588	3,900	1,077	0,5330	0,897	0,906	2,430	1200	45,70
1,025	0,563	3,120	1,065	0,5290	0,900	0,940	1,636	1200	35,00

TABLE 1 (contd)

1.003	0.576	3.315	1.068	0.5300	0.899	0.921	1.882	1200	37.40
0.980	0.588	3.385	1.070	0.5320	0.900	0.904	1.950	1200	39.60
1.331	0.563	3.230	1.068	0.5310	0.899	0.944	1.799	1200	37.00
1.305	0.576	3.415	1.076	0.5350	0.908	0.929	1.885	1200	50.00
1.271	0.588	3.720	1.074	0.5340	0.900	0.907	2.267	1200	47.00
1.694	0.563	3.275	1.065	0.5300	0.901	0.943	1.880	1200	34.00
1.655	0.576	3.630	1.068	0.5310	0.900	0.923	2.267	1200	38.00
1.617	0.588	3.570	1.071	0.5330	0.900	0.906	2.160	1200	42.50
1.025	0.563	2.230	1.067	0.5280	0.899	0.939	0.558	1150	30.80
1.003	0.576	2.640	1.066	0.5270	0.899	0.915	1.075	1150	30.40
0.980	0.588	2.880	1.066	0.5275	0.900	0.898	1.404	1150	31.00
1.331	0.563	3.040	1.069	0.5290	0.898	0.940	1.576	1150	34.00
1.305	0.576	2.854	1.068	0.5283	0.898	0.917	1.340	1150	35.00
1.271	0.588	3.115	1.070	0.5300	0.898	0.901	1.655	1150	37.00
1.694	0.563	2.900	1.065	0.5280	0.901	0.939	1.443	1150	24.30
1.655	0.576	2.948	1.062	0.5250	0.897	0.911	1.508	1150	24.10
1.617	0.588	2.930	1.062	0.5255	0.898	0.894	1.489	1150	26.20
1.025	0.560	3.780	1.156	0.5076	0.633	0.907	1.800	1250	37.20
1.003	0.570	3.930	1.219	0.5114	0.606	0.898	1.845	1250	39.20
0.980	0.585	4.097	1.219	0.5143	0.608	0.879	1.985	1250	45.00
1.331	0.558	3.714	1.125	0.5017	0.643	0.899	1.595	1250	37.00
1.305	0.572	4.160	1.188	0.5085	0.618	0.890	2.176	1250	40.00
1.655	0.575	4.225	1.125	0.4962	0.635	0.862	2.180	1250	38.50
1.617	0.584	4.327	1.219	0.4947	0.586	0.847	2.199	1250	52.00
1.025	0.552	3.300	1.133	0.5036	0.637	0.931	1.150	1150	36.20
1.003	0.562	3.310	1.152	0.5106	0.633	0.909	1.126	1150	44.20
0.980	0.577	3.660	1.183	0.5179	0.624	0.898	1.566	1150	48.80
1.331	0.548	3.472	1.100	0.4966	0.645	0.905	1.320	1150	37.30
1.305	0.566	3.630	1.150	0.5099	0.634	0.901	1.470	1150	48.00
1.271	0.579	3.740	1.162	0.5143	0.634	0.889	1.598	1150	48.80
1.694	0.553	3.675	1.100	0.4923	0.640	0.890	1.562	1150	44.20
1.655	0.564	3.840	1.117	0.4979	0.638	0.883	1.741	1150	46.50
1.617	0.575	3.975	1.150	0.5009	0.623	0.870	1.883	1150	48.80
1.025	0.558	3.580	1.150	0.5034	0.624	0.903	1.642	1150	53.10
1.003	0.574	3.975	1.150	0.5085	0.630	0.887	2.260	1150	58.00
0.980	0.578	3.890	1.162	0.5140	0.632	0.889	1.965	1150	66.00

TABLE 1 (contd)

1.331	0.559	3.837	1.153	0.4995	0.620	0.894	1.991	1150	52.00
1.305	0.572	4.020	1.147	0.5065	0.629	0.886	2.111	1150	61.50
1.271	0.587	4.190	1.175	0.5096	0.621	0.869	2.233	1150	69.30
1.694	0.560	4.060	1.125	0.4893	0.621	0.874	2.212	1150	58.40
1.655	0.573	4.290	1.150	0.4973	0.618	0.868	2.518	1150	60.00
1.617	0.585	4.380	1.162	0.5008	0.614	0.856	2.560	1150	64.00
1.025	0.562	3.830	1.162	0.5054	0.623	0.900	2.000	1200	54.30
1.003	0.572	3.960	1.167	0.5121	0.626	0.896	2.052	1200	62.90
0.980	0.587	4.230	1.167	0.5159	0.630	0.880	2.332	1200	68.80
1.331	0.560	4.000	1.183	0.5031	0.609	0.899	2.230	1200	58.00
1.305	0.573	4.180	1.183	0.5093	0.616	0.888	2.322	1200	64.00
1.271	0.587	4.350	1.186	0.5147	0.618	0.877	2.460	1200	71.80
1.694	0.558	4.110	1.133	0.4967	0.627	0.889	2.380	1200	50.00
1.655	0.572	4.400	1.162	0.5003	0.615	0.875	2.607	1200	60.00
1.617	0.585	4.520	1.175	0.5052	0.613	0.864	2.657	1200	67.20
1.025	0.522	3.125	1.125	0.4842	0.617	0.928	1.245	1200	39.80
1.003	0.538	3.385	1.150	0.4972	0.618	0.924	1.584	1200	50.00
0.980	0.545	3.540	1.150	0.4956	0.615	0.909	1.833	1200	51.00
1.331	0.537	3.685	1.150	0.4915	0.613	0.915	2.040	1200	48.80
1.305	0.552	3.960	1.150	0.4996	0.620	0.905	2.291	1200	61.00
1.271	0.553	3.927	1.150	0.4989	0.620	0.901	2.274	1200	61.50
1.694	0.526	3.680	1.150	0.4780	0.594	0.910	2.154	1200	40.90
1.655	0.543	4.027	1.125	0.4878	0.619	0.898	2.550	1200	52.00
1.617	0.548	3.975	1.150	0.4888	0.612	0.892	2.500	1200	51.00
1.025	0.560	3.976	1.160	0.5097	0.631	0.910	2.230	1250	71.80
1.003	0.573	4.461	1.160	0.5079	0.628	0.886	2.793	1250	76.00
0.980	0.587	4.720	1.165	0.5109	0.627	0.871	3.179	1250	82.00
1.331	0.559	4.150	1.150	0.5067	0.629	0.906	2.451	1250	68.30
1.305	0.570	4.460	1.160	0.5090	0.628	0.894	2.783	1250	72.70
1.271	0.586	4.640	1.170	0.5095	0.622	0.870	2.852	1250	79.80
1.694	0.560	4.540	1.135	0.4897	0.616	0.875	2.891	1250	73.30
1.655	0.574	4.940	1.150	0.4920	0.611	0.856	3.160	1250	83.10
1.617	0.584	4.880	1.160	0.4995	0.604	0.855	3.140	1250	83.10
1.146	0.650	5.660	0.666	0.5508	0.788	0.848	1.735	1250	70.20
1.124	0.665	5.770	0.665	0.5558	0.793	0.837	1.785	1250	70.20
1.100	0.679	5.930	0.663	0.5522	0.788	0.813	1.905	1250	69.00

TABLE 1 (contd)

1.457	0.650	5.480	0.666	0.5602	0.795	0.863	1.506	1250	72.40
1.428	0.665	5.850	0.668	0.5658	0.798	0.850	1.755	1250	80.00
1.400	0.679	5.830	0.665	0.5591	0.794	0.824	1.790	1250	72.30
1.146	0.650	5.100	0.670	0.5713	0.798	0.878	1.148	1150	84.50
1.457	0.602	4.375	0.654	0.5394	0.787	0.894	0.639	1150	44.00
1.428	0.625	4.440	0.665	0.5558	0.798	0.889	0.688	1150	53.00
1.400	0.619	4.600	0.664	0.5482	0.785	0.886	0.800	1150	48.70
1.146	0.673	5.625	0.658	0.5575	0.800	0.828	1.705	1150	83.00
1.124	0.702	6.200	0.663	0.5585	0.796	0.796	2.108	1150	93.00
1.100	0.673	5.800	0.655	0.5493	0.795	0.816	1.868	1150	88.70
1.457	0.693	5.850	0.665	0.5635	0.799	0.813	1.795	1150	77.70
1.428	0.687	6.000	0.657	0.5542	0.794	0.808	2.050	1150	82.00
1.400	0.698	6.150	0.660	0.5566	0.798	0.796	2.080	1150	86.40
1.146	0.653	6.030	0.654	0.5498	0.798	0.841	2.114	1200	75.20
1.124	0.668	6.320	0.656	0.5508	0.798	0.824	2.300	1200	77.60
1.100	0.678	6.570	0.656	0.5495	0.794	0.810	2.462	1200	81.60
1.457	0.658	6.300	0.652	0.5485	0.789	0.834	2.355	1200	76.00
1.428	0.669	6.360	0.654	0.5513	0.799	0.824	2.346	1200	75.00
1.400	0.681	6.523	0.657	0.5546	0.802	0.814	2.454	1200	79.00
1.197	0.625	4.950	0.657	0.5485	0.794	0.878	1.166	1200	71.00
1.170	0.638	5.305	0.655	0.5501	0.795	0.861	1.485	1200	72.00
1.148	0.647	5.550	0.649	0.5436	0.784	0.840	1.765	1200	68.00
1.515	0.625	5.380	0.649	0.5361	0.785	0.858	1.633	1200	60.00
1.487	0.641	5.650	0.649	0.5450	0.785	0.850	1.829	1200	70.00
1.457	0.651	5.634	0.649	0.5423	0.792	0.833	1.845	1200	64.00
1.197	0.624	5.660	0.648	0.5449	0.790	0.873	1.860	1250	70.00
1.170	0.637	5.920	0.648	0.5478	0.808	0.860	2.098	1250	65.00
1.148	0.650	6.080	0.651	0.5453	0.794	0.839	2.141	1250	69.00
1.515	0.627	5.660	0.646	0.5405	0.795	0.862	1.898	1250	63.00
1.487	0.641	5.940	0.652	0.5418	0.791	0.845	2.035	1250	71.00
1.457	0.653	6.100	0.654	0.5423	0.788	0.830	2.104	1250	74.00
1.015	0.564	4.615	0.822	0.4730	0.814	0.840	2.546	1250	57.50
0.989	0.577	4.960	0.828	0.4730	0.807	0.821	2.766	1250	73.40
1.270	0.582	4.961	0.830	0.4730	0.814	0.814	2.766	1250	77.00
1.230	0.605	5.260	0.834	0.4730	0.802	0.782	2.990	1250	82.80
1.015	0.566	5.075	0.819	0.4740	0.818	0.838	3.132	1200	80.00

TABLE 1 (contd)

0.989	0.578	5.260	0.826	0.4740	0.812	0.820	3.161	1200	101.40
1.270	0.583	5.350	0.830	0.4740	0.807	0.813	3.180	1200	105.50
1.230	0.607	5.700	0.832	0.4740	0.806	0.782	3.367	1200	111.00
1.015	0.567	4.485	0.830	0.4770	0.811	0.841	2.340	1150	75.00
0.989	0.578	4.900	0.830	0.4770	0.811	0.825	2.703	1150	79.00
1.270	0.584	4.822	0.831	0.4770	0.810	0.817	2.602	1150	81.00
1.230	0.607	5.200	0.830	0.4770	0.811	0.786	2.742	1150	97.00
1.015	0.567	4.840	0.822	0.4730	0.814	0.835	2.815	1150	93.00
0.989	0.578	5.110	0.827	0.4730	0.810	0.819	2.970	1150	103.50
1.270	0.586	5.225	0.829	0.4730	0.807	0.808	3.100	1150	103.50
1.230	0.607	5.430	0.831	0.4730	0.805	0.780	3.192	1150	113.00
1.401	0.676	6.090	0.751	0.5600	0.699	0.829	2.180	1200	98.00
1.155	0.644	5.735	0.746	0.5600	0.703	0.869	2.010	1200	89.30
1.110	0.670	6.200	0.757	0.5600	0.694	0.836	2.290	1200	103.50
1.425	0.667	5.830	0.761	0.5650	0.696	0.848	1.907	1200	76.00
1.401	0.675	6.000	0.761	0.5650	0.696	0.837	2.060	1200	77.00
1.155	0.645	5.210	0.766	0.5640	0.690	0.875	1.343	1250	76.00
1.110	0.671	5.570	0.771	0.5640	0.687	0.841	1.593	1250	87.50
1.425	0.663	5.680	0.758	0.5640	0.698	0.850	1.805	1250	75.00
1.401	0.675	5.543	0.767	0.5640	0.690	0.835	2.045	1250	72.60
1.155	0.645	5.600	0.746	0.5520	0.693	0.855	1.928	1250	79.00
1.110	0.665	6.110	0.745	0.5520	0.694	0.830	2.371	1250	88.60
1.425	0.665	6.025	0.748	0.5520	0.691	0.830	2.250	1250	85.00
1.401	0.676	5.875	0.748	0.5520	0.691	0.816	2.160	1250	86.70

TABLE-2

1.015	0.563	4.340	0.806	0.463	0.813	0.823	2.254	1150	67.0
0.989	0.580	4.785	0.805	0.462	0.812	0.796	2.742	1150	63.2
1.270	0.584	4.665	0.806	0.463	0.813	0.794	2.624	1150	66.0
1.230	0.608	5.455	0.805	0.462	0.812	0.758	3.410	1150	64.0
1.015	0.563	5.296	0.785	0.442	0.796	0.784	3.868	1150	71.3
0.989	0.580	5.440	0.785	0.442	0.796	0.762	3.971	1150	78.0
1.270	0.586	5.800	0.784	0.441	0.796	0.752	4.435	1150	71.2
1.230	0.607	5.850	0.791	0.443	0.793	0.731	4.380	1150	79.0
1.015	0.564	3.973	0.824	0.473	0.812	0.839	1.615	1200	53.8
0.989	0.579	4.397	0.824	0.473	0.812	0.817	2.009	1200	52.9
1.270	0.584	4.485	0.824	0.473	0.812	0.810	2.095	1200	55.5
1.230	0.608	4.715	0.824	0.473	0.812	0.778	2.305	1200	55.5
1.015	0.564	4.340	0.798	0.452	0.800	0.800	2.420	1250	55.5
0.989	0.579	4.440	0.803	0.455	0.801	0.786	2.418	1250	64.0
1.270	0.586	4.461	0.792	0.448	0.801	0.766	2.657	1250	49.4
1.230	0.607	5.340	0.795	0.451	0.802	0.743	3.580	1250	54.8
1.154	0.646	5.800	0.652	0.539	0.781	0.835	1.815	1190	82.0
1.128	0.663	6.160	0.655	0.540	0.777	0.814	2.114	1190	79.0
1.438	0.656	5.800	0.652	0.539	0.781	0.823	1.815	1190	82.0
1.400	0.676	6.465	0.656	0.541	0.777	0.800	2.328	1190	84.0
1.154	0.645	6.200	0.645	0.530	0.774	0.822	2.302	1190	93.1
1.128	0.662	6.900	0.642	0.529	0.777	0.800	2.940	1190	90.4
1.438	0.654	6.770	0.640	0.528	0.778	0.808	2.865	1190	89.5
1.400	0.676	6.900	0.642	0.529	0.777	0.783	2.920	1190	91.3
1.154	0.646	6.270	0.644	0.530	0.776	0.821	2.388	1260	91.2
1.128	0.662	6.860	0.641	0.529	0.779	0.800	2.923	1260	90.2
1.438	0.652	6.440	0.643	0.530	0.778	0.814	2.497	1260	95.0
1.400	0.676	6.685	0.644	0.530	0.776	0.784	2.690	1260	91.2
1.154	0.646	5.380	0.663	0.549	0.780	0.850	1.394	1260	68.8
1.128	0.662	5.800	0.663	0.549	0.780	0.830	1.710	1260	70.5
1.438	0.654	5.435	0.667	0.552	0.780	0.843	1.408	1260	73.5
1.400	0.674	5.643	0.665	0.551	0.781	0.817	1.588	1260	69.0
1.154	0.645	4.850	0.771	0.568	0.695	0.881	1.035	1140	72.5
1.128	0.659	5.150	0.771	0.568	0.695	0.862	1.295	1140	73.6
1.438	0.653	4.887	0.774	0.570	0.695	0.873	1.076	1140	74.1
1.400	0.676	5.342	0.774	0.570	0.695	0.844	1.443	1140	82.0

TABLE 2 (contd)

1.154	0.646	5.300	0.759	0.561	0.697	0.868	1.557	1140	88.5
1.128	0.663	6.090	0.756	0.558	0.697	0.842	2.270	1140	86.0
1.438	0.654	5.700	0.757	0.560	0.698	0.856	1.946	1140	87.0
1.400	0.676	5.890	0.758	0.561	0.698	0.829	2.091	1140	87.3
1.154	0.645	5.400	0.755	0.556	0.695	0.862	1.700	1220	79.0
1.128	0.663	5.950	0.753	0.555	0.695	0.837	2.228	1220	81.0
1.438	0.654	5.700	0.753	0.555	0.695	0.848	2.000	1220	76.0
1.400	0.676	5.875	0.757	0.557	0.694	0.824	2.106	1220	86.8
1.154	0.646	5.730	0.739	0.535	0.683	0.828	2.252	1220	87.7
1.438	0.654	6.200	0.738	0.535	0.685	0.818	2.781	1220	86.0
1.400	0.674	6.353	0.742	0.537	0.683	0.796	2.852	1220	91.3
1.154	0.646	6.110	0.761	0.524	0.644	0.812	2.194	1230	75.2
1.128	0.658	6.250	0.765	0.527	0.645	0.800	2.284	1230	84.0
1.438	0.656	6.240	0.765	0.527	0.645	0.803	2.268	1230	83.0
1.400	0.675	6.380	0.762	0.525	0.645	0.778	2.438	1230	80.0
1.154	0.647	6.400	0.751	0.511	0.637	0.790	2.737	1230	89.5
1.128	0.660	6.910	0.749	0.510	0.638	0.773	3.190	1230	90.4
1.438	0.656	6.790	0.745	0.508	0.638	0.775	3.137	1230	85.0
1.400	0.675	6.870	0.745	0.508	0.638	0.753	3.264	1230	85.4
0.989	0.579	3.430	0.931	0.513	0.779	0.886	1.420	1200	57.4
1.270	0.588	3.696	0.930	0.512	0.778	0.870	1.810	1200	59.4
1.230	0.606	4.270	0.930	0.512	0.778	0.845	2.583	1200	60.7
1.015	0.564	3.430	0.922	0.507	0.775	0.898	1.535	1200	60.7
0.989	0.578	3.700	0.925	0.508	0.775	0.879	1.980	1200	68.0
1.270	0.586	4.250	0.923	0.507	0.775	0.865	2.795	1200	66.0
1.230	0.605	4.730	0.921	0.507	0.777	0.837	3.456	1200	66.0
0.989	0.580	4.360	0.913	0.498	0.771	0.859	3.326	1250	63.5
1.270	0.584	4.470	0.915	0.499	0.770	0.854	3.400	1250	65.0
1.230	0.605	4.490	0.915	0.499	0.770	0.825	3.443	1250	66.0
0.989	0.579	3.580	0.925	0.510	0.779	0.881	1.796	1250	58.5
1.270	0.586	3.720	0.928	0.511	0.779	0.873	1.931	1250	63.3
1.230	0.607	4.110	0.928	0.511	0.779	0.843	2.461	1250	65.1
1.200	0.624	4.900	0.656	0.565	0.805	0.905	1.071	1150	79.0
1.153	0.649	5.515	0.652	0.563	0.809	0.868	1.635	1150	81.0
1.438	0.660	5.600	0.654	0.564	0.805	0.854	1.688	1150	86.8
1.400	0.676	6.070	0.654	0.564	0.805	0.834	2.079	1150	86.0

TABLE 2 (contd)

1.153	0.648	5.295	0.664	0.570	0.803	0.879	1.315	1150	78.0
1.438	0.659	5.585	0.667	0.573	0.803	0.868	1.544	1150	79.0
1.400	0.675	5.651	0.670	0.574	0.801	0.850	1.585	1150	82.4
1.153	0.647	5.300	0.666	0.574	0.804	0.888	1.331	1200	73.4
1.438	0.658	5.400	0.666	0.574	0.804	0.872	1.393	1200	80.0
1.400	0.675	5.570	0.668	0.575	0.804	0.852	1.536	1200	80.0
1.200	0.623	5.175	0.640	0.551	0.804	0.884	1.465	1200	83.0
1.153	0.647	5.790	0.643	0.552	0.802	0.853	2.009	1200	91.2
1.438	0.658	5.985	0.644	0.552	0.801	0.839	2.188	1200	90.7
1.400	0.675	6.110	0.645	0.552	0.801	0.819	2.284	1200	93.2
1.111	0.672	5.480	0.638	0.584	0.860	0.869	1.725	1200	87.5
1.438	0.658	5.480	0.634	0.583	0.878	0.886	1.794	1200	85.0
1.400	0.677	5.596	0.632	0.582	0.879	0.860	1.897	1200	80.8
1.111	0.672	5.450	0.644	0.593	0.866	0.883	1.640	1200	71.4
1.438	0.659	5.050	0.644	0.593	0.866	0.900	1.270	1200	76.0
1.400	0.675	5.404	0.640	0.591	0.868	0.875	1.620	1200	71.6
1.111	0.672	5.538	0.641	0.589	0.865	0.878	1.650	1250	69.5
1.438	0.657	4.810	0.639	0.588	0.865	0.897	1.440	1250	68.8
1.400	0.675	5.325	0.639	0.588	0.865	0.872	1.552	1250	70.5
1.111	0.672	6.370	0.610	0.561	0.864	0.835	3.174	1250	82.0
1.438	0.658	6.020	0.611	0.561	0.865	0.852	2.711	1250	86.8
1.400	0.677	6.030	0.616	0.563	0.860	0.832	2.680	1250	91.2
1.154	0.646	4.560	0.758	0.583	0.719	0.903	0.794	1160	71.4
1.127	0.658	4.770	0.758	0.583	0.719	0.886	1.008	1160	72.3
1.154	0.645	4.710	0.745	0.571	0.716	0.885	1.067	1160	86.0
1.127	0.659	5.100	0.746	0.572	0.717	0.868	1.502	1160	89.5
1.452	0.655	4.985	0.742	0.570	0.718	0.870	1.374	1160	84.5
1.154	0.645	4.913	0.734	0.559	0.712	0.867	1.354	1200	70.6
1.127	0.658	5.380	0.734	0.559	0.712	0.849	1.946	1200	80.0
1.452	0.654	4.900	0.731	0.557	0.712	0.851	1.382	1200	66.8
1.015	0.565	4.270	0.828	0.477	0.804	0.844	2.130	1150	58.0
0.989	0.582	4.613	0.827	0.476	0.804	0.818	2.478	1150	59.0
1.270	0.588	4.530	0.830	0.477	0.803	0.810	2.346	1150	63.3
1.230	0.606	4.970	0.834	0.477	0.800	0.786	2.723	1150	69.5
1.015	0.565	4.800	0.816	0.468	0.801	0.828	2.966	1150	65.0
0.989	0.582	5.240	0.819	0.468	0.800	0.805	3.363	1150	68.0

TABLE 2 (contd)

1.270	0.587	5.260	0.819	0.468	0.801	0.798	3.390	1150	68.3
1.230	0.608	5.525	0.823	0.469	0.798	0.772	3.570	1150	75.0
1.015	0.565	4.660	0.816	0.465	0.798	0.822	2.786	1200	66.0
0.989	0.580	5.145	0.817	0.465	0.796	0.802	3.290	1200	66.8
1.270	0.587	5.400	0.815	0.465	0.798	0.793	3.580	1200	63.1
1.230	0.605	5.442	0.819	0.466	0.797	0.770	3.570	1200	68.8
1.015	0.567	5.150	0.798	0.453	0.795	0.800	4.150	1200	66.8
0.989	0.580	5.540	0.798	0.453	0.795	0.782	4.610	1200	66.0
1.270	0.587	5.600	0.799	0.453	0.794	0.774	4.635	1200	69.5
1.230	0.608	5.755	0.802	0.454	0.793	0.747	4.580	1200	73.0
1.015	0.565	4.280	1.049	0.468	0.620	0.829	2.190	1200	60.4
0.989	0.581	4.850	1.048	0.468	0.620	0.807	2.850	1200	59.7
1.270	0.586	4.700	1.050	0.468	0.619	0.800	2.640	1200	62.3
1.230	0.609	5.270	1.051	0.468	0.618	0.769	3.192	1200	64.0
1.015	0.565	5.050	1.037	0.459	0.616	0.813	3.550	1200	84.0
0.989	0.579	5.585	1.032	0.457	0.615	0.788	4.210	1200	76.0
1.270	0.587	5.835	1.031	0.457	0.615	0.778	4.590	1200	74.3
1.230	0.609	5.936	1.037	0.459	0.615	0.754	4.480	1200	84.0
1.015	0.565	5.083	1.033	0.456	0.613	0.807	3.580	1250	74.0
0.989	0.581	5.510	1.032	0.456	0.614	0.785	4.170	1250	74.0
1.270	0.585	5.850	1.033	0.456	0.613	0.779	4.960	1250	64.1
1.230	0.606	6.120	1.037	0.459	0.615	0.758	5.110	1250	67.8
1.015	0.565	4.722	1.038	0.459	0.615	0.813	3.055	1250	59.4
0.989	0.580	4.943	1.038	0.459	0.615	0.792	3.350	1250	60.5
1.270	0.584	5.170	1.036	0.458	0.616	0.785	3.615	1250	60.4
1.230	0.607	5.450	1.038	0.459	0.615	0.757	3.887	1250	61.3
0.989	0.579	3.550	1.175	0.525	0.625	0.907	1.576	1150	60.3
1.230	0.607	4.186	1.188	0.527	0.619	0.868	2.284	1150	80.0
1.015	0.565	3.483	1.170	0.517	0.616	0.914	1.625	1150	68.0
0.989	0.579	3.922	1.173	0.518	0.617	0.895	2.221	1150	76.8
1.270	0.583	4.110	1.173	0.518	0.617	0.888	2.450	1150	76.6
1.230	0.608	4.580	1.173	0.518	0.617	0.851	3.140	1150	80.0
0.989	0.578	3.910	1.163	0.508	0.611	0.879	2.307	1250	68.8
1.270	0.588	4.010	1.162	0.507	0.609	0.861	2.393	1250	72.4
1.230	0.607	4.615	1.161	0.507	0.610	0.836	3.340	1250	73.4
0.989	0.579	4.075	1.155	0.507	0.613	0.875	2.870	1250	73.4

TABLE 2 (contd)

1.270	0.585	3.960	1.152	0.506	0.613	0.865	2.660	1250	68.8
1.230	0.608	4.475	1.159	0.508	0.613	0.835	3.392	1250	80.0
1.010	0.567	2.910	1.067	0.520	0.874	0.918	1.370	1200	42.8
0.989	0.582	3.310	1.069	0.520	0.873	0.894	1.850	1200	46.5
0.968	0.592	3.450	1.073	0.520	0.870	0.879	1.970	1200	52.0
0.948	0.605	3.900	1.072	0.520	0.870	0.860	2.505	1200	54.0
0.928	0.621	4.220	1.074	0.520	0.868	0.838	2.815	1200	56.5
1.010	0.566	3.200	1.057	0.511	0.866	0.903	1.904	1200	55.6
0.989	0.577	3.550	1.057	0.511	0.866	0.885	2.630	1200	52.9
0.968	0.590	3.910	1.057	0.511	0.866	0.865	2.870	1200	54.0
0.948	0.605	4.350	1.057	0.511	0.866	0.844	3.405	1200	54.7
0.928	0.619	4.620	1.061	0.511	0.864	0.825	3.630	1200	59.0
1.010	0.568	3.250	1.054	0.510	0.868	0.898	2.055	1200	70.5
0.989	0.582	4.100	1.048	0.510	0.872	0.876	3.337	1200	63.2
0.968	0.592	4.340	1.046	0.510	0.874	0.862	3.767	1200	57.5
0.948	0.605	4.700	1.047	0.510	0.873	0.843	4.230	1200	58.0
0.928	0.619	4.710	1.046	0.510	0.874	0.823	4.290	1200	62.3
0.980	0.586	4.610	1.139	0.508	0.640	0.868	3.186	1200	73.0
0.959	0.599	4.860	1.140	0.508	0.639	0.848	3.500	1200	76.0
0.938	0.610	4.900	1.133	0.508	0.643	0.846	3.860	1200	73.0
1.271	0.587	4.485	1.133	0.508	0.643	0.866	3.100	1200	65.0
1.245	0.599	4.900	1.136	0.508	0.641	0.848	3.521	1200	73.0
1.218	0.612	4.950	1.142	0.508	0.638	0.831	3.480	1200	76.1
0.980	0.587	5.255	1.124	0.501	0.637	0.854	4.840	1250	83.0
0.959	0.598	5.510	1.127	0.501	0.635	0.837	4.990	1250	78.5
0.938	0.610	5.655	1.128	0.501	0.635	0.833	5.010	1250	81.0
1.271	0.586	5.100	1.127	0.501	0.635	0.854	4.230	1250	78.5
1.245	0.598	5.325	1.131	0.501	0.633	0.837	4.370	1250	84.3
1.218	0.611	5.910	1.125	0.501	0.637	0.833	5.060	1250	74.0
1.003	0.570	4.100	1.140	0.506	0.634	0.887	2.535	1150	99.0
0.980	0.585	4.560	1.138	0.506	0.635	0.864	3.192	1150	96.8
0.959	0.598	4.940	1.130	0.506	0.640	0.845	4.070	1150	93.2
1.305	0.570	4.610	1.130	0.506	0.640	0.887	3.490	1150	83.0
1.271	0.585	5.100	1.130	0.506	0.640	0.864	4.180	1150	84.2
1.245	0.598	5.165	1.138	0.506	0.635	0.845	4.080	1150	77.0
1.003	0.570	4.180	1.140	0.514	0.645	0.902	2.601	1150	80.0

TABLE 2 (contd)

0.980	0.585	4.650	1.139	0.514	0.642	0.879	3.370	1150	80.0
0.959	0.598	4.770	1.144	0.514	0.642	0.859	3.295	1150	78.4
1.305	0.570	4.110	1.137	0.514	0.646	0.902	2.552	1150	70.5
1.271	0.586	4.438	1.140	0.514	0.644	0.878	2.905	1150	77.0
1.245	0.597	4.593	1.140	0.514	0.644	0.861	3.103	1150	78.5
0.991	0.587	3.990	1.167	0.517	0.618	0.882	2.025	1200	58.8
0.959	0.600	4.080	1.172	0.520	0.619	0.867	2.132	1200	59.5
1.291	0.586	4.200	1.169	0.519	0.619	0.887	2.287	1200	58.0
1.245	0.603	4.410	1.172	0.520	0.619	0.862	2.495	1200	63.5
0.991	0.580	3.790	1.165	0.512	0.613	0.882	1.839	1250	52.0
0.959	0.590	4.210	1.167	0.513	0.613	0.870	2.302	1250	55.6
1.291	0.581	3.950	1.163	0.511	0.611	0.881	2.028	1250	48.0
1.245	0.595	4.140	1.166	0.512	0.633	0.860	2.442	1250	53.0

APPENDIX 3

	Billet Diameter / Billet Height	Billet Weight	Parting Area	Maximum Forging Height	Parting Dia. / Max Forging Height	Weight Of Forging
Billet Diameter / Billet Height	1.00000	-0.02317	-0.00854	0.06953	-0.04389	0.03993
Billet Weight	-0.02317	1.00000	0.82340	-0.84216	0.88481	0.73887
Parting Area	-0.00854	0.82340	1.00000	-0.80334	0.91757	0.31622
Maximum Forging Height	0.06953	-0.84216	-0.80334	1.00000	-0.96605	-0.52662
Parting Diameter / Max Forging Height	-0.04389	0.88481	0.91757	-0.96605	1.00000	0.50200
Weight Of Forging	0.03993	0.73887	0.31622	-0.52662	0.50200	1.00000
Shape Complexity	-0.01593	0.08939	-0.23296	-0.24839	0.04565	0.30447
Process Yield	0.06902	-0.68601	-0.88346	0.68421	-0.77295	-0.01934
Flash Thickness	-0.02703	0.76375	0.57740	-0.75939	0.73054	0.56801
Flash Width	0.04937	0.26431	0.58169	-0.25179	0.34875	-0.27070
Flash Width / Flash Thickness	0.07655	-0.04741	0.32837	0.05825	0.04619	-0.46139
$\left(\frac{\text{Flash Width}}{\text{Flash Thickness}}\right)^2$	0.04944	-0.07717	0.29391	0.05312	0.03185	-0.48139
Slug Temperature	0.01069	0.12916	0.22573	-0.07929	0.13463	0.11307
Forging Load	-0.14376	0.57125	0.83742	-0.57456	0.67244	0.00420
Flash Width / Clipped Forging Diameter	0.07662	-0.09359	0.18911	0.08910	-0.03847	-0.46320

The Correlation Matrix

APPENDIX 3 (continued)

	Shape Complexity	Process Yield	Flash Thickness	Flash Width	$\frac{\text{Flash Width}}{\text{Flash Thickness}}$	$\left(\frac{\text{Flash Width}}{\text{Flash Thickness}}\right)^2$
$\frac{\text{Billet Diameter}}{\text{Billet Height}}$	-0.01593	0.06902	-0.02703	0.04938	0.07655	0.04944
Billet Weight	0.08939	-0.68601	0.76375	0.26431	-0.04741	-0.07717
Parting Area	-0.23295	-0.88346	0.57740	0.58169	0.32837	0.29391
Maximum Forging Height	-0.24839	0.68421	-0.75939	-0.25179	0.05825	0.05312
$\frac{\text{Parting Diameter}}{\text{Max Forging Height}}$	0.04565	-0.77295	0.73054	0.34875	0.04619	0.03185
Weight Of Forging	0.30447	-0.01934	0.56801	-0.27070	-0.46139	-0.48139
Shape Complexity	1.00000	0.19065	0.24961	-0.01896	-0.11684	-0.07705
Process Yield	0.19065	1.00000	-0.52762	-0.69432	-0.43747	-0.41568
Flash Thickness	0.24961	-0.52762	1.00000	0.11012	-0.30234	-0.30565
Flash Width	-0.01896	-0.69432	0.11012	1.00000	0.90642	0.87546
$\frac{\text{Flash Width}}{\text{Flash Thickness}}$	-0.11684	-0.43747	-0.30234	0.90642	1.00000	0.98180
$\left(\frac{\text{Flash Width}}{\text{Flash Thickness}}\right)^2$	-0.07705	-0.41568	-0.30565	0.87546	0.98180	1.00000
Slug Temperature	-0.04858	-0.08262	-0.09567	0.27118	0.32080	0.29954
Forging Load	-0.24291	-0.84740	0.32836	0.72783	0.56798	0.56125
$\frac{\text{Flash Width}}{\text{Clipped Forging Diameter}}$	0.12930	-0.37432	-0.14954	0.90541	0.92447	0.91173

The Correlation Matrix (continued)

APPENDIX 3 (continued)

	Slug Temperature	Forging Load	Flash Width / Clipped Forging Diameter
Billet Diameter / Billet Height	0.01069	-0.14376	0.07662
Billet Weight	0.12916	0.57125	-0.09359
Parting Area	0.22573	0.83742	0.18911
Maximum Forging Height	-0.07929	-0.57456	0.08910
Parting Diameter / Max Forging Height	0.13463	0.67244	-0.03848
Weight Of Forging	0.11307	0.00420	-0.46320
Shape Complexity	-0.04858	-0.24291	0.12930
Process Yield	-0.08262	-0.84740	-0.37432
Flash Thickness	-0.09567	0.32836	-0.14954
Flash Width	0.27118	0.72783	0.90541
Flash Width / Flash Thickness	0.32080	0.56798	0.92447
$\left(\frac{\text{Flash Width}}{\text{Flash Thickness}}\right)^2$	0.29954	0.56125	0.91173
Slug Temperature	1.00000	0.10774	0.22132
Forging Load	0.10774	1.00000	0.44856
Flash Width / Clipped Forging Diameter	0.22132	0.44856	1.00000

The Correlation Matrix (continued)

APPENDIX 4

The author has conducted cold compression tests on brown plasticene slugs to investigate the effects of aspect ratio on the flow of billet material. Results similar to those of Schey et al[25] were obtained.

A power press was used for the tests and the lubricating fluid was a 50/50 mixture of glycerine and teepol. Slugs differing in aspect ratio but equal in volume were cut from 1.6 inch, 2 inch and 2.4 inch diameter bars and compressed between flat platens at the same speed to a final height of one inch.

Visual inspection and measurements of the slugs' widest sections after compression revealed that all the billets barrelled and that the bulgings were maximum about half way up their (billets') heights. It was also observed that the tallest billet barrelled most and the widest least. This confirms that when upset a tall slug contacts the die walls sooner than the shorter one.

A further observation made was that little or no slug widening occured at the billet-tool interfaces. This later observation suggests that except the slug very nearly fits the die impression, billet edges do not form the corners of closed die forged components. This was confirmed in the laboratory study where faint rings indicating the original edges of the billets were seen on the faces in contact with the bottom of the die impressions. Fig 1 shows diagramatically the shapes of the slugs before and after compression.

APPENDIX 4 (contd.)

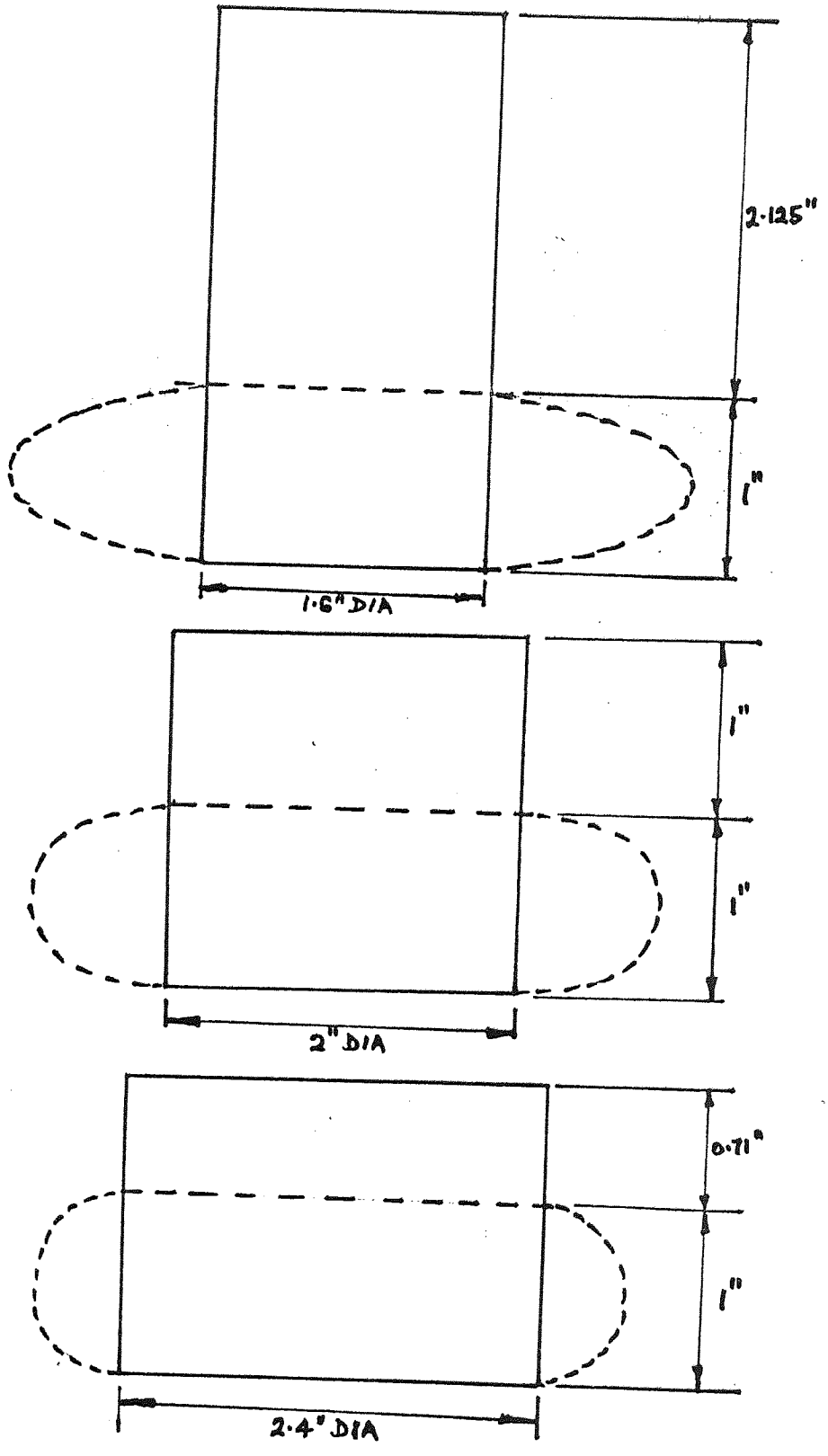

Fig 1

REFERENCES

1 C B Aston
Garringtons Limited, Bromsgrove.
Personal Communication.

2 J Hughes
Forging and Presswork Limited, Witton, Birmingham.
Personal Communication.

3 F Benton
Halladays Drop Forging Limited, Birmingham.
Personal Communication.

4 E Siebel
Die Formgebung im Bildsamen Zustand
Stahl Eisen, Dusseldorf, 1932.

5 A Geleji
Bildsame Formung der Metalle in Rechnung und
Versudi Akademie Verlag Berlin, 1960.

6 H Lippmann
"Elementary Methods For The Analysis Of Certain Forging Processes"
Int. Jou. Mech. Sci. Vol 1 (109-120), 1960.

7 R L Dietrich and G Ansel
Trans. A S M 38(709-727), 1947.

8 G L Baraya, W Johnson, R A C Slater
Int. Jou. Mech. Sci. Vol 7 (621-645), 1965.

9 W Schroeder and A Webster
Jou. Appl. Mech. 1949 (289-294).

10 V V Sokolovskii
Theory of Plasticity (In Russian)
Izd. Akad Nauk SSSR, 1946.

11 E P Unksov
An Engineering Theory of Plasticity
Butterworths, 1961.

12 S Kobayashi, R Herzog, J T Lapsley Jnr, E G Thomsen
Trans. ASME, August 1959.

13 H F Massey
The Flow Of Metal During Forging
presented to Manchester Assoc. of Engineers, November 1921.

14 B Zünkler
Determination of Stresses and Loads in Plain Strain Closed Die Forging.
Industrie Anzeiger, 84 67-74 (1964).

15 A T Male and M G Cookcroft
Jou. Inst. Metals, 1964.

16 J Stöter
"Forchungsberichte des landes Nordrhein"
Westfaren Nr 848, Westdeutscher verlag, Köln und Opladen, 1960.

17 M W Storoschev, E A Popov
Fundamentals of Forming (In German)
V E B. Verlag, Berlin, 1968.

18 J L Aston
University of Aston in Birmingham
Personal Communication.

19 K Lange
Determination of Load and Energy Requirements in Closed Die Forging (In German)
Industrie Anzeiger 80 631-34 (1958)

20 T Altan, R J Florentino
Prediction of Loads and Stresses in Closed Die Forging
Submitted for ASME Winter 1970 meeting.

21 S I Gubkin
Engineering Method for Calculating Metal Forming Processes.
The Scientific and Technical Soc. for Engineering Industry
Book 42, Mashgiz 1957.

22 J F Nye
ASME Jou. App. Mech. (337-346) 1951.

23 R A Slater, W Johnson, S Y Aku
Experiments in the Fast Upsetting of Short Pure Lead Cylinders and a Tentative Analysis
Int. Jou. Mech. Sci. Vol 10 (169-186) 1968.

24 H Mäkelt
Mechanische pressen (Mechanical presses)
Carl Hanser Verlag, Münich 1961.

25 J A Schey, P W Wallace and F A Shunk
Research Report on "Metal Flow in Closed Die Press Forging of Steel".
American Iron & Steel Institute.

26 T Altan, H J Henning
Material Savings Through Improved Flash Design in Round Closed Die Forging
Submitted to Precision Metal, 1970.

27 H J Henning, A M Sabroff, F W Boulger
A Study of Forging Variables
Technical Documentary Report No MLTDR 64-95,
Battelle Memorial Inst. Columbus, Ohio (March 1964).

28 R A Fisher
The Design of Experiments
Oliver & Boyd, 1960.

29 O L Davis
Statistical Methods in Research and Production
Oliver & Boyd, 1967.

30 E A Barry
"A statistical study, with the aid of a computer, of some of the factors which affect die life in drop forging".
MSc Dissertation, University of Aston, 1967.

31 J F Tognarelli
"An examination of the estimating method for aluminium alloy forgings".
MSc Dissertation, University of Aston, 1969.

32 W Naujoks and D C Fabel
"Forging Handbook"
American Society for Metals, Metals Park, Ohio, 1939.

33 A G Macdonald, S Kobayashi, E G Thomsen
Some Problems of Press Forging Lead and Aluminium
Trans ASME, August 1960.

34 S Kalpakjian
"A survey of the feasibility of an analytical approach to die design in closed die forging".
Battelle Memo. Inst. DIMC Memorandum, June 1966.

35 K Vieregge
"Effect of the Flash Gap in Drop Forging".
Industrie Anzeiger 92(1970), 49 pp 1119-21.

36 K Vieregge
"Design of the Flash Gap on Forging Dies".
Industrie Anzeiger 92(1970), 65 pp 1561-4.

37 S C Jain, A N Bramley
"Experiments in Extrusion Forgings".
Research Report No 102, Dept. of Mech. Eng.,
University of Birmingham.

38 G P Teterin et al
"Shape Difficulty Criteria for Forgings" (In Russian)
Kuznecho Stamporocnoe Proizvodstvo, 8(1966) p 6-9.

39 Y Yarnitsky, J Bergman
"Blank Design for Drop Forging of Hand Tools"
Metal Treatment and Drop Forging, April 1966.

40 A M Sabroff, F W Boulger, H J Henning
Forging Materials and Practices
Reinhold Book Corporation, 1968.

41 H K Ihrig
"The Effect of Various Elements on the Workability of Steels".
Trans. AIME 167, 736 (1946).

42 C L Clark, J J Russ
"A Laboratory Evaluation of Hot Workability Characteristics
of Metals".
Trans. AIME 167, 736 (1946)

43 J S Byam-Grounds
"Technical Developments in Modern Drop Stamps and Forging Presses".
Metal Treatment, 27 (1960) p 415.

44 K Lange
"Theory and Basic Principles of Drop Forging".
Metal Treatment and Drop Forging, 32 (236), 184-195 (May 1965)
32 (237), 210-220 (June 1965), 32 (238), 264-270 (July 1965).

45 J L Aston, A Muir
"Some Factors Affecting the Life of Drop Forge Dies"
DFRA Publication.

46 B Winch
Garringtons Limited, Bromsgrove.
Personal Communication.

47 E Orowan
BISRA Report No MWF/20/50.

48 E C Larke
The Rolling of Strip, Sheet and Plate.
Chapman and Hall Limited, 1967.

49 S K Samanta
"Resistance to dynamic compression of low carbon steel and alloy steels at elevated temperatures and high strain rates".
Int. Jou. Mech. Sci. 1968, Vol. 10 (613-637).

50 J F Alder, V A Phillips
"The effect of strain rate and temperature on the resistance of aluminium, copper and steel to compression".
J. Inst. Met. 1954 (83) p 80.

51 Shaw, Boulger and Lorig
"Development of Die Lubricants"
Battelle Memorial Inst. Columbus, Ohio.
Summary Report on Contract AF 33 (600) - 26272, October 1955.

52 H Tolkien
"Lubrication Effect in Drop Forging Dies".
Werkstattstehnik, 51 (1961) S102-105.

53 H Tolkien
"Effect of Lubrication in Die Wear".
Werkstattstechnik, 51 (1961), S431-435.

54 H Meyer-Nolkemper
"Studies of Die Lubricants".
DFRA Publication.

55 C Hopper
Acheson Colloids United, Plymouth.
Personal Communication.

56 E J Breznyak, J F Wallace
"Lubricating During Hot Forging of Steel".
Forging Industry Education and Research Foundation,
Cleveland, Ohio, 1965.

57 H Takahashi, J M Alexander
"Friction in the Plain Strain Compression Test".
Jou. Inst. Met. 1961-62, 90.

58 J F Bishop
"On the Effect of Friction on Compression and Identation
Between Flat Dies".
Jou. of Mechanics and Physics of Solids 6 (1958) 132-144.

59 G T Van Rooyen, W A Backofen
"A Study of Interface Friction in Plastic Compression".
Int. Jou. Mech. Sci. 1960 (1), 1-27.

60 B & S Massey Limited, Manchester,
Personal Communication.

61 A Thomas
"Wear Tests on Die Materials".
DFRA Report.

62 U Klafs
"Determination of Temperature Distribution in the Workpiece of Hot Forming".
Industrie Anzeiger 91 (1969) 48.

63 D Bauer and G Muhs
"Calculation of Temperature Distribution in Drop Forgings".
Industrie Anzeiger 91 (1969) No 48, 83/84.

64 A Thomas
"Stresses and Temperature in Forging Dies".
DFRA Publication.

65 M A Kellow, A N Bramley and F K Bannister
"The Measurement of Temperatures in Forging Dies".
Presented at the 9th M.T.D.R. Conference, Birmingham 1968.

66 T Altan, S Kobayashi and V Ostafiev
"Numerical Calculation of the Temperature Distribution in Orthogonal Metal Cutting".
ASME Publication, 67-Prod-17.

67 T Altan, S Kobayashi
"A Numerical Method of Estimating the Temperature Distributions in Extrusion Through Conical Dies".
ASME Publication, 67-Prod-8.

68 J L Maulbetsch
"Thermal Stresses in Plates".
Trans. ASME Jou. Appl. Mech. 2, A141-A146 (1935).

69 B E Gatewood
"Thermal Stresses in Moderately Thick Elastic Plates".
Trans. ASME, Jou. Appl. Mech. 26. 432-436 (1959).

70 Carslaw and Jaeger
Conduction of Heat in Solids.

71 R D Mindlin, D H Cheng
"Thermoelastic Stresses in the Semi-infinite Solid".
Jou. App. Phy. 21 (931-933) (1950).

72 Z Zudans, T C Yen, W H Steigelmann
Thermal Stress Techniques
By the Franklin Inst. Research Laboratories.

73 N O Mykelstad
"Two Problems of Thermal Stress in the Infinite Solid".
Trans. ASME, Jou. Appl. Mech. 9, 136-143 (1942).

74 O J Horger
"Residual Stress". Handbook of Experimental Stress Analysis.
John Wiley & Sons Inc., New York, 1950.

75 G E Dieter, Jnr.
Mechanical Metallurgy, McGraw-Hill Co, New York, 1961.

76 A W Hendry
Photoelastic Analysis
Pergamon Press, 1966.

77 E G Coker, L N G Filon
A Treatise of Photoelasticity
Cambridge University Press, 1931.

78 M M Frocht
Photoelasticity
John Wiley, Vol I 1941, Vol II 1948.

79 H T Jessop and F C Harris
Photoelasticity. Principles and Methods.
Cleaver-Hume Press, 1949.

80 R B Heywood
Photoelasticity for Designers.
Pergamon Press, 1969.

81 M Hetenyi
Handbook of Experimental Stress Analysis.
John Wiley, 1950.

82 R W Goranson & L H Adams
"A Method for the Precise Measurement of Optical Path Difference".
J Franklin Inst. V216, n 4, pp 475-504 (October 1933).

83 T Altan, H J Henning and A M Sabroff
"The Use of Model Materials in Predicting Forming Loads in Metal Working".
Trans. ASME, November 1969.

84 A P Green
"The Use of Plasticene Models to Simulate the Plastic Flow of Metals".
Phil. Mag. Series 7 42 (329), 365-373 (1951).

85 R Weller and G H Shortley
"Calculation of Stresses Within the Boundary of Photoelastic Models".
Jou. App. Mech. 1939, A71-A78.

86 A M Freudenthal
Introduction to the Mechanics of Solids
John Wiley, 1966.

87 E G Thomsen, C T Yang and S Kobayashi
Mechanics of Plastic Deformation in Metal Processing
The Macmillan Co (New York) 1964.

88 R N Bayliss
"Metallurgical Developments Relevant to Forging Dies".
DFRA Publication.

89 T Altan and A M Sabroff
"Important Factors in Selection and Use of Forging Equipment".
Precision Metal, June 1970.

90 H Fessler and R T Rose
"Photoelastic Determination of stresses in a cylindrical shell".
Brit. Jou. Appl. Phys. 4 (1953), 76-79.

91 M Clutterbuck

"The dependence of stress distribution on elastic constants".
Brit.Jou.Appl.Phys.9 (1958) 323-329

92 D J Duncan
Physical similarity and Dimensional analysis
Edward A rnold 1953.

93 H Fessler and B H Lewin
"Study of large strains and the effect of different values of poisson's ratio".
Brit.Jou.Appl.Phys.11,1960 273-279

94 P W Bridgman
Dimensional Analysis
Yale university press 1927

95 D H Sansome
Dept. of Mechanical Engineering
Personal communication.

96 N Bott
Formerly of the Dept.of Mechanical Engineering
Personal communication

97 J Forster
B & S Massey Ltd. Manchester
Personal communication

98 M B Peterson and R L Johnson
" Frictional studies of graphite and mixtures of graphite with several metallic oxides and salts at temperatures up to 1000°F "
N A C A technical note No 3657, Feb.1956

ACKNOWLEDGEMENT

I wish to thank Dr J.L.Aston, the project supervisor, for his guidance, Mr A.D.Hopkins, for his advice and the Commonwealth Scholarship Commission and the University of Aston Grants Committee for their financial support.

The co-operation of Messrs Forging and Presswork Ltd. and Garringtons Ltd., in whose works the industrial study was carried out, and the technical assistances of Messrs S.J.Cross and D.C.Whyley are thankfully acknowledged.

My gratitude also goes to Messrs F.Benton of Halladays Drop Forging Ltd., C.B.Aston of Garringtons Ltd., H.Coulsons of the GKN Technological Centre, and B.H.Lewin of the Department of Mechanical Engineering for the useful discussions I had with them.